THESIS FOR THE DEGREE OF DOCTOR OF PHILOSOPHY

Partial Discharges at Fast Rising Voltages

THOMAS HAMMARSTRÖM

High Voltage Engineering
Department of Materials and Manufacturing Technology

CHALMERS UNIVERSITY OF TECHNOLOGY

Gothenburg, Sweden 2014

Partial Discharges at Fast Rising Voltages
THOMAS HAMMARSTRÖM
ISBN: 978-91-7597-054-7

ISSN 0346-718X
Technical report no. 3735/2014

High Voltage Engineering
Department of Materials and Manufacturing Technology
Chalmers University of Technology
SE-412 96 Gothenburg
Sweden
Telephone + 46 (0)31-772 1000

Chalmers Bibliotek, Reproservice
Gothenburg, Sweden 2014

Abstract

The present demand for higher efficiency and flexibility in the energy sector has led to an increased use of power electronic generated waveforms as these allow energy conversion between different frequencies including DC. The generated waveforms are usually synthesized by so called Pulse Width Modulation (PWM) techniques, where the desired waveform is approximated by a number of square shaped pulses with a short rise time. Applications such as variable speed drives and reactive power compensation are saving vast amount of energy. This makes it important to understand how rapidly rising voltages affect insulation systems. In particular this applies to partial discharges (PDs), which are considered as affecting the life time of insulation considerably. This thesis presents an investigation regarding the behavior of PDs for different voltage waveforms characterized by steep rise times. The analysis method is based on moderately sharp frequency filters in the PD decoupler, high-resolution digitizers and time-domain stochastic filtering. Although entirely passive, the PD decoupler filter suppression can be made to change two orders of magnitude in half a decade of frequency enabling studies down to nanoseconds in the PD rise time. Voltages of different rise times are employed, which resulted in significant differences in the PD behavior. Applying square-like voltages to cavities with dielectrically insulated electrodes significantly affects the discharge amplitude, its rise time, the extinction voltage and the distribution shape. The investigation shows that the amplitude of the PDs increases considerably while the rise time of the PD signal decreases for shorter voltage rise times.

Thus continued investigations applying PWM waveform of different level of filtering (smoothness) is important. An approach is presented which accepts both timing jitter and a non-integer relation between carrier and modulating frequency. The modified method is first used on the cavity test object and the observations found for semi-square wave forms were confirmed also on other insulation system such as a motor stator and a twisted pair test object. For the phase resolved PD (PRPD) pattern to become similar to the normal AC pattern, it is required that the remains from PWM steps are lower than the extinction voltage. Thus limits for a sufficient smoothing level are found, which is of importance when designing insulation systems exposed to fast transients. To illustrate the degradation process, microscopic images show how the rise times affect the cavity surface deterioration, observations that are consistent with the electrical measurements. The same observations were found valid on motor insulation. Finally a simulation model was introduced with sufficient detail to reproduce the observations. A relation between over voltage level and PD quench voltage was found necessary to enable the reproduction of the measured results.. This also results in a lower extinction voltage for short rise times.

Keywords: Partial discharges, square like voltages, measurements, cavities, repetitive voltages, short rise time, high dV/dt.

Acknowledgements

I would like to thank a number of persons especially. Prof. Stanislaw Gubanski for his supervision of the project and for his valuable guidance, which has been very important to me. My supervisor Prof Tord Bengtsson for his great input which has taught me a lot of new things and for always been ready to discuss new things. My supervisor Prof. Jörgen Blennow which in almost all hours during the days were ready for discussing my project as well as other topics. All the members of the reference group are gratefully acknowledged.

The work presented in this publication has been performed within the ELEKTRA program, projects 36036 and 360137, with financial support from the Swedish Energy Agency, Elforsk, ABB AB and Trafikverket which is gratefully acknowledged. Financial support from Schneider Electric's fund in memorial of Erik Feuk as well as Wilhelm and Martina Lundgrens Vetenskapsfond for participation in courses and conferences are also acknowledged. A special thanks to my family who patiently have been forced to accept all the hours I have been working (as I always tend to do through the years..), friends, all present and new colleagues at the department and other people really close to me, without you things should have been so much different.

And at moments when nothing else works:"Tag rak backhand(" för den är jag säker på")!"

Table of Contents

1. Introduction

The presence of partial discharges, PDs, is often considered as a sign of weakness when occurring in insulation systems and may be a cause of accelerated degradation. Extensive investigations have been reported in literature concerning various PD measurement techniques as well as consequences of PD exposure in insulation systems operating at 50 and 60 Hz sinusoidal voltages. The increased use of Pulse Width Modulated voltages (PWM) by power electronics motivates however further investigations in this area [1].

A number of time-to-breakdown studies have indicated that the frequency of the applied sinusoidal voltage plays the most important role [2, 3] in this context, as at increased frequency also an increased amount of PDs occurs during a given time period, assuming that their properties do not change with time. Therefore the service life of an insulation system depends inversely on the frequency of voltage at which it operates and, as far as known to the author of this thesis, no exceptions from this rule have been reported.

1.1 Description of the project

The conventional PD detection technique [4] is primarily utilizing the vast difference in frequency content between the applied voltage and the PD signal itself. Direct detection of partial discharges at steeply rising voltages is therefore difficult, as the frequency contents of such voltages are much higher than at the power frequency and close to the characteristic frequency content of the PD. An IEC task force had studied this issue, mainly suggesting the use of steeper filters compared to previous approaches [5]. Additionally a number of non-conventional techniques have also been employed [6, 7, 8].

To overcome the difficulties arising when using the conventional circuits, a time domain technique, utilizing the stochastic nature of PDs for separating them from the applied voltage, has recently been developed [9]. To explore the feasibility of this approach and to investigate properties of PDs at varying voltage rise times, a number of different PD sources were studied [10, 11]. Some of the sources exhibited insignificant dependence on the rise time, which agreed with the expectations arising from the time-to-breakdown studies. In contrast however, a strong reduction of the PD extinction voltage was observed for short (~2 μs) rise times as compared to long

(~100 μs) ones for enameled-wire insulation of electric motors and for dielectrically insulated cavities [11]. Moreover, the number of discharges per cycle clearly displayed different voltage dependency at the short rise times for the cavity, whereas this behavior remained quite similar and independent of the rise time for the motor insulation. It has been considered in [12] that the evolving PD degradation in gas filled cavities does cause changes in the discharge mechanism. However, the differences described in [11] reflect behavior attributed to the rise time of the applied voltage but not to degradation. Thus the implications of rise time on the PD characteristics should be investigated further and the validity of the observations tested on other insulation systems.

One essential motive for initiating the work presented in this thesis was therefore to elucidate the observed differences in PD behavior (extinction voltage, rise time and number of PDs per period) appearing in dielectric cavities of different dimensions under different rise times of the applied voltage. Additionally the PD magnitude should be included in the investigation since this is considered a vital parameter in the degradation process of the insulation system [12].These measurements needed to be reproduced on several different cavity sizes to verify that the earlier observations were robust. This work combines both theoretical and experimental approaches to study the PD phenomena occurring within cavities. Several rise times, selected in between the two earlier employed ones [11] were used for analyzing the PD amplitude, its time and voltage distribution as well as PD signal rise time in cavities with dielectric insulated electrodes. However, to allow detailed analyses of the studied cases, the earlier developed measuring system had to be modified; the bandwidth of the measurement needed to be extended for resolving the rise times of the PDs themselves. This allowed a detailed analysis of how the different rise times affect the PD characteristics for semi-square voltage waveforms.

In addition, effects of voltage waveforms resembling actual applications were also elucidated. A two level PWM waveform utilizing different levels of filtering, from sharp edges gradually smoothed until sinusoidal shape, were employed to elucidate how the Phase Resolved PD (PRPD) patterns are influenced. This to verify the previous findings and provided new insights into the PD characteristic behavior. This task required a considerable modification of the data processing algorithm to make it possible to take phase jitter into account. As a result, both offline and online measurements became possible based on the modified principle. The latter approach was used to demonstrate the validity of the presented observations on other insulation systems exposed to a range of voltage waveform with various frequency contents and amplitudes. The tests were performed on simple twisted pair test objects as well as on a complete motor stator. For verifying the similarity of electrical observations with degradation patterns appearing on the PD treated surfaces of the investigated objects an optical microscope was used. A simulation model is also presented that allows predicting the PRPD patterns resulting from applications of voltage waveforms similar to the ones applied in the experimental investigations for different level of filtering. Thus the important parameters that influence the dependence of rise time of the PD characteristics can be identified.

1.2 Outline of the thesis

Chapter 2 of this thesis presents a literature review on the recent development within the field of PD measurements at steeply rising voltages and places the current work in context of previously presented investigations. Most relevant simulation approaches describing the conditions for appearance and the properties of PDs are also discussed.

Chapter 3 describes the algorithm applied to detect PDs at steep rising voltage waveforms. Further, the method is presented for identifying individual PDs as well as the suitable trigger level. It is followed by theoretical considerations on how to select suitable filters for amplifying PD signals and for suppressing remnants of the applied voltage. Limitations of the developed measurement system are clarified by comparing them to the earlier employed circuit, followed by suggestions for two alternative new circuits. It is further discussed how the actually applied voltage can be recreated from the PD signal for calibrating the measurement system and relevant results are presented for the different insulation systems used.

Chapter 4 contains results of investigations clarifying the question on whether extinction voltage measurements are suitable for robust representation of significant PD properties. This is followed by a detailed analysis of how the rise time of the applied voltage affects the number of PDs taking place in dielectrically isolated cavities of different dimensions. Furthermore measurements of the rise time of the PDs are discussed. This section ends with presentation of PD caused degradation on cavity wall surfaces.

Chapter 5 presents the modified algorithm that is applicable for studies of PD activity under PWM voltage waveform excitation at various levels of filtering. Initially the results presented in chapter 4 are verified for the cavity test object under this kind of exposure, which results in a recommendation on filtering level for reducing the stress on the insulation system to meet the effect of PD exposure similar to that under sinusoidal excitation. Subsequently, the validity of the recommendation is tested on the motor insulation systems.

In Chapters 6 the simulation approach is described. It uses the measurement based information for obtaining the model parameters with the goal of reproducing the experimental observations.

In chapter 7, conclusions of the work are summarized and finally in chapter 8 suggestions on future work are provided.

1.3 List of publications

1. Thomas Hammarström, Tord Bengtsson, Jörgen Blennow, Stanislaw Gubanski, "Resonant PD signal decoupling circuit for rapidly changing voltages", Proc. of 22 nd Nordic Insulation Symposium (NORDIS 11), Tampere, Finland, pp. 149-152. ISBN/ISSN: 978-952-15-2562-9, 2011.

2. Thomas Hammarström, Tord Bengtsson, Jörgen Blennow, Stanislaw Gubanski, "Changes in PD Properties with Decreasing Voltage Rise Time in Dielectrically Insulated Cavities", Proc. of the 17th International Symposium on High Voltage Engineering, ISBN/ISSN: 978-3-8007-3364-4, 2011.

3. Thomas Hammarström, Tord Bengtsson, Jörgen Blennow, Stanislaw Gubanski, "Evidence for Changing PD Properties at Short Voltage Rise Times", in IEEE Transactions on Dielectrics and Electrical Insulation, Volume: 18, Issue: 5, pp. 1686-1692, 2011.

4. Thomas Hammarström, "Detection of Partial Discharges in Cavities at Fast Rising Voltages", Thesis for the Degree of Licentiate of Engineering, Chalmers University of Technology, Gothenburg, Sweden, ISSN 1652-8891, Technical report no. 70/2011.

5. Thomas Hammarström, Tord Bengtsson, Jörgen Blennow, Stanislaw Gubanski, "PD Properties at PWM Voltages of Varying Smoothness", in IEEE Transactions on Dielectrics and Electrical Insulation, Vol. 20, Issue 6, pp. 2035-2042, 2013.

6. Tord Bengtsson, Elisabeth Lindell, Thomas Hammarström "Stochastic Detection of Partial Discharges" in IEEE Transactions on Dielectrics and Electrical Insulation, Vol. 20, Issue 6, pp. 2203-2211, 2013.

7. Thomas Hammarström, Tord Bengtsson, Jörgen Blennow, Stanislaw Gubanski "Partial Discharges in a stator under synthesized voltage waveforms", Proc. of the 18th International Symposium on High Voltage Engineering, Seoul, South Korea 2013.

8. Thomas Hammarström*, Tord Bengtsson, Jörgen Blennow and Stanislaw Gubanski "Partial Discharges in Motor Wires at PWM Voltages of Different Smoothness", Proc. of 7th International Symposium on Electrical Insulating Materials, Niigata City, Japan, pp.184-187, 2014.

1.3.1 Out of scope of this thesis

9. Becky Bergman, Ann-Marie Eriksson, Jörgen Blennow, Jens Groot and Thomas Hammarström "University students' first encounter with Electrical Engineering: Reflections on a Project-based Design of a Technical Communication course", Journal of Academic Writing, ISSN 2225-8973, pp.1-14, October 22 th 2012.

10. Anette Johansson, Thomas Hammarström, Markus Jarvid and Stanislaw Gubanski, “Analysis of multiple electrical trees incepted at wire electrode test object by means of PD detection”, Jicable HVDC’13 workshop, Perpignan, France, November 18-20th, 2013.

11. Anh T. Hoang, Thomas Hammarström, Tord Bengtsson, Yuriy V. Serdyuk, and Stanislaw M. Gubanski, “Partial Discharge Behavior of a Newly Developed Enamel Insulation at Various Voltage Rise Times”, Proc. of 7th International Symposium on Electrical Insulating Materials, Niigata City, Japan, pp.241-244, 2014.

12. Xiangdong Xu, Tord Bengtsson, Thomas Hammarström, Jörgen Blennow, and Stanislaw Gubanski, "Loss Current Studies of Partial Discharge Activity", accepted for publication in IEEE Transactions on Dielectrics and Electrical Insulation, 2014.

2. Background and Literature Review

PDs have been known to affect the insulation material in several ways due to exposure of ultra-violet radiation, heating and generation of ozone. Commonly all these factors have been known to potentially degrade insulation materials. Particularly damages in polymeric materials due to eroded chain structures have been found to be harmful and is a characteristic sign of degradation when appearing in a solid insulation. The likelihood of electrical trees increases due to the PD activity. It is important to note that these damages will not heal unlike PDs in liquids or gases.

Insulation systems for high voltage applications vary considerably depending on voltage level and applications which will influence where the PDs are most likely to occur. In some applications it is easy to gain access for measurement equipment close to the PD source to reduce influence of external noise but this is most often not the case. Thus measuring and localizing PDs has always been a challenging task, particularly in field applications. It is an advantage, when possible, to apply non-destructive approaches to identify weaker points in the insulation system by means of suitable measurement techniques to gain information about defects for preventing premature failure. To facilitate this diagnosis, various kinds of possible PD defects have been shown to generate typical signal patterns, which can be identified when applying different kinds of detectors [13, 14].

The work presented in this thesis is a continuation of earlier investigations regarding effects imposed by the exposure of electric insulation to voltage waveforms having frequency content higher than the traditional 50-60 Hz. The previous work [15] has provided an extensive overview of the achievements published in this field so far and this chapter aims to continue this task. It reports on recently published information regarding implications due to the PDs, mainly in dielectrically insulated cavities, as well as on the progress regarding development of measurements procedures.

This chapter presents previous attempts to analyze PD characteristics as well as adequate measurement techniques and different simulation approaches employed to illuminate the PD mechanism and properties within insulation systems.

2.1 PD source types

In this section a brief survey of the recent literature regarding exposure of insulating material to high frequency containing voltage waveforms is presented. The dominating belief is that the frequency of the applied voltage is the most important parameter contributing to a reduction of insulation life time, as for example revealed by measurements on twisted pair test objects [16]. However, for windings exposed to voltage shapes characterized by considerable voltage gradients, such as for example PWM voltage shapes, over-voltages appear due to wave reflections which distribute the electrical stress unevenly between the windings [17]. As a consequence, an increased degree of insulation degradation is often found. It is discussed in [18] that different shapes of the applied voltage to which an insulation system is exposed indeed affect it differently, even if the peak-to-peak value of the applied voltage remains the same. Recent results of investigations performed on a needle plane electrode system have shown that different PD characteristics depend not only on the type of insulation system (in this case solid or liquid) but also on the shape of the applied voltage [19]. This further emphasizes the importance of inventing suitable detection methods, allowing for identifying different source types and different PD characteristics. Dependent on the type of insulation system and the defect, the PDs appearing will differ considerably in number and magnitude as will be discussed in this thesis.

2.1.1 PD mechanisms

One important parameter when discussing the probability of PD appearance, apart from the electric field strength affecting the defect, is the number of free electrons available to start an avalanche. The time between when the conditions for a PD to occur are fulfilled until it actually occurs is usually named the statistical time lag and depends on the time needed for the first free electron to be available. In an insulation defect, such as a cavity, the number of free electrons emitted from the wall depends on the electric field according to the Richardson-Schottky law [20, 21]. Thus with increasing electric field strengths the amount of electrons emitted increases and the statistical time lag decreases. An additional time delay until a PD becomes fully developed is the formative time lag which is described in detail in [13].

Numerous approaches to categorize and model the partial discharge mechanisms have been presented in the literature and the most common mechanisms considered in cavities with dielectrically insulated walls are streamer, Townsend and pitting phenomena [12, 14]. The active mechanism in a particular case depends on the specific conditions in the defect. Townsend discharges are, according to [12], characterized by longer rise time and lower amplitude in particular when compared to streamer discharges. One important factor for the possibility of a Townsend

discharge to occur is the presence of a feedback mechanism in the defect to maintain the avalanche. For a dielectrically insulated cavity, such a feedback mechanism does not exist initially but may appear as the cavity surface degrades. The pressure and the size of the cavity are here important, as described by the Paschen cure [14, 22]. On the other hand, in a dielectrically insulated cavity, increase of either the pressure or the cavity size increases the likelihood for the appearance of a streamer discharge [14]. It is however still debated and not fully investigated which of these mechanisms can be most harmful to the insulation system. Another aspect here is that some insulation defects commonly described as cavities have shown the tendency of a change in PD mechanism as the degradation proceeds and this is further discussed in the next section.

2.1.2 PDs in dielectrically insulated cavities

Although investigations of PD properties in cavities, both in terms of measurements on real defects as well as on their models, are well described in literature, one of the important challenges for this thesis has been to design a suitable test object for such studies. A commonly used approach is to use three plates of insulating material pressed together with a hole in the middle one. An alternative way is to create a spherical defect in a solid material body, which is considerably more difficult to manufacture. Some reports claim that the spherical void has an advantage in that influences from the cavity edges are avoided and so the cavity PD pattern is not disturbed [23]. On the other hand, an attempt to avoid such influences in a three layer cavity object was made by employing cavities with dimensions considerably larger than those of the spherical electrodes connected to the endplates [24]. The roughness of the cavity surface is also another important factor. It was indicated in [25] that one significant factor determining the degradation process of a cavity surface in LDPE was related to hot-electron induced bond breaking processes, which eventually will create a breakdown within the material. The charges due to PDs accumulate on the cavity surface and affect the electric field distribution within the cavity and therefore also the subsequent discharges [23]. According to [12] significant changes in the PD mechanism could in particular be observed within LDPE cavities when exposed to a sinusoidal voltage of 50 Hz. The PD mechanism was believed to change between streamer, Townsend and pitting as the degradation proceeded and finally initiated electrical treeing. Also in [24] evidence was presented indicating changes in the PD characteristics, believed to be partly due to reduction in cavity wall surface resistance, being the consequence of changes in their chemical structure. To compare simulations and measurements, the model endplates were covered with copper [26] to ensure an even charge accumulation on the cavity surface. This can however influence several important factors for the discharge mechanism, such as the feedback mechanism.

It was suggested in [27] that the location of a cavity influenced the PD pattern, which was demonstrated by comparing cavities with both insulated and non-insulated electrodes as well as with different roughness of the electrodes. As the resistivity of the surface of the cavity obviously is an important factor influencing the PD mechanism, the frequency of applied voltage indeed has an effect on the PD appearance for sinusoidal voltage shapes, according to several simulations and measurement approaches. In the next section some of these observations are presented and discussed.

2.1.3 PD dependency of voltage shape

Measurements of PD patterns in a liquid insulation system are presented in [19], where the phase location of the PDs was found to be substantially dependent on the shape of the applied voltage. In this case sinusoidal and triangular voltage shapes were applied across a pin-plate PD source. In both cases, the PD occurrences followed the shape of the applied voltage. However, when the same measurement was repeated on a solid insulation object, the width of the statistical PD distribution increased significantly, indicating that the dependence on the voltage derivative was considerably more significant for the solid insulation object than for the liquid insulation one. This can be compared with the observations made in [15] where tests with oil/paper insulation type of objects revealed a considerable delay in the time before PDs started and where at a frequency of about 120 Hz, no PDs could be measured at all. This time delay before the PD appearance indicated that the derivative of the voltage signal was not as important as the main frequency of the pulse shape.

The use of HVDC technology with increased stress on oil/paper insulated cables and transformers may, according to [28], reduce the insulation life considerably. It was shown that both the PD inception voltage and the actual breakdown voltage were reduced due to changing voltage shape, though more measurement is needed to determine how the voltage shape parameters affect the oil/paper insulation system.

Further [29, 30] presents investigations where an EPR insulated high voltage cable was exposed to an electrical stress consisting of a sinusoidal voltage combined with superimposed steep voltage impulses. The results obtained indicated that PD measurement was an excellent tool to monitor the degradation process and that the utilized voltage shape caused an accelerated degradation process when compared to that of a pure sinusoidal excitation. This result further underlines the importance of studying PWM voltage shapes where higher frequency content increases the operating stress.

For motor winding test samples subjected to both unipolar and bipolar pulses, as demonstrated by [31], short rise times of the pulses reduced the inception voltage for

PDs while the behavior under pulses with longer rise times was more dependent on the main pulse frequency. As compared to the results of [15], this finding agrees well with the observation that the extinction voltage level becomes reduced for the shorter rise times.

Reference [32] demonstrated an approach were different levels of harmonics were added to the sinusoidal waveforms for a fixed RMS value. The PD pattern revealed a strong influence from the superimposed high frequency contribution; although whether this was connected to peak amplitude or voltage derivative remains to be investigated. Similarly tests were performed in [33] to simulate stress on the insulation system due to remains from the conversion between AC and DC in HVDC substations.

In [34] it was presented how enamel insulation modified by addition of Cr_2O_3 on the outer coat layer provided an up to 20- 30 longer time to failure. During the same investigation, when a 1 kHz square voltage waveform with 1 µs rise time was applied, it was noted that the new material still provided improved performance; however the difference was considerably lower, less than 10 times. Since PDs are considered such an important contribution to the degradation process within insulation systems, the reason behind this should be largely attributed to how the PD characteristics changes due to the waveform applied.

2.2 Measurement techniques

Several principles are employed to detect PDs, such as acoustic, chemical, electromagnetic wave propagation (UHF - Ultra High Frequency), electrical methods and detection of light emission. Each of them has its own advantages and disadvantages [14]. This work however focuses almost entirely on electrical PD detection. The conventional electrical methods [3, 4, 14] primarily utilize the vast difference between the frequency content of the applied voltage and the PD signal itself. Therefore it is difficult to use this approach together with voltage sources with steeply rising fronts, as the frequency contents of the stress is in the same frequency range as the PDs, both of which are much higher than that of the sinusoidal power frequency. An IEC task force (IEC 61934) has studied this issue for repetitive wave forms with rise times up to 50 µs [5]. To detect PDs according to the elaborated procedure the main principle is to employ filters of increased steepness to separate the applied voltage from the PD signals. However, several alternative approaches to overcome the problem have also been presented and these utilize various time domain based techniques that in a general sense take the stochastic nature of PDs into consideration for separating them from the applied voltage. A more detailed description of this approach is provided in section 2.3.

The principles discussed below cover both the traditional methods as well as some novel ideas within this area.

2.2.1 Sinusoidal waveforms

For sinusoidal voltage shapes a considerable amount of material has been presented, but the standard IEC 60270 [4] only covers electrical measurements from DC up to 400 Hz. This standard also discusses the different bandwidth options that should be applied. In general terms the measurements are performed at a bandwidth below 1 MHz, usually by means of narrow or wide band instruments. A decoupling capacitor is placed in parallel with the measurement object and an impedance, often named quadrupole, enables PD measurements. The impedance is either connected in series with the decoupling capacitor or with the measurement object. Any PD occurring creates a voltage drop across the cavity resulting in a current pulse that can be measured across the measurement impedance, the PD decoupler. Further, the apparent charge can be obtained by integration, i.e. low-pass filtering, of the current pulse.

One approach with the aim to act both as an alternative and a complement to the traditional 50/60 Hz IEC 60270 sinusoidal PD measurements, were suggested by [35]. The method combines the classical approach with dielectric response measurements to evaluate the frequency dependence of the appearing electrical stress on for example a stator bar test objects. By applying both low and higher frequencies the diagnostic of an insulation system could be facilitated. Observations by [35, 36] suggests that various low frequency wave shapes could be applied to the test object during offline testing, in turn suggesting that relevant information about the physical characteristics such as charge decay could be elucidated.

2.2.2 Short voltage rise time

Measurement of PDs at steep voltage shapes has according to [3] been performed using a resistor in series with a coupling detector together with suitable band pass filter techniques. However, the problem with the overlapping frequency content between the PDs and the applied voltage makes this approach considerably more difficult.

One recently presented method uses differential probes to remove the contribution from other sources than the PDs. This is basically a similar method as the balancing methods presented in [14]. In [37] a limited amount of data was available for the analysis, 10 cycles were collected each time, obviously increasing the difficulty to monitor changes in the PD characteristics. In principle no obstacles exist for expanding this principle to cover a larger amount of data for statistical analyses. However the probes need to be very accurately balanced, since even small deviations

will have a considerable impact on the result. An additional observation is that use of higher voltages imposes additional difficulties, as the voltage range of the probes is limited and use of voltage dividers further increases the difficulties in balancing. Therefore, the method is at present only applicable at lower voltage levels.

In [38] a UHF antenna and an ultra-wide band transformer were used to detect PDs at different rise times of applied voltages. The rise times studied in this case ranged from 0.1 to 140 μs semi-square voltage, except for the shortest rise time which was surge shaped. Based on these measurements it was concluded that the inception voltage was reduced for steeper voltages. However, the design of the PD measurement system is not clearly described in [38]. It is claimed that it is based on a time pattern approach and the system most probably captures a series of measurements to calculate the average value corresponding to the applied voltage shape and uses this to resolve the PD pattern. This approach to utilize the random occurrence of the PDs is thus similar to the system introduced in [15]. It has also to be pointed out that if a UHF antenna is used to capture the PDs, calibration of the PD amplitude in terms of apparent charge is almost impossible. In some special cases where the PDs can be measured both with a capacitive decoupler and an UHF antenna simultaneously, an estimation of the relation between the detectors can be obtained according to [39]. However such estimates depend heavily on the position of the PD source and the antenna. If the location of the PD source remains the same then the sensitivity will mainly be affected by the accuracy in the positioning of the antenna and a reasonable relation between the two sensors can be obtained. However if the PDs occur in different locations such as in a transformer winding, then the relation between the outputs of the sensors will differ considerably.

The UHF method is can be successfully applied to determine the presence of changes in PD characteristics, particularly in transformer applications [40]. The bandwidth when applying the UHF method is normally within the interval of 0.3 to 3 GHz, however results have been presented where up to 13 GHz has been utilized [41]. Although this system is not electrically connected to the insulation the same way as the capacitive connection, this sensor can be disturbed by noise from surrounding equipment such as inverters and motors which may cause severe problems. One approach to reduce interference was presented by [42] who proposed a twin antenna sensor to suppress disturbances from PWM converters together with a steep high pass filter with a cut-off filter of 5 MHz. This approach was utilized for low voltage measurements ($\leq$1 kV) on a twisted pair test object exposed to square voltage waves with about 500 V/μs steep voltage fronts. The use of twisted pair test objects has become more important due to the increasing use of electric motors controlled by inverters.

An electromagnetic non-decoupled sensor suitable for positioning close to motor voltage supply for offline surge testing was suggested in [43] and enables PD measurements at lower frequencies compared to the UHF method; 20 MHz up to 100 MHz were illustrated. However not having the possibility to connect to the test object electrically implies an uncertainty when it comes to calibrations, since it needs to be related to other sensors with different bandwidths.

Another method suggested in [44] has demonstrated the possibilities to evaluate the PD exposure on both twisted pair test objects as well as within dielectrically insulated cavities. It is based on principles similar to dielectric response measurement where the changes in the complex capacitance of the insulation system can be used to determine the change inflicted by PDs appearing. Steep voltage waveforms can be applied since this approach uses the harmonic content of the applied waveform to obtain the PD current. This method estimates the total charge well as well as providing information about slowly decaying charges, but does not provide information about the magnitude of the individual PDs within the defect. Thus the results need to be complemented with other approaches as well.

In [45] ways of measuring temperature by means of UV camera to determine the presence and influence of PDs are presented. In common with the previously discussed method its application has the drawback that only average influences can be monitored. One significant property of PDs is the statistical occurrence, which is the principle of the detection method discussed in the next section.

2.3 Stochastic PD measurements

In [15] a measurement system was presented that makes use of the stochastic nature of PDs to limit the influence from the applied voltage. This is an advantage since the applied voltage has significantly higher amplitude compared to the amplitudes of the PDs and there will be remnants of the applied voltage if not extremely steep high-pass filters are employed.

The initially employed measurement system is illustrated in Figure 2.1. It comprises a capacitive decoupler, which is connected in parallel to the measurement object, and a high voltage source is used to generate unipolar or bipolar voltage pulses. An electrical filter consisting of a coaxial cable, and a resistor R_m is connected to a 14 bit NI-DAQ digitizer with a sampling rate of 100 MS/s employing a 10x probe. The coaxial cable acts as a resonance cavity for the PD signal at higher frequencies. The high-resolution digitizer is a central part in this circuit as the voltage remnant is usually substantially larger than the PD signals due to the use of low-order filtering.

To facilitate PD detection with a remnant of the applied voltage present in the measured signal, a moving average of the voltage remnant measured across R_m is calculated. Since each PD occurrence is random, the remnant can be eliminated by subtracting the moving average from the measured signal, leaving only the contribution from the PDs as shown in Figure 2.2. This limits the demand for steep filters, although some filtering is still needed. The most important property of the filter is to adjust the signal to noise ratio properly to facilitate the detection in cases where the voltage remnant is considerably larger than the remaining PD information. This system has successfully been applied to detect PDs using sources such as corona needle and twisted pair. However, for steeper voltages and for cavities with insulated electrodes, the resolution should further be increased to facilitate measurements closer to polarity changes. A further drawback of this set-up is that the time resolution is limited to 100 MS/s, which is too small to resolve PD rise times in the range of 1 - 10 ns which is considered a typical case for streamer discharges [13].

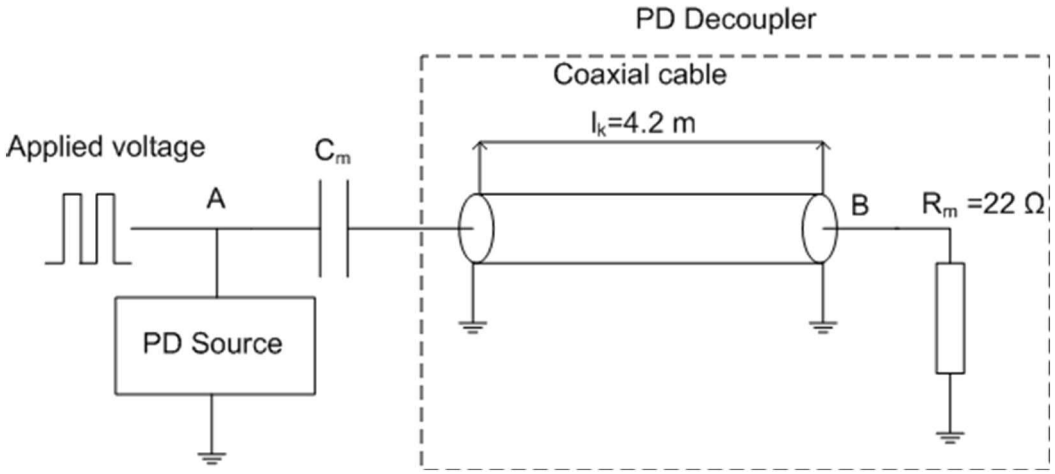

Figure 2.1 PD measurement setup used in [15].

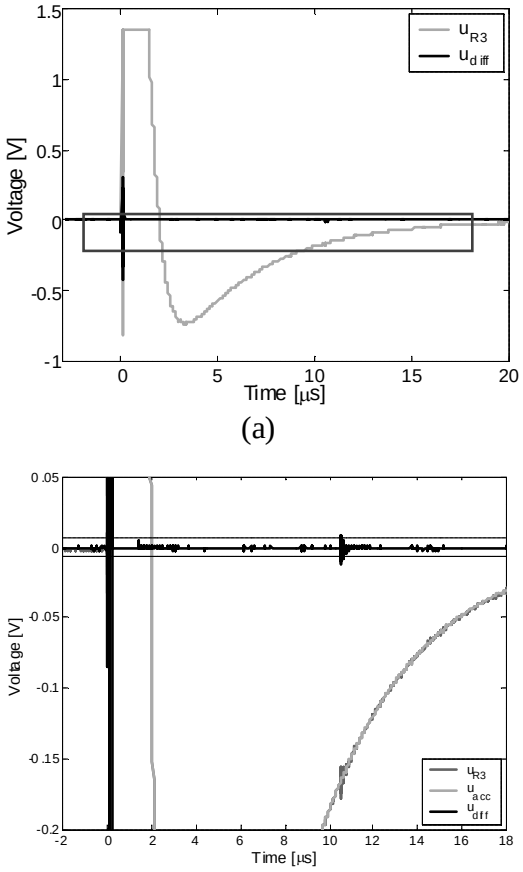

Figure 2.2 Principles of the stochastic PD detection (from [15]). Figure a) shows the original recorded signal and the difference to the moving average. The boxed area in figure a) is enlarged in figure b) where the moving average is included.

In Figure 2.2 an example of the measured signal across R_m, u_{meas}, is illustrated. The accumulated signal is evaluated for each new measurement according to Equation 2.1:

$$u_{acc}(t,k) = \frac{u_{meas}(t,k) + n \cdot u_{acc}(t,k-1)}{n+1} \tag{2.1}$$

The accumulated signal is thus a moving average of length n. PDs are detected in the difference signal u_{diff}:

$$u_{diff}(t,k) = u_{meas}(t,k) - u_{acc}(t,k-1) \tag{2.2}$$

These calculations are repeated online in the measurement system to allow efficient monitoring of PDs.

2.4 Simulation approaches

For improving the performance of insulation systems and for increasing the understanding of physical processes involved in PD activity, it is desirable to be able to simulate the phenomenon as a complement to measurements. This section presents some of the techniques employed in the past. Due to the complexity of the PD development process different simulation models have been proposed, dependent on the scope of different investigations. The main limiting factors in this development have been the availability of efficient computational tools as well as reliable measurement data sets for verifications. Anyhow, simulation techniques of several levels of advancements have been suggested and a short review is presented below.

The first attempts to simulate and schematically describe the PD behaviour resulted in the so called "ABC-model", where the defect as well as surrounding dielectric material were presented as lumped capacitors [13, 46]. This approach implies that an equipotential field distribution is assumed within both components. The PD occurrence and the leakage associated with it are included by introducing a resistor across the discharging capacitor. As this model can easily be implemented in a circuit simulator, it has been applied and discussed in many papers. One drawback with this approach is the built-in difficulty to include the influence of space charges, which in particular affects the estimation of the electric field level within the insulation system. Modifications of the ABC model have been introduced in [47, 48], which extend the possibility to approximate the influence of space charges. The circuit-based ABC model is equivalent to a model based on electric field calculations based on Gauss's law and the equation of continuity [49].

In [20] a fundamentally updated ABC model was proposed, in which a physical description of the discharge event was utilized, including pressure and temperature as parameters responsible for the statistical distribution of discharge events during different stages of degradation in insulation defects. The key element was to include the rate of electron emission (per time unit) from the surface of the cavity wall. Further Paschen's curve was utilized to determine suitable conditions for PDs initiation, with an adaptation of pressure for adjusting the PD pattern. An even distribution of surface charges was however assumed after each PD. A similar approach was introduced in [50], suggesting that the reason behind different PD patterns during aging could relate more to changes in the gas constitution and the work function than to the variation of pressure. A further advancement of the PD modelling introduced estimation of a cylindrical discharge channel within a cavity defect by means of a finite element (FEM) software [21, 51, 52]. The specific radius and conductivity of the channel were assumed based on the estimated number of

available free electrons in the defect. Here, the advantage is that the defect can be separated into sections to facilitate the appearance of several PDs occurring almost simultaneously. When applying the above mentioned models [20, 21, 50-52], the common feature is that PD occurrence is determined by a probability function dependent on various parameters. Simple methods are used to calculate the electrical field distribution and the effects of space charges.

A kinetic PD pulse model, which essentially is based on a hybrid approach between FEM analysis of the discharge process and traditional circuit analysis, was proposed by [53]. It centres on a kinetic Monte-Carlo simulation and is able to predict some PD properties in sub-mm cavities with both dielectrically insulated walls and with conducting electrodes. The limited cavity size implicates, according to [53] that the PD event does not develop as a streamer but as a Townsend discharge.

A model of electrical discharge in air based on consideration of charge transport phenomena has been proposed in [54, 55], in which multiple interactions between electronic and ionic charges as well as photon ionization mechanism are considered. This model is implemented by applying rotational 2D geometry and provides qualitative agreement with measurements on single discharges presented in [49]. The drawback with this type of modelling is the need for providing a large number of various physical parameters to adapt the simulation results to the measurements and a considerable simulation time.

As already mentioned, the common problem with the various simulation approaches is the long time needed for the calculations. In some cases a few days of calculation time is required for a single discharge. Naturally, this will limit the possibility to reproduce a complex PD pattern. To avoid this difficulty and to understand the statistical behaviour of PDs occurring in dielectrically insulated cavities, the ABC approach is utilized in this work, as this approach requires the least computational effort.

3. Stochastic PD Detection

The stochastic PD detection method introduced in this chapter exploits the random nature of PDs to facilitate their detection at steep rise times. Modifications to the algorithm as well as a new type of PD decoupler is introduced to extend the abilities of this approach as the previous has shown some limitations at rise times shorter than 2.5 µs. Further, possible calibration procedures and sensitivity estimations are presented.

3.1 Stochastic PD algorithm

This chapter describes details and improvements of the method introduced in section 2.3. The overall structure of the adopted analysis and technical details regarding the calculation of moving average are presented, the choice of trigger level and the requirements on voltage stability are discussed.

The analyses are performed on signals that contain contributions from the applied voltage, here denoted the “remnant”, as well as from the PDs and other interferences. Mainly, the task is thus to separate the PD signals from contributions from the other two sources. The remnant is eliminated by use of the moving average, whereas the elimination of other interferences may be more difficult. If these interferences come from the voltage supply, however, they are phase-locked to the waveform and can thus be identified.

The procedural elements of the used algorithm are presented in the flow chart in Figure 3.1. In practice, the processing may either be performed online or on recorded data. The sequential steps of the numbered flowchart are:

1. and 2. The start of the procedure begins with recording of the data traces. Before their processing, time adjustment is made to certify that voltage changes occur at the same time in all analyzed traces. This is necessary for an efficient use of the moving average and is further discussed and exemplified in [56].

3. and 4. The calculation of the moving average is made. Each new trace is used to update the moving average value, see section 3.1.1.

5. Based on the noise level and the number of iterations performed, n, the trigger level is determined and the position and peak-to-peak value of the PDs in each trace are identified, see section 3.1.3.

6. Some interference that may originate from the voltage supply system is not properly suppressed by the moving average calculations, partly due to inadequate sampling frequency. This problem, if it appears, is eliminated by ignoring pulses in a narrow time interval around phase-locked interference [56].

7. For each measurement, a finite but not necessarily limited number of traces should be recorded.

When using the stochastic approach in case of non-phase stable waveforms, such as PWM waveforms, additional processing steps are however required, see chapter 5.

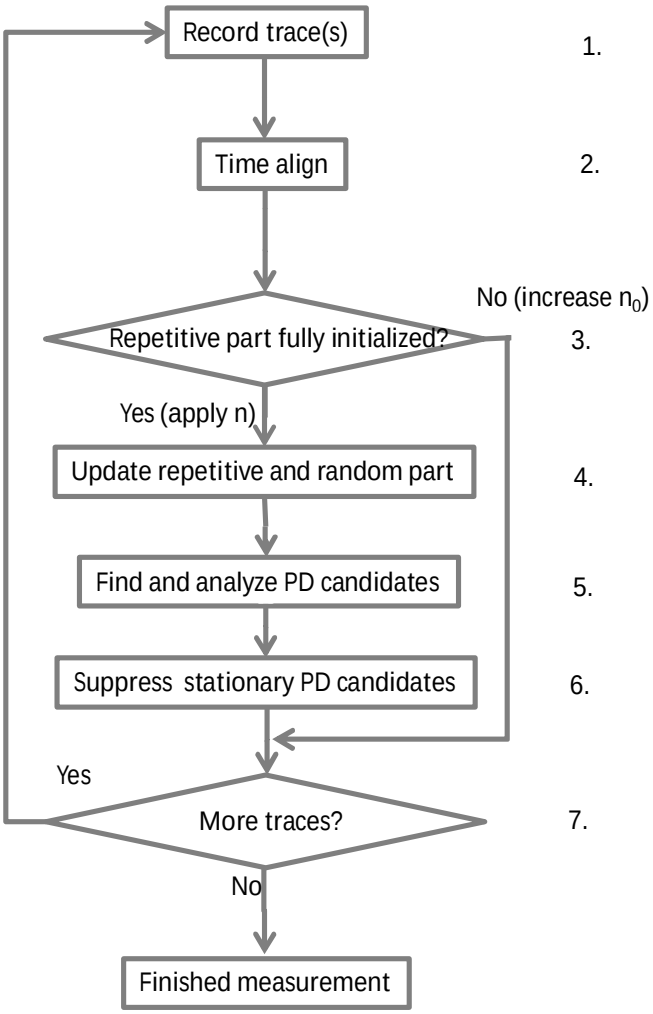

Figure 3.1 Flow chart of the stochastic PD detection algorithm.

Different strategies can be used to make the PD data collection and analysis efficient. If each captured trace utilizes a high sample rate or contains many PD events, the data processing time increases if performed online. In such cases more data could be collected during a given time by only capturing the traces and then performing the analysis offline after the measurements are completed.

If the data analysis is performed online, a recommended approach is to start the data collection below the inception voltage for initiating and stabilizing the moving average calculation. This approach prevents the influence of large PDs, which may corrupt the results if their initial contributions are not suppressed properly in the subsequent traces. Afterwards the voltage can gradually be increased until PDs appear, see section 3.3.5 for a discussion on allowable voltage changes. The data collection can then be started with a minimal influence of the moving average for separating the repeating and the random events in the recorded traces where the PD signals are detectable in the random parts.

On the other hand, when performing data analysis offline, one possible approach is to first use some of the collected data for stabilizing the moving average and then repeating the procedure on all the collected data as described above.

The initial method introduced in [9] to calculate the moving average has some drawbacks, particularly at the beginning of the measurement. PDs appearing in the initial traces may result in a false detection in the subsequent acquisitions and long initialization periods are therefore required. A modified approach is thus introduced, as defined in Equation 3.1, which reduces the time necessary for obtaining a stable moving average.

$$u_{acc}(t,n) = \frac{u_{meas}(t,n) + \min(n, n_0) \cdot u_{acc}(t, n-1)}{\min(n, n_0) + 1} \tag{3.1}$$

For each new trace, n increases until a maximum value n_0 is reached. As long as $n<n_0$, n is used in the calculation. To exemplify this, assume that a PD appears within a trace at iteration $n<n_0$ before the moving average is stabilized. The contribution in the calculated moving average of this PD will be suppressed by a factor $n+1$at the next iteration:

$$u_{PDrem}(t,n) = \frac{u_{meas}(t,n)}{n+1} \tag{3.2}$$

When calculating the moving average at the next iteration (n+1), the contribution related to the previous PD will further be reduced:

$$u_{PDrem}(t,n+1) = \frac{(n+1) \cdot u_{meas}(t,n)}{(n+1)(n+2)} \tag{3.3}$$

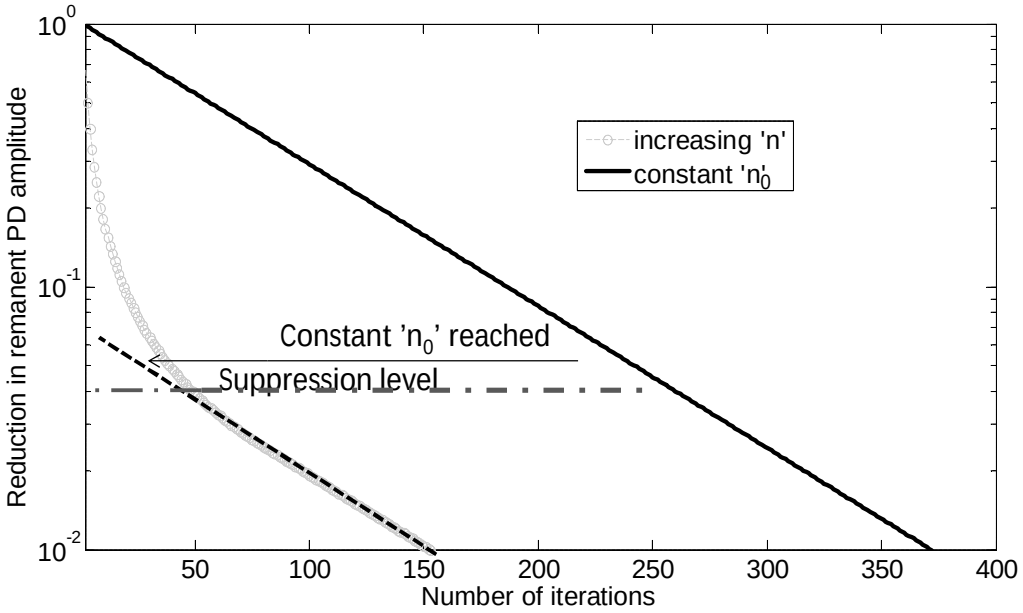

Figure 3.2 The decay of remnant of PDs occurring in the first trace for n_0=80. After 150 iterations, the PDs in the initial trace are supressed by a factor 10^{-2} as compared with 0.2 for the constant n_0 approach.

The total suppression when the trace number eventually reaches $n=n_0$ will be $\frac{1}{(n_0+1)}$ independently of n as long as $n<n_0$. The limited initiation time required facilitates a consistent initiation of the moving average. This is illustrated in Figure 3.2 for a case where a PD occurs at the first captured trace and n_0 is set to 80. The number of iterations required until the maximal trigger level $\frac{1}{n_0} = \frac{1}{80}$ is reached is also indicated in the figure. As a comparison Figure 3.2 also includes the moving average calculation when applying $n=n_0$ from the first trace onwards, as presented in chapter 2.3, which increases the required number of iterations about five times.

3.2 Design of resonant PD decoupler

To enable a detailed study of PD signals with various rise times and amplitudes, it is important to use a detection method with high enough bandwidth. Little signal attenuation is thus required in the frequency band of the PDs (above about 1 MHz) while the attenuation should be considerably higher at lower frequencies.

This section describes how an electrical measurement system can be designed to facilitate the desired properties. Both theoretical considerations and practical experiments aid in selecting suitable circuit alternatives. As the considered voltage rise times are in the µs range, this calls for very steep filters. With the use of the stochastic

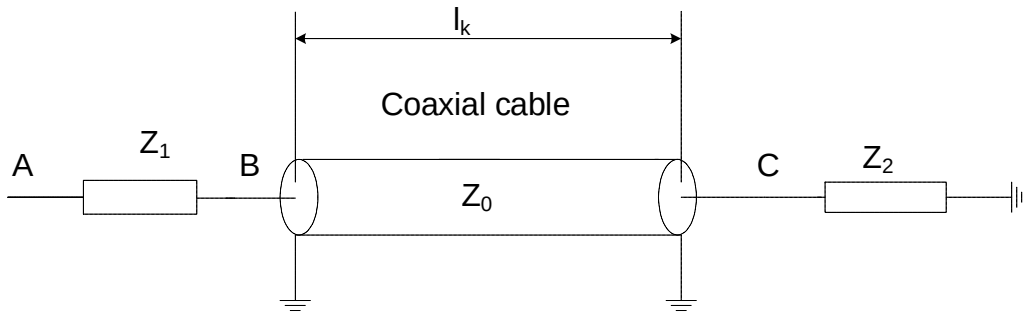

Figure 3.3 A coaxial cable with length l_k and characteristic impedance Z_0 with connected end impedances Z_1 and Z_2.

time domain technique, the filters do not need however to completely suppress the applied voltage; some remains of similar or larger magnitude as the PD signals are acceptable or even desirable, depending on the resolution of the measurement system, i.e. the digitizer. The filters in the PD decoupler should therefore be optimized for voltage slew rate and PD magnitude, allowing easy adaptability of the filter to different properties of the test voltage and PD magnitudes.

3.2.1 Enhancing resonances

A resonant PD decoupler, comprising of a coaxial cable together with end impedance terminations, was introduced in the previous work [15] to provide resonance amplification of the measured signals at higher frequencies. It is important to demonstrate how the terminating impedances of the cable should be selected to introduce as high resonance peaks as possible.

The transfer function between points 'A' and 'C', as shown in Figure 3.4, is expressed by Equation 3.4, assuming the travelling wave speed within the cable is v and the angular frequency ω:

$$H(j\omega) = \frac{Z_2 Z_0}{(Z_1 + Z_2) Z_0 \cos(l_k \cdot \omega / v) + j \cdot (Z_1 Z_2 + Z_0^{\,2}) \sin(l_k \cdot \omega / v)} \tag{3.4}$$

To simplify this expression, we introduce the following symbols: $Z_2 = Z_0 z_2$, $Z_1 = Z_0 z_1$ and $x = l_k \cdot \omega / v$.

We thus normalize each terminating load Z_1 and Z_2 with the characteristic impedance Z_0. Introducing identical loads ($z_1 = z_2 = z$) in each end of the cable yields the following expression, only dependent on two variables, x and z:

$$H(jx) = \frac{z}{2 \cdot z \cdot \cos(x) + j \cdot 2 \cdot (1 + z^2) \cdot \sin(x)} \tag{3.5}$$

A further simplification is to express:

$a = \left(1+z^2\right)/z$ and $H(j\omega) = 2 \cdot H^{'}(j\omega)$ which together with Equation 3.5 results in the following expression:

$$H^{'}(jx) = \frac{1}{\cos(x) + j \cdot a \cdot \sin(x)} \tag{3.6}$$

Equation 3.6 indicates that infinite resonance amplitudes can be reached if the denominator in the equation become equal to zero, i.e. the constant a is chosen as an imaginary number. Infinite resonance amplitudes are not possible in practice, but this is a condition for obtaining very strong resonances and implies that capacitive terminations would be advantageous. Additional studies of the resonance properties have shown that the resonances are maintained even for different capacitive terminations on the condition that they substantially differ from the cable impedance.

The possibility to utilize the resonant amplification of the coaxial cable is a vital part of the new PD decoupler and the terminations Z_1 and Z_2 should be maintained as capacitive as possible. Inductors are not as attractive as capacitors for this purpose because of the appearance of low-frequency resonance at $x>0$ for large $|a|$, if $j\,a\,>0$.

3.2.2 Realization of a resonant PD decoupler

The transfer function of a transmission line, capacitively terminated at both ends, generates several resonance frequencies with high amplification. An efficient attenuation of the applied voltage also requires use of a proper high pass filter, which must be accomplished without significantly affecting the terminating impedance Z_1 as this would reduce the resonance peaks and thus the PD amplification. Another important factor is to limit the use of components with values comparable to those of parasitic elements in the appropriate frequency range. Including a capacitor connected to ground at point 'B' in Figure 3.4 ensures sufficiently large imaginary impedance to maintain the resonance peaks and also to decrease the influence of the parasitic capacitances. A 5 pF capacitor provides an impedance of about 3 kΩ at 10 MHz, which is relatively low impedance in the part of the spectra where the resonance peaks occur. The other termination point 'C' should preferably be connected to an oscilloscope, with an impedance of a 1 MΩ resistor in parallel with a 20 pF capacitor. At PD frequencies, the load will then be almost totally dominated by the capacitive part of the oscilloscope input impedance. These and similar considerations have led to the circuit solution presented in Figure 3.4 and certain details of this solution deserve further discussion.

To increase the suppression of the applied voltage by decreasing the time constant of the high pass filter, it is possible to use either a low value of R_m or C_m. HV capacitors are expensive and not easily adjustable. R_m cannot be made arbitrarily small as a realistic parasitic inductance of 1 µH may appear in series with R_m, and may add more

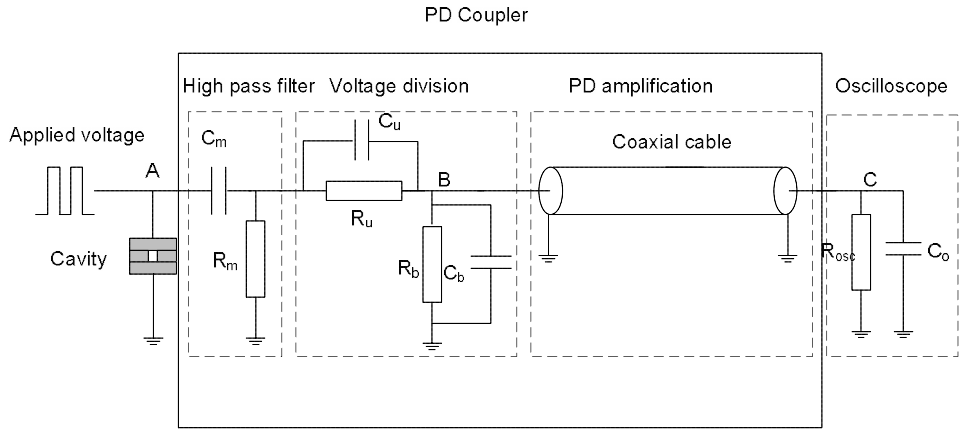

Figure 3.4 Modified PD decoupler with point 'C' connected to an oscilloscope, the cavity indicates measured object.

than 1 Ω already at 160 kHz. Thus, parasitic inductances will affect the characteristics of the decoupler for small values of the resistor R_m. To avoid the necessity of using a too small value of R_m while still reducing the voltage remnant, a frequency dependent voltage division, connected as shown in Figure 3.4, is suggested. At low frequencies this is dominated by the resistive chain and at high frequencies by the capacitive one. Thus we can have different divider ratios at high and low frequencies and the cable termination is dominantly capacitive in the resonant region. The high pass filter reduces the input voltage for frequencies corresponding to the frequency content of the applied voltage, whereas PD signals on the other hand are not strongly attenuated by the presence of this frequency depended voltage division. The capacitors C_u and C_b also reduce the influence of stray capacitances and for this purpose they should preferably be larger than about 5 pF.

The modified measurement circuit can thus be considered to consist of three different parts, the high pass filter, the voltage divider and the amplification part realized by resonances in the coaxial cable. The analytical expression of the transfer function of the whole circuit is quite complex and therefore not presented here. Instead the most significant influences of changes in the component values are indicated in Table 3.1.

Table 3.1 Influence of increasing component values on amplitude of the transfer function of the modified measurement circuit; the signs + or – indicated a relative amplitude variation.

Frequency interval	R_b	R_u	C_b	C_u	R_m
Low f (< 5 MHz)	++	--	-	++	++
High f (> 5 MHz)	0	0	+	+	+

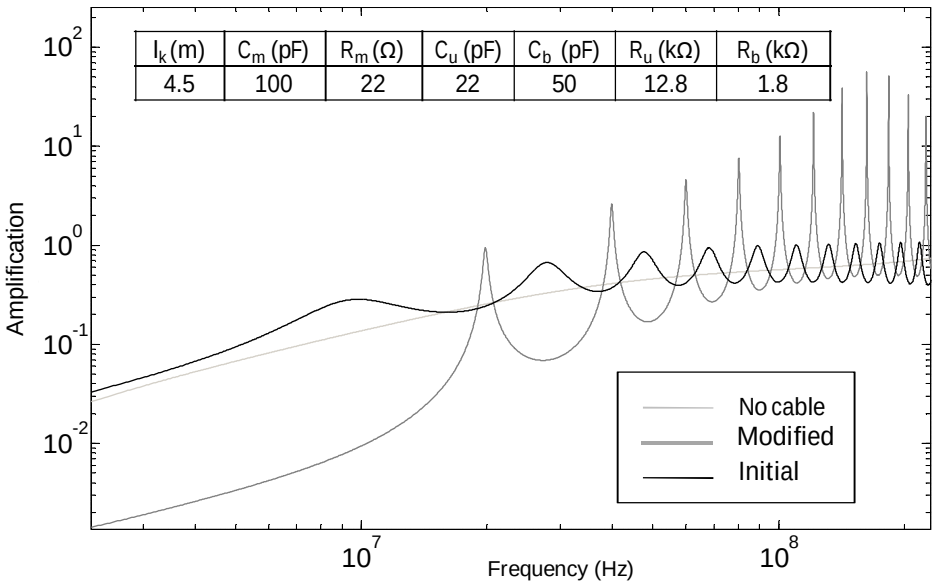

Figure 3.5 Comparison of transfer functions of the modified and initial (Figure 2.1) PD decouplers. The circuit parameters are included in the table and the transfer function of the modified circuit without a coaxial cable is provided as a reference.

The table shows that a suitable way to decrease the voltage remnant would be to increase R_u, or alternatively to decrease the shunt resistors R_m or R_b. An increase of the amplification at higher frequencies can be accomplished by increasing C_u, see chapter 3.3.3 for details regarding optimization of the transfer function. However, the important factor is the relation between the amplification at low and at higher frequencies rather than the absolute amplification level. Figure 3.5 shows the transfer function of the modified circuit in comparison to the one of the initial circuit containing only the high pass filter C_m, R_m and the coaxial cable (Figure 2.1). It is obvious that the suppression of the voltage remnant now is significantly more efficient up to 10 MHz and that the resonance peaks are higher.

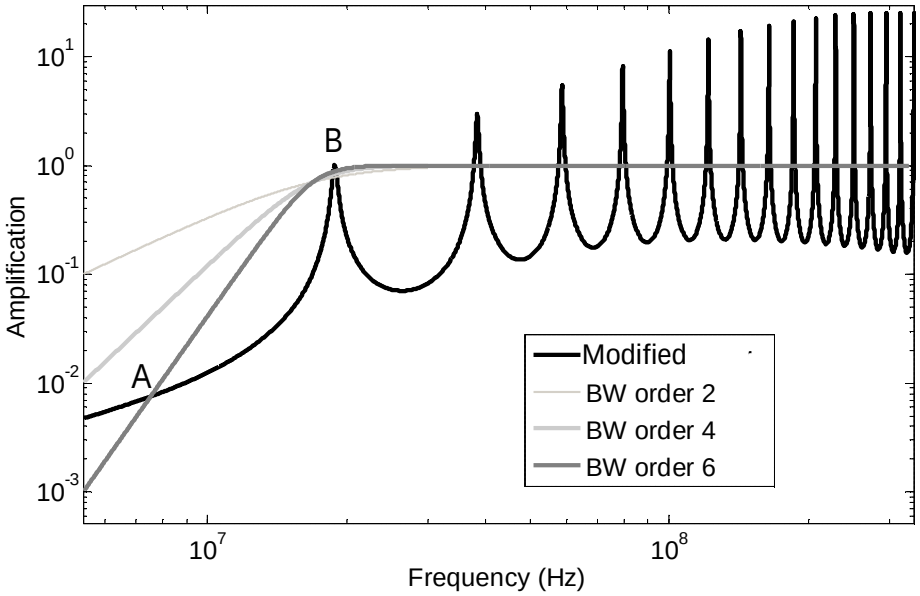

Figure 3.6 Transfer function of modified decoupler compared to Butterworth filter characteristics (orders of 2,4 and 6 indicated). A very high Butterworth filter order is required to resemble the steepness of the modified decoupler.

At higher frequencies the amplification is improved and capacitive terminations of the coaxial cable ensure high resonance peaks.

In Figure 3.6 the obtained transfer function is compared to a Butterworth filter function [57]; given by Equation 3.8 and dependent on the filter order n:

$$\left|T(j\omega)\right| = \frac{1}{\sqrt{1+\varepsilon^2\left(\frac{\omega_p}{\omega}\right)^{2n}}} \tag{3.7}$$

Where ε is related to the ripple in the pass band, Amax, according to the equation

$$\varepsilon = \sqrt{10^{Amax/10}-1} \tag{3.8}$$

The parameters used for the comparison presented in Figure 3.7 are shown in Table 3.2.

Table 3.2 Filter parameters.

ε	Amax	ω_p
1	$10\cdot\log(2)$	$2\pi\cdot 17.5E6$

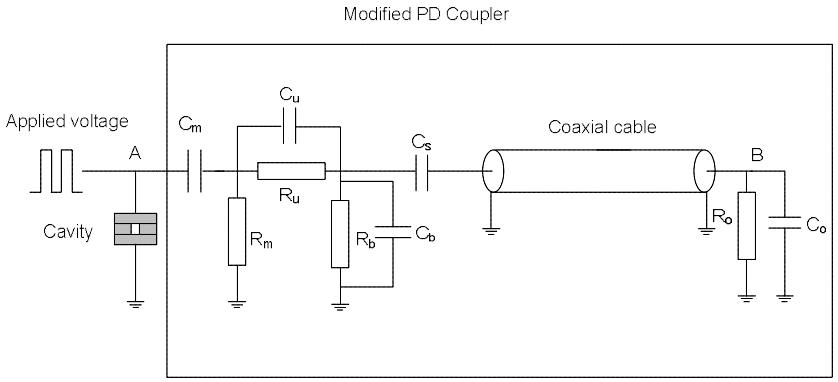

Figure 3.7 Alternative modified decoupler; the termination of the cable is enhanced by a series capacitor C_s.

As can be observed in Figure 3.6, the steepness of the transfer function of the modified decoupler is comparable to the steepness of a Butterworth filter of 6 th or higher order at frequencies between 7 and 20 MHz, marked as 'A' and 'B' in the figure.

By additionally applying a capacitor C_s in series with the coaxial cable, as illustrated in Figure 3.7, the voltage remnant at lower frequencies can be suppressed even further without significantly affecting the high frequency part of the spectrum, as illustrated in Figure 3.8. This alternative decoupler can be very useful particularly for voltages with shorter rise times than the ones applied in this work, thanks to additional further suppression of the voltage remnant at the lower part of the spectrum.

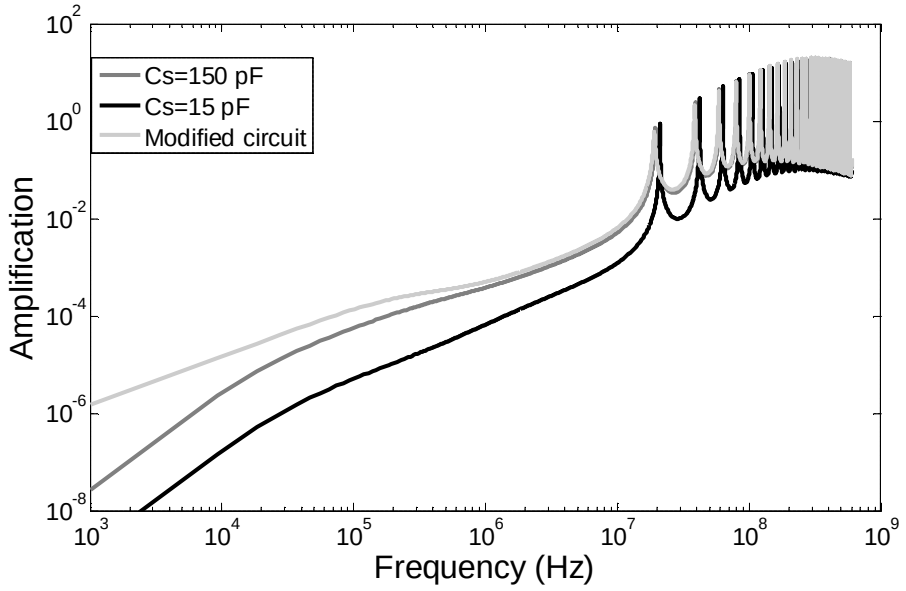

Figure 3.8 Transfer function of circuit alternative with a capacitor C_s in series with the cable.

3.3 Measurement and verification

To verify the solutions presented above, the transfer function is measured on a real circuit and the results are compared with the theoretical considerations. The final indicator of success is the result of a comparison of PD signals obtained with the initial decoupler and the new one.

3.3.1 Transfer functions

The transfer function for a realization of the modified decoupler with component values indicated in Figure 3.5 was measured up to 400 MHz. To capture the actual transfer function for this system up to as high frequency as possible, some special measures had to be taken. An HP arbitrary wave generator was applied, which could provide sinusoidal voltages up to 20 MHz, and the complex voltage amplitude was measured both at the input and the output of the decoupler. To enable analyses at higher frequencies, a square voltage shape was used instead. By utilizing high harmonic frequencies of this signal, the transfer function measurement could be extended as shown in Figure 3.9. This figure demonstrates that the frequency positions of the resonance peaks relatively well agree (up to at least 250 MHz) with the expected spectrum.

When comparing the measured and the theoretical transfer functions, especially above 100 MHz, it appears that the resonance peaks are additionally affected by factors not included in the theoretical analyses. It could be caused by, for example,

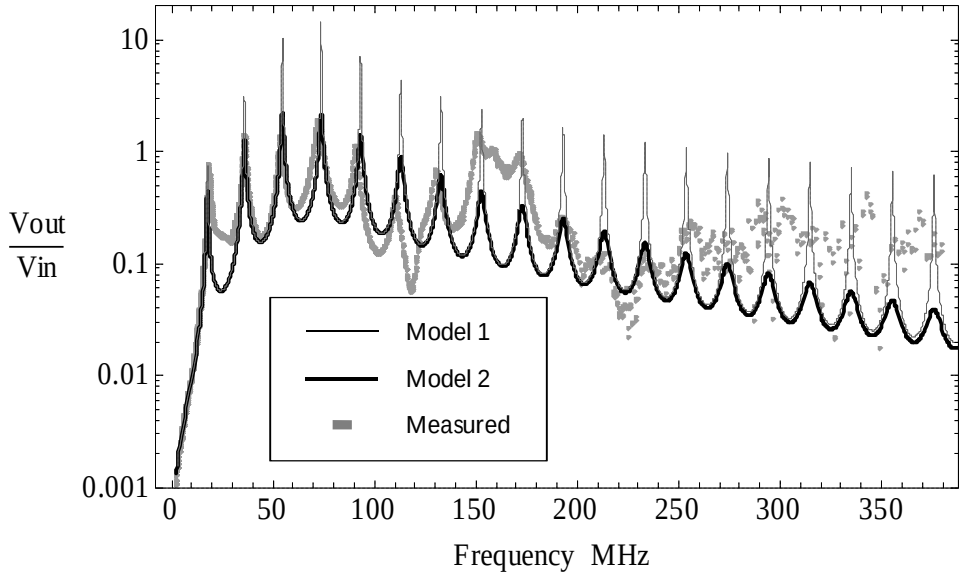

Figure 3.9 Comparison between theoretical and measured transfer functions of the modified decoupler. Model 1 represents a non-resistive coaxial cable whereas Model 2 includes a frequency dependent cable conductor resistance R_c.

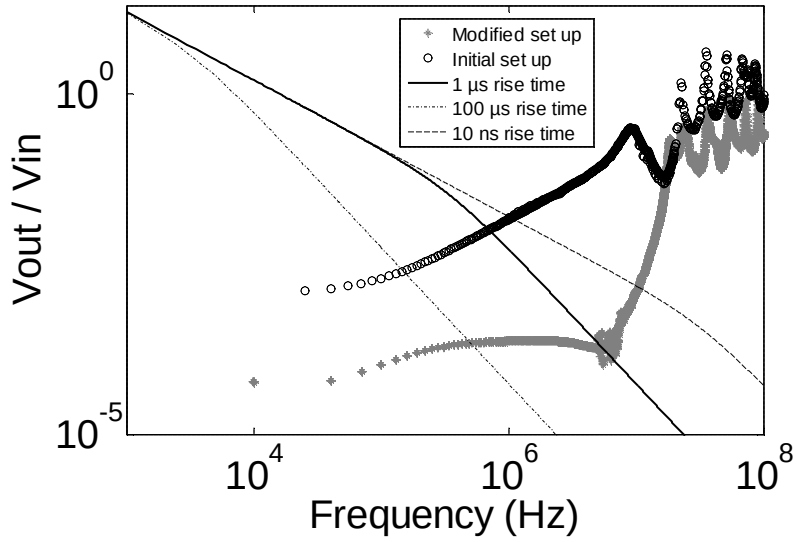

Figure 3.10 Transfer functions of the modified and initial circuits. Note the increased attenuation for applied voltages by the modified circuit. For comparison, the frequency content of voltage waveforms with different rise times are included as well as of typical PD signals (10 ns).

skin effects in the coaxial cable and by other parasitic components present in the physical implementation of the circuit. To explore a possible improvement of the model, Figure 3.9 additionally show the result of a model taking into account frequency dependent loss in the cable conductor [58]. This is realized by introducing a series resistance per unit length in the coaxial cable, $R_c = R_c(1+\gamma \cdot \omega)$, where $R_c = 0.1\ \Omega/m$ and $\gamma = 4 \cdot 10^{-9} s/rad$. The result obtained indicates that the reduction in resonance amplitude may at least partly be due to this effect.

When the measured transfer function is compared in Figure 3.10 with the one used earlier, obtained by the solution presented in Figure 2.1 (here marked: 'initial'), it becomes apparent that the signal is significantly attenuated in the modified decoupler at frequencies below 10 MHz. Another benefit is that the increased attenuation of the remnants of the applied voltage makes it possible to detect PD pulses closer to the polarity reversal, which enables the analysis of even steeper voltage shapes than the ones discussed here.

3.3.2 PD response

The new PD coupler was tested by measuring PDs in a dielectrically insulated cavity of the same type as the one used in [11]. It was composed of three polycarbonate plates pressed together, where a hole of 2 mm diameter was made in the central plate. The thickness of the polycarbonate plates was 0.75 mm and the rise time of the applied voltage was 2.5 µs. One important purpose of this test was to demonstrate

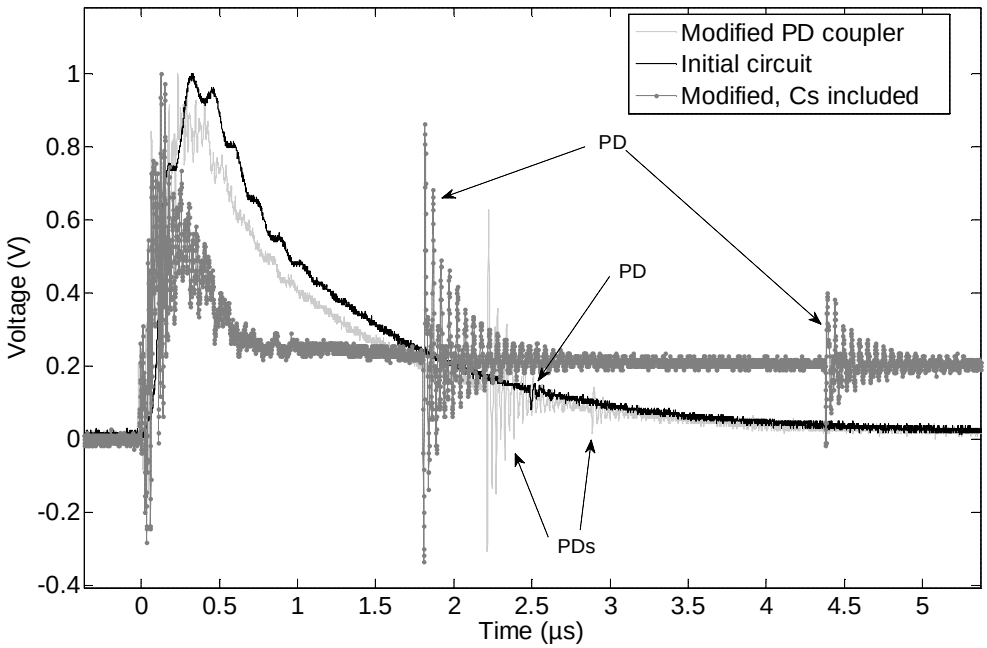

Figure 3.11 Signals scaled to similar remnant level as measured at voltage reversal by initial and modified decoupler alternatives. Both of them contain at least one PD event, as indicated by the arrows. Note the considerably reduced voltage remnant in the circuit with in series connected capacitor C_s.

that the suggested circuit modifications result in significantly improved possibilities for PD detection at steep voltages.

As it was not possible to use the decoupling circuits simultaneously, the same PD events could not be compared. Three subsequent tests were performed instead, one with the initial circuit and two with the modified alternatives. All other conditions were the same and the test duration was kept short to minimize the effects of PD source ageing and potentially changing ambient conditions. Figure 3.11 shows the signals measured. The polarity reversal in the applied voltage is clearly visible in all of them as the bump starting at t=0, which is the remnant of the rapid voltage change. To facilitate the comparison, the signals are scaled so that these bumps have similar magnitudes. The signals show PD events at about 2 µs after the polarity reversal and it is apparent that the signals from the modified decouplers are substantially easier to recognize than the one from the initial circuit. The decoupler with a capacitor C_s in series allows for increasing the resolution as its voltage remnant is of shorter duration than in the other alternatives. An important comment is that none of the presented circuits needs to be particularly optimized for securing frequency characteristics good enough for the measurements, suggesting that the solutions are robust for these types of applications.

One observation from Figure 3.11 is that the signal of the circuit with in series connected capacitor C_s remains at an elevated level (a slow decay) after the polarity reversal due to charging of the capacitor C_s. In cases when this becomes a problem, a resistor can be connected in parallel to C_s. This option is not exploited further, since the modified decoupler without series connected capacitor C_s appeared to be sufficient for the investigations presented in this work.

3.3.3 Example of circuit optimization

As the proposed circuit modification allows additional suppression of the remnant from the applied voltage, even shorter rise times or higher voltage amplitudes can be analyzed. Thus at such conditions, a lower resolution A/D converter might be necessary to resolve the voltage magnitude of a complete PD trace. This however reduces the available dynamic range and lowers the sensitivity of the measurement. Therefore an adaption of the component parameters of PD decoupler is probably needed for matching various rise times.

To illustrate how this can be accomplished, the parameters of the circuit in Figure 3.5 are adjusted with the aim to reduce the voltage remnant in relation to the PD amplitude and to resolve PDs occurring close to polarity reversals. The procedure is based on the considerations presented in section 3.2, in which the relevant filter parameters determine the transfer function of the PD decoupler are defined. Increasing the value of resistor R_u, while maintaining the other parameter values constant, should increase the suppression at lower frequencies with only a minor reduction at higher ones. Studying the transfer function for R_u increased to 100 kΩ shows that this is the case, as exemplified in Figure 3.12.

However if the remnant at frequencies up to 10 MHz needs to be further decreased, the transfer function can be further adjusted. As indicated in the Table 3.1, a lower value of C_u influences the magnitude of the amplification at lower frequencies. Modifying the circuit by using C_u=5 pF increases the suppression more below the resonances than it decreases the peaks.

To improve the resolution of a captured PD trace, a reduction of the ratio between the voltage remnant and the PD amplitude is desired. Transient simulations are helpful here.

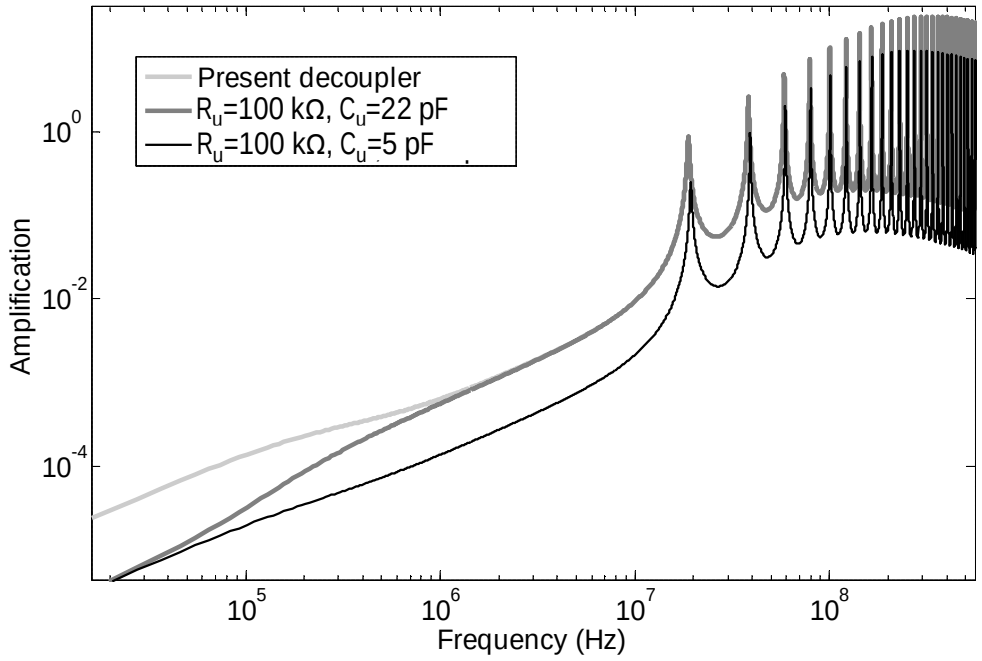

Figure 3.12 Transfer function characteristics for different parameter values. Note that increased suppression below 10 MHz needs adjustment of both the resistive and capacitive contribution in the frequency dependent voltage divider.

To simulate PDs appearing at polarity reversals, a circuit model presented in Figure 3.13 is used. It illustrates an Orcad model [59] of the system generating the high voltage waveform. A high voltage switch (Behlke HTS 301-03-GSM) is modeled as two voltage controlled switches (Sbreak) with defined on- and off resistance values (1 Ω and 100 MΩ). The PD decoupler is implemented similarly as shown in Figure 3.7. In addition, a simple 'ABC'- model [14] illustrated in Figure 3.14 is included to simulate the PD signal. The capacitance values included in the latter figure are chosen to resemble properties of the dielectrically insulated cavity. To simulate the discharge a resistor with fixed on– and off value is used. The off/on transition time is consistently chosen to be about 1 ns. This rapid increase in resistance ensures the high frequency content in the simulated PD event. The advantage with such a simulation is that it provides PDs with equal magnitude and frequency content.

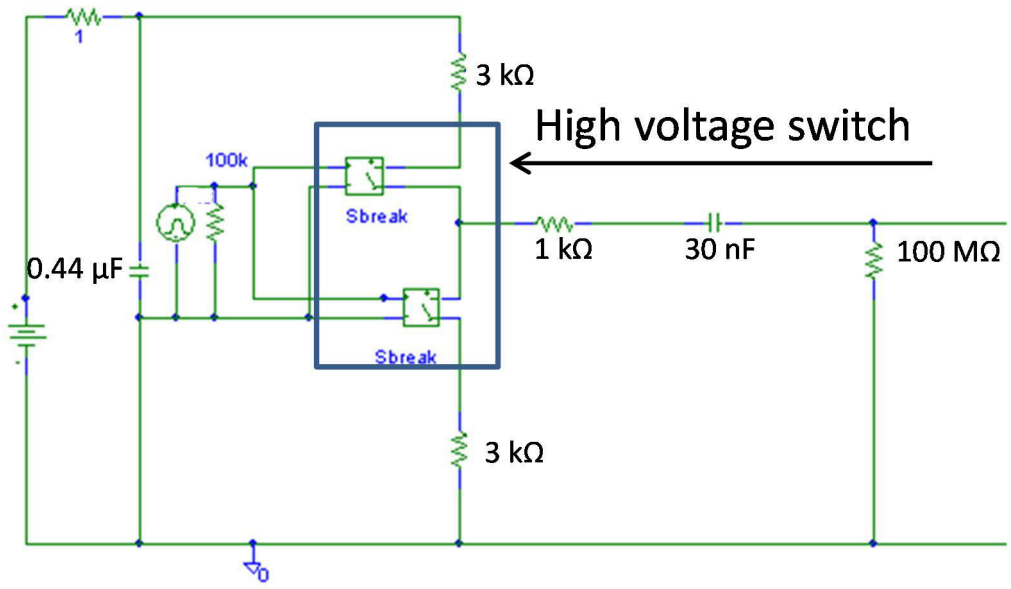

Figure 3.13 A model of bipolar voltage generation part of the test set-up. The two voltage controlled switches (Sbreak) simulates the high voltage switch (Behlke HTS 301-03-GSM).

Applying a semi-square voltage waveform with 2 µs rise time in the transient simulation shows for the different parameter values explored previously that the voltage remnant decreases when the resistance R_u increases. Additionally, the influence on the PD magnitude is small, as expected. Worth commenting is that increasing C_u increases the PD amplitude, as exemplified in Figure 3.15 for C_u=22 pF, but, at the same time, the oscillation at the polarity reversal increases due to the increase in amplification at lower frequencies. The presented simulation is an aid in finding the most suitable circuit parameters for matching the PD magnitude in relation to the voltage remnant.

C_1 (pF)	C_2 (pF)	C_3 (pF)
50	0.15	0.1

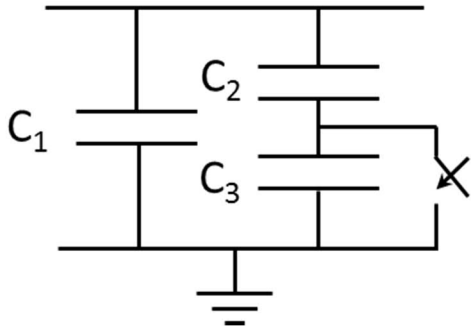

Figure 3.14 A basic ABC-model used to simulate PD in the circuit evaluation process. C_1 and C_2 resembles the surrounding insulation and C_3 the defect.

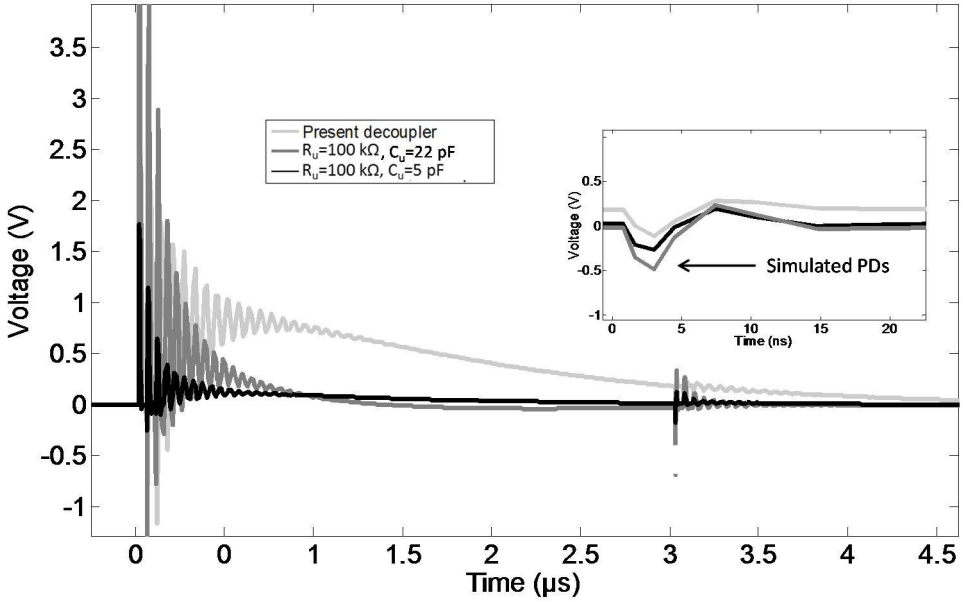

Figure 3.15 Simulated PD traces for three different circuit alternatives. Note that the combination of increased R_u and reduced C_u is used to minimize the ratio of the remnant and the PD amplitude.

To verify the results of the simulation, the measured voltage remnant in the modified circuit is compared in Figure 3.16 with a measurement by means of a similar circuit, but with increased R_u and decreased C_u. As can be observed, the main finding of the simulations regarding the voltage remnant suppression is clearly recreated in the actual measured results. Figure 3.16 illustrates that PDs generated in the test object exposed to 8 kV_p and 2.5 µs rise time can easily be identified shortly after the polarity reversal in the signal recorded by the circuit with R_u value of 100 kΩ and decreased C_u. The remnant and the high frequency interference from the switch decay in this case already before the externally applied voltage reached its half value. As the voltage remnant after these modifications mainly consists of rapidly decaying high frequency oscillations, detection of PDs of small PD magnitudes becomes possible close to polarity reversals. As observed in Figure 3.12, the decreased C_u lowers the resonance peaks; it is however clear, based on results presented in Figures 3.15 and 3.16, that the reduction of the remnant is larger than the decrease in PD amplitude. Thus the relation between voltage remnant and PD amplitude is improved for the modified R_u and C_u parameter values.

The considerations presented above provide an example on how the decoupler could be modified for higher voltages and shorter rise times. However, for the investigations presented later in this thesis the parameters indicated in Figure 3.5 are used, as they appear to be more suited for the analyses below in which the remnant signal is utilized for detailed reconstructions of the applied voltage and for measurement calibration.

3.3.4 PD Trigger level

Each time the moving average is subtracted from a trace potentially containing PDs, special procedures need to be performed in order to find the voltage level suitable to separate noise from useful information (the trigger level) as well as determination of the length of each PD pulse.

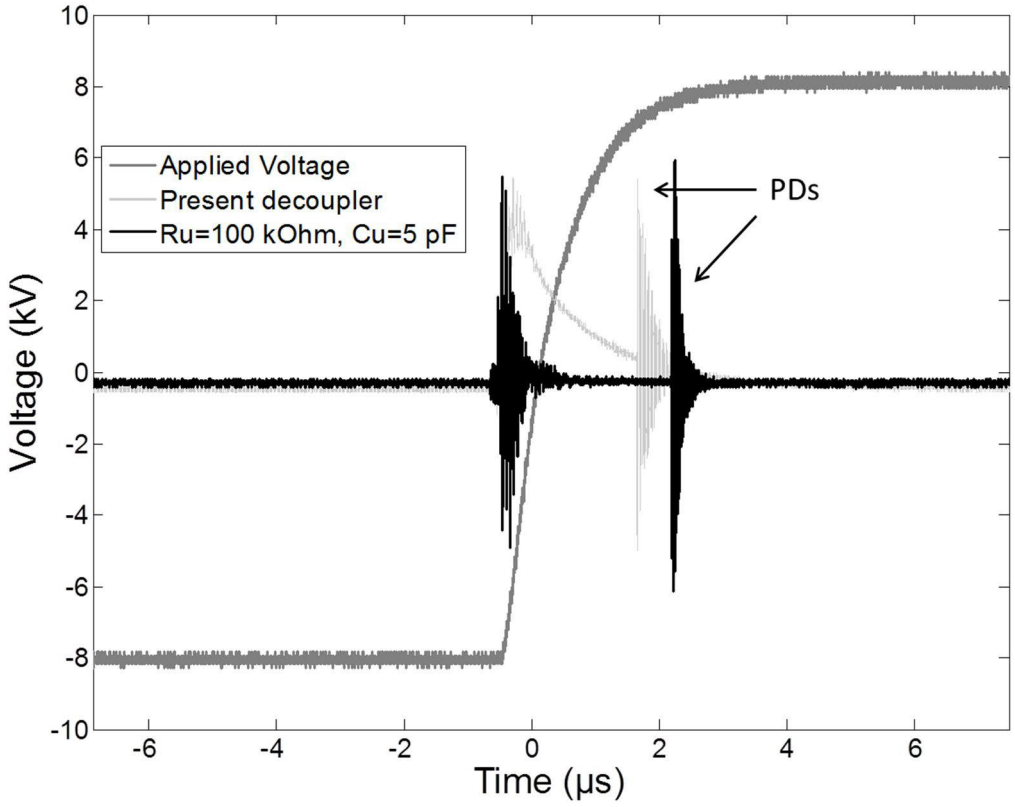

Figure 3.16 PD events and the resulting voltage remnant measured in a dielectrically insulated cavity exposed to voltage step of 8 kV_p for both the present decoupler and with changed component values. The PD traces are magnified in the figure to facilitate comparisons.

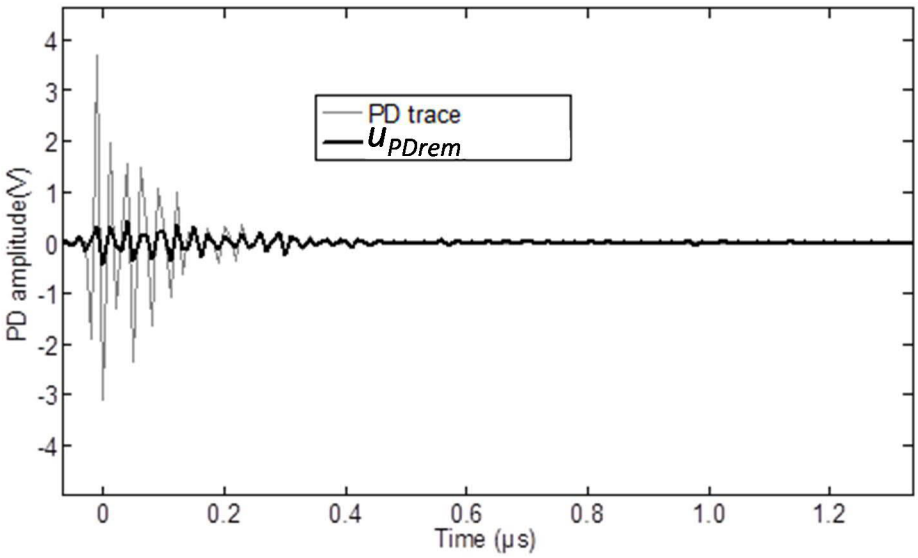

Figure 3.17 Single PD trace in comparison to a signal from previous traces after subtracting the moving average for a low n_0 value (n_0=10).

Figure 3.17 shows a PD appearing in one trace as well as the next moving average, calculated for a low averaging length $n_0 = 10$. As can be observed here, the remains of previous PDs u_{PDrem} is clearly noticeable in the figure. Therefore a higher n_0 value is applied in the investigations presented in this thesis, typically $n_0 = 80$, to further decrease the remnants.

The trigger level can either be manually or automatically determined to adapt to different signal to noise- ratios. Presently the automatic detection level is determined by applying the largest value of the following alternatives: either the maximum amplitude detected on the previous trace divided by the number of averages n_0, or the median value of all the captured data in one trace multiplied by a factor 1.5. The latter principle seems suitable since the amount of trace values corresponding to noise is higher than what is related to PDs. A similar approach is discussed in [60] where a procedure to remove Gaussian noise is described by applying wavelets that resemble the properties of PDs.

After a PD is identified, the duration of the signal response must be determined. This is important to obtain the highest reliable detection rate. The procedure employed consists of constructing an envelope considering the lowest resonance frequency in the PD decoupler, which should relate to the transient response from the high-pass filter. Here 5 MHz has been selected since, according to Figure 3.5, the first resonance is at 20 MHz, well above this frequency. The starting point of a PD event is defined as the time when it passes above the trigger level. The end is found by requiring that a specific time must pass, where the envelop remains below trigger level. A typical time used is a few times the period of the lowest resonance frequency. In Figure 3.18 a PD event is illustrated together with its envelop. The length before the

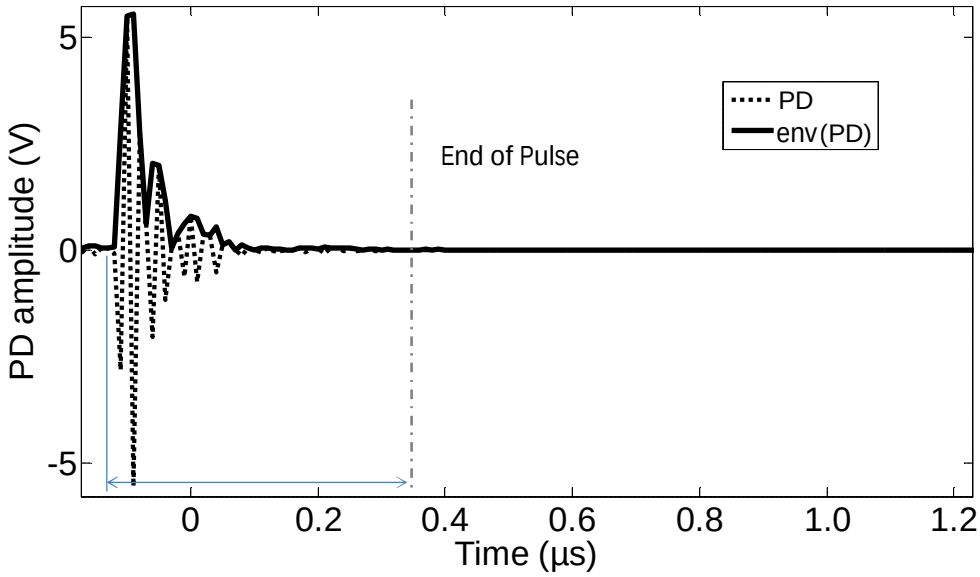

Figure 3.18 Envelope of a captured PD signal with indication of the time after which detection of a new PD becomes possible (End of Pulse).

next PD can be identified is indicated and thus a typical duration of one PD signal is 0.1- 0.5 µs. The shortest detection interval possible is given by the PD pulse length, which, with this detection circuit, is determined by the resonances. A high resonance value also means a long duration when PDs are detected. Thus there is a trade-of between possibilities to detect weak and dense PDs. In cases where less suppression of the applied voltage remnant is needed, the filters in the PD decoupler can be adjusted to shorten the resonant response from each PD further to increase the PD time resolution.

When PDs occur so closely in time that individual detection is impossible, only the amplitude of the largest ones can be obtained but this value is not overestimated, as may occur when applying other amplitude extraction methods based on integration. Therefore there is no risk of falsely considering several small PDs as one large.

3.3.5 Requirements on voltage stability

It is important to consider the effect of voltage source instability, in terms of varying amplitude of the applied pulses, on the stochastic PD detection procedure. In practice, a slightly varying voltage can be handled if the PD trigger level is higher than the change introduced to the moving average.

Let us assume a sudden change in the applied voltage amplitude between two captured traces from u_{meas} to $u_{meas} + \Delta u_{meas}$,. Further assume that the moving average value was stable and that the applied voltage remnant has the peak value u_{rem}. The change in applied voltage will thus be seen in the following trace as an increase of the voltage remnant amplitude by $u_{rem}\ \Delta u_{meas}/u_{meas}$. If this increase is not to be considered

as a PD, the trigger level, u_{trig}, must be larger. This provides a relatively simple condition for the limit of allowable increase in voltage change between captured traces:

$$\frac{\Delta u_{meas}}{u_{meas}} < \frac{u_{trig}}{u_{rem}} \tag{3.9}$$

From this rule, it is obvious that voltage variation is most critical when the PD trace contain an appreciable remnant of the applied voltage, such as for very short rise times. For longer rise times and sinusoidal waveforms, voltage variation is of less concern.

When the voltage varies substantially, it may no longer be possible to rely on the automatic trigger level procedure. A fixed trigger level should be used instead. For example, consider a measurement on a test object containing PD generating defect, exposed to 6 kV_p. The moving average is stabilized during the measurement. Suddenly the voltage level is increased to 8 kV_p. Figure 3.19 exemplifies how the remnant u_{rem} increases up to 1 V, while the peak of the moving average before the increase is 0.65 V. This implies a difference of 0.35 V, as shown in the figure, indicating that the minimum trigger level should be above this limit.

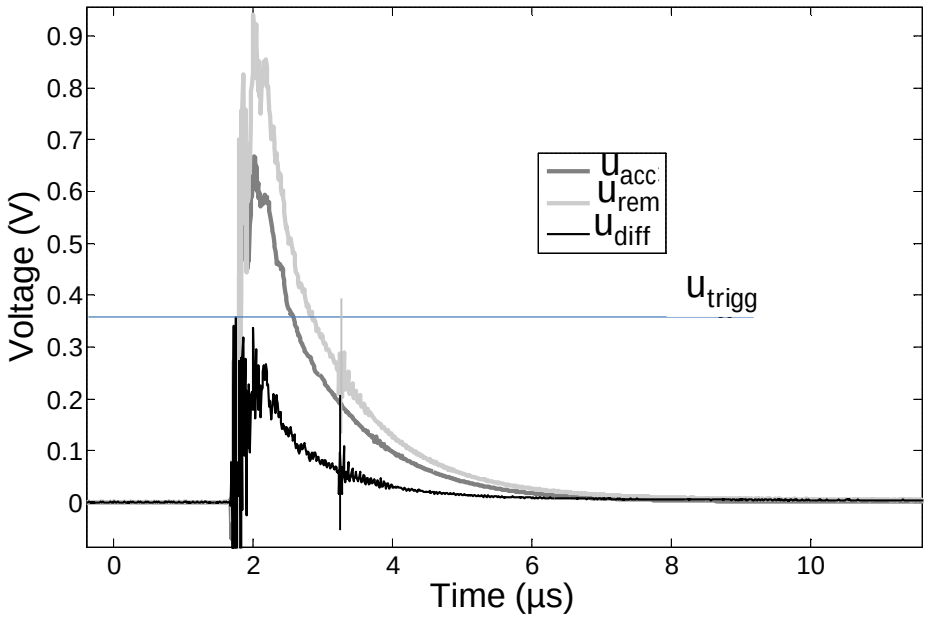

Figure 3.19 Voltage remnants after increasing voltage from 6 to 8 kV_p.

To quantify the minimum rate of voltage change, assume a specific trigger level u_{trig} of 0.01 V required to detect PDs. Performing tests at u_{meas} of 6 kV_p (u_{rem}=0.65 as indicated in Figure 3.19) would result, based on Equation 3.10, in a maximally allowed increase or variation in voltage level Δu_{meas} of 79 V for each trace captured. If PDs

can be neglected for some time after polarity reversal, then naturally a lower trigger level can be employed.

Thus the rate of acceptable voltage change depends on the rate of the data collection as well as the number of averages. It is therefore possible to allow a gradual voltage variation if measurement quantities are properly adjusted.

3.4 Sensitivity estimate

So far three different PD decoupler circuits (initial, modified and alternative modified) were employed mainly for demonstrating how the PDs can be studied with increased resolution. To theoretically evaluate their capabilities in relation to the initial circuit, with parameters presented in Figure 3.5, the peak voltage from the remnant of the applied voltage is compared with the peak-to-peak value of the voltage output, U_{PD-pp}, when 1 pC PD is injected at the input. The dynamic range for a digitizer with number of bits, b, is expressed as:

$$N_D = \frac{1}{2^b} \tag{3.10}$$

This estimate is also valid for a general noise, if b is treated as an indication of the resolution in the employed measurement system. In order to resolve a PD event at a given rise time the peak to peak value of the PD signal should be larger than the resolution limit when compared to the voltage remnant:

$$\frac{U_{PD\_pp}}{U_{a\_pp}} > 2^{-b} \tag{3.11}$$

This evaluation compares digitizer options with 8 and 10 bits resolution for the different circuit alternatives. Although the DAQ used has 14 bits resolution, only 10 of them are actually applicable at the highest sample rate. The first step is to calculate the response from a PD of 1 pC with infinitely short rise time. In this case the voltage drop across the decoupling capacitor is equal to the ratio between PD charge and its capacitance. Further, the response to a voltage with a specified rise time applied to the same circuits is calculated. This investigation is repeated for six rise times between 10 ns and 1 ms for all circuit alternatives. By calculating the ratio between the voltage remnant for each rise time and the available resolution of the digitizer employed, the minimum resolvable charge for each circuit alternative can be obtained by means of the relation between the apparent charge and the voltage U_{PD-pp}. The output when using the modified circuit becomes 8.0 mVpp for a 1 pC applied to the PD decoupler

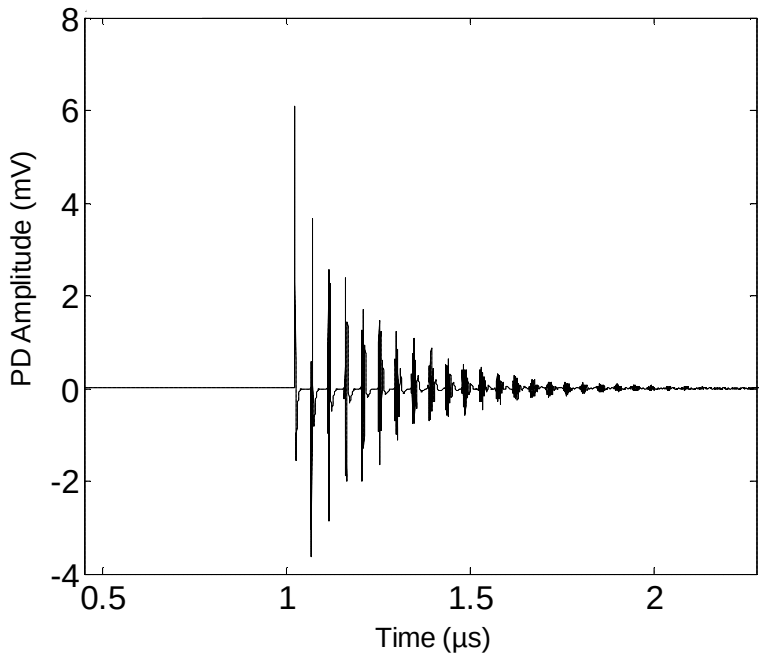

Figure 3.20 The voltage output U_{PD_pp} from modified circuit when applying a simulated PD of 1 pC with infinitely fast rise time at its input.

input, as exemplified in Figure 3.20. For the circuit with a series capacitor C_s of 47 pF (alternative modified) the result is 6.9 mVpp while the initial circuit provides 6.0 mV_{pp}. The voltage remnants for all the circuit alternatives are illustrated in Figure 3.21.

For both the modified cases the voltage remnant is considerably reduced compared to the initial circuit at all rise times. To determine the sensitivity of the obtained

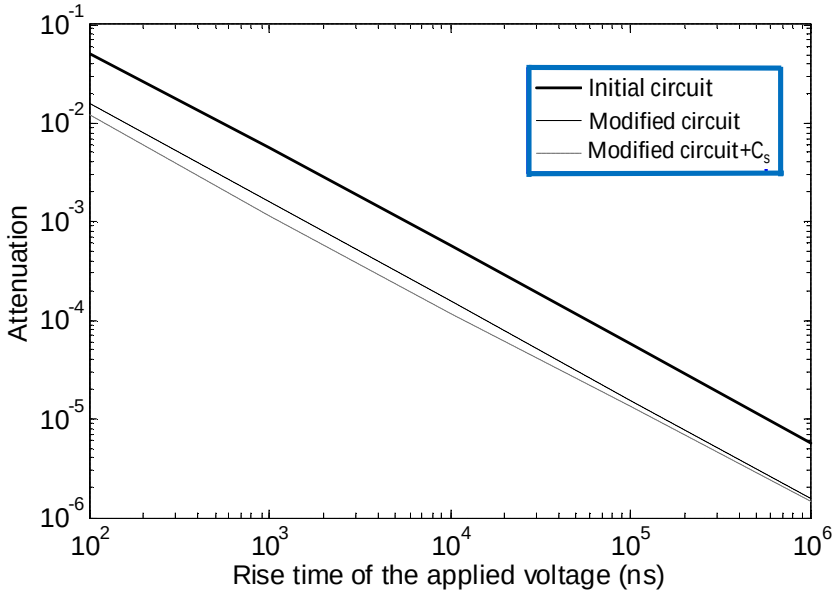

Figure 3.21 Voltage remnants for three different circuit alternatives. Note that the difference in remnant between modified and alternative modified circuits is rather small as compared with initial circuit.

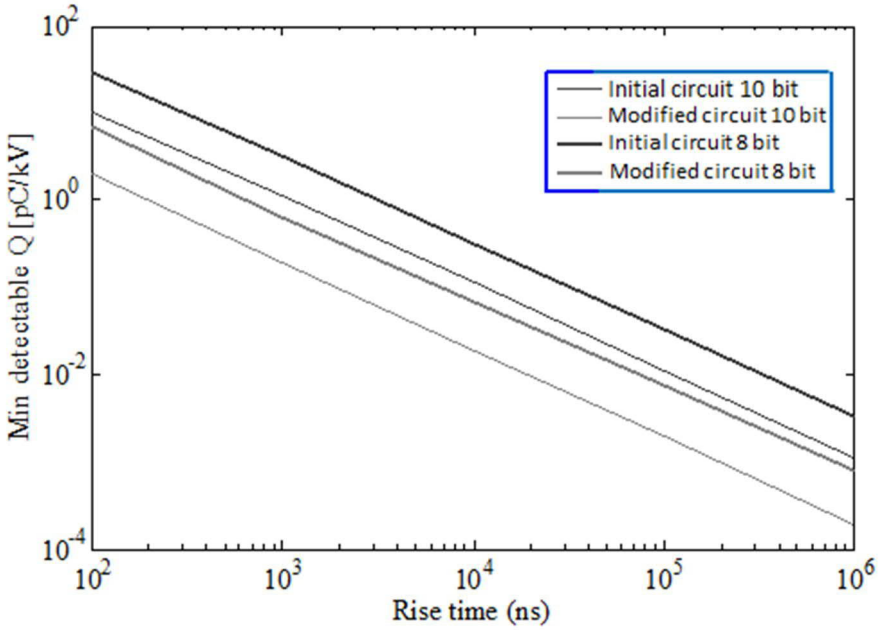

Figure 3.22 Sensitivity estimates of initial and modified PD decouplers. Note that the sensitivity increases for the modified circuit.

solutions, the digitizer properties need to be taken into account. This is exemplified with 8 or 10 bits resolution. Equation (3.11) is utilized to determine the minimum charge per kV and the result is presented in Figure 3.22. If, for example, a rise time of 1 µs is employed, then the theoretical sensitivity of the modified circuit becomes 0.1 or 0.9 pC/kV respectively with 10 or 8 bits digitizer resolution. For the initial circuit the sensitivity is 2 or 10 pC/kV.

The results shows that both the modified circuits with 8 bits digitizers can theoretically resolve smaller PD signals than a 10 bits digitizer using the initial circuit. In this example, the choice of circuit parameters is adjusted to fit the applications in this thesis regarding PD amplitude and voltage rise times in the µs range. Naturally, is it possible to optimize the circuit for higher or lower sensitivity demands than those considered in Figure 3.22.

3.5 PD signal properties

3.5.1 Signal rise time

The main limiting factor in detecting rapid changes in PD rise time is the data acquisition sampling rate. To obtain the highest possible rate, the resolution in amplitude has to be sacrificed. An oscilloscope with sampling rate of 2.5 GS/s and 8 bits resolution is used. For any of the circuit solutions, the shape of the PD response is affected by the electrical filters utilized and is especially the case when the circuit contains a resonant amplification of the input signal. For a detailed investigation of

PD properties, estimation of discharge rise time or the duration of the event is of importance as a significant decrease in rise time to about 1 ns or less is expected for a change from Townsend to streamer mechanisms [13].

Two possible approaches to estimate the PD signal rise time are presented here. One employs a mathematical model of the circuit subjected to simulated PD signals of different rise times, where the corresponding rise time of the output signal is calculated, which provides a relation between the actual and the observed rise times. A conceivably more accurate method is to recreate the original signal at the circuit input by utilizing the measured output and the transfer function of the employed circuit. Below, we will find that the latter approach seems more feasible but demands extra development before it can regularly be utilized.

To evaluate the first approach, an approximate mathematical model of the measurement circuit shown in Figure 3.5 was made in order to compare the calculated PD signal at point 'C' with the signal introduced in point 'A'. The steepness of the simulated PD pulse in point 'A' was then compared to the corresponding steepness at point 'C' and the result obtained is shown in Figure 3.23 which suggests that, due to the influences from the electric circuit, a PD with 1 ns rise time is to be measured as having a rise time of about 4 ns. This is in the range of what it expected of a streamer discharge. However, at longer actual rise times, say of about 7 ns, the same rise time of the output signal should be measured. The maximum PD rise time possible to measure seems theoretically limited to about 20 ns using this approach.

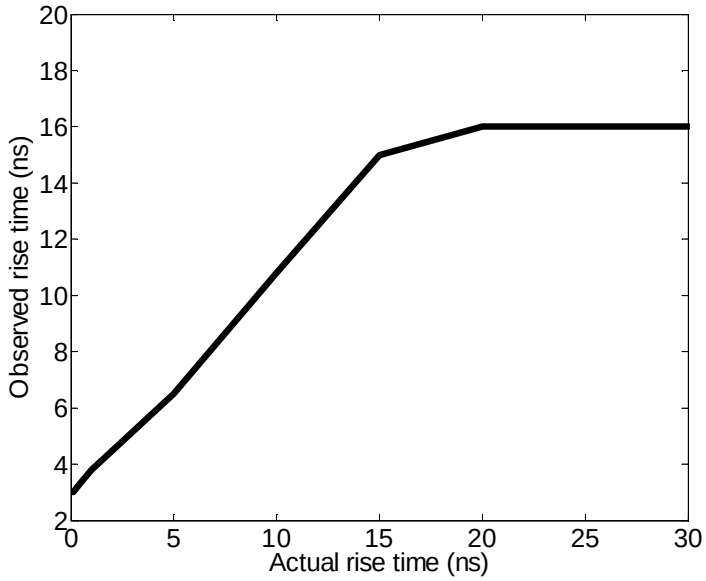

Figure 3.23 Relation between original rise time of PD event and rise time of the signal after passing measurement circuit.

3.5.2 Recreation of original voltages

The transfer function, as defined in section 3.3, facilitate recreation of both the initial shape of the applied voltage as well as the voltage dip caused on the coupling capacitor by a PD. The shape of the voltage at the PD source can theoretically be obtained by dividing the Fourier transform of the signal measured across R_{osc} by the transfer function. Transforming the result of this calculation back to the time domain yields the original shape of the voltage pulse. The vital component here is therefore the transfer function. As discussed previously in this chapter the difficulty to accurately model the transfer function increases considerably at higher frequencies. At low frequencies the estimates will also be less accurate due to the very large suppression of the voltage remnant. Figure 3.24 displays two types of transfer functions applied in these calculations. These are obtained from the analytical model and from fitting of the measured data by interpolation.

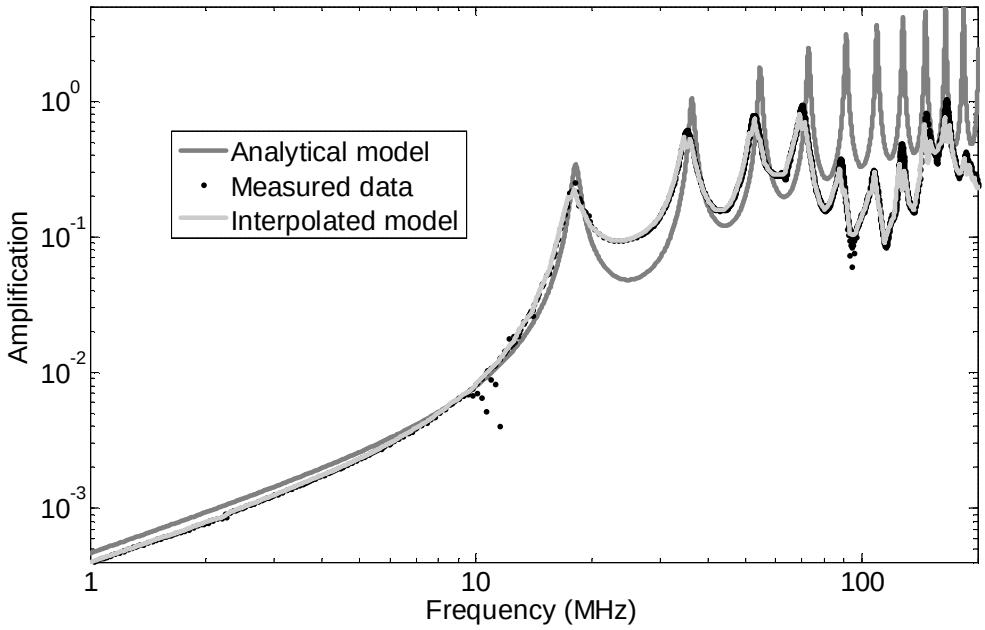

Figure 3.24 Transfer functions of the modified circuit used for recreating the voltage at the PD source.

Regardless of which of the alternatives is used, any DC offset will not be correctly transformed between the output and the input signal. Thus in order to properly recreate the initial shape of the applied voltage, this needs be compensated for after the transformation is performed.

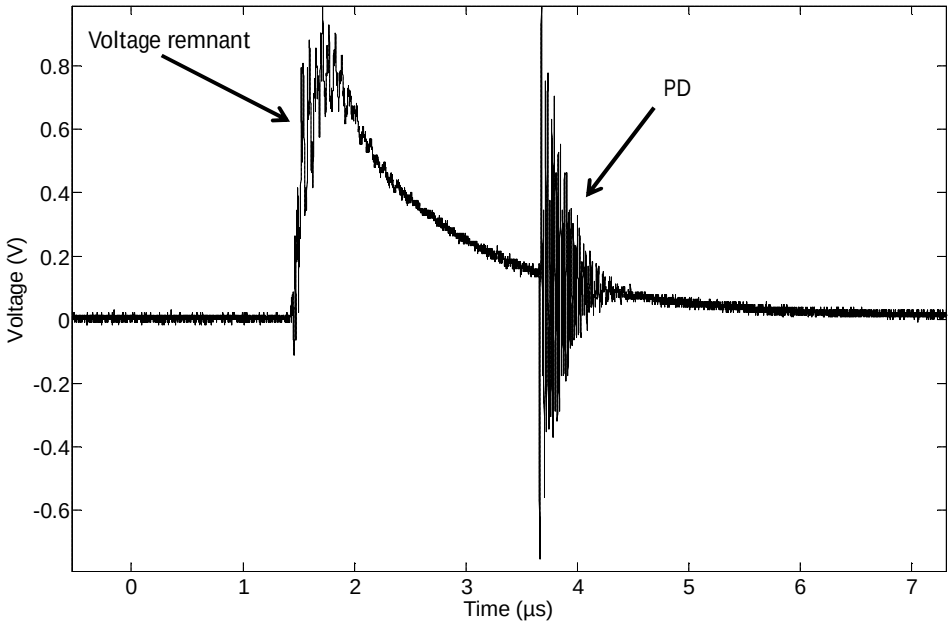

Figure 3.25 Voltage remnant and PD signal from a dielectrically insulated cavity. The rise time of the applied voltage is 2.5 μs.

Figure 3.25 illustrates the measured voltage remnant measured across R_{osc} including one PD for an applied voltage of amplitude of 8 kV_p with rise time of 2.5 µs to a dielectrically insulated cavity with a diameter of 3.5 mm. In addition to the signal from the PD circuit, the applied voltage was simultaneously recorded by a 1000x Tektronix probe. When using the complete remnant signal to recreate the applied voltage by means of the analytical transfer function, the result follows the voltage shape measured by the probe very well, as illustrated in Figure 3.26. The slight deviation that is observed might well be caused by the probe itself, which is complicated to calibrate properly.

In contrast, the recreation based on the measured transfer function suffers from variations in slope and step amplitude. Note that the PD info in the insert of Figure 3.26 is enlarged 100 times and yet is not very prominent.

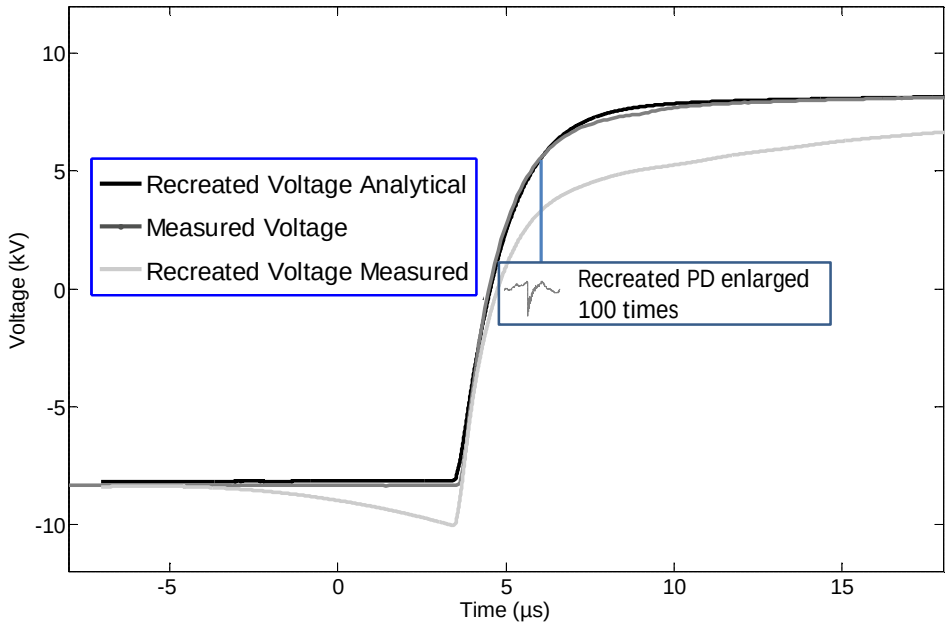

Figure 3.26 Reconstructed and measured voltages across decoupling capacitor. Both the analytical and interpolated transfer functions are used to recreate the voltage step from the remnant.

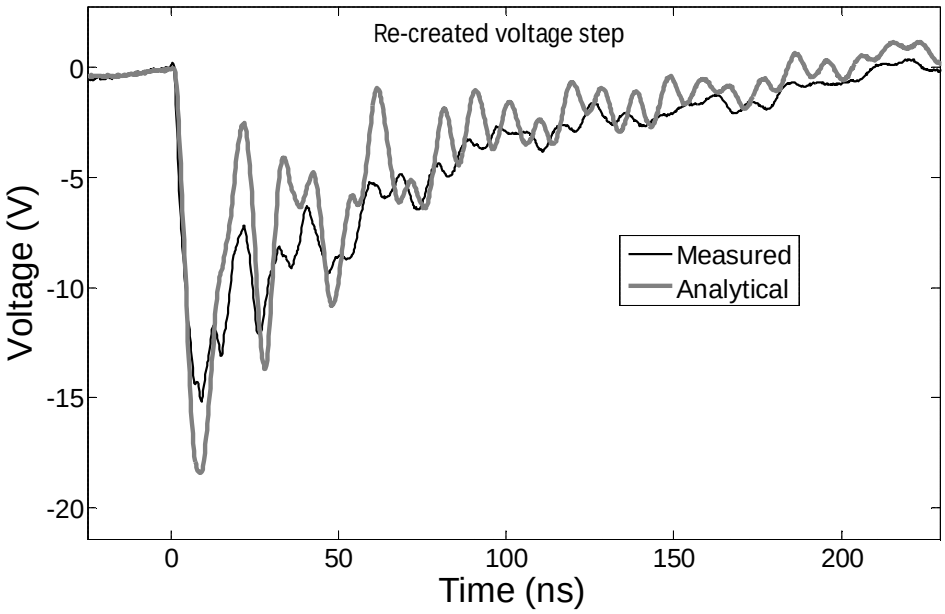

Figure 3.27 Recreated voltage step due to a PD event. Note that the amplitude is about the same in both cases, but the measured transfer function shows considerably less oscillations in the

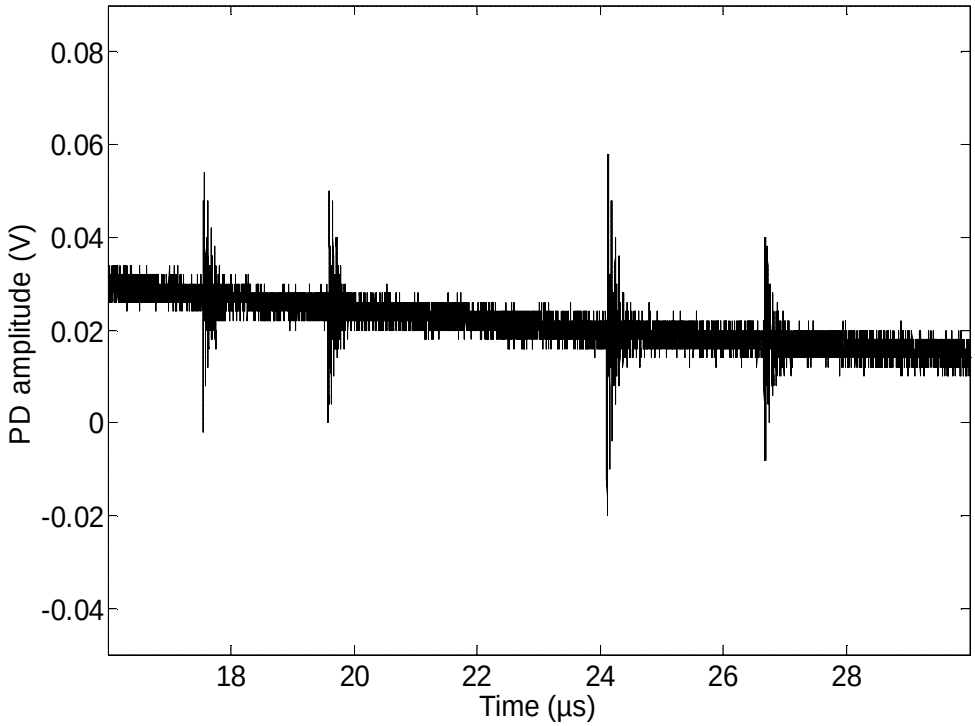

Figure 3.28 Signal of voltage remnant and PDs from dielectrically insulated cavity. The rise time of the applied voltage is 40 µs.

One possible reason that the analytical model performs better might be a consequence of the increased suppression of the voltage remnant in the modified PD decoupler. This results in a decreased accuracy of the measured transfer function at low frequencies. The waveform generator used to measure the transfer function

provided 8 V in peak amplitude and gives a very low response signal at these frequencies.

Both the measured and the analytical transfer functions are employed to recreate the PD signal. Here only a short time surrounding the PD is recreated to limit the influence from the applied voltage. In Figure 3.27 the recreated PD voltage step is illustrated using both functions.

When comparing these results it can be noticed that the ripple level is a bit lower for the measured transfer function. This is most likely caused by the differences in the high frequency region of the spectra. The peak levels for both alternatives are between 15 and 18 V.

To further investigate the recreation technique, a voltage of longer rise time although with the same amplitude is considered. Based on the voltage remnant (including PDs) presented in Figure 3.28, one concludes that more but weaker PDs appear at this case and that the voltage remnant is considerably lower. It is however important to elucidate how this fact affects the amplitude of the original PDs. Since the voltage remnant is attenuated more efficiently, a longer part of the signal may be recreated.

When analyzing the recreated signal across the cavity, a low frequency signal disturbs the result, as shown in Figure 3.29. The magnitude of this signal is in the volt range, which is very low compared to the applied voltage and therefore this contribution is likely due to noise. However by comparing with the measured signal in Figure 3.28, the positions of the PDs can be identified in the recreated signals as well.

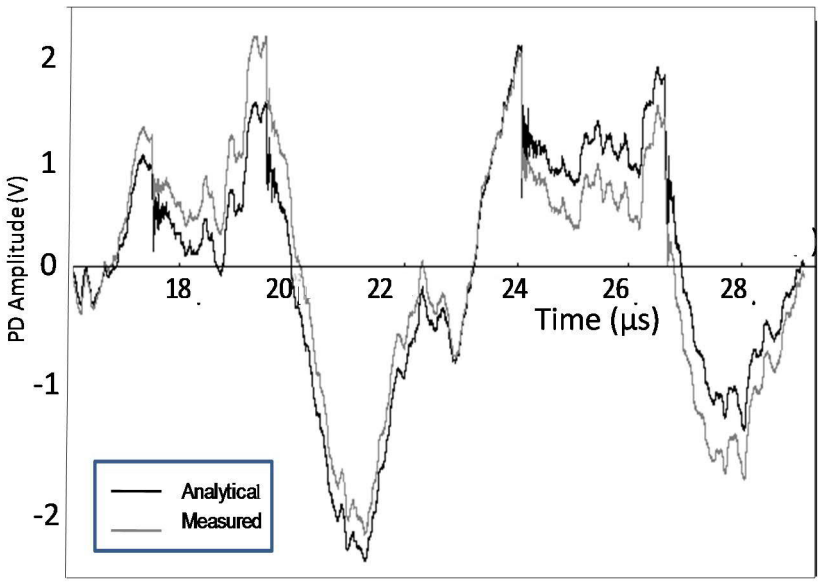

Figure 3.29 PD signal recreated from the remnant of Figure 2.28 at time interval between 18 µs and 27 µs. Note that the locations of the PDs can possibly be found.

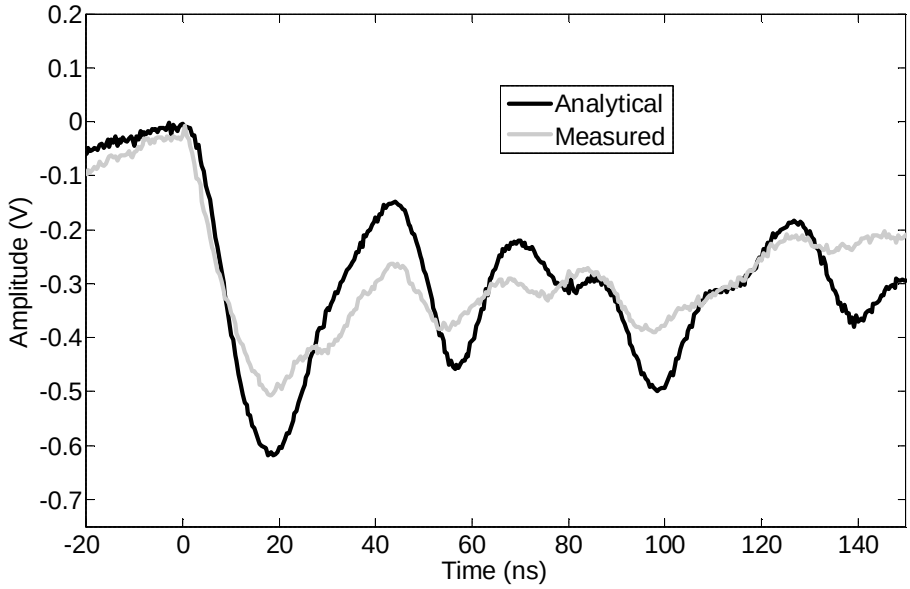

Figure 3.30 Recreated PD signal at voltage waveform with 40 μs rise time.

A detailed view of the first PD in Figure 3.29 is shown in Figure 3.30 for both transfer functions. The recreated PD signal is considerably smaller than the one for the shorter rise time of 2.5 µs. Again the measured transfer function give less oscillations after the initial step and this is taken as an indication that it is slightly more accurate. At the same time the amplitude ratio between the signals are almost identical for the measured and the recalculated PDs. Table 3.3 shows a comparison between measured PD amplitudes for the different rise times.

A problem with utilizing resonant amplification is the oscillations in the measured output signal which make identifications of two PDs occurring close in time more difficult. This can be as exemplified in Figure 3.31 illustrating PDs from an applied voltage of 80 μs rise time and 8 kV_p in amplitude. Three PDs occur with very little time difference in between them, so that the oscillations interfere. It would indeed be beneficial to more clearly separate them by reducing the amount of oscillation. This can possibly be achieved by recreation, as indicated in the figure. Despite of theprevailing noise, the three PDs are more unambiguously identified in the recreated signal from either the transfer functions.

Table 3.3: Ratio between PD amplitudes measured and recreated for voltage waveforms of 2.5 and 40 µs rise times.

Ratio PD measured	Ratio PD recreated (analytical transfer function)	Ratio PD recreated (interpolated transfer function)
(1.7/0.055)=31	(18/0.6)=30	15/0.48=31

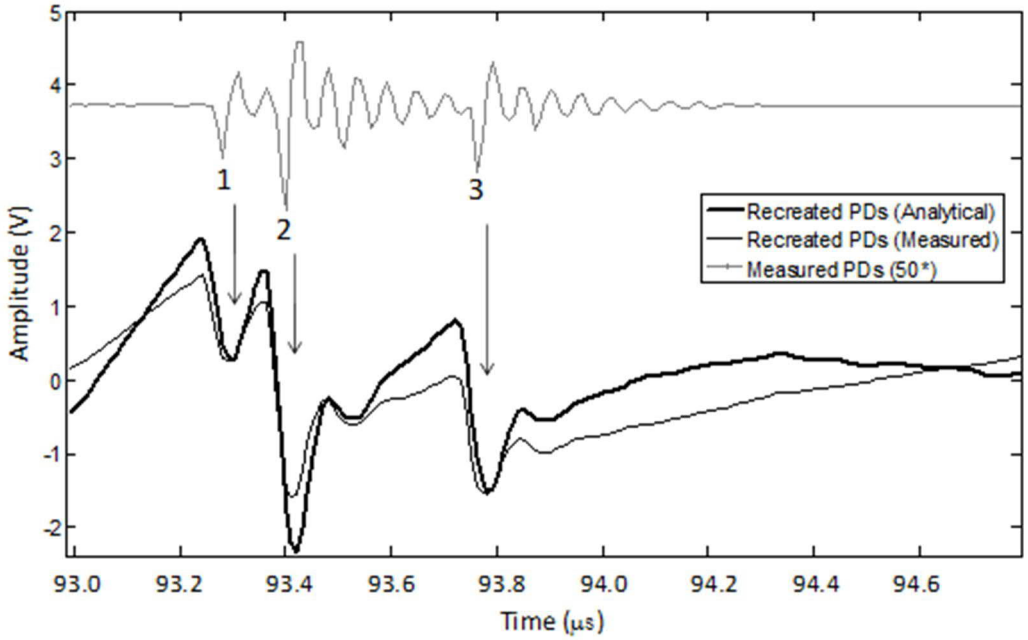

Figure 3.31 Measured and recreated signals from three PDs that occur closely to each other. Note that the three PDs are clearly separated in the recreated signal.

3.6 Calibration

In most PD tests, it is important to calibrate the measurement system. This is a challenging and sometimes even impossible task, particularly in PD detection methods using antennas, such as UHF, and acoustical principles. In capacitive decoupled PD detectors the calibration is customary done by injecting a known charge into the circuit. Since the PD decoupler suppresses lower frequencies considerably, the need to use calibration pulses similar to actual PD signals is imminent. If such equipment is unavailable, it is necessary to use other approaches. In this chapter such an approach is presented and compared with results obtained by applying a commercial PD calibrator. One of them is based on using the recreation method introduced in previous section. Based on the recreated PD amplitudes together with the 100 pF capacitance of the decoupling capacitor and the 50 pF test object (the dielectrically insulated cavity), the real apparent charge in the examples in section 3.5.2 can be estimated to be between 2.25 and 2.55 nC for the short rise time. For the longer rise times the value is between 72 to 90 pC. Using the amplitudes of the originally measured PD signal and relating this to the apparent charge across the decoupling capacitor suggests that 1 mV corresponds to about 1.5 pC for the cavity test object. The recreation method may thus be useful for calibration purposes. Verification of such a method requires however a test object where the voltage dip from a PD is directly measurable in the voltage signal.

An example of such a test-object is a twisted pair sample, resembling insulation of a motor winding, in which the voltage level needed to create PDs is about 0.5 - 1 kV_p and facilitates detection of the voltage dips. For illustration, a twisted pair sample having capacitance of about 13 pF is exposed to a semi- square voltage with a rise time of about 1.8 µs and amplitude of 1.3 kV_p. Figure 3.32 shows a voltage dip of about 68 V (7.8 nC), as measured with a Tektronix 1000x probe (see Table 3.4), while the PD signal has 13.3 V amplitude. 1 mV in PD decoupling signal should thus correspond to about 1.75 pC since the total capacitance of the test object and the decoupling capacitor is about 113 pF. This relation differs somewhat from the one for the cavity test object and to resolve the cause of this discrepancy another probe with increased bandwidth (LeCroy) is used.

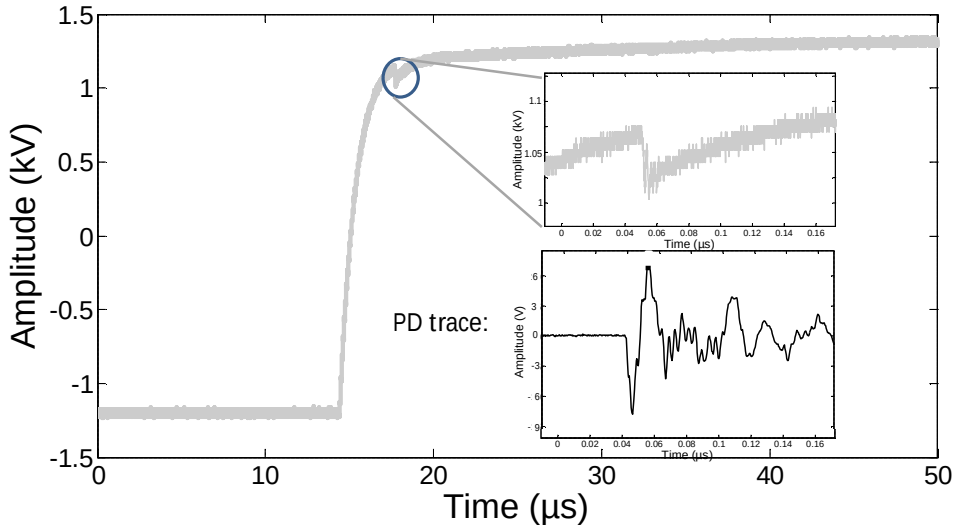

Figure 3.32 Voltage dip and measured PD amplitude for a twisted pair test object. Note that the voltage dip measured by a high voltage probe is directly observable.

Table 3.4 The characteristics of the applied high voltage probes for measurements of voltage dips. The voltage for the LeCroy probe is limited to 6 kV_p.

Probe	Attenuation	Bandwidth (MHz)	Impedance (MΩ)
Tektronix P6015A	1000	50	100
LeCroy PPE 6 kV	1000	400	50

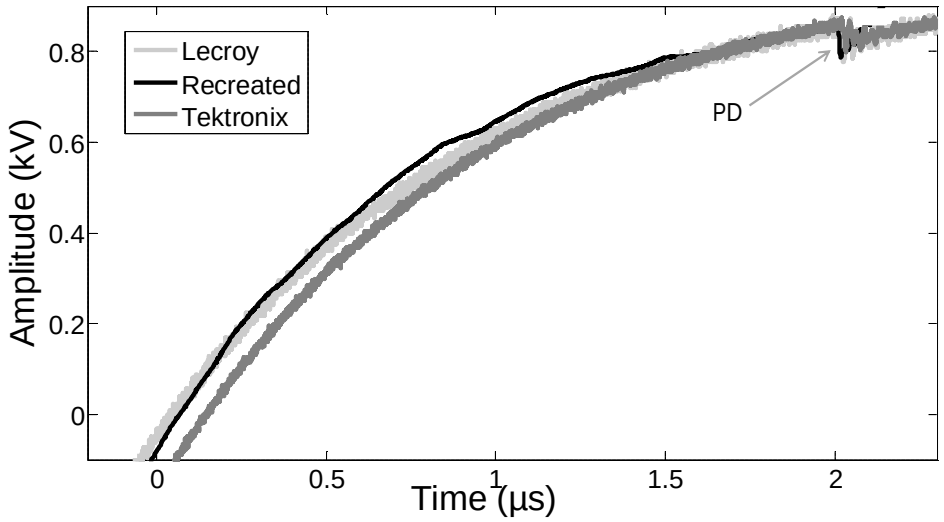

Figure 3.33 Measured and recreated voltage during a PD event for a twisted pair test object. The voltage dip is measured utilizing two different 1000x probes.

A comparison of the recreated and measured voltage shapes, showing similar magnitudes of both the applied voltage waveform and the voltage dip can be found in Figure 3.33. An enlargement of the PD event measured by both the probes is shown in Figure 3.34. Interestingly, the oscillations are less in the recreated results than from the probes, in section 3.5.2 the amount of oscillations was regarded as a quality measure. An estimation of the recalculated voltage step is about 75 V, with corresponding apparent charge of about 8.5 nC. The deviation between measured and

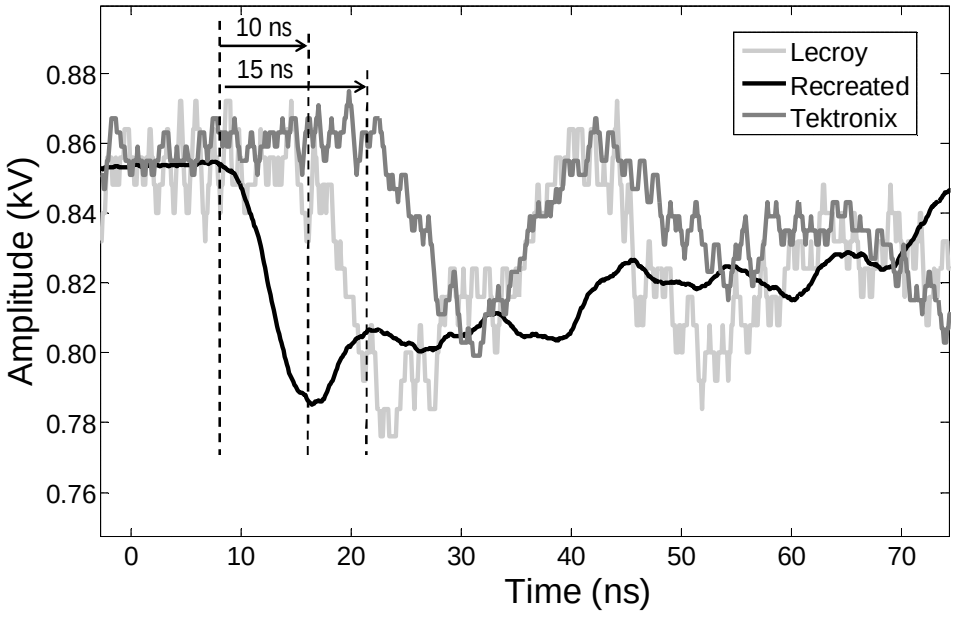

Figure 3.34 Recreated and measured voltage dips, using both the 50 as well as the 400 MHz probe. Note that the slope of the dip is closer to the recreated result when applying higher bandwidth.

Table 3.5 Calibration constant for different alternatives of measuring the charge dip across the test object and relating it to the measured PD amplitude.

Probe	LeCroy	Tektronix	Recreated (twisted pair)	Recreated (cavity)
Calibration constant (pC/mV)	1.52	1.7	1.56	1.5

recreated results is about 10% respectively: 9 nC (LeCroy) and 7.7 nC (Tektronix). The LeCroy probe closely follows the recreated result and the resulting calibration constants are shown in Table 3.5. One reason for the deviation between probes could be that the recreated voltage dip has a shorter rise time than the one measured with Tektronix probe, as seen in Figure 3.34. The difference is smaller between the LeCroy probe and the recreated results.

Additionally, the delay between the signal measured by the Tektronix probe and the recreated one is about 15 ns, which, assuming a speed of wave propagation of 200 m/µs within the cable, provides an estimate of the probe cable of 3 m. In reality, the cable was 2.9 m long. Similar estimate for the LeCroy probe shows a time delay of only 10 ns, corresponding to the delay in a 2 m long cable, again similar to the actual length of 1.95 m. When considering the time difference between the measured PD signal and the recreated waveform of about 25 ns, illustrated in Figure 3.35, the influence of the 5 m coaxial cable length in the PD decoupler becomes visible and proves that the recreation facilitates detailed analysis of the measured data. Despite the difference in

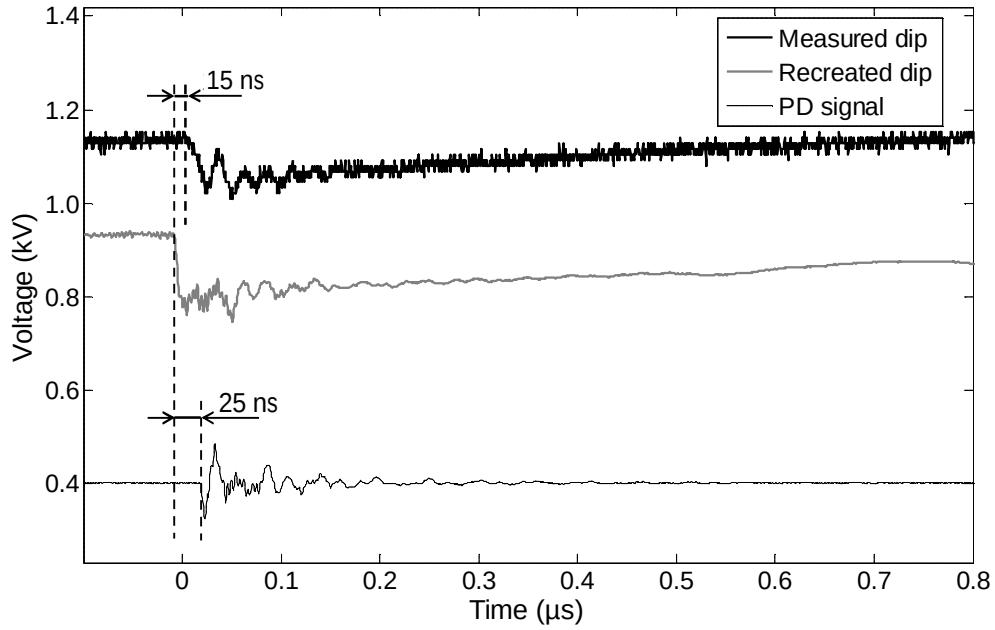

Figure 3.35 Time shifts between recreated and measured voltage dips as well as detected PD trace. Note the curves are shifted in voltage level to facilitate comparison.

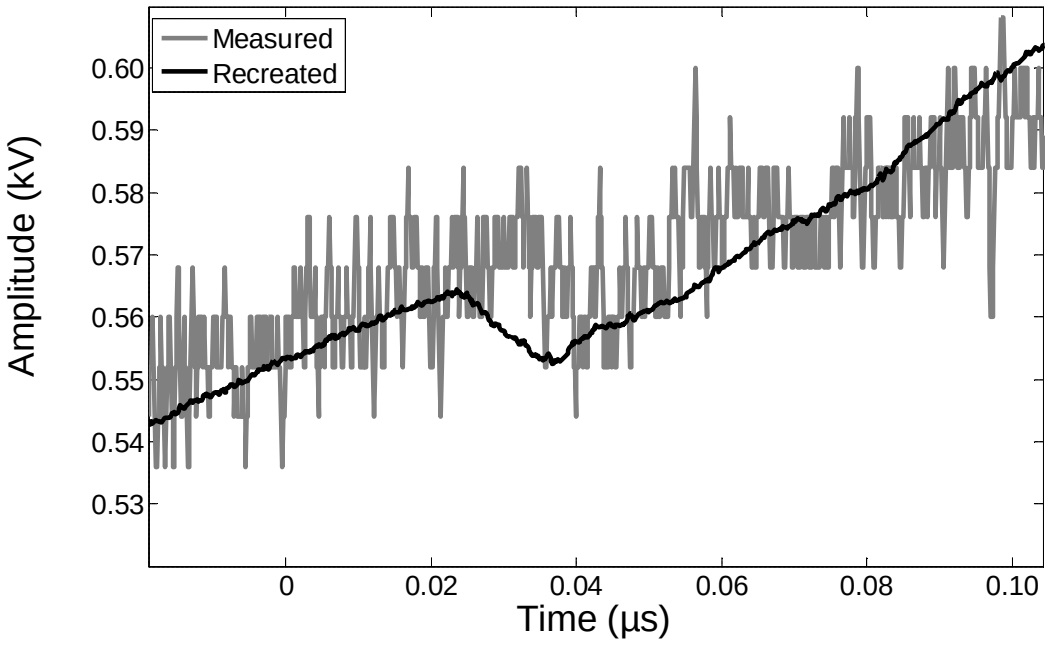

Figure 3.36 Recreated voltage dip together with measured signal by LeCroy probe in case of a weak PD.

bandwidths, both the probes capture sufficient details concerning the voltage dip for this test object. To further illustrate the advantages with the recreation method, consider weak PDs where the voltage dip is barely resolvable as exemplified in Figure 3.36. In the probe trace, although measured with the high precision LeCroy 1000x probe, the dip is hard to identify. The recreated result shows however clearly the pulse with a

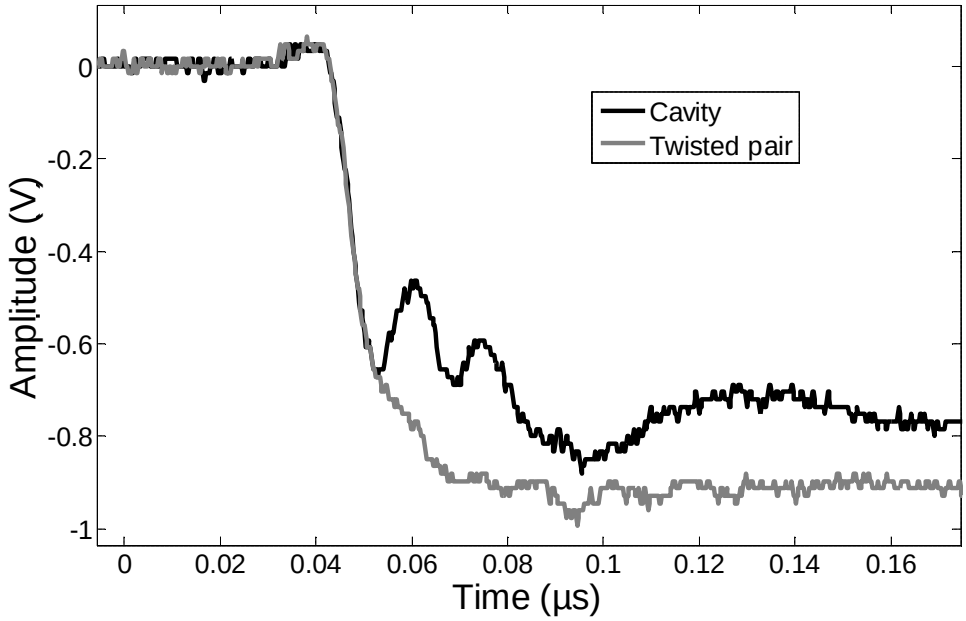

Figure 3.37 Voltage dips measured by means of Haefely calibrator on cavity and twisted pair test objects.

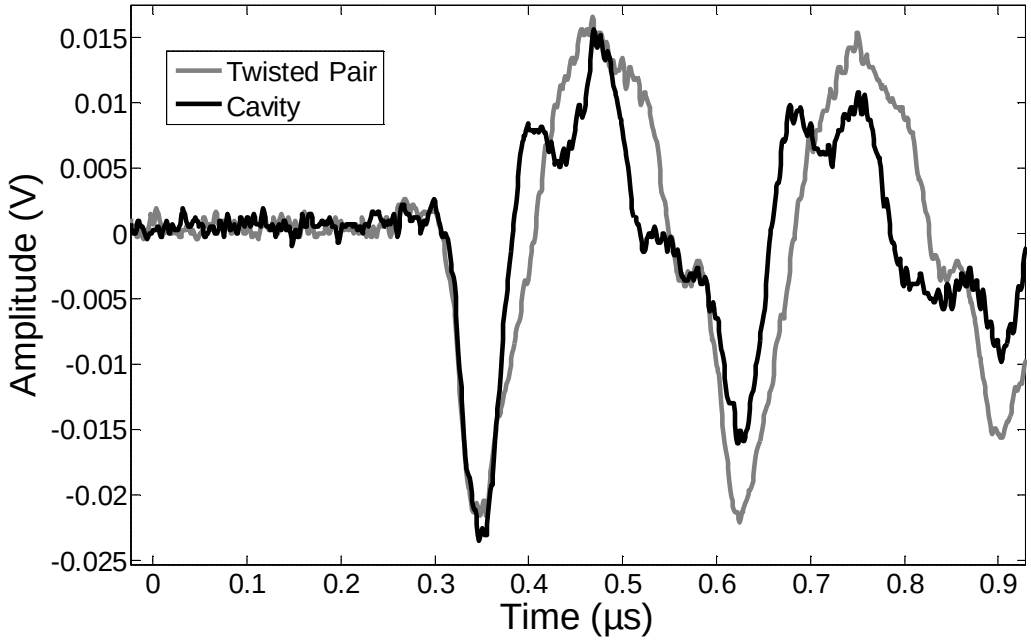

Figure 3.38 PD signals measured for cavity and twisted pair test objects after injecting calibrating charge of 200 pC to decoupling capacitor.

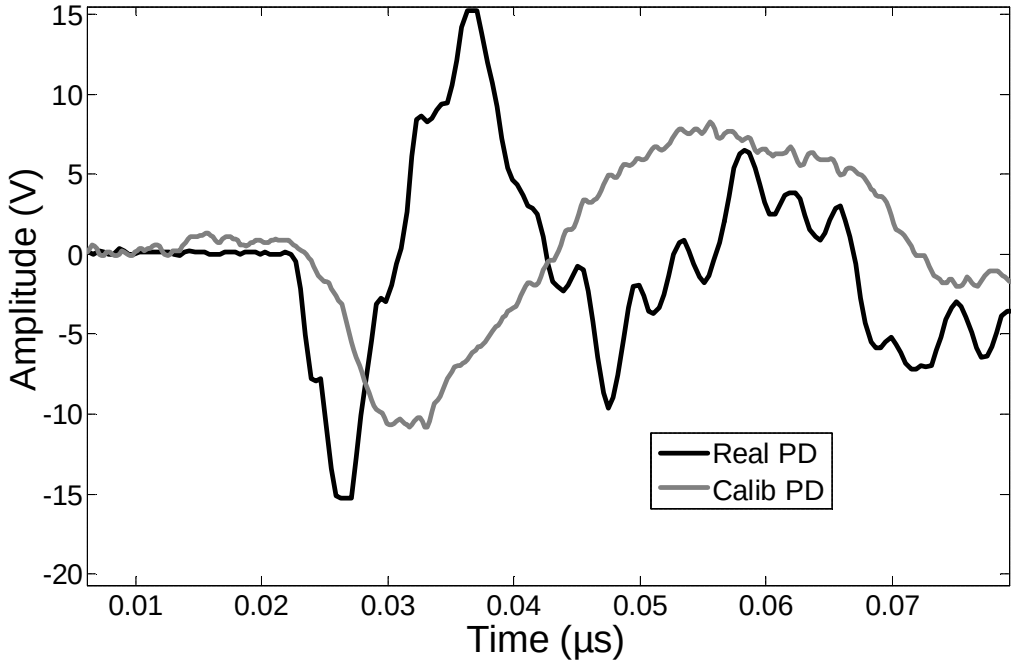

Figure 3.39 Comparison between actual and calibrator PD signals in a twisted pair test object. The calibrated signal is amplified to facilitate comparisons. Note that the rise times differ by more than a factor of 2.

considerably lower noise level, indicating that the recreation method provides better accuracy than a voltage probe.

Commercially available PD calibrators are commonly applied for estimation of PD detection sensitivity. A Haefely PD calibrator type 451 was applied in this work. The calibrator was placed across the test objects (dielectrically insulated cavity and twisted pair) for measuring the voltage dip. A sufficient sample rate of 2.6 GS/s, was used to resolve the rise time. Figure 3.37 shows the resulting voltage dips across the test objects for 200 pC input charge, which differ slightly in magnitude because of a difference in object's capacitance. The about 1 V dip observed in the figure results from voltage division between the calibrator, 100 pF, and the decoupling capacitance, 100 pF.

The corresponding output signal from the decoupler was about 40 mV, as illustrated in Figure 3.38 for both objects. Thus 1 mV would correspond to about 5 pC. When comparing this value with the results obtained when using actual PDs, the calibration constant differs more than 3 times. The reason behind it is most probably the difference in frequency content between actual PDs and calibration signals, as shown in Figure 3.39 where rise times of an actual PD and the calibrating signal are compared (the calibrator is intended for use on PD equipment with a maximum operating frequency of 1 MHz).

As a result of the presented investigations, the recommended calibration approach is thus either by using real signals (if available) or by voltage recreation. Another possibility is to apply a calibrator unit with steep enough front.

3.7 Concluding remarks

This chapter presents the structure of an enhanced algorithm applicable for extraction of PD signals from voltage traces by subtracting a moving average signal from a measured data trace. The stochastic nature of the discharges is utilized in this approach. As compared to previously developed approaches, the presence of PDs when calculating the moving average is more efficiently suppressed. Additionally, a method is introduced to automatically establish suitable trigger levels as well as to identify the beginning and the end of each PD event.

Two alternative PD decoupler circuits are also presented, which enable use of low resolution digitizers, such for example as an oscilloscope, and allow achieving a considerably higher sample rate. It is also demonstrated how the initial voltage step can be recreated based on measured output signal, which may further be utilized to calibrate the measurement system, instead of using a PD calibrator. This is particularly important in cases where the voltage dip due to a PD at the capacitive decoupler is too small.

4 PD Properties in Dielectrically Insulated Cavities

This chapter presents investigations on PD characteristics in a dielectrically insulated cavity. Sections 4.1 - 4.3.3 describes results when measuring PDs within a cavity (3.5 mm in diameter) when applying a PD decoupler similar to the one shown in Figure 2.1. From sections 4.3.4 onwards, the demand for increased time resolution when studying PD rise time made it necessary to utilize the PD decoupler introduced in section 3.2. The final section in this chapter presents studies on different cavity thickness and it ends with a non-electrical investigation as a support to the electrical measurements.

4.1 PD source set up

Due to the stochastic nature of partial discharges, it is often non-trivial to reproduce measurements exactly. To measure PD extinction voltage, the circuit with a capacitive decoupling was used. The main components of the circuit are shown in Figure 2.1. The test object was made out of three 0.75 mm thick polycarbonate discs pressed together. Before the assembly, a cavity was made by drilling a hole in the middle plate, as indicated in Figure 4.1. The object was connected between point 'A' of the measuring set-up and ground. A bipolar voltage source was connected to point 'A', offering a possibility to use different rise times as well as its levels. A 100 pF decoupling capacitor C_m was connected to the cavity as shown in Figure 3.2. The semi-square shaped voltage applied during all the following tests had a fundamental frequency of 313 Hz to eliminate disturbances from external power sources running at 50 Hz and to limit the memory required for the signal processing of the data. The PD signal in point "B" was measured by connection to the input channel of an oscilloscope with 8 bits resolution. Data from 200 positive voltage changes were collected during each of the measurements since earlier investigations have shown that the behavior at negative voltage change was similar. To ensure that no PDs occur outside the cavity, an initial test used three massive polycarbonate plates. No PDs were than observed at the voltage levels investigated. For further details regarding measurement procedures, see [10].

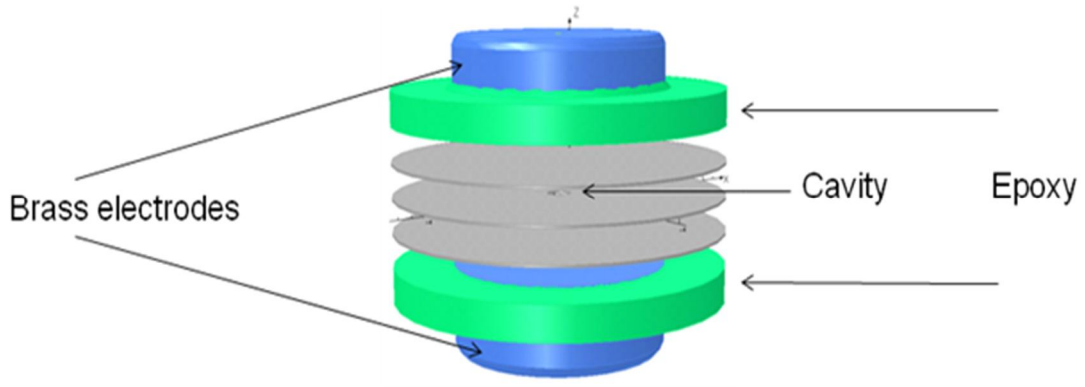

Figure 4.1 *The PD source used to measure extinction voltage in a dielectrically insulated cavity.*

4.2 PD extinction voltage

In this section the focus is on a basic PD property, namely the lowest voltage at which PDs can persistently appear. It is known that the lowest voltage at which PDs first appear as the voltage is increased can be higher than the voltage at which they disappear when the voltage is decreased. The former is conventionally called PD Inception Voltage (PDIV) and the later PD Extinction Voltage (PDEV). In the next subsection, the difference between these will be investigated for the test object of interest at different rise times. The result is that the extinction voltage seems more reliable and more dependent on the voltage rise time and thus this parameter is used for more detailed investigations.

4.2.1 Inception or extinction voltage

Measurement of extinction voltage is a relevant test to find the voltage level below which no PDs should be present in the insulation system. A more common approach has however been to measure inception voltage at which PDs starts to occur regularly. Both quantities are important. The extinction voltage test is done by increasing the applied voltage until a significant amount of PD occurs and then gradually decreasing it until no PD can be detected. When measuring the inception voltage level, the applied voltage is increased until PDs are first observed, following the measurement procedure described in the standard IEC 60270 [4]. To elucidate the differences between extinction and inception voltage levels in the cavity, semi-square bipolar voltages with 4 and 40 μs rise times were used. The measurements for the shorter rise time were repeated three times and the electrodes connected to the cavity endplates were grounded for about 20 minutes between each of them. To enable a statistical evaluation, identical tests was performed three times, with a break of 24 hour in between. The cavity electrodes were short-circuited during the break to prevent influences from remaining surface charges. After a three days long rest, an identical series of measurements was performed for the longer rise time.

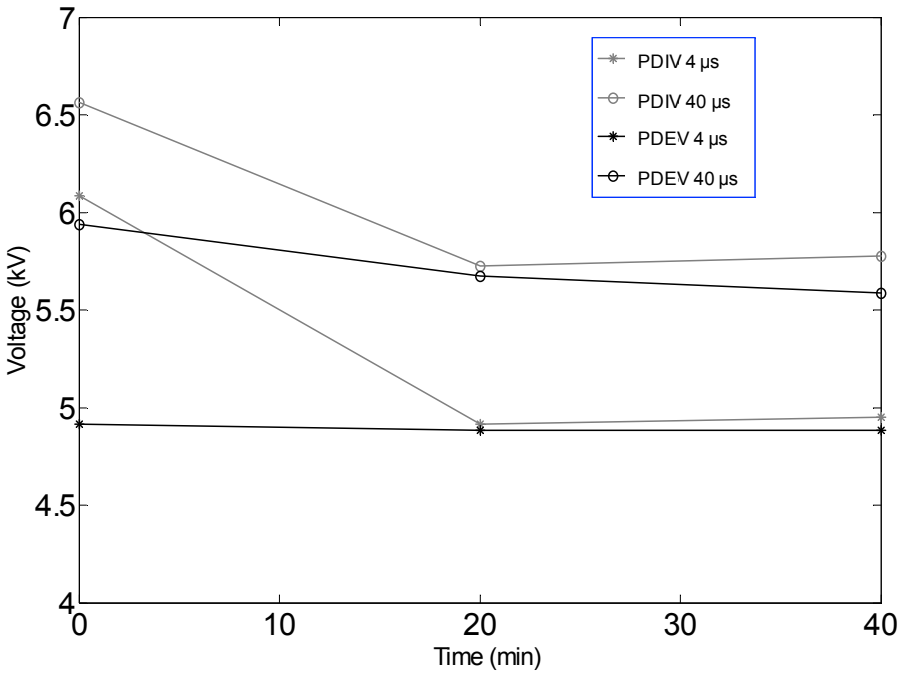

Figure 4.2 *Measurement of the average inception and extinction voltage. Note the difference in inception voltage between first, second and third measurement occasion for both the used rise times (the time scale indicates here the lapse time between the consecutive measurements).*

A significant difference in the extinction voltage level for the short and the long rise time was found, whereas the difference in inception voltages was considerably smaller for a fully relaxed insulation system. However, the consecutive measurements, after the PDs have been initiated for the first time, presented in all cases a much smaller difference between the inception and the extinction voltage levels, despite that the extinction voltage method always remained considerably lower and almost constant, as seen in Figure 4.2.

As can be seen from the figure, during the first inception voltage measurements only a small influence of rise time could be observed, while for the following measurements the difference became larger. This further emphasizes the importance of choosing the extinction voltage as the primary indicator in this work.

4.2.2 Extinction voltage and rise time

In this investigation, as discussed and concluded in the previous section, the extinction voltage method is chosen since it can be considered more important for service lifetime and be measured with a better repeatability. However, in order to perform the measurement as consistently as possible a procedure is defined that avoids the subjectivity, which easily may occur when using only a visual inspection of the oscilloscope screen. Therefore, an approach is used where the measurement system collects information from a fixed number of cycles at each voltage level before proceeding to the next lower voltage level. The number of PDs observed is noted for each voltage level and the measurement sequence terminates when no PD is found in

any of the recorded cycles. This is performed for all the tested cases. In many cases, the extinction voltage level can be found by extrapolating the number of PDs detected as function of voltage level to the highest voltage at which no PDs are detected. Here we additionally observe a quite unusual case that the number of PDs remains constant down to a voltage level where no PD is observed; the PD extinction voltage is thus bounded by the lowest voltage with PD and the highest without. If these bounds are too wide, it is possible to increase the voltage above inception and repeat the procedure with a smaller voltage step. Such a refinement is not possible with the inception voltage measurement, as discussed above.

To find the critical rise time at which PD characteristics change, rise times of 4, 7, 16, 20 and 40 μs were therefore applied here, hereafter respectively marked as T_1 to T_5. The rise time is here defined as the time difference from attainment 10% to 90% of the voltage change.

To measure the extinction voltage level, amplitudes between 8.0 and 4.0 kV were applied, starting from 8.0 kV downwards. The voltage amplitude connected to the cavity was reduced in steps of first 1, then 0.5 and finally 0.3 kV until the extinction voltage level was reached. This procedure with the same voltage levels was repeated for all the rise times investigated.

The measured number of PDs per period for the investigated rise times is shown in Figure 4.3, from which the extinction voltages can be estimated. From this figure, it is clear that a short rise time results in an almost constant number of PDs at all investigated voltages above the extinction, whereas the longer rise times yield a progressively increasing number of discharges and a higher extinction voltage. The critical region differentiating these two features seems to be between T_3 and T_4, i.e., between 16 and 20 μs and indicates for a change in PD behavior.

This type of observation has not been noticed for other types of PD sources, for which investigations of extinction voltage are reported [10]. Thus the observed behavior of a cavity with dielectrically insulated walls might be the first observation indicating a possible change of PD character with varying voltage rise time.

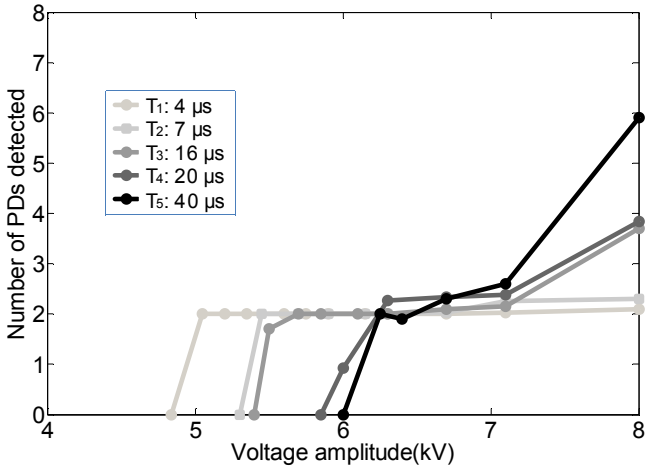

Figure 4.3 *Number of PDs detected per period at different rise times, note that shorter rise times yield almost a constant number of PDs per period.*

To better understand and confirm existence this effect, a study on how other PD parameters, like amplitude, voltage and time distribution as well as PD signal rise time, become affected by the voltage rise time has been carried out and the results are presented below.

4.3 Other PD characteristics

4.3.1 PD time distribution

In Figure 4.4 the PD occurrences during the voltage rise are illustrated for the studied rise times. It is apparent that the spread in time and number of PDs decrease significantly for shorter rise time and accordingly, as can be found from Figure 4.3, only two PDs per period can be detected for the 4 μs voltage pulse.

Another important observation from Figure 4.4 is that the voltage drop over the cavity must be significantly different from the applied voltage since the first PDs occur close to 0 kV, indicating that the cavity must be pre-charged for making a PD event possible. The position of the occurrence of individual PDs on the voltage waveform has been found to be quite informative in many respects. It becomes clear from Figure 4.3 that the voltage range between 7.1 and 8.0 kV must be important, since the detected number of PDs increases significantly for the longer rise times (T_3 to T_5), while it remains practically constant for the faster ones. In Figures 4.4 and 4.5 these two voltage levels are compared in time domain for all the rise times by indicating the positions where the PDs occurred. It is apparent that the spread of PDs in time decreases when the applied voltage decreases, especially for the shorter rise times. This is mainly because less PDs are detected per period at the lower voltage level (7.1 kV). We also find from Figure 4.3 that at 7.1 kV only two PDs per period could be detected for the shortest rise time T_1. For 8.0 kV, more PDs are detected (on average 2.14 PDs per period) and a short gap is observed, which is associated with occurrence of a second PD close to or at the voltage maximum. This gradually changes as the rise time is increased (from T_2 to T_5), mainly due to the fact that more PDs occur per period. Other investigated PD sources, such as needles and twisted pairs [9], have not exhibited any influence of rise time on the PD distribution.

Another way to study the PD distribution is by using the first discharge rate, which is a concept introduced in [15] that basically defines the probability for a PD to occur at a given time within the period. This is similar to the phase resolved analysis at sinusoidal voltages. The main factor influencing the first discharge rate is however the rise time. Therefore, to make the comparison between the different cases investigated here easier, the first discharge rate is preferably normalized for each of the wave forms by the respective rise times, T_r, as indicated in Equation 4.1 where the multiplication with T_r ensures that the integral of the normalized first discharge rate over one period is equal to the average number of PDs per period. The normalized probability for the first PD to occur at a certain time instant:

$$P_{FD}^{N}(T/T_r) = T_r P_{FD}(T) \qquad (4.1)$$

For first discharges, the maximum value is 2 but could be less if PDs are not observed in every period. This operation effectively makes all rising voltage flanks follow approximately the same curve and a result is shown in Figure 4.6. This figure shows that, at the longer rise times (T_3 to T_5) PDs occur relatively earlier than at the shortest rise time T_1. The presently obtained result indicates that the shape of the applied voltage has an impact on the PD characteristics in the cavity, i.e. increase in normalized time delay for the shorter rise times, which implies higher voltage level for their initiation. When we compare the normalized characteristics for several voltage levels it is apparent from Figure 4.7 that this delay prevails. When considering the half-width of the PD distributions shown in Figure 4.8 for all the investigated voltage levels, it is clear that the time width of the first discharge distribution decreases with increasing voltage and decreasing rise time.

With decreasing voltage, the first PD after each polarity reversal occurs more and more at the voltage maximum and thus the time width of the first discharge rate distribution increases considerably. This effect is here most clearly seen for the longest rise time T_5. For the shortest rise time, T_1, there is a smoother decrease in the width, from 1 to 0.5 µs, in the studied voltage range as the PD always occur on the voltage flank. By comparing the distributions of time width for different rise times, we find that they scale rather well. The width of the normalized distributions at 6 – 6.5 kV is about the same. This indicates that the observed time width may rather be controlled by the voltage waveform than by the physical process of PD formation.

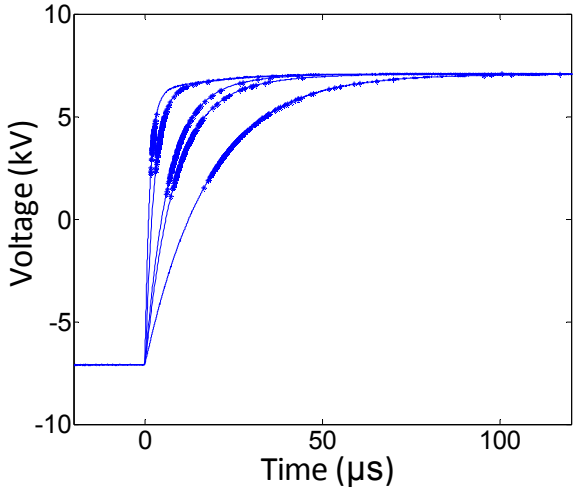

Figure 4.4 *PDs at different voltage rise times T_1 to T_5 at 7.1 kV peak voltage; note that the PD generally starts at higher voltage levels for shorter rise time.*

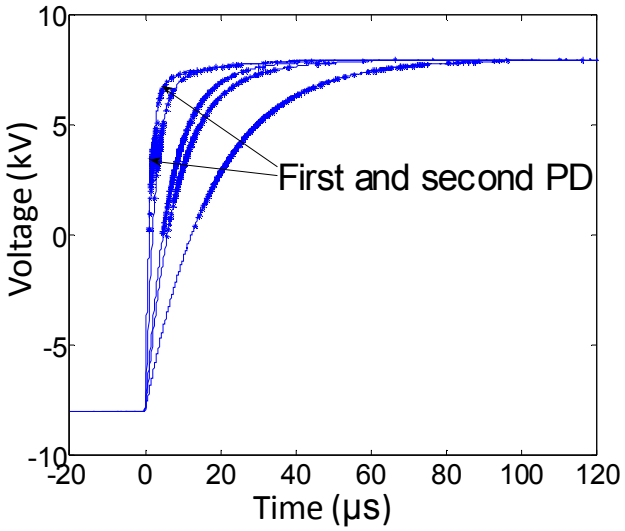

Figure 4.5 *PDs at different voltage rise times T_1 to T_5 at 8 kV peak voltage. Here a second cluster of PDs is visible also at short rise times, while even a third cluster can be seen for the longest ones.*

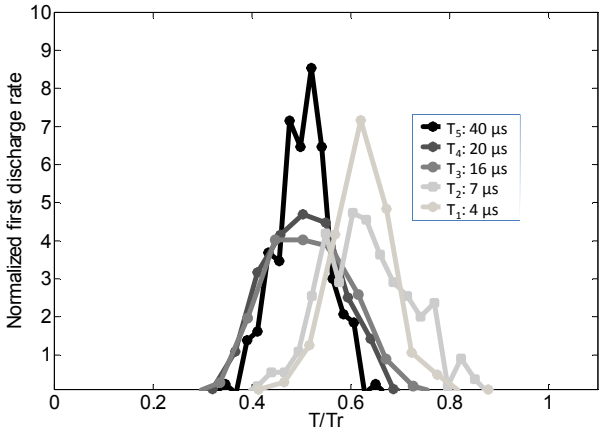

Figure 4.6 *Normalized first discharge rate at 7.1 kV, note the delay of the PD distribution for shorter rise times.*

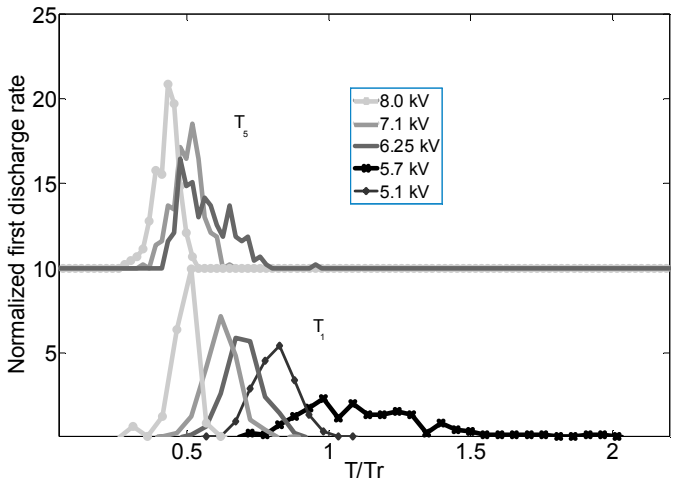

Figure 4.7 *Normalized first discharge rates at various voltage levels. The delay between short (4 µs) and long (40 µs) rise time remains at all the levels down to the extinction voltage (note that the T_5 y-scale is offset by 10 for clarity).*

4.3.2 Distribution of PD amplitude

To better understand the discharge process in the cavity, clearly more indications are needed. Indeed the most common property associated with PDs is their amplitude (in V or apparent charge (pC)). In this section, the original PD decoupler, shown in Figure 2.1, was employed.

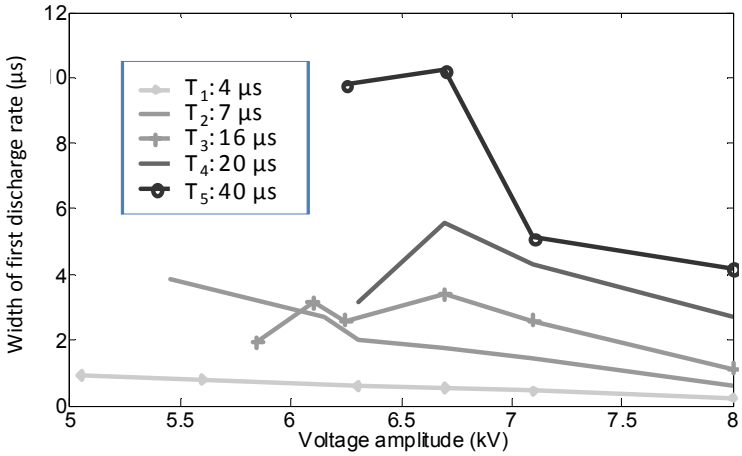

Figure 4.8 *Time half-width of the discharge rate distributions, the difference decreases at higher voltage levels.*

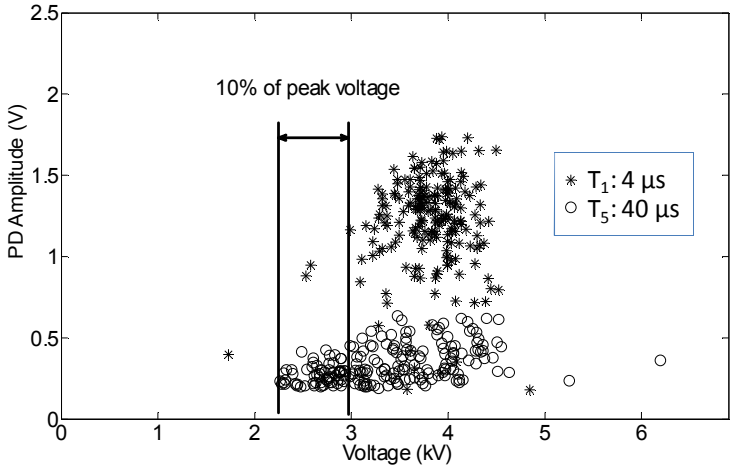

Figure 4.9 *Amplitude of PDs as function of the voltage when they appear for peak voltage of 6.2 kV. Note that the shorter rise time has larger amplitude and is displaced to higher voltages by about 10% of the peak-to-peak voltage.*

By measuring the PD amplitude as a function of the applied voltage, differences could be observed in both the amplitude and in the voltage level at which PDs occur for the shortest (T_1) and the longest (T_5) rise times. It is shown in Figures. 4.9 – 4.10 for voltages of 6.2 and 7.1 kV respectively. It can be concluded from the figures that the measured PD amplitudes are larger at shorter rise times, but that they also appear at higher voltage, which was already illustrated in Figure 4.4. At the shorter rise time T_1 PDs are on average displaced to higher voltage levels by about 10% of the peak level as compared to longer one, which again indicates that the shape of the applied voltage has a significant influence.

It is also apparent from Figures 4.9 – 4.10 that the PD amplitude increases when the applied voltage is raised from 6.2 kV up to 7.1 kV for the shorter rise time T_1, which is not the case for the longer rise time. Here instead of two large discharges per period,

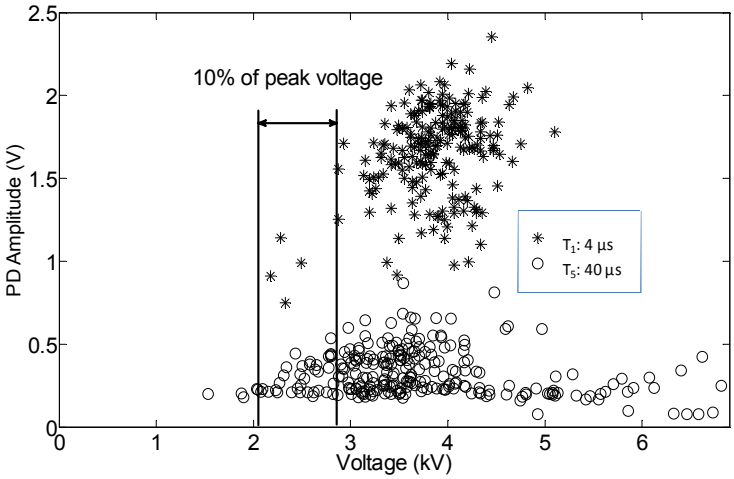

Figure 4.10 *Amplitude of PDs as function of the voltage when they appear for peak voltage of 7.1 kV. Here the amplitude difference for PDs at T_1 and T_5 is even more pronounced than in Figure 4.9.*

several smaller discharges are registered. An important observation is that at 6.2 kV on average two PDs per period are detected for all rise times. The PD amplitudes are however 3 - 4 times higher for T_1 than for T_5, which should certainly influence the charge distribution in the cavity and thus contribute to the large difference in extinction and inception voltage as seen in Figure 4.3.

According to [13] the voltage level required for breakdown in a dielectrically isolated cavity is approximately 5% higher for streamer than for Townsend types of discharges. The fact that PDs starts to occur at a higher voltage level for the short rise time T_1 as compared to the long one T_5, motivates a belief that one perhaps deals with discharges of different nature. This hypothesis is further strengthened by the fact that discharge amplitudes also differ significantly, as it is known that Townsend and streamer mechanisms show large differences both in amplitude and rise time of the discharge signal [12, 13].

4.3.3 Correlation between first and second PD

The relation between the first and second PDs in the same half-period when both are observed may provide additional evidence for changing the discharge mechanism. The following Figures 4.11 - 4.13 compare the second PD amplitude to the peak amplitude of the first one at 8 kV_p. Based on these results it can be noticed that the sum of the first and second PD amplitudes seems to be limited by an expression of the form:

$$a \cdot pd_1 + b \cdot pd_2 = 1 \qquad (4.2)$$

where a and b are constants. If $a \approx b$, this equation implies that the summed amplitude of all PDs occurring during a period is roughly constant and the PDs are dependent on each other. In contrast, if a is significantly different from b or such a limit cannot be observed, the PD amplitudes are not limited by the sum rule and may be independent. The estimated location of this limit is indicated in each of the figures.

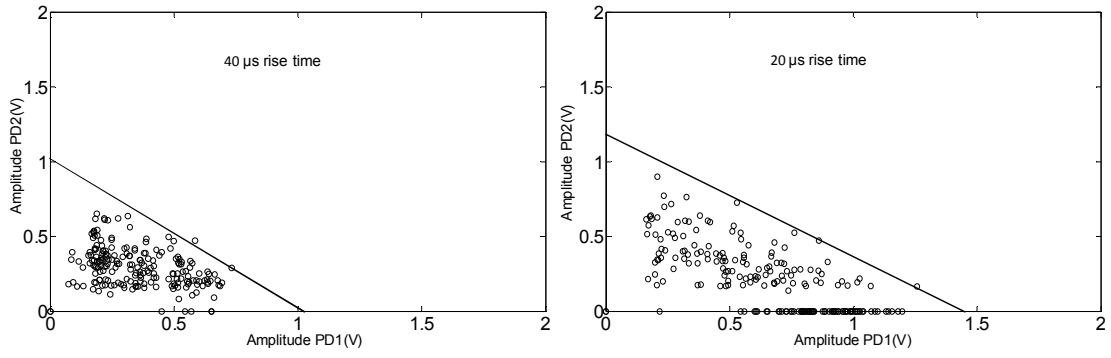

Figure 4.11 *Second PD amplitude as function of first one for 40 and 20 µs rise times. Note that for steeper voltages the amplitude increases particularly for the first PD.*

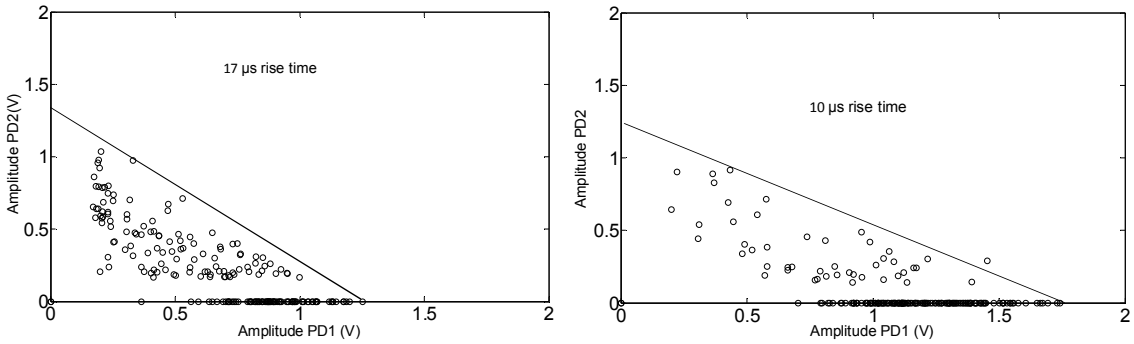

Figure 4.12 *As the rise time is decreased from 17 down to 10 µs, the second PD has about the same amplitude while the first keeps increasing.*

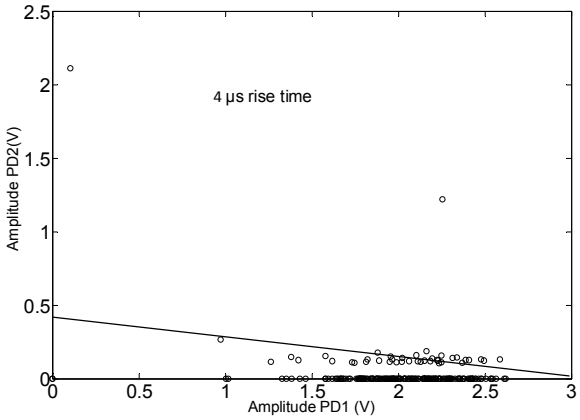

Figure 4.13 *At 4 µs, the second PD shows severely reduced amplitude when observed.*

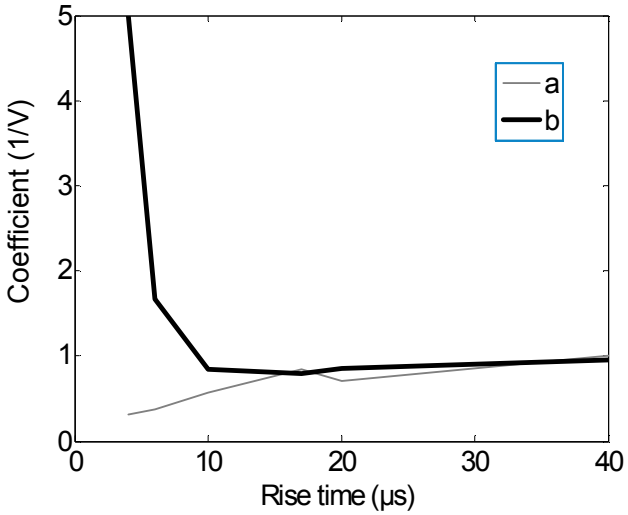

Figure 4.14 *Coefficients a and b of Equation 4.2 diverge for short voltage rise times.*

For the shorter rise times usually one PD occurs at each polarity change but in a few cases a secondary one could be observed at this voltage level. For decreasing rise times, the amplitude of the first PD will increase considerably especially when compared to the second PD (as far as a second PD appears). This makes the

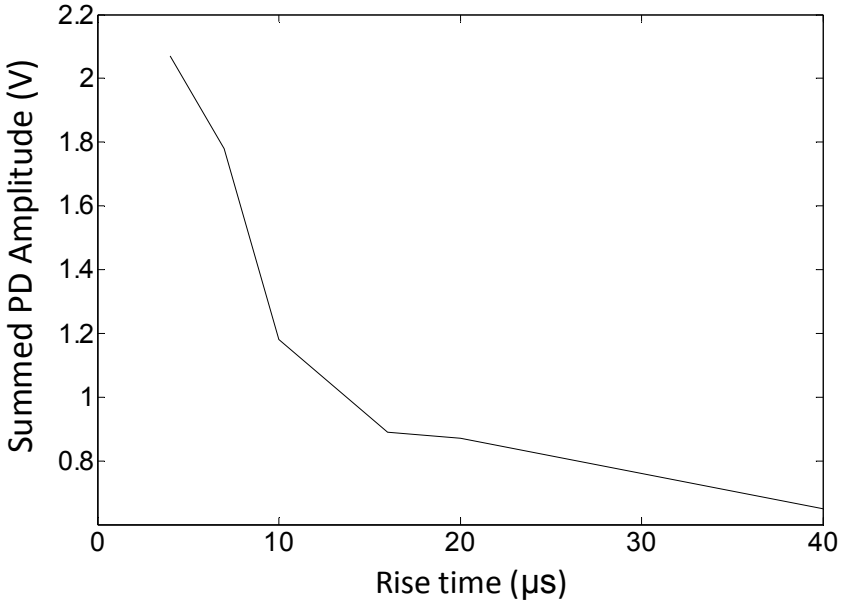

Figure 4.15 *Summed PD amplitude (in V) per polarity reversal as a function of voltage rise times for a cavity of 3.5 mm in diameter at 8 kV_p voltage.*

estimation of a limit in Figure 4.13 more difficult. If the coefficients *a* and *b* of Equation 4.2 are estimated for each of the rise times investigated, as shown in Figure 4.14, the influence of rise time becomes especially obvious at rise times shorter than 10 – 17 µs. Thus the amplitude relation between the first and the second PD gives further evidence that the transition, noticed in Figure 4.2 is a consequence of a significant change of PD properties.

Although the number of PDs increases at longer rise times of the applied voltage it can be noticed, as seen in Figure 4.15, that the total summed PD apparent charge increases considerably at shorter voltage rise times. This, together with the indication from Figure 4.14, definitely motivates the conclusion that the rise time of the applied voltage influences the magnitude and distribution of the occurring PDs considerably.

4.3.4 PD signal rise time

The rise time of the actual PD event is a characteristic indicator of the discharge mechanism [12, 13]. Due to the resonant character of the used PD decoupling, the actual PD rise time or its duration is here reflected in the acquired signal of the observed PD event. To investigate possible differences, it is necessary to resolve transient signals in the range of ns. To enable the use of a fast digitizer with low resolution, an improved PD decoupler circuit had to be employed, circuit alternative 1 as described in chapter 3. An example of measured PD signals for two different rise times (2.5 and 40 µs) occurring in a cavity with 3. 5 mm diameter exhibits a considerable difference in rise time, as shown in Figure 4.16.

The rise times of the PD signals were measured to be approximately 8 and 4 ns, respectively for the 40 and 2.5 µs voltage rise times. The average PD rise times and

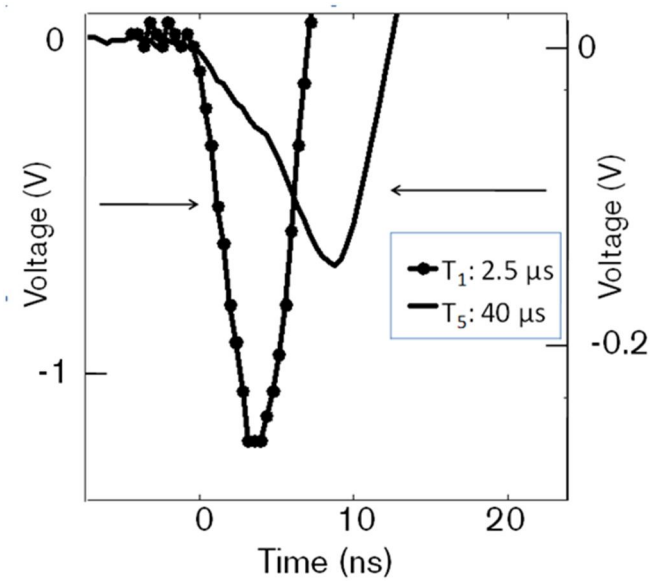

Figure 4.16 *PD signals measured at two different voltage rise times, the shorter rise time results in a faster rising and stronger PD signal. Note the different y-scales for the two signals.*

the standard deviations for both the voltage rise times, based on data from 100 recorded periods, are presented in Table 4.1.

Table 4.1 *Comparison of PD signal rise time.*

Applied voltage rise time (µs)	2.5	40
Average PD rise time (ns)	4.3	7.0
Std. dev. (ns)	0.8	2.3
Corrected PD rise time *	1	7

*From Figure 3.24.

The standard deviation values indicate that the difference seen in Figure 4.16 has some statistical significance, even for a reasonably large number of discharges. It is apparent from Table 4.1 that the measured PD rise time is shorter for the shorter rise time of the applied voltage but the difference is not large enough to firmly conclude that it is due to a change of the actual PD mechanism. In [61] a difference in spectral content has been observed for different rise times, which agrees with the results presented here.

One method to correct for the distortion of the PD signal rise time is to simulate the response of the decoupling circuit, as discussed in chapter 3.5. Figure 3.12 indicates that, for the shorter voltage rise time, the measured PD rise time should correspond to about 1 ns and for the longer to about 7 ns, as for the latter the circuit responds approximately correctly. This means that the PD rise time for the shorter voltage rise time could indeed be in the range of what is expected of a streamer type of discharge. It was illustrated in chapter 3.6 how the measured PD signal could be employed to recreate the initial signal, which allows providing both the shape and the amplitude of applied voltage as well as the voltage step caused by PD.

The recreation approach is applied here to two measured PDs signals, each similar to the data shown in Table 4.1. Both the analytical and the measured transfer function are used. For the short rise time, the original signal used in this comparison is illustrated in Figure 3.28. Figure 4.17 shows the recreated voltage steps due to a PD using both the transfer function alternatives as well as the measured PD signal.

The rise time of the recreated PD step is in both cases estimated to be about 10 ns, which is longer than the 4 ns measured in the original signal. This is in a strong contrast to the simulated circuit response discussed above, which suggests 1 ns as the actual PD rise time. Clearly, more work is required before the actual rise time can be obtained by recreation of the voltage on the coupling capacitor.

After recreation of the first PD for a longer rise time, 40 μs, following the same approach, the resulting signals are shown in Figure 4.18, from which it can be concluded that the voltage drop is smaller and the rise time is estimated to be about 20 ns. This is again longer than the 7 ns of the original signal. However, the PD rise time has increased as compared to the shorter voltage rise time.

In conclusion, this study of PD signal rise times has shown that there is a clear difference depending on the voltage rise time, which is a further indication of a possible change in the PD mechanism. Regarding the true actual PD rise time, the methods applied here provide different results and thus further work is needed to obtain more reliable results.

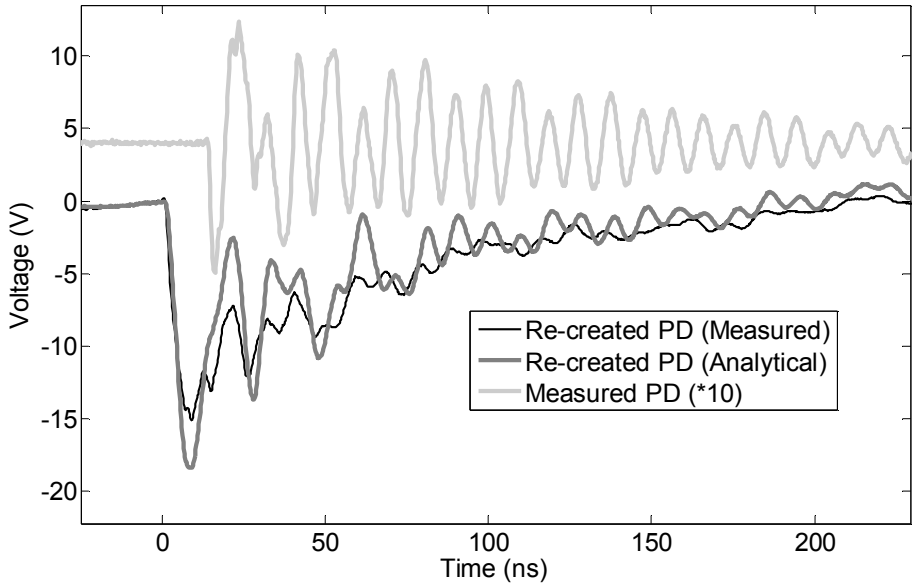

Figure 4.17 *Recreated signal for the first PD occurring for an applied voltage of 2.4 μs rise time. The measured PD signal is enlarged 10 times.*

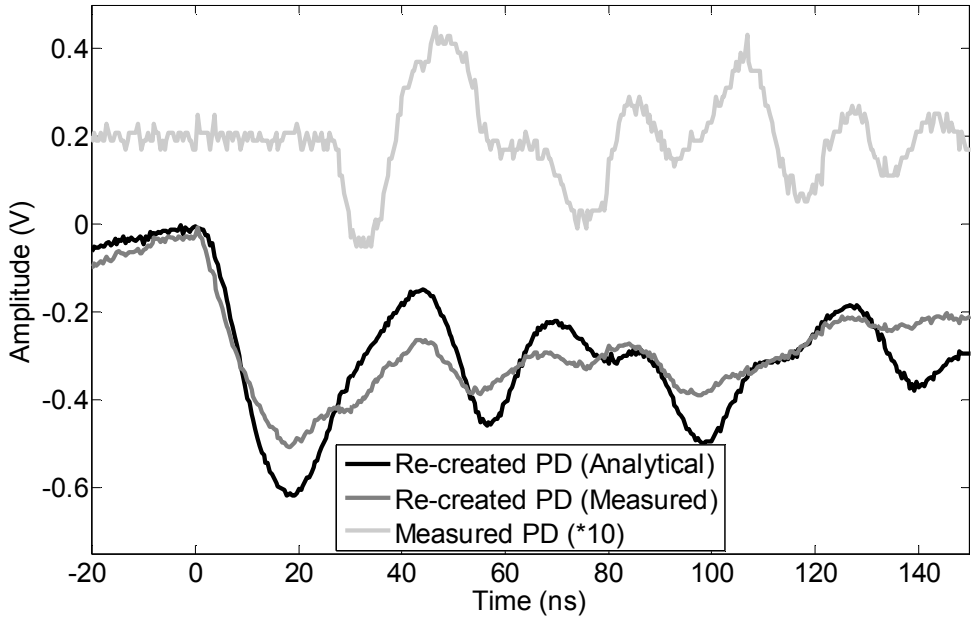

Figure 4.18 *Recreated signal for the first PD occurring for an applied voltage of 40 μs rise time. The measured PD signal is enlarged 10 times.*

4.4 Cavity exposed to unipolar voltage

The results presented so far all suggest that the use of voltage waveforms with steeper rise times increases the PD amplitude considerably. In [49] the concept of active insulation was introduced whereby charging the surface of dielectrically insulated electrodes with unipolar impulses could increase the breakdown voltage level considerably. Different rise and tail times were utilized in form of standard impulses for testing lightning (1.2/50 μs) and switching (250/2500 μs) insulation characteristics. As in the present study bipolar waveform has been applied in all the cases, it is thus important to find out whether the observations presented seem to be valid also for unipolar voltages. A broader range of the voltage rise times of positive voltage pulses was applied and a similar cavity as the one used in the previous investigations was employed (4 mm in diameter). Further the waveform used a frequency of 313 Hz as well as 50 % duty cycle. Applying a 2.5 μs rise time resulted in PD amplitude with about the same order of magnitude as for the bipolar waveform, as shown in Figure 4.19. It can be observed how the PDs closely follow the shape of the applied voltage waveform and increases in amplitude when occurring at the top of the pulse.

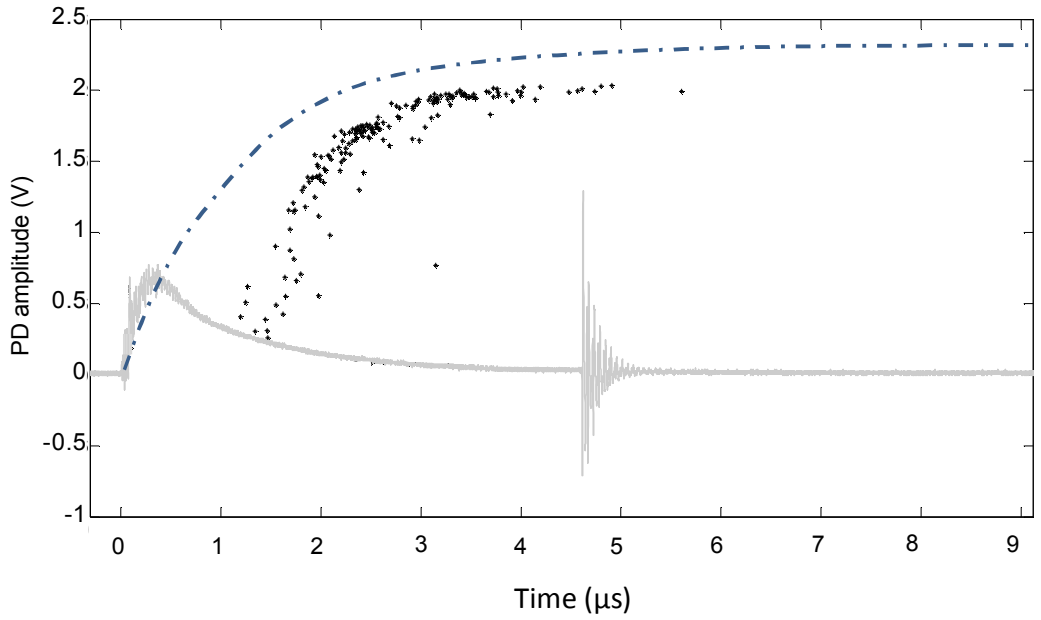

Figure 4.19 *PD amplitudes for unipolar pulses of 2.5 µs rise time and +6.5 kV peak value in relation to time. One of the measured PD signals is shown as an example.*

Increasing the rise time to 7 µs reveals that the distributions start to show less influence of the applied voltage shape, as seen in Figure 4.20.

Figure 4.21 shows that for a long rise time, 160 µs, the PD amplitude is considerably reduced by at least a factor of 4, similarly to the results for bipolar voltage.

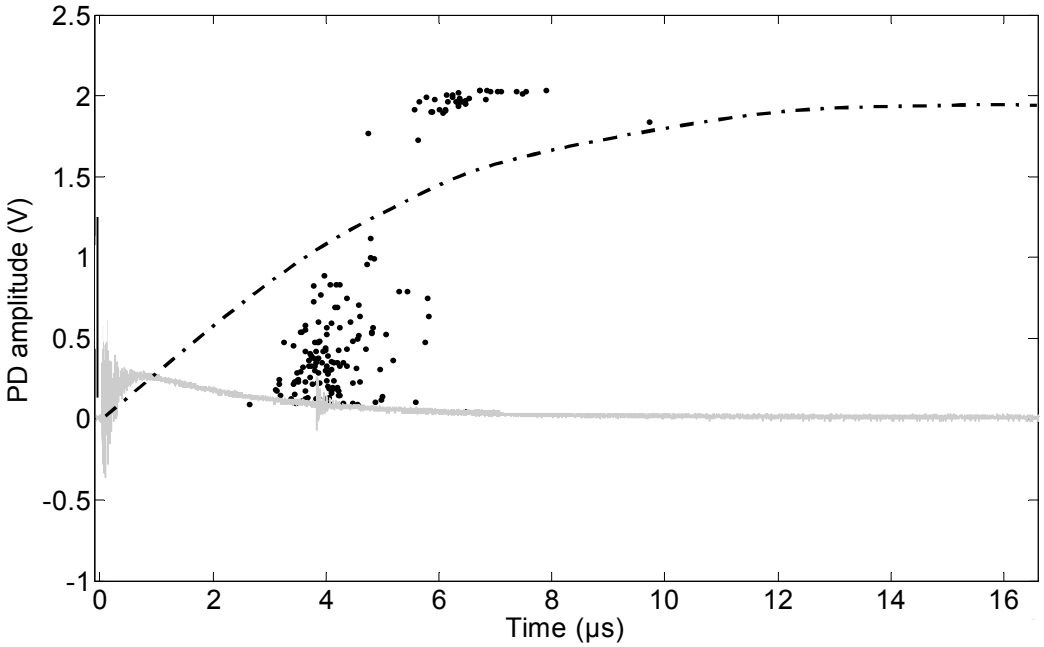

Figure 4.20 *PD amplitudes for unipolar pulses of 7 µs rise time and +6.5 kV peak value in relation to time. Note the changes in the distribution.*

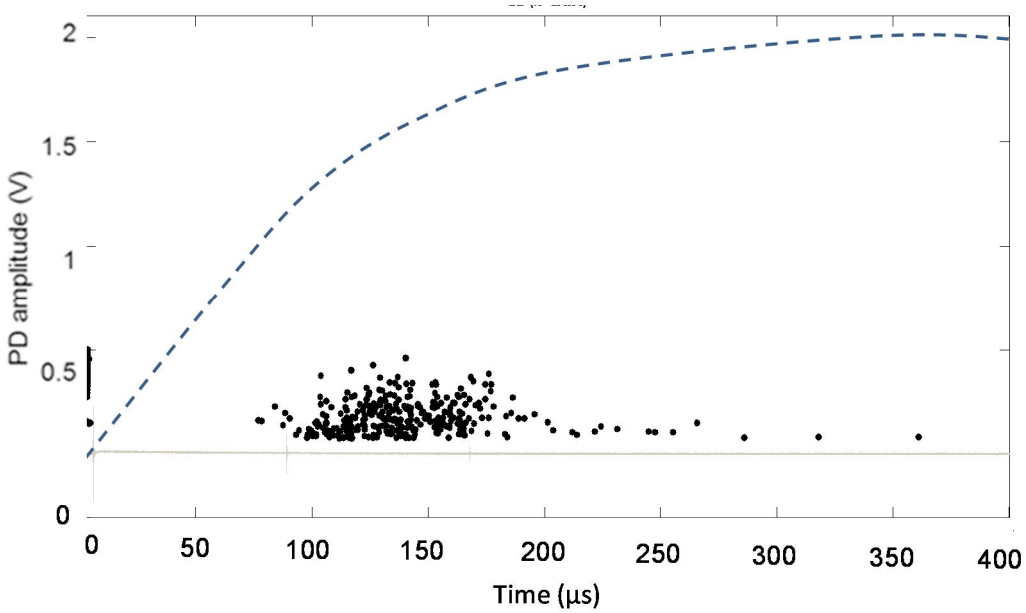

Figure 4.21 *PD amplitudes for unipolar pulses of 160 µs rise time and +6.5 kV peak value in relation to time. Note that the shape of the voltage flank is no longer reflected in the PD pattern.*

To facilitate the comparisons between different rise times the distribution of normalized first discharge rate were employed similarly as for the bipolar case.

In a case a PD takes place, positive and negative charges are deposited on cavity walls and if not decaying completely between two consecutive flanks they will delay occurrence of the next PD until the voltage across the cavity reaches high enough level. The likely implication is that the PDs, on average, will occur at a higher voltage level. Figure 4.22 shows the relevant first discharge rates for voltage rise times ranging

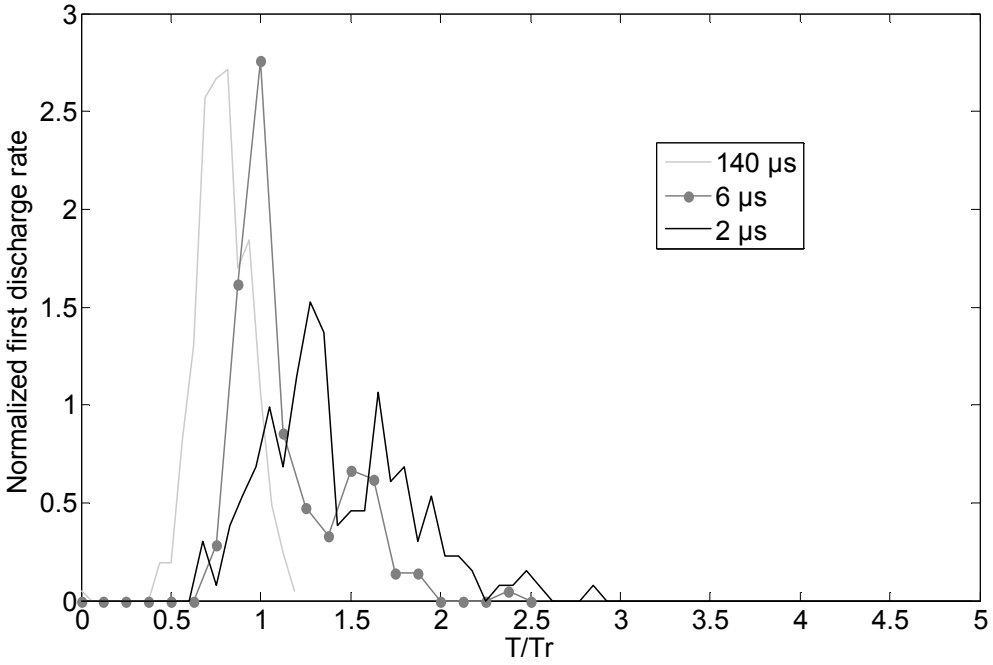

Figure 4.22 *Normalized first discharge rate. As observed the delay in relation to the flank increases for shorter rise times.*

between 2.5 and 160 µs. Compared to the previously shown in Figure 4.7 distributions for bipolar wave shapes, the normalized time until PDs start do not increase, however the spread becomes broader with decreasing voltage rise time. This feature may probably result as an effect of the unrelaxed charges on the cavity walls. The correlation between the rise time and PD amplitude still remains apparent for the unipolar waveforms.

Table 4.2 *PD characteristics for different rise times with unipolar voltage at 6.5 kV_p.*

Rise time (µs)	2.5	7	160
Number of PDs/cycle	2	2.05	2.4
Total amplitude (V)/cycle	1.6	0.7	0.24
Extinction voltage level	10	10.2	12.5

The difference in extinction voltage between the exploited rise time extremes was larger than 2 kV, which confirmed the observations presented earlier in Figure 4.3. Thus both the tests utilizing bipolar and unipolar waveform indicated a stronger PD impact at shorter rise times. Additionally, it has been shown that the PDs behave similarly at both increasing and decreasing voltage flanks. Data presented in Table 4.2 shows that the total summed amplitude of PDs differs between 2 to 8 times for the rise times applied. This means that using a wave shape with different rise and fall time would imply variations in the net charge deposited on insulation walls.

4.5 Varying cavity dimension

The investigations presented hitherto have been based on a cavity of 3.5 mm in diameter. This will now be expanded to other dimensions; both the cavity diameter and height will be varied to investigate whether the change of PD properties can still

be observed. If so, possible variations will be very interesting to note. These investigations were all performed with the modified decoupling circuit alternative, discussed in section 3.2.

4.5.1 Cavity diameter

Several cavity diameters were tested: 1, 2, 4 and 10 mm. Here one short and one long rise time, 2.5 and 160 μs respectively, were applied. The extinction voltage plots for 2 and 10 mm cavities are shown in Figure 4.23, further confirming that the observations presented in Figure 4.3 and in [10] remain, at least quantitatively, valid for the different cavity diameters.

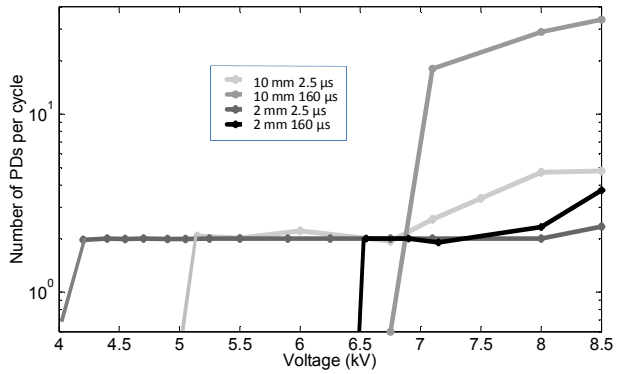

Figure 4.23 *Extinction voltage plot for cavities of 2 and 10 mm in diameter. Note that the prevailing difference in PD characteristics discussed in section 4.2.*

By plotting the PD amplitudes as a function of the instantaneous voltage one could observe differences in both the amplitude and the voltage level at which PDs occur for all the investigated dimensions, as shown in Figures 4.24-4.27 for 1 to 10 mm cavities, respectively. For the 3.5 mm cavity, it was observed that the decreasing rise times gradually changed the PD characteristics from a linear to no dependence on the number of PDs detected as function of the applied voltage. Here two rise times were applied, 2.5 and 160 μs, and these were intentionally chosen shorter and longer as the ones presented in Figure 4.3. At the shorter voltage rise time (2.5 μs) PDs are on average displaced to higher voltage levels by about 10% of the peak value in all the cavities tested, which again indicates that the shape of the applied voltage has a significant influence. The PD amplitude for the long rise time (160 μs) remained about the same in all cavity dimensions whereas it increased with cavity diameter for the short rise time.

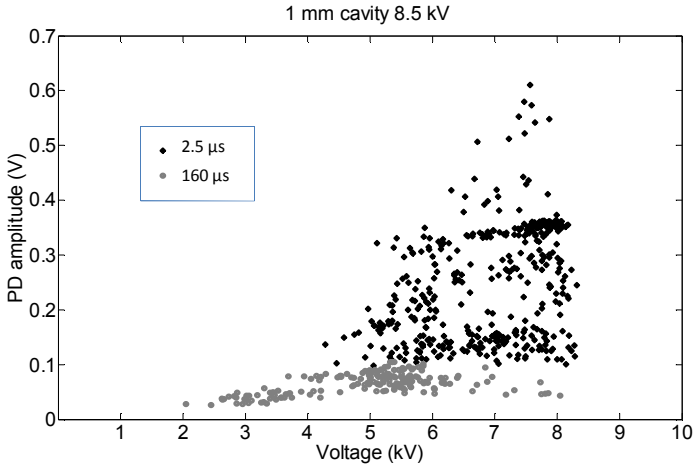

Figure 4.24 *Amplitude of PDs occurring in a cavity of 1 mm in diameter as a function of the applied voltage. The PDs occur at significantly higher voltage levels for the shorter rise time and have considerably higher amplitude.*

The electric field level (not considering space charges) will for a given external voltage be higher in the cavities with larger diameter, which might influence inception and extinction voltage. As the number of discharges for long and short rise times is different, it is interesting to compare the summed PD amplitude during each cycle. Figure 4.28 shows the average single PD amplitude and the total summed PD amplitude per cycle for all the cavity dimensions. It is apparent that although the total number of PDs increases at longer rise times, the total summed amplitude remains considerably lower. This was also observed for the 3.5 mm cavity and appears now to be valid also at several cavity dimensions. The PD amplitudes are on average 3 - 4 times higher for the short rise time than the long one, which should certainly influence the charge distribution in the cavity and thus contribute to the large difference in extinction and inception voltage, as seen in Figure 4.2 for different rise times.

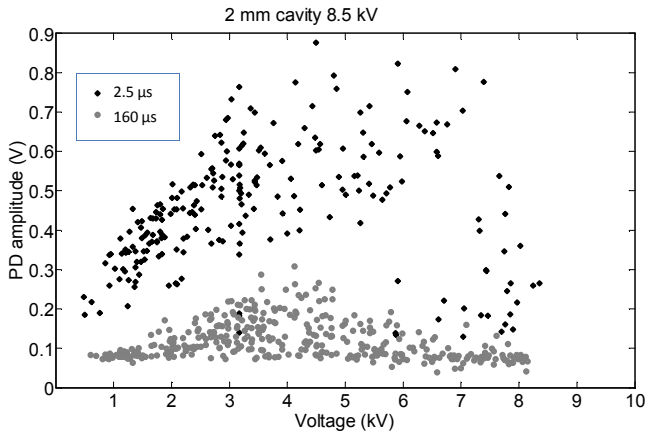

Figure 4.25 *Amplitude of PDs occurring in a cavity of 2 mm in diameter as a function of the applied voltage. At this cavity size there is no significant difference in the voltage of PD occurrence in contrast to all the other cavity sizes. This may be a statistical effect.*

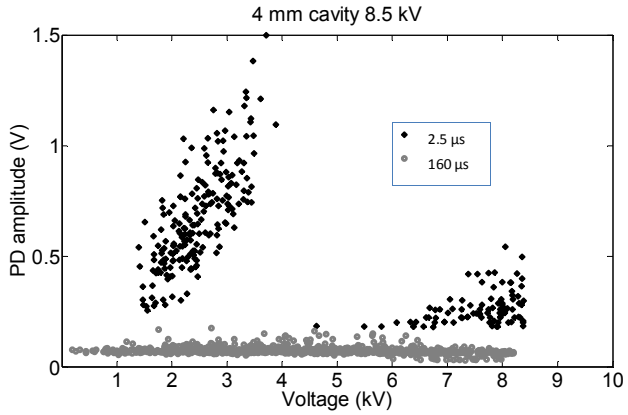

Figure 4.26 *Amplitude of PDs occurring in a cavity of 4 mm in diameter as a function of the applied voltage. In this figure two generations of PD are visible for the short rise time. Note that the amplitude scale is about twice as large as in Figures 4.24 – 4.25.*

The delay until a PD occurs depends on the available electrons in the defect but also on the electric field strength. Considering the electric field from an electrostatic calculation as in Figures 4.29 – 4.30, where a fixed voltage potential is applied on one side of the polycarbonate material and the other is grounded, one observes a more homogenous field distributions for larger cavity diameters and, at the same time, the smaller cavities do not reach the same peak of field strength as in the larger ones. This result suggests that the voltage required for initiating PDs should increase at smaller cavity diameters. However, as the electric field in the actual case is additionally influenced by surface and volume charges, the appearance of lower extinction voltage for the smaller cavity dimensions can be explained as being affected by charges remaining on the defect walls.

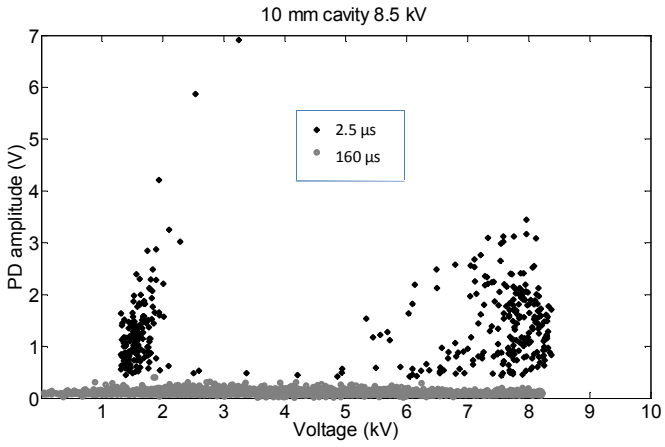

Figure 4.27 *Amplitude of PDs occurring in a cavity of 10 mm in diameter as a function of the applied voltage. The PD amplitudes have increased considerably as compared to those presented in figure 4.25.*

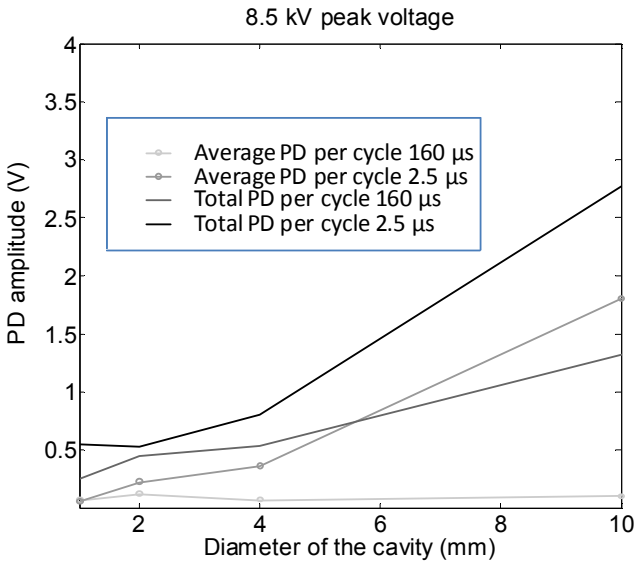

Figure 4.28 *Total and average PD amplitudes in cavities of different diameters. Note that the average PD increases significantly with increased diameter.*

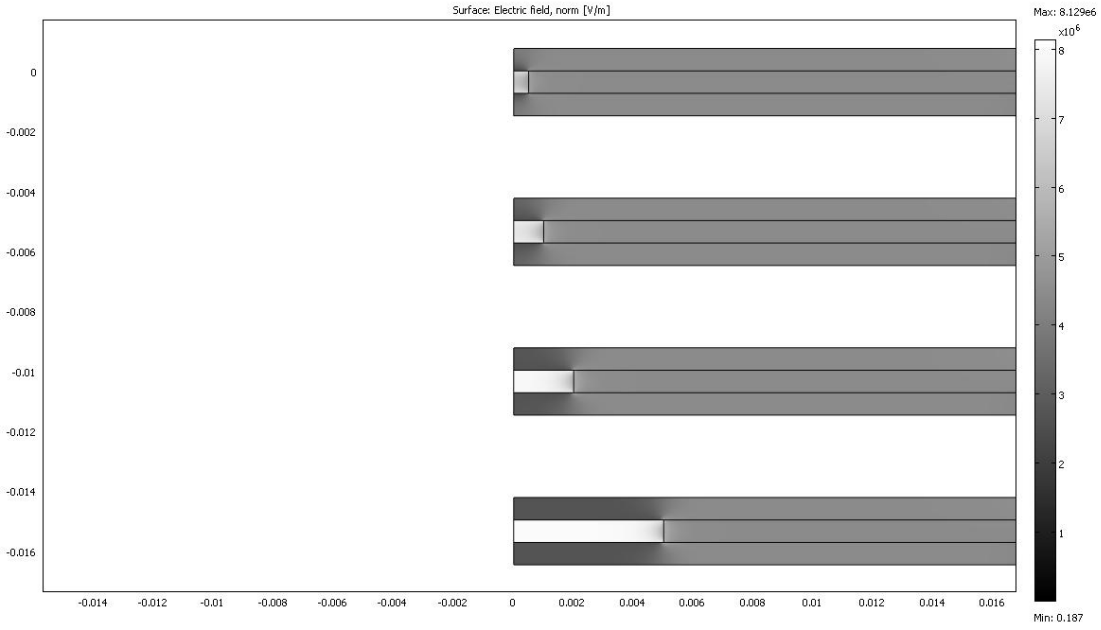

Figure 4.29 *Total simulated electric field in each of the tested cavities (1, 2, 4 & 10 mm in diameter).*

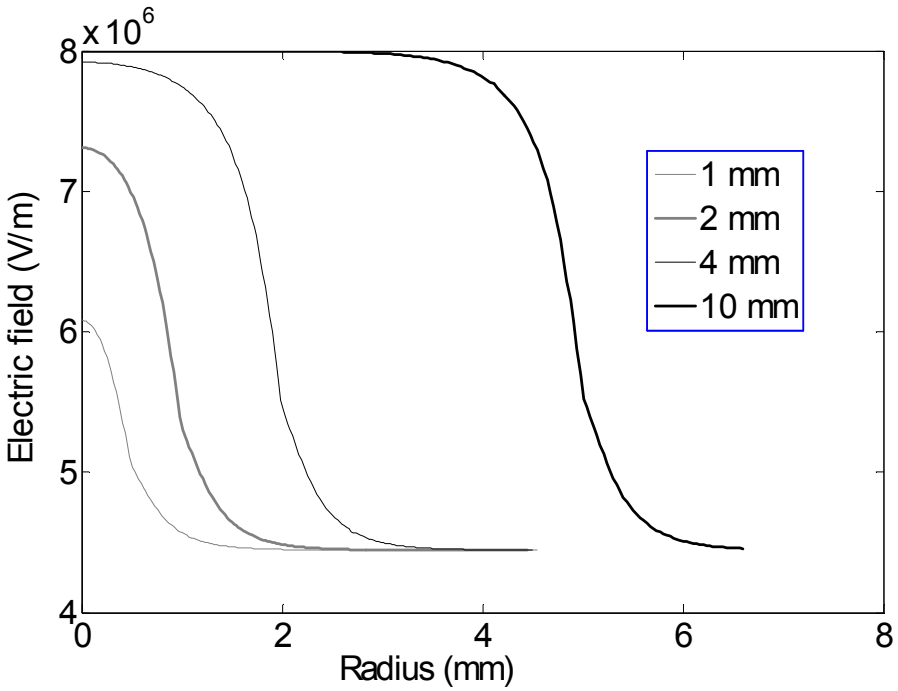

Figure 4.30 *Total simulated electric field across the central part in investigated cavities. Note that a cavity with smaller diameter implies less homogenous electric field distribution for the same applied voltage.*

4.5.2 Cavity height

To investigate how the PD characteristics are affected by the cavity height, a test with two different rise times of the applied voltage was performed on two cavities, each 10 mm in diameter. One cavity was formed in a 0.75 mm thick polycarbonate material and the other was in a 0.1 mm thick PET film. The measurement procedures were in all other aspects identical to the previously presented approaches.

The first investigation regarded the number of detected PDs at different voltage levels for 2.5 and 160 μs voltage rise time and the results are illustrated in Figure 4.31.

An obvious observation is that the difference in extinction voltage prevails despite a considerable reduction of the cavity volume. The transition between linear and a constant number of PDs detected per period is however less pronounced.. The number of PDs detected in the thinner cavity is smaller for the longer rise time, which is likely to be connected to the reduced volume.

If the distribution of first PDs occurring at one voltage level is compared, a reduction in the delay between the different investigated rise times can be noticed for the thinner cavity, see Figure 4.32. The normalized probability distribution for the first PD to occur is similar for both cavities exposed to the longer rise time, however for the shorter rise time the probability decreases for the smaller thickness.

Due to the significant thickness decrease, the electric field in the cavity becomes considerably higher for the same voltage, which will affect the generation of free

electrons and according to the Paschen curve also the extinction voltage levels. This effect is clearly seen in Figure 4.26.

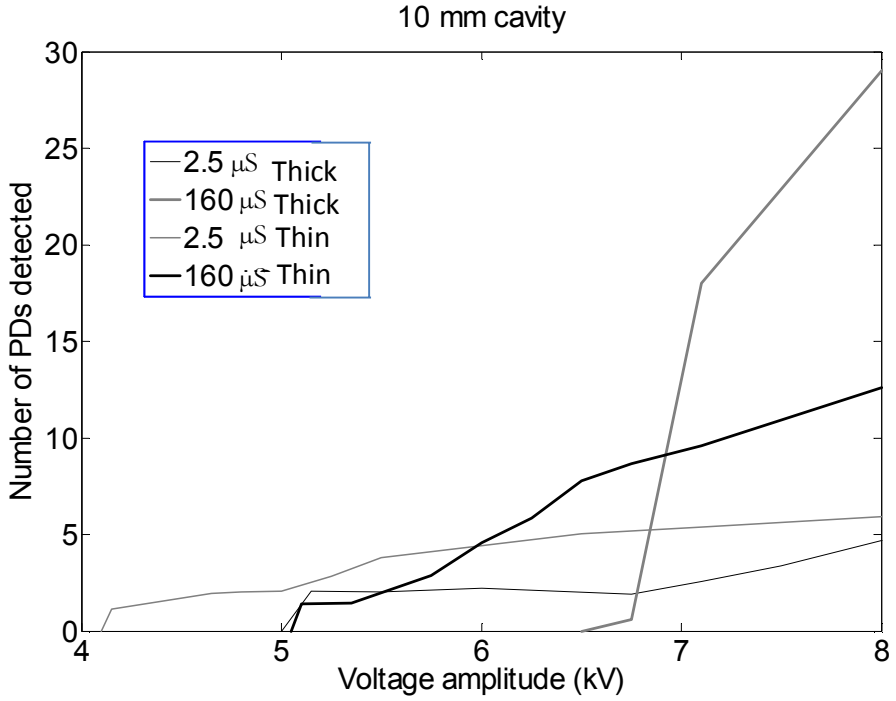

Figure 4.31 *Number of PDs detected at two voltage rise times for cavities of two different heights, 10 mm in diameter each.*

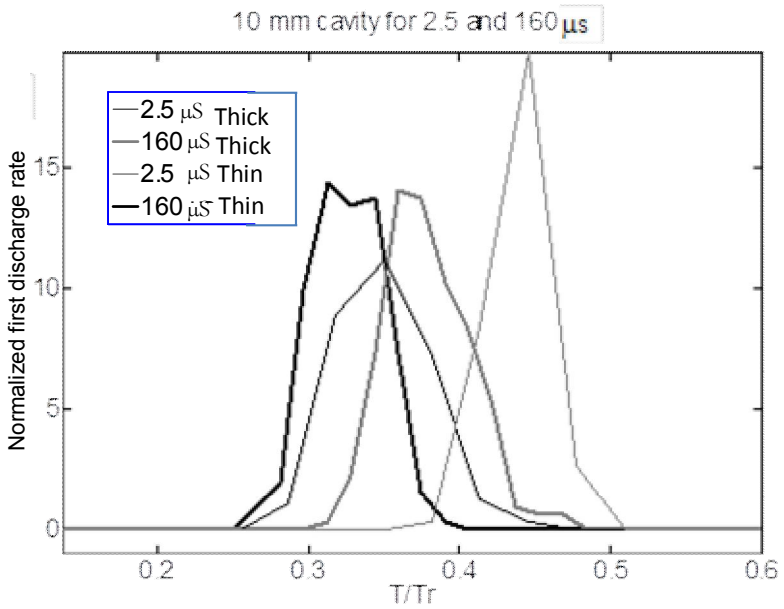

Figure 4.32 *PD distribution for two different cavity thicknesses. Note that the difference in time delay decreases for the thinner cavity thickness.*

When summarizing the total amount of charge released, it is seen that the total apparent charge increases considerably when a shorter rise time is applied, see

Table 4.3. This agrees well with the results presented in sections 4.2 and 4.3. Based on this result it is clear that the PD amplitudes remain larger for the shorter rise time in the thin cavity, although a significant change in volume has been introduced. Additionally it can be noted that for the longer rise time the total PD charge increase is more dependent on thickness than for the short one. This resembles the observations made in [62] for Townsend discharges where the charge amount closely follows the height of the cavity.

The conclusion based on all the observations presented in this chapter is that the total apparent charge released during a PD event increases at steeper voltages. This further emphasizes the importance of continuing investigations regarding how the change of PD mechanism influences the associated material degradation.

Table 4.3 *The total apparent charge deposited at cavity surface at 8 kV_p.*

Thickness (mm)	Charge (2.5 μs) nC	Charge (160 μs) nC
0.75	10	6.8
0.1	8.5	3.5

4.6 Non-electrical observations

In order to elucidate the effect of voltage rise time on the material degradation, two polycarbonate cavities, 1 mm in diameter each, were exposed to 9.5 kV_p voltage pulses with 2.5 and 40 μs rise times. The voltage amplitude was selected to be well above the inception level. Results of a microscopic observations of the defects appearing on the surfaces of the cavity endplates are shown in Figures 4.33 and 4.34. The pictures reveal that for the longer rise time considerably smaller pit but of larger concentration occur on the surface of polycarbonate as compared to the one exposed to the pulses of shorter duration. This agrees well with the observations presented in the previous sections indicating that for shorter rise times the number of PDs decreases but the amplitude increases considerably. Thus the electrical measurements and the optical observations confirm a larger severity of the short rise times in a PD degradation process.

In particular, these results prove that the changed PD properties have an impact on how insulation materials degrade under PD exposure. It seems therefore likely that the effect discussed throughout this chapter will contribute to a reduced service lifetime, if certain conditions are fulfilled. Presently, we have only obtained some indications on what the "certain conditions" may be. More work is needed to identify and understand them in detail.

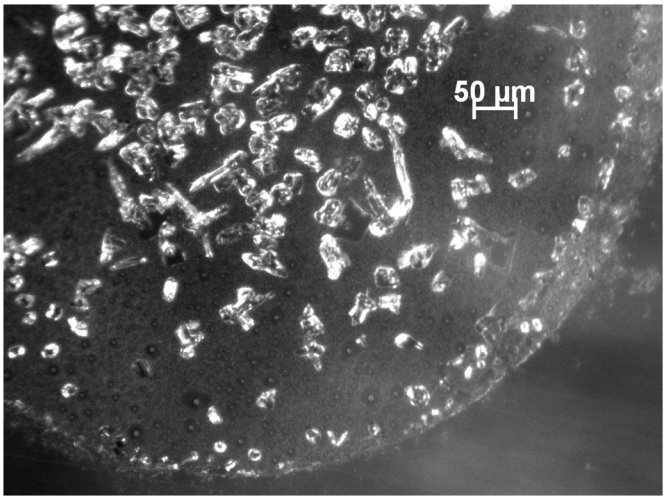

Figure 4.33 *Microscopic view of one of two cavity endplates after exposure to 2 million cycles at 2.5 µs rise time. Larger but fewer pits as compared to the endplate exposed to a longer voltage rise time are seen.*

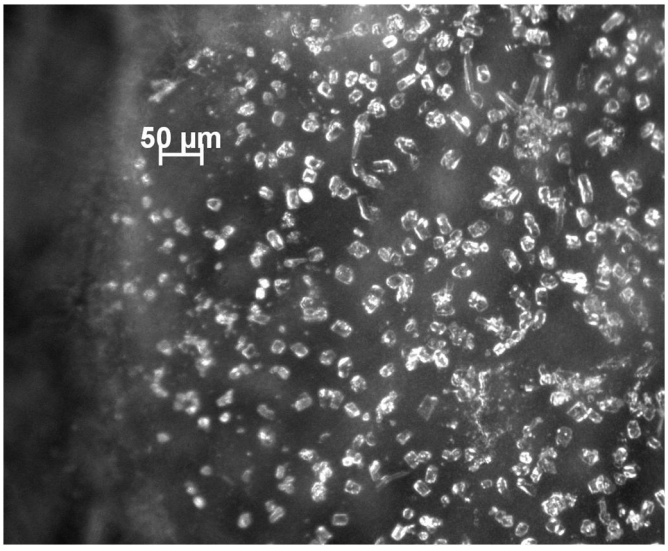

Figure 4.34 *Microscopic view of one of two cavity endplates after exposure to 2 million cycles at 40 µs rise time. A large number of small pits appear, approximately similar in size.*

A further observation is that the distributions of pits are not especially concentrated to the surroundings of the edges of the cavity, but rather evenly spread across the endplates. This suggests that the edge does not significantly influence the measured results other than reducing the electric field as indicated in the static simulations. Additionally, one may observe from Figure 4.34 that the field strength at the cavity wall is quite reduced for a 1 mm cavity as compared to the interior.

4.7 The critical rise time

It was shown in section 4.4 how the PD pattern changes at different rise times for unipolar waveforms and that for shorter rise times the PD distributions closely follows the shape of the semi-square voltage front. When a PD occurs at higher applied voltage its amplitude increases accordingly. For longer rise times this tendency gradually ceases and discharges of considerably smaller amplitudes, less related to the waveform itself, are observed. Thus investigations on how well the PRPD pattern resembles the waveform can possibly elucidate if similar behavior remains true for bipolar waveforms.

The bipolar case is therefore reanalyzed below. It should be noted that the results were obtained with the original PD decoupler (explained in Figure 2.1), in which the remnant of the applied voltage was considerably higher, thus influencing the accuracy. When applying a 4 μs rise time, a similar relation between PD amplitude and waveform as the one presented in Figure 4.19 seems to be present, see Figure 4.35. However, the relation is less pronounced than for the unipolar case, partly due to a smaller distribution width in relation to the rise time. Further it can also be noted that the spread in PD amplitude is larger and no PDs occur at the voltage maximum. At short rise times we thus observe similar but less clear tendencies for the bipolar case.

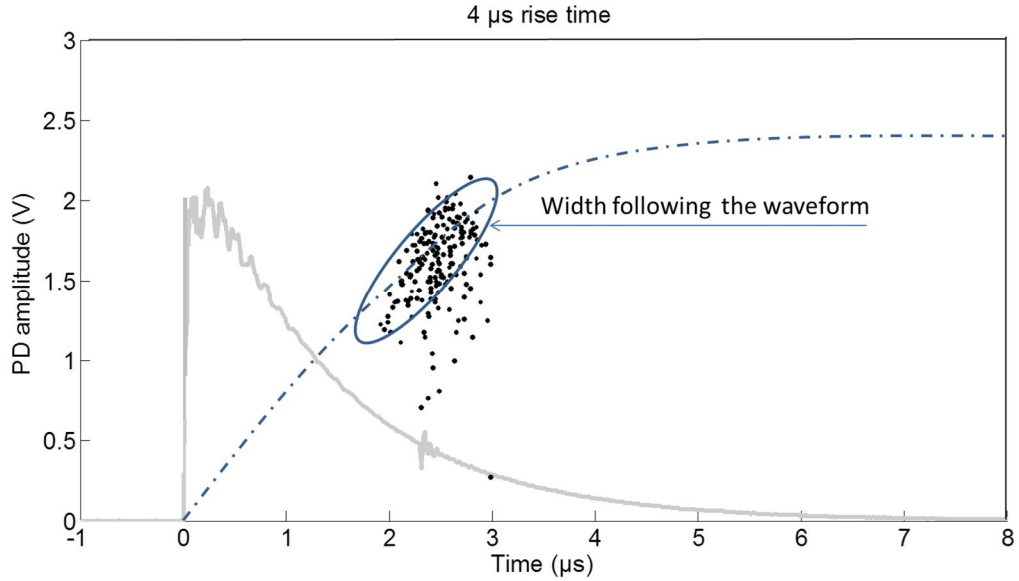

Figure 4.35 *PD amplitudes for bipolar pulses of 4 μs rise time and 7.1 kV peak value in relation to time.*

For the unipolar case with 7 μs rise time both large PDs close to voltage maximum and small ones at earlier stage are observed as illustrated in fig. 4.20. The same rise time for bipolar voltages shows less resemblance between applied waveform and PD amplitude, although some similarities are still present, Figure 4.36. The first PDs of a larger amplitude, are followed by a second group of PDs with much lower amplitudes. When increasing the rise time further to 40 μs the tendency of less dependence on waveshape continues, as can be observed in Figure 4.37. The average amplitude is considerably lower and more PDs occur closer to the polarity shift as indicated earlier in section 4.3.

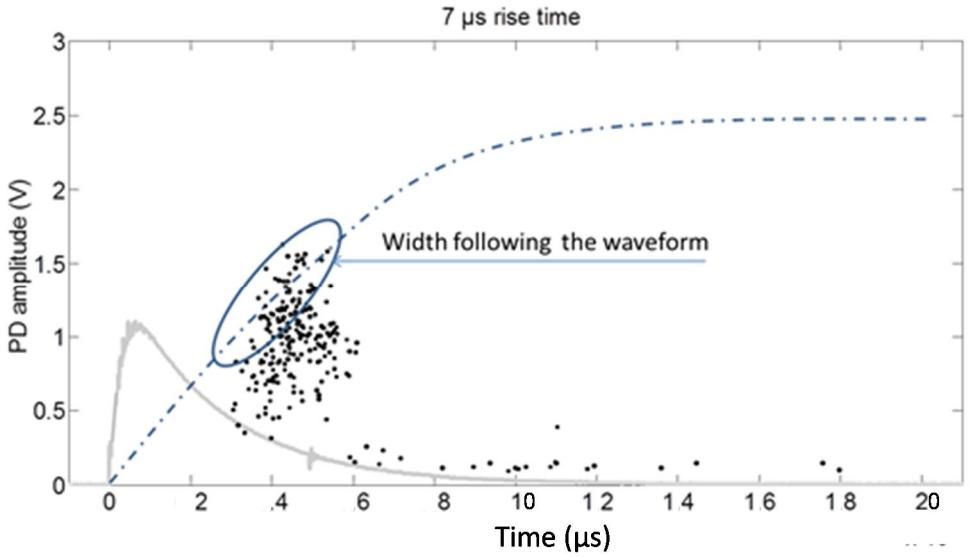

Figure 4.36 *PD amplitudes for bipolar pulses of 7 µs rise time and 7.1 kV peak value in relation to time. Note that the main difference is that PDs are observed earlier than for the unipolar case.*

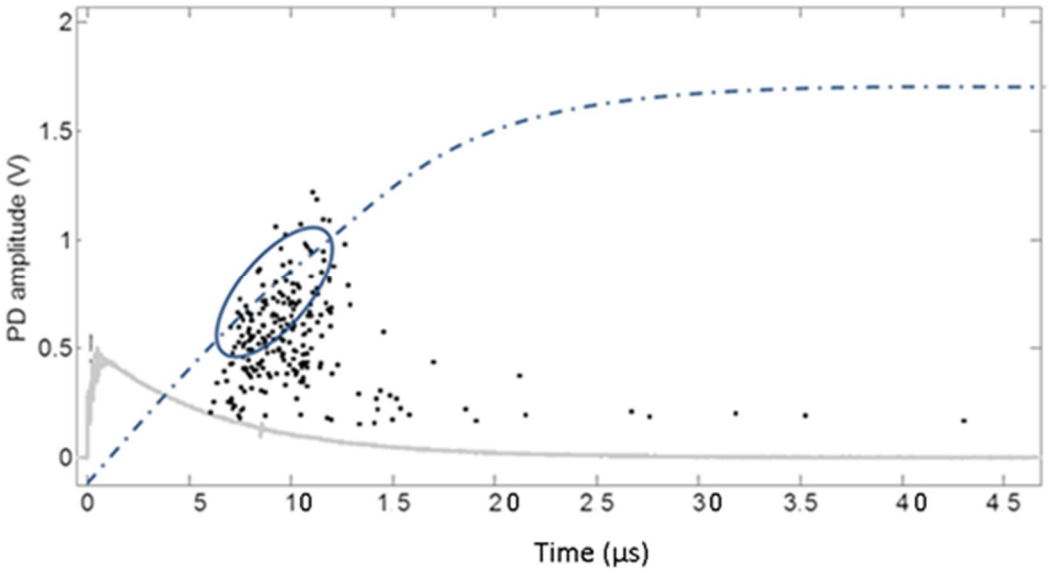

Figure 4.37 *PD amplitudes for bipolar pulses of 15 µs rise time and 7.1 kV peak value in relation to time.*

Table 4.4 lists the characteristic parameters for the bipolar case, which indeed indicates similarities regarding amplitude distribution, extinction voltage level as well as the number of PDs detected per cycle.

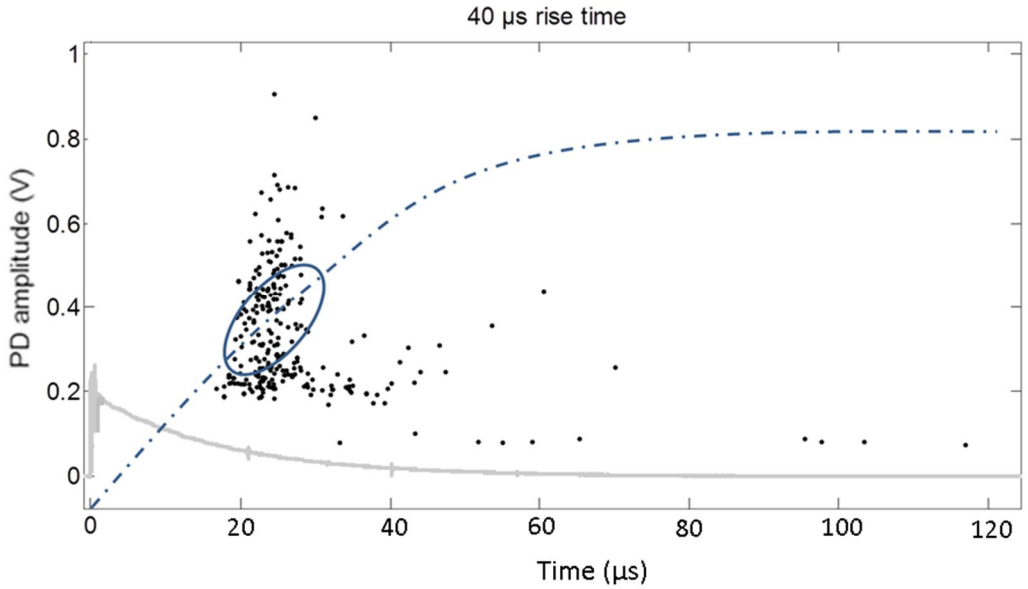

Figure 4.38 *PD amplitudes for bipolar pulses of 40 µs rise time and 7.1 kV peak value in relation to time. Note the reduced scale of PD amplitude and the elongated time scale.*

Table 4.4 *PD characteristics for different rise times with bipolar voltage.*

Rise time (µs)	4	7	15	40
Number of PDs/cycle	2	2	2.1	2.5
Total amplitude (V)/cycle	1.5	1.0	0.63	0.42
Extinction voltage level (kV)	9	10.6	11	12

4.8 Summary

It is shown in this chapter that PD extinction voltage characteristics change when a cavity is exposed to voltage pulses with shorter rise times, independent if unipolar or bipolar waveforms are applied. The dependence on voltage rise time becomes also apparent when other PD properties are analyzed, such as amplitude, time delay, correlation between consecutive discharges and discharge rise time. The effect seems to be repeatable and valid for different dimensions of cylindrical cavities, including large variation of cavity height as well as its diameter. This is an important observation from a practical point of view since defects in real insulation systems may considerably vary in size.

We have additionally showed that there are possibilities for a change in the cavity discharge mechanism when reducing the rise time of applied voltage pulses, manifested by enhanced discharge amplitude and shortening PD signal rise time. It is postulated that for the short rise times a streamer like discharges are likely to dominate, possibly yielding a stronger deterioration of the cavity walls. The results of electrical measurements were confirmed by microscopic observations of the damage patterns on cavity walls. The PD activities during shorter rise time result in a fewer

but deeper pits. This emphasizes the need to investigate how the long time degradation of polycarbonate and other materials can be affected by voltage waveforms of different rise times to extend investigations on internal PDs within insulations system as presented in [63].

5 PWM Waveforms

5.1 PD detection under PWM voltages

The time domain technique described in the previous chapters allows for exploration of the properties of PDs at varying voltage rise times and in various PD sources when applying semi square voltage pulses. The same approach can, in theory, be utilized to measure PDs at synthesized voltage shapes, such as Pulse Width Modulated (PWM) waveforms. However, some characteristics of PWM sources make the technique less suitable. It is possible, for example, to relate position of PDs with respect to specific polarity reversals, but it is not possible to relate these events to the phase position within the modulated waveform. Thus it becomes impossible to create a phase resolved PD (PRPD) pattern, which makes a direct comparison with sinusoidal conditions difficult. The way to overcome this issue is discussed in this chapter and a solution is presented. Also the degree of PWM waveform smoothness yielding the same level of PD activity as for sinusoidal waveforms is defined.

5.1.1 PWM waveform properties

In a PWM voltage pulse train the pulse width changes in relation to the phase position on the modulated waveform, as illustrated in Figure 5.1. The generated sinusoidal form defines the modulation frequency, whereas the pulse repetition rate is denoted the carrier frequency. PWM waveforms are further characterized by a modulation depth that reflects how much of the available pulse width is used for the modulation, less modulation means that pulse width variation is reduced. What is necessary to consider, is the phase drift between the carrier and modulation frequency, as indicated in the figure. This is especially important in cases when the ratio between the carrier and modular frequencies is not an integer, as the switching events do not appear at the same phase positions in different voltage periods. Further, there may appear jitters in the firing of the steps in addition to the phase drift, which altogether cause that pulses may vary by several μs in length at the same phase positions.

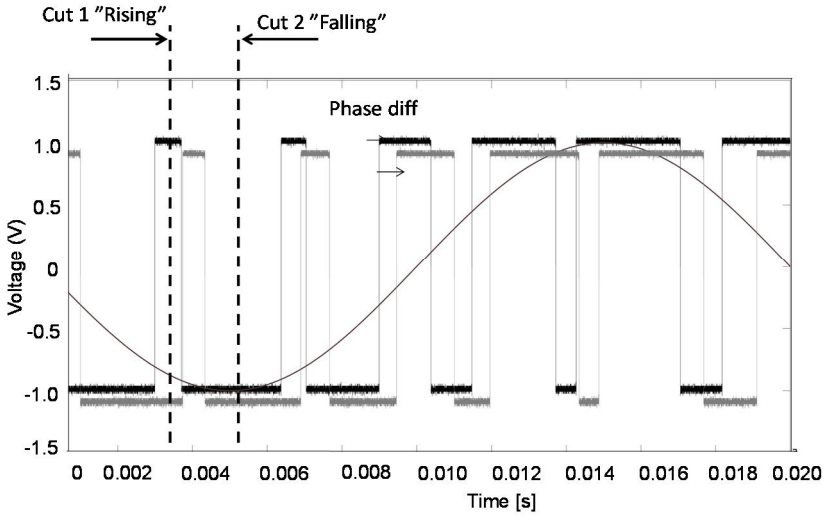

Figure 5.1 *A sinusoidal voltage shape synthesized by a bipolar two level PWM converter with carrier frequency 300 Hz. Two PWM waves recorded at different times are shown. The phase drift between the carrier and modulation is indicated, whereas the timing jitter is invisible in the scale of the figure. The PWM waves are displaced in amplitude to facilitate the readability and the indicated cuts refer to the black PWM wave.*

If the PWM carrier waveform and the modulated waveform were in perfectly stable phase match, it would be straightforward to make PRPD analysis for the individual steps and the entire generated period by applying the stochastic PD detection as presented in chapter 3. As this is often not the case, the approach has to be modified substantially for taking the drift and the jitter into account.

5.1.2 Adaptions to detect PDs under PWM waveform

To analyse PDs, two traces are captured during each acquisition event, described as step '1' in Figure 5.2. One trace contains the PD information and the other the non-smoothed PWM waveform where the times of the polarity reversals should be clearly detectable in the captured trace. This facilitates the detection of the voltage flanks positions in the PWM trace, which is done in the next step of the algorithm, indicated as step '2'. Here each flank is taken out of the total time trace in such a way that the maximum and minimum of voltage step are cut in the centre as indicated in Figure 5.1.

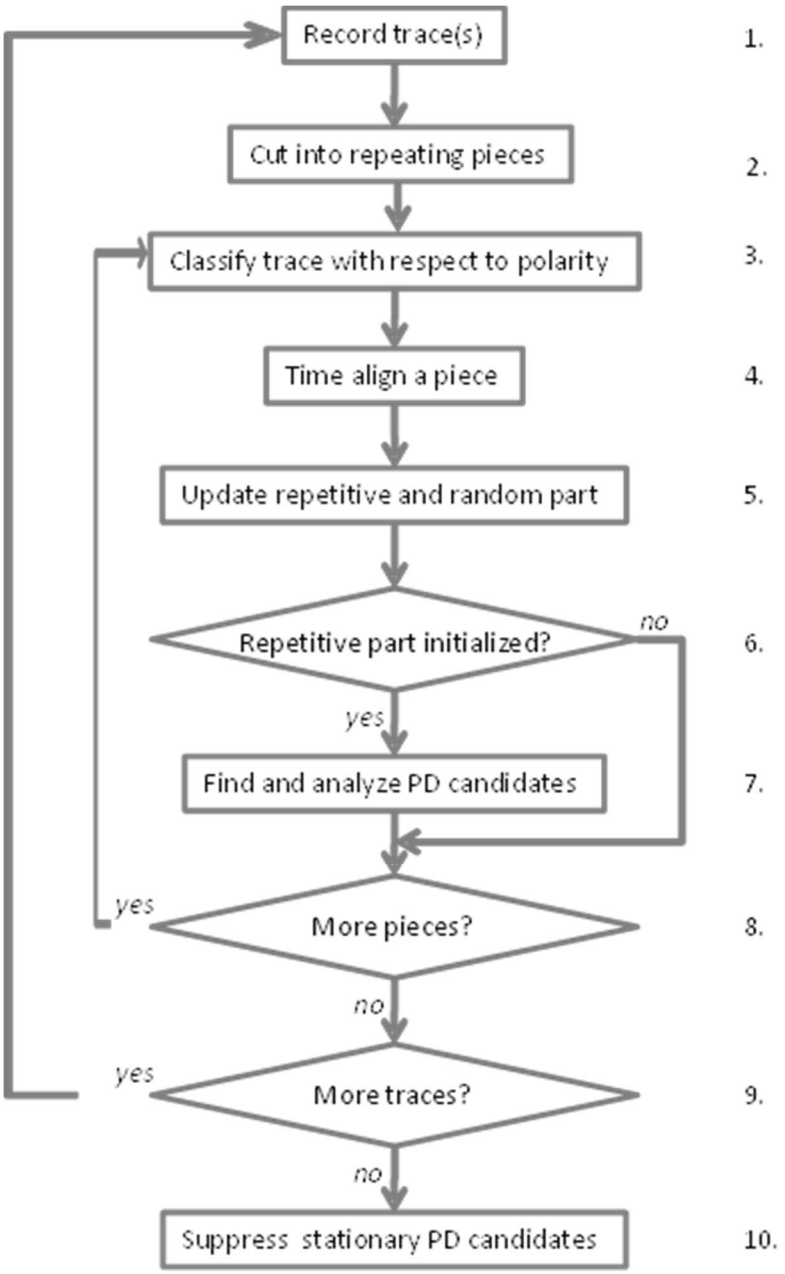

Figure 5.2 *The structure of the algorithm proposed in this work*

Each cut is then classified in step '3' (Figure 5.2) depending on its polarity, as illustrated in Figure 5.3, where the different polarity steps are separated into classes, "Rising" and "Falling", as suitable for a two level inverter. In Figure 5.1 the PWM trace contains eleven flanks, implicating a total of eleven cuts, where five are classified as "Falling" and six as "Rising".

In step '4', during each measurement series, the first cut of the PWM trace of either class is used as a reference to synchronize the following flanks within the same class. As the initial step of data processing, each new cut is time adjusted before the floating average calculation is undertaken in the following step. The starting position k of each

new cut is repeatedly adjusted in relation to the reference vector until the summed square difference is minimized:

$$\Delta(k) = \sum_{i=1}^{length\_reference\_cut} (x(i) - y(i-k))^2 \qquad (5.1)$$

where x and y represent the floating average vector and the cut from the latest trace respectively. As the voltage flanks often create the largest voltage remnants in each PD cut, particularly for short rise times, a good fit between consecutive flanks are essential. This reduces the influence of rapid changes in the applied waveform.

At the next stage, step '5' of Figure 5.2, one floating average per class is calculated to eliminate repetitive elements from the PD cut, which implicates that two of them are needed, one for the 'Falling' and the other for the 'Rising' cases. Each cut in one particular class contributes to the calculation of its floating average value to obtain PD information, as illustrated in Figure 5.4.

Since each voltage step cut can differ considerably in length, the same applies to the PD step cut. Thus the adjustment in the starting point between the cuts and the difference of lengths prevents a part of the floating average vector from being updated. The proposed solution aims at increasing the size of the floating average vector until its length becomes at least the same as the longest of the appearing cuts. For each of the iterations, when a new cut is processed, the parts in the floating average value, covering the same time as the cut, are updated while the others remain the same. The number of iterations undertaken on a specific sample within the floating average vector is noted in a specific vector. Until the maximum number of iterations has been reached for all parts of the floating average vectors, the numbers

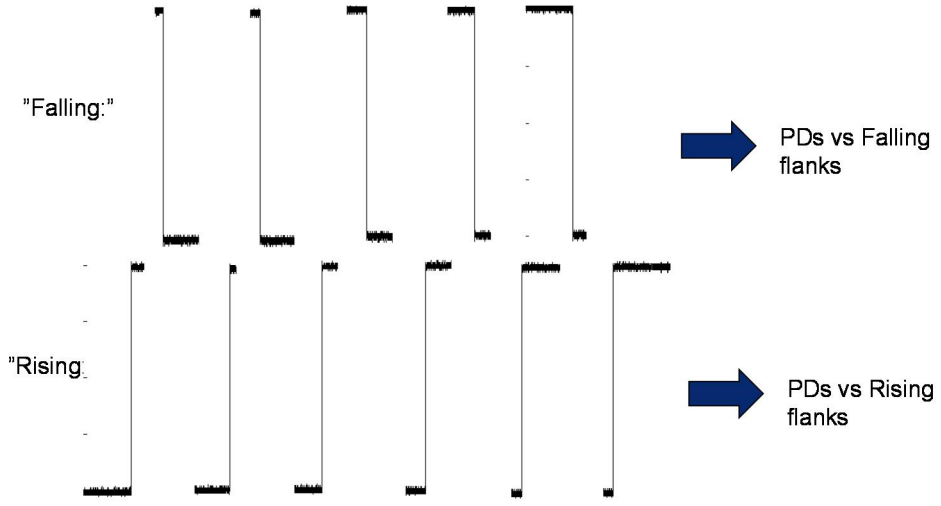

Figure 5.3 *Classification of races from Figure 5.1. Note that each cut is to be processed separately with respect to reference values for reducing voltage remnant in the PD channel.*

of averages for a specific class increases each time a long enough trace appears in the calculations. This is in principle similar to the initiation phase described for obtaining the floating average value described in chapter 3 for one cut with a fix length.

In step '7' of Figure 5.2, each time the present floating average is subtracted from a new cut containing potential PDs, procedures such as finding the voltage level suitable to separate noise from useful information (the trigger level) as well as determination of the length of each PD pulse, is performed.

The calculation of floating averages are performed for all cuts in a specific trace and for all captured traces in steps '8' and '9'. The processing may be performed either during recording or on subsequently stored traces.

The suppression of repetitive bursts is best performed when a large number of PDs is found, marked in Figure 5.2 as step '10', thus it should be performed at the latest stage. To aid the supervision of an ongoing measurement, this processing element may also be performed inside the loops, for details see [56].

The measurement technique introduced in this chapter enables characterization of PD properties in an object exposed to PWM shaped voltages of different level of smoothness and is implemented as a Labview based software. It can, in principle, relatively easily be also adapted to a case with a multi-level waveform, by extending the introduced classification. One additional advantage with classifying the PWM

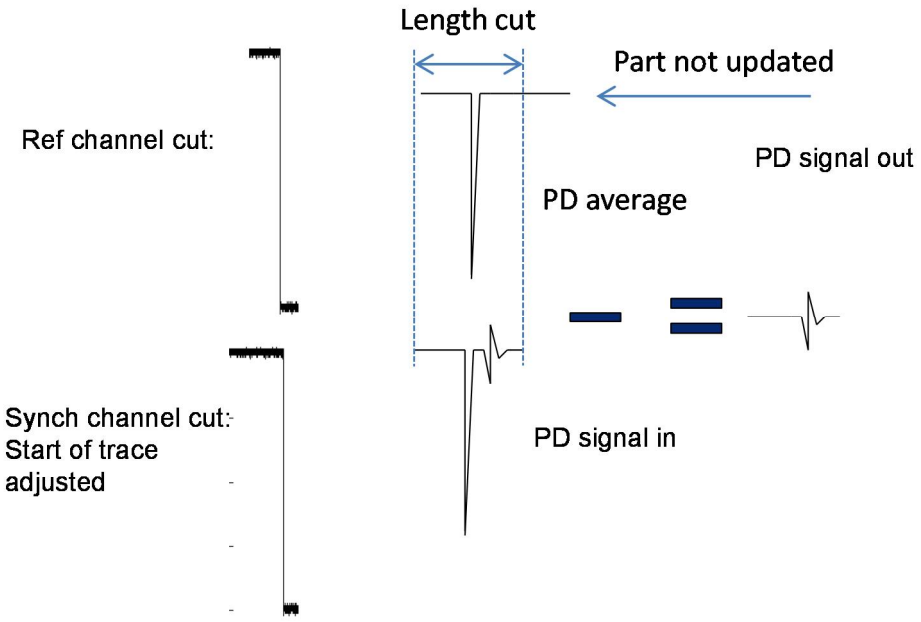

Figure 5.4 *Time adaption illustrating 'falling' class where the PD channel contains both remnant from the polarity reversal and PDs. This remnant is minimized when the synch channel cut is properly fitted in relation to the reference trace.*

signal depending on the polarity of the flanks is that non-symmetrical behaviour of PD characteristics can easily be analysed. Two special cases where a simpler approach can be utilized should be commented. One is when no additional trigger trace is required. In this case the PDs occurring need to be much lower in amplitude than the voltage remnant. Then the PD channel itself can be employed as the trigger signal. The other case is when the PDs are much larger than the remnant, so the influence of changes in the positions of the polarity shifts may cause very small additions in the total remnant for requiring an extra trigger channel and subsequently in classification into separate steps.

The presented approach uses non-filtered PWM signal as a synchronization channel to classify the captured trace. This can be avoided if the transfer function between non-filtered PWM signal and the PD detector voltage is known. In such a case the non-smoothed signal can be recreated by Fourier transforming the PD detector voltage and multiplying by the transfer function. This calculation may thus be applied as the synchronization channel, which implicates that only one measurement channel is needed. However, this would require a considerable amount of memory and calculational effort.

5.1.3 PD PWM voltage shapes of different smoothness

The harmonic spectrum of the applied PWM pulse train can be utilized to classify the level of smoothness by taking the ratio between the harmonic and the modulation frequency amplitude, commonly denoted as total harmonic distortion (THD) [45]. Thus a lower smoothness implies an increased degree of harmonic distortion in the waveform.

As the distortion cannot properly reflect the differences between fast rise times, a

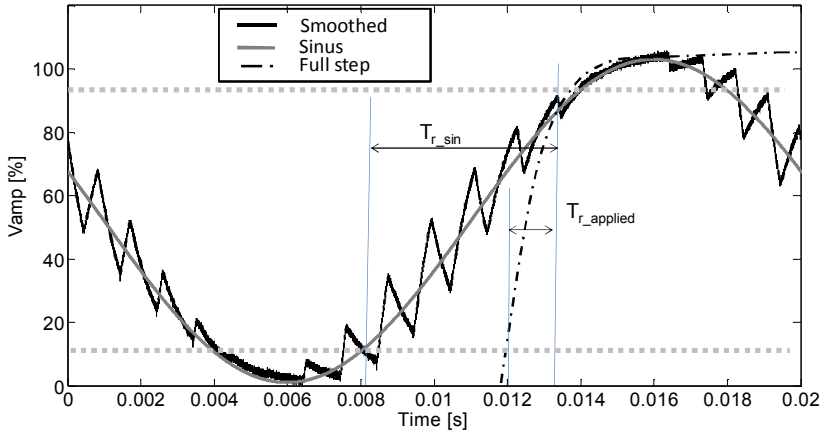

Figure 5.5 *The definition of smoothness applied relates the rise time of the smoothed and the ideal sinusoidal voltage waveform. Note that the rise time is defined between 10 and 90 % of the magnitude*

different approach is chosen in this investigation, both to enable a more intuitive correlation between the different levels of smoothness investigated but also with the possibility to clearly include the influence of the rise time of the applied PWM pulse train maintaining the same peak- to peak ratio. To quantify the level of smoothness, the relation between the rise time of the applied voltage and a sinusoidal voltage at power frequency was used, as shown in Equation 5.2. Note that the equation assumes that the rise times for both signals are measured between 10 and 90 % of the peak- to peak value, thus the rise time of a 50 Hz sinus is 6.7 ms. An example is illustrated in Figure 5.5, for both the rise time of a full step, representative for the PWM pulse train, and a sinusoidal wave used as reference. With this approach the smoothness value reflects not only the peak-to-peak value of the individual steps but also the rise time of the applied voltage. Thus, it enables a quantification of the full range of waveforms investigated in the following sections within this chapter.

$$S = \frac{T_{r\_applied}}{T_{r\_\sin}} \qquad (5.2)$$

Utilization of the described method is demonstrated below by analysing the behaviour of three different test objects.

5.2 Dielectrically insulated cavity

A cylindrical cavity (diameter of 4 mm) formed in an object consisting of three polycarbonate discs pressed together, as described in chapter 4.1, was used in a system presented in Figure 5.6. The object was connected between point "A" of the measuring set-up and ground. A two level bipolar PWM source was connected to point "B", offering a possibility to use different rise times, modulation and carrier frequencies as well as voltage levels. The same switch as employed in the previous investigations was here controlled by a unipolar PWM pulse, generated by an Agilent 33220A oscillator, set at 34 % duty cycle variation. The applied carrier frequency was 1 kHz and the modulation frequency was 50 Hz. The relation between the two

Table 5.1. Filter components in the circuit from Figure 5.6 and the resulting waveform smoothness.

Level	R_4 (kΩ)	R_5 (kΩ)	C_2 (pF)	Smoothness	T_r (μs)	TD (%)
1	2	-	-	0.0003	2	128
2	12	-	-	0.0018	12	127
3	100	100	-	0.006	40	126
4	300	100	-	0.028	160	108
5	1300	100	-	0.11	730	63.6
6	1300	100	100	0.18	1200	15.8
7	2300	100	100	0.29	1900	15.5

R_1(kΩ)	R_2(kΩ)	R_3(MΩ)	C_1(nF)
3	1	100	68

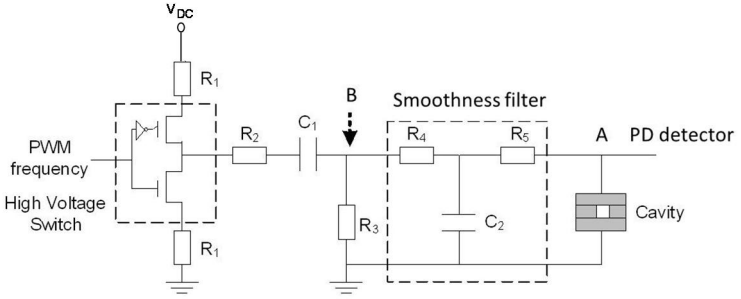

Figure 5.6 *Test setup including two level bipolar PWM generation circuit and a smoothing filter. The high voltage switch is a Behlke HTS 301-03-GSM.*

frequencies was an integer multiplier, which facilitates the illustration of PD patterns in relation to the modulation frequency. This however is not a necessary condition to enable the measurements and analyses. Parameters of the circuit elements utilized to smooth the PWM signals are listed in in Table 5.1.

Other means of quantifying the level of high frequency contributions within the synthesized waveform than smoothness is however possible. The benefit of using smoothness as a parameter in the investigation in favour of other possible measures is illustrated in Table 5.1 by the TD column, which lists the total distortion of the generated wave shape. The total distortion is calculated as

$$TD = \sqrt{\frac{\int_0^T \left(U_{sin}(t) - U(t)\right)^2 dt}{\int_0^T U_{sin}^2(t) dt}} \qquad (5.2)$$

where $U(t)$ is the generated wave shape and $U_{sin}(t)$ is the target sinusoidal with period T. It is apparent from the last column of Table 5.1 that the TD measure is not very effective in separating between the three shortest rise times, whereas these have a large impact on PD properties.

To enable a comparison of the PD characteristics arising at various PWM voltage shapes, a sinusoidal wave form was utilized as a reference. This voltage was obtained from a regulated 20 kV_p voltage transformer.

When measuring PDs in the cavity test object, the peak- to peak voltage level was adjusted to 8.75 kV_p for all the rise times investigated, the main objective was to study the PD pattern for a gradually increased smoothness of the PWM voltage waveform.

Before each test, the specimen was conditioned so stable PD characteristics were obtained. To further ensure reliable test results, repeated investigations were performed on the same test specimen for different levels of smoothness, showing the

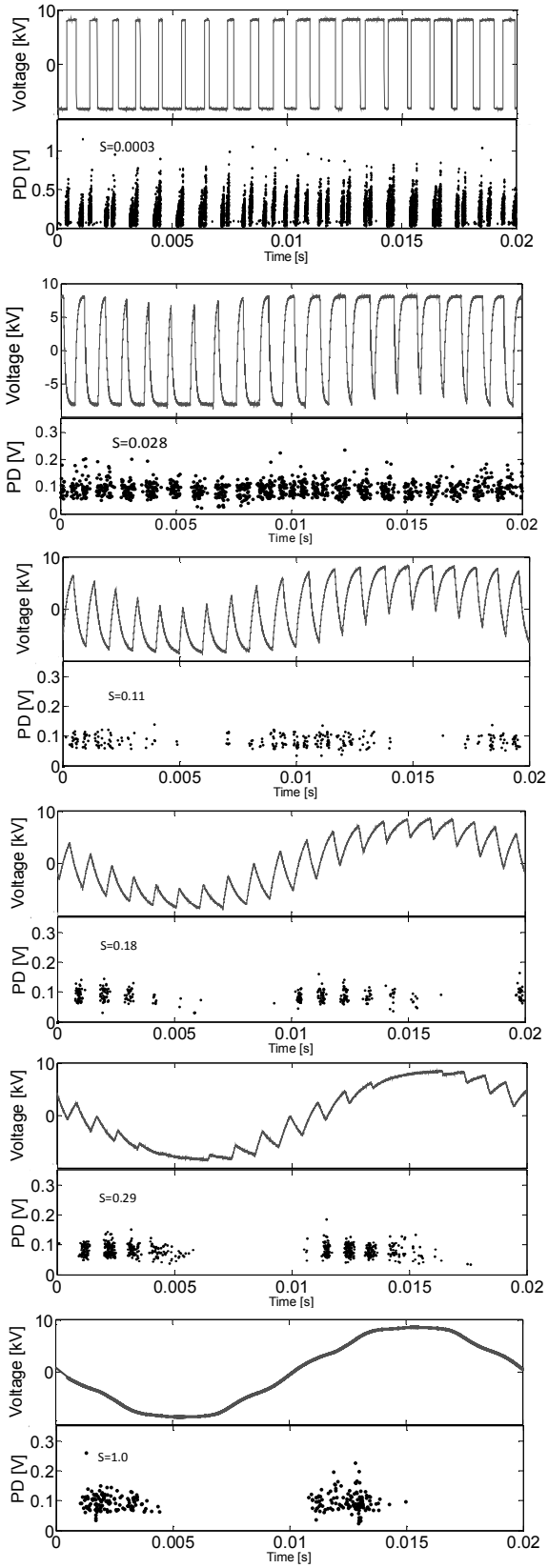

Figure 5.7 *PD patterns at different levels of PWM voltage smoothness and for a sinusoidal waveform. In each figure, the applied voltage is shown in the top panel and the observed PD pattern in the lower one. Note that the PD amplitude scale is larger for the lowest level of smoothness.*

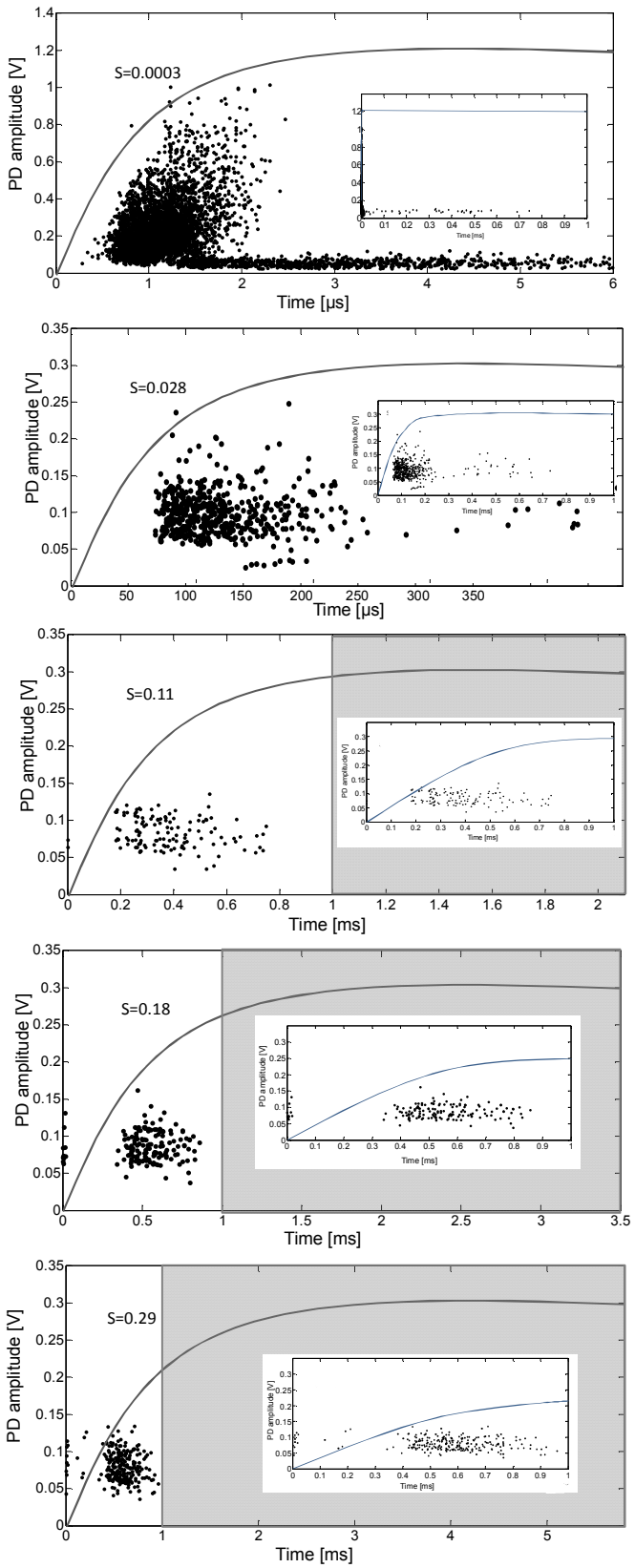

Figure 5.8 *PD pattern in relation to the voltage flank at different smoothness levels. For each smoothness level the time scale is adjusted to show the same portion of the flank. In the inserts, the same data are shown at the same time scale. Note that no PD can be detected after 1 ms and that PD amplitude is approximately constant for all but the smallest smoothness.*

observations are consistent; this suggests that degradation of the cavity endplates was negligible and did not influence the presented results.

The investigations concentrated on analysing the amplitude and the number of PDs. Figure 5.7 illustrates the shape of applied voltage as well as the corresponding PD pattern for the increasing level of smoothness, until sinusoidal conditions are reached. It is apparent that PDs occur on each voltage flank at the low smoothness levels. It further appears that the PD pattern is clearly influenced by the phase shift and jitter in the PWM signal. If the PDs were occurring only on the voltage flanks, the pattern would consist of thin vertical lines for a stable PWM waveform. The width of the pattern reveals the presence of phase shift and jitter. Despite of this, it is still possible to clearly distinguish the positions of the PWM train edges, as the modulation and carrier frequency are almost synchronized. For increasing smoothness the PD pattern gradually transforms in number, amplitude and phase position, which becomes particularly obvious when the smoothness level is above 0.03, for which the PDs occur only at some of the edges. Although the spread in PDs increases, the presence of the edges is still visible. This increase in spread is affected by the rise time of the applied voltage, as it becomes longer than for the cases of lower smoothness. Figure 5.7 also shows an additional behaviour apparent for the higher smoothness levels, e.g. appearance of distinct areas where no PDs occur. These areas are reflecting the decreasing amplitude contributions from the smoothed voltage steps on the modulated waveform, which temporarily reduces the externally applied electric field. In relation to the space and surface charges, the total electric field level in the cavity is lowered and thus reduces the chance for PD appearance. For the smoothness 0.1 and above, PDs start to concentrate in the vicinity of the largest peak-to-peak steps of the PWM waveform. At this level of smoothness both the modulation and the carrier frequency still influence the PD pattern. At a further increased smoothness level, the most significant change is in the phase distribution.

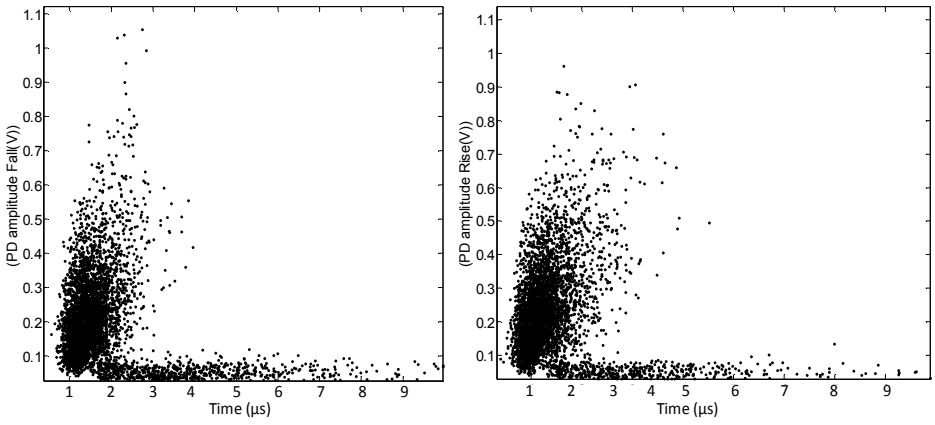

Figure 5.9 *PD amplitude at "Falling" and "Rising" voltage flanks.*

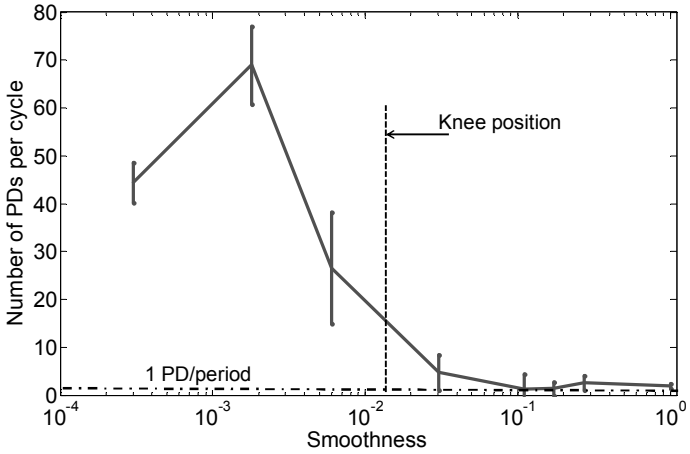

Figure 5.10 *Number of PDs detected for exposure of PWM voltage shapes as a function of PWM smoothness. Here a 1 kHz carrier frequency and 8.75 kV_p are applied, thus 1 PD per flank gives 40 PD per period. The standard deviation is indicated for each measured value.*

To illustrate this in detail, the PD position and amplitude relative to the voltage flanks are indicated for some different rise times in Figure 5.8. Only positive flanks are displayed in the figure because the PD pattern is symmetrical, as shown in Figure 5.9 for the lowest smoothness level.

The PD distribution relative to the flanks experiences only minor changes, despite that the rise time increases considerably for the larger smoothness levels. However, since some of the PDs start already very close to the polarity reversals, they show less dependence on the position of the smoothed voltage step.

To properly quantify the relation between PD characteristics and smoothness,

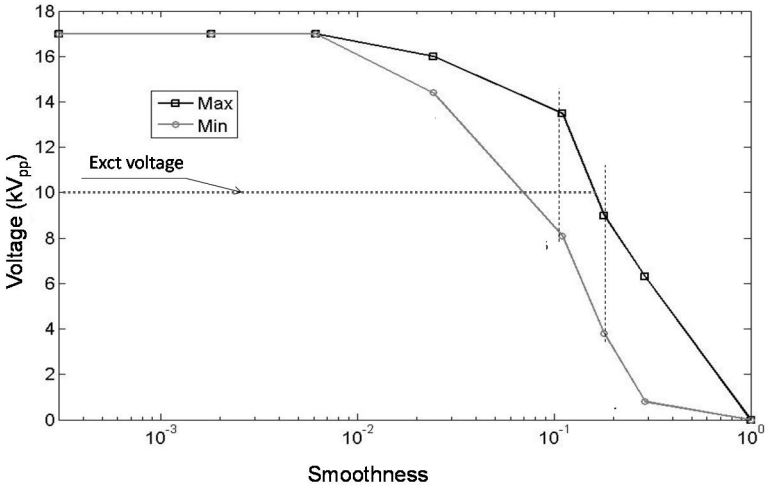

Figure 5.11 *Peak-to-peak value of voltage steps in PWM waveforms of various smoothness levels. Note the indicated area where the PD pattern gradually approaches the sinusoidal PRPD pattern as well as the indicated extinction voltage level for smoothness levels larger than 0.01.*

additional examinations involve determinations of the number of PDs occurring and the average PD amplitude per cycle. The investigated cases reveal that the number of PDs changes, particularly for the lower smoothness levels. This is particularly obvious when analysing Figure 5.10. At the lowest smoothness level, the average total number of PDs per cycle is practically equal to the number of voltage flanks appearing in each modulated cycle. With increasing smoothness, the number of PDs initially increases, which agrees with the observations reported in chapter 4. The smoothness level required to reach about the same number of PDs as for the sinusoidal waveform is between 0.006 and 0.028. The centre of this interval is marked as the knee position in Figure 5.10. At still increasing smoothness level the detected number of PDs decays rapidly. However, this observation is in contrast to the results presented in chapter 3 and remains mainly the consequence of not using 50% duty cycle and allowing the voltage steps to decrease below the peak-to-peak value for smoothness levels above 0.006, as exemplified in Figure 5.11. The dependence of the average PD amplitude as a function of smoothness level is illustrated in Figure 5.12. It can be noticed that PD amplitudes become reduced with increasing smoothness. When the PWM waveform is smoothened to between 0.0018 and 0.006, constant PD amplitude of about 70 mV per 50 Hz period is reached. For yet higher smoothness levels only minor differences can be observed. This suggests that possibly different phenomena may be influencing the change in PDs amplitude and their number at low smoothness. This effect is further discussed in chapter 6.

The correlation between the height of voltage steps and the smoothness of PWM voltage waveform is illustrated in Figure 5.11. As the level of PD extinction threshold is about 5 kV_p, one may conclude that the qualitative change of the PD characteristics starts taking place already at smoothness level above 0.1 where the step magnitude reaches this limit. It is therefore postulated that at this point the way the insulation

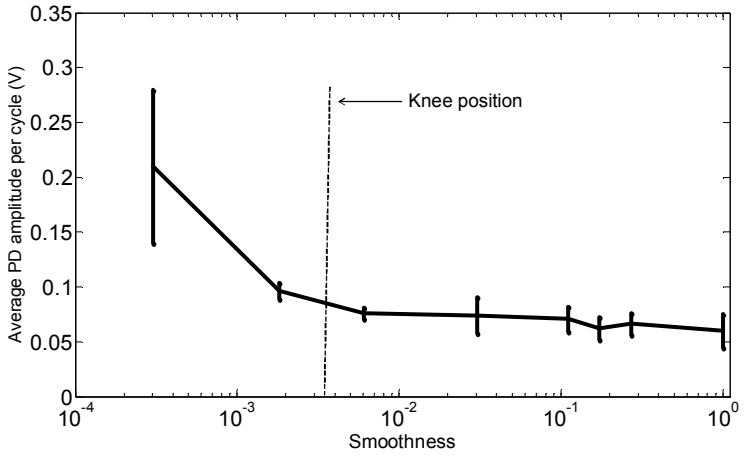

Figure 5.12 *Average PD amplitude with standard deviation indicated. Note that the PD amplitude increases significantly at shorter rise times. The standard deviation is indicated for each measured value.*

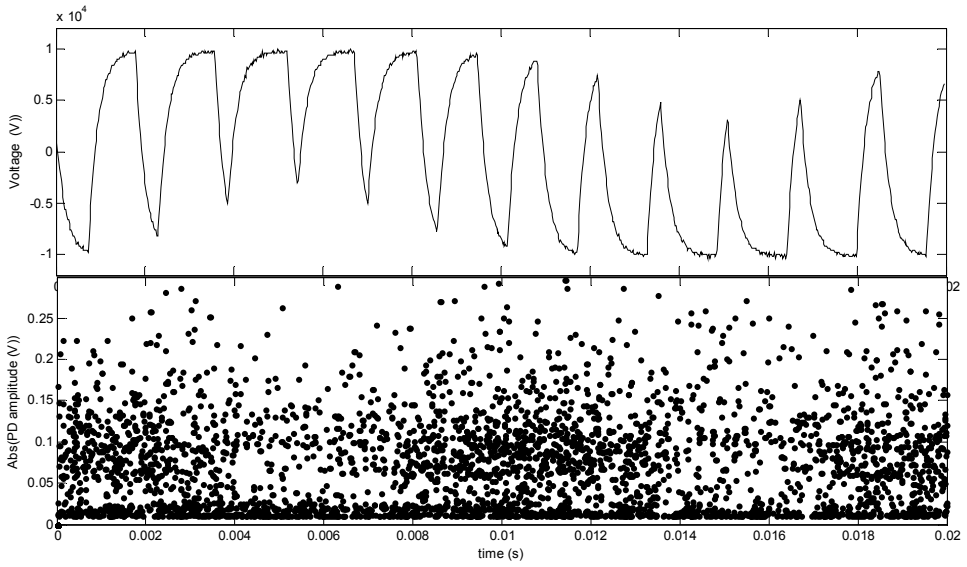

Figure 5.13 *Non-integer relation between carrier (637 Hz) and modulated frequency (50 Hz). Note that the smoothed waveform varies considerably in phase in relation to the PD pattern although a more dense PD distribution can be observed at the zero crossing.*

system degrades will also change, gradually approaching the rate under sinusoidal excitation.

To demonstrate how the presented approach works with a drift in phase between carrier and modulating frequency, a test was run with carrier frequencies of 637 Hz. and 600 Hz at 10.5 kV_p. The results are illustrated in Figures 5.13 and 5.14 and indicate that at the integer relation between carrier and modulated frequencies it is indeed easier to analyse the data.

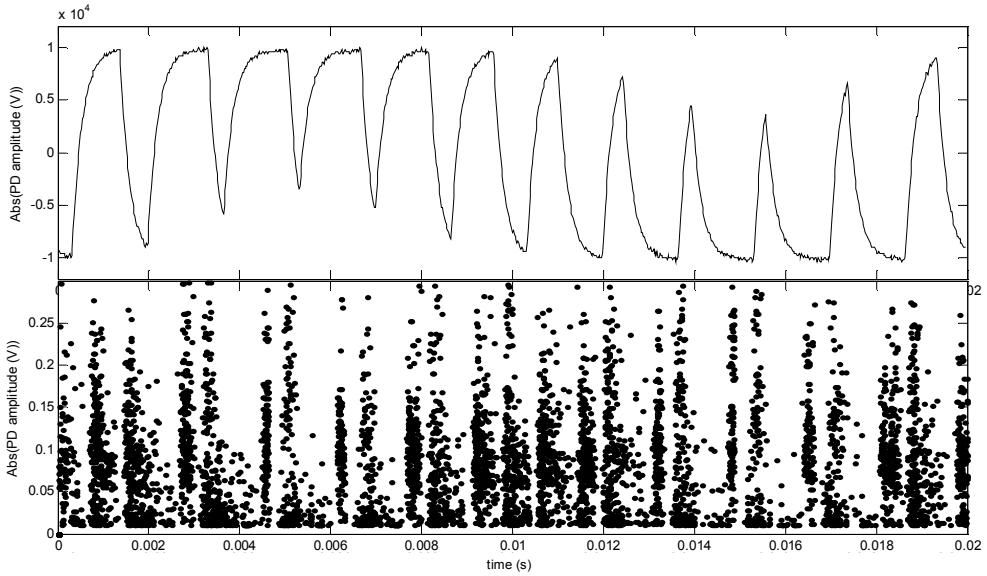

Figure 5.14 *Integer relation between carrier (600 Hz) and modulated frequency (50 Hz). The flanks are distinct.*

5.3 Motor stator insulation

To evaluate the presented test method on a more geometrically complex insulation system than the cavity test object, an electric motor with a high number of turns provides an relevant challenge. For this test a three phase motor stator designed for low power applications (< 1kW) is selected. A photo of this object is shown in Figure 5.15. The diameter of winding wire was 0.7 mm and, as this stator was picked "off the shelf", a detailed information regarding the insulation material of the wire is not available. One characteristic feature of this test object is that its capacitance is considerably high, about 500 pF, which increases, as compared to the cavity object, the shortest rise time possible to apply from about 0.5 to 2 μs. However, the main goal with this work was to use the developed method to analyse PD characteristics of this object at varying smoothness of the PWM voltage waveform.

Figure 5.16 and Table 5.2 provide information on the measuring system and the components utilized to filter the voltage waveform to different smoothness levels. Also in this case the modulating frequency was 50 Hz and a carrier frequency was 1 kHz. A peak-to-peak voltage of 2.4 kV_p, which is well above the inception voltage level for this winding, was selected in all measurements reported here. Data from 200 cycles were collected at each smoothness level. Compared to studies utilizing dielectrically insulated cavities, the use of PWM waveform on a stator introduces wave reflections, which change the PD distribution considerably.

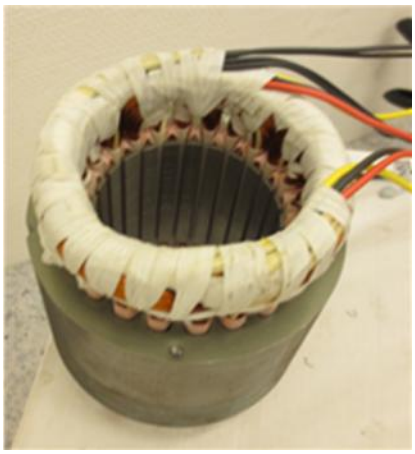

Figure 5.15 *A three phase motor stator for low voltage applications (outer diameter of 70 mm and height of 120 mm). Two phases are grounded and one exposed to a PWM voltage shape of different levels of smoothness.*

R_1 (kΩ)	R_2 (kΩ)	R_3 (MΩ)	C_1 (nF)
3 (0.8* for smoothness=1))	1	100	68

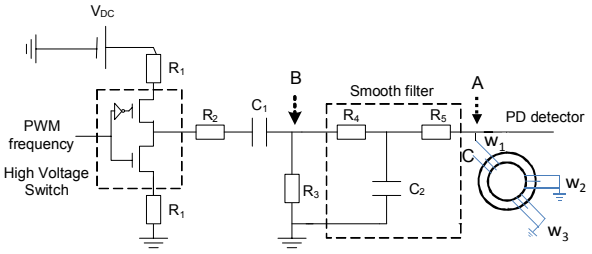

Figure 5.16 *The test set-up presenting location of PD signal detector and components used to smooth the applied PWM voltage.*

Table 5.2 *Electric filter components and their characteristics. Rise times marked with * are approximate as the wave shape is affected by propagation through the winding*

Level	R_4 (kΩ)	R_5 (kΩ)	C_2 (pF)	Smoothness	T_r (μs)
1	0	-	-	0.00003	2*
2	0	-	-	0.0006	3.65*
3	2	-	-	0.0007	4.42*
4	12	-	-	0.0016	10.2*
5	100	100	-	0.027	178
6	300	100	-	0.11	727
7	1300	100	-	0.35	2320
8	1300	100	100	0.39	2575
9	2300	100	100	0.72	4800

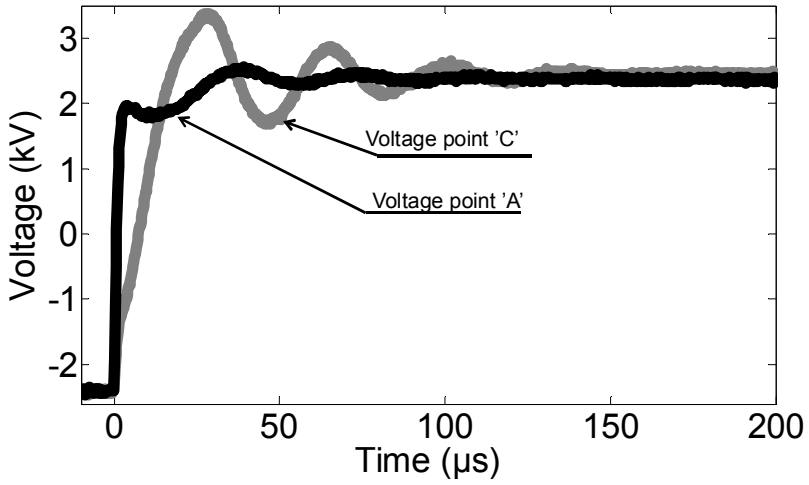

Figure 5.17 *Shape of the incoming pulse and its modification after travelling through the stator winding for the shortest rise time applied (2 μs). Overvoltage of about 3.4 kVp is observed due to reflections within the winding.*

The investigations were performed with the stator windings connected as illustrated in Figure 5.16; one terminal of the energized winding was connected to point 'A' and the other remained open, point 'C'. In service this point would either be connected to neutral ground or to some of the other windings, i.e 'Delta' or 'Y' connection. To properly elucidate how overvoltages affect the PD distribution and the PRPD pattern, the voltage was measured simultaneously at points 'A' and 'C'. An example is illustrated in Figure 5.17, a voltage wave is transmitted through the winding and reflected at the open termination. When examining the resulting voltage output in point 'C' for the lowest smoothness level applied, an overvoltage of at least 0.9 kV_p was measured, i.e., 41 % overvoltage.

The shapes of voltage transient in point 'C' reveals that both inductive and capacitive couplings are responsible for its formation. The amount of overvoltage is dependent on the relation between the rise time of the signal and the travelling time through the stator. For shorter rise times, the influence of reflections is apparent on both terminals of the winding. As the rise time increases the voltage increases more uniformly across the complete winding and little or no influence of the reflections are present for the higher levels of smoothness.

Figure 5.18 shows the measured PD signals as compared with the waveform of the applied voltage. For the lower smoothness, PDs starts to appear at the voltage front and continue until about 30 μs later, about the time for the the overvoltage peak at the winding end, point 'C'. This indicates that the reflections within the winding have a considerable influence on the PD distribution. For PDs occurring very closely in time, as observed here, it becomes challenging to resolve them separately, if possible at all, because of the signal distortion due to wave propagation.

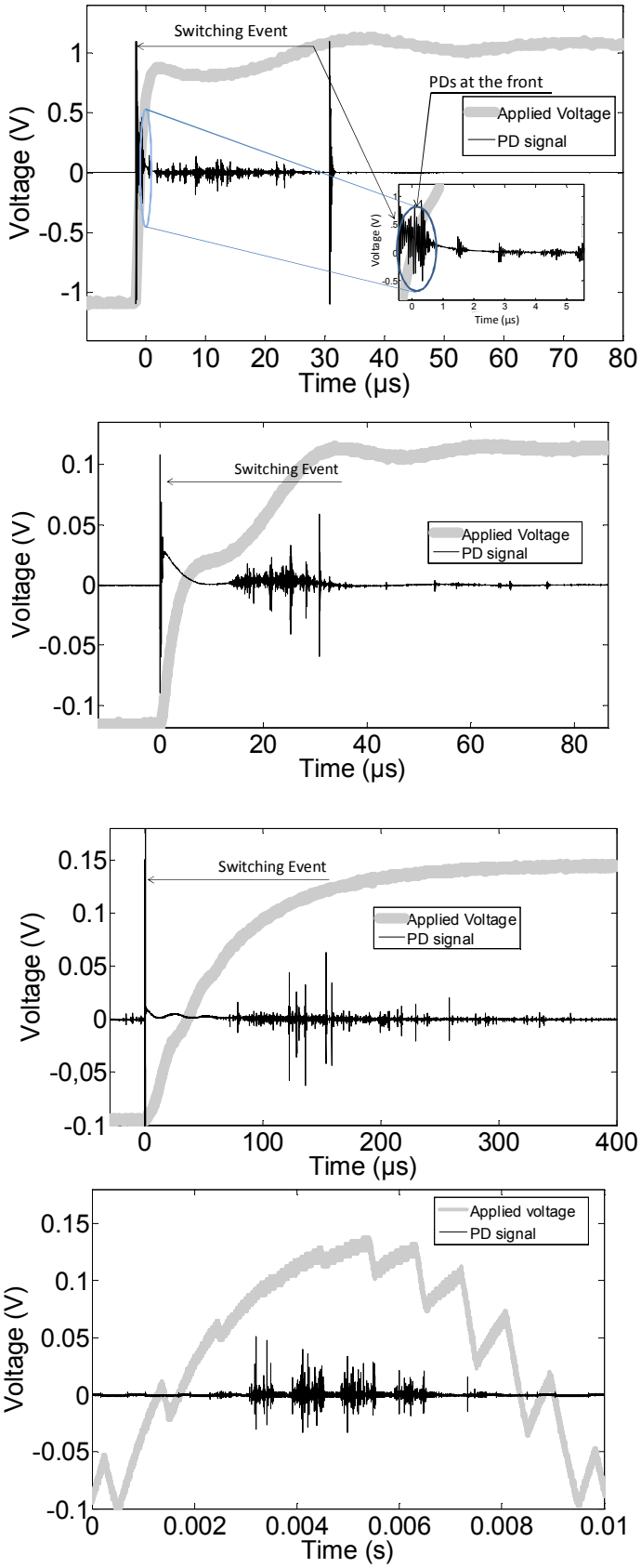

Figure 5.18 *Registered PD traces in relation to the applied voltage waveform at different level of smoothness (1, 4, 5 and 9 in Table 5.2). At the lowest smoothness level(s), the first PD's take place 1 – 3 µs after polarity reversal, as illustrated in the insert.*

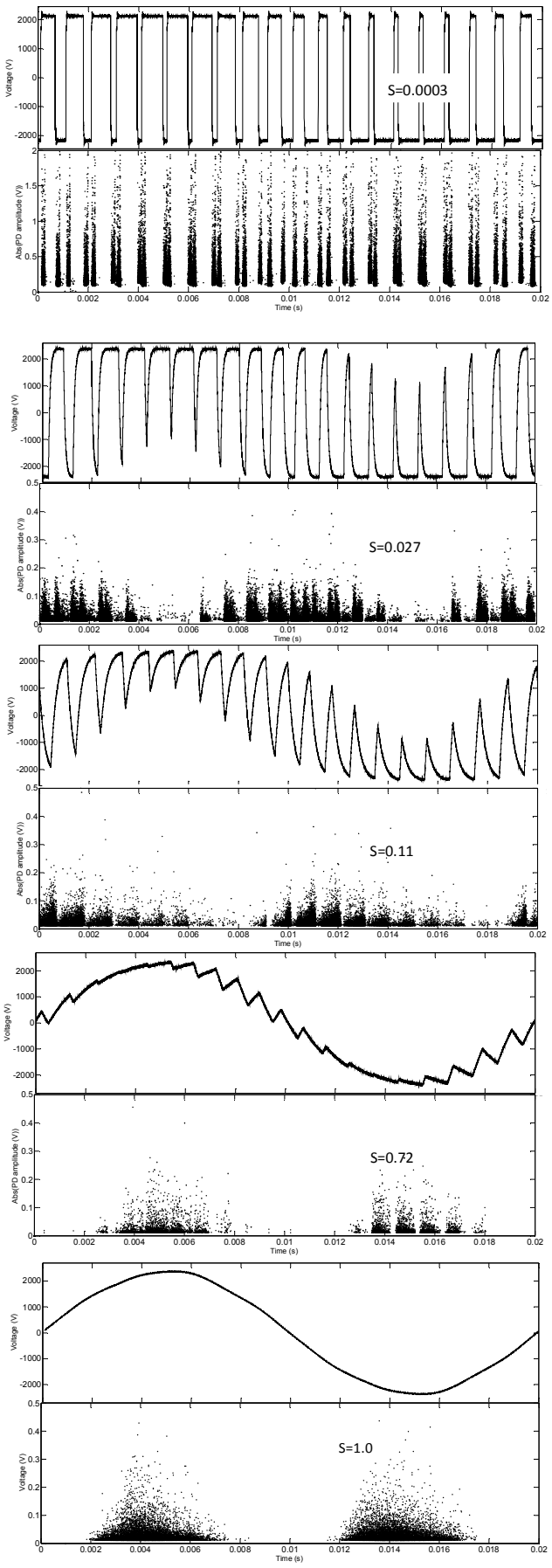

Figure 5.19 *Phase resolved PD patterns at different levels of smoothness. In each figure, the shape of applied voltage is shown in the top panel.*

For increasing smoothness, the PDs close to the voltage flanks vanish and concentrate instead close to the positions of local voltage maxima. Another feature is that their amplitude gradually decreases. For long enough rise times, such as for smoothness level 0.027 and higher, where the voltage is distributed evenly across the winding length it becomes easier to resolve individual PDs. In Figure 5.19 the PRPD patterns obtained from 200 cycles are presented. For the investigated stator the number of PDs detected per cycle is very high, on average more than 1000 at the lower smoothness levels. Since several PDs appear closely in time the resolution of individual PDs is difficult. It can also be observed that the PD amplitude gradually decreases for higher smoothness levels and the phase distribution change towards the sinusoidal conditions as the remnant of the carrier waveform decreases. For the investigated stator, this gradual transformation of PD occurrence in relation to phase position becomes obvious particularly for smoothness levels of 0.027 and higher. At low smoothness levels, the PDs are mainly located close to the polarity reversals. When the smoothness increases, the carrier frequency modulates the PD pattern and areas with decreased amount of PDs appear, until the PD distribution resembles the pattern at sinusoidal voltage condition.

To quantify the condition for reaching sinusoidal-like PRPD pattern, the maxima of PD amplitude per cycle in the cycle interval centre, 9.5 and 10.5 ms (denoted Zero crossing), are compared with the rest of the interval (denoted Peak) in Figure 5.20. Already at the smoothness of 0.027 and higher the same maximum PD level as for sinusoidal conditions is obtained. Particularly at the smoothness level of 0.35 no PDs can be detected at the centre.

The hypothesis formulated in previous chapter suggested that the amplitude of the

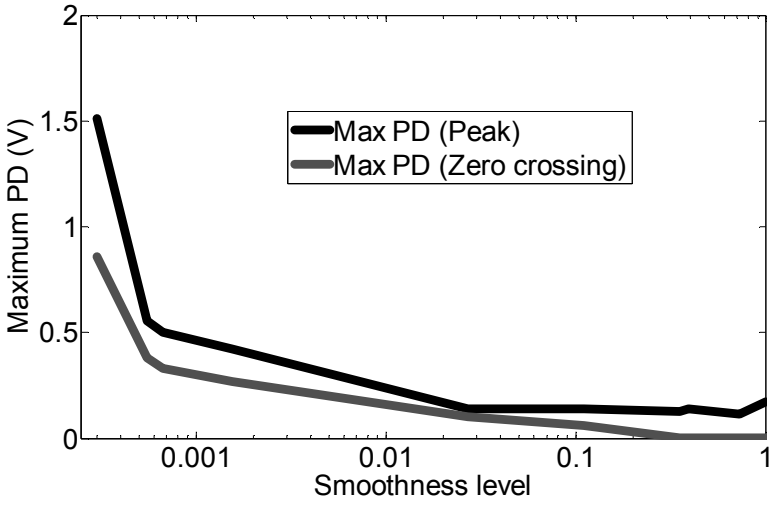

Figure 5.20 *Maximum PD amplitude related to the time interval where it is detected. Note that the PD amplitude reaches sinusoidal conditions between smoothness levels 0.027 – 0.35.*

remaining steps of the voltage waveform in relation to the extinction voltage level is an important factor for the transition to the sinusoidal-like PRPD pattern. A similar observation is also valid for the stator winding and suggests a solution for reducing the adverse effect of fast steep voltage fronts on motor insulation deterioration.

A final comment of this section refers to a possibility for performing on-line measurements by means of the presented system. The open ended winding applied here when using Y-connection will of course introduce reflections compared to voltage stiff online testing, however the latter will instead introduce reflections at the input of the winding due to the long cables often connected to the stator used, see [46]. Thus off-line measurements are relevant tests, while the suggested approach allows online use as well. However, a modified test-setup including Rogowski coil or antenna would be required instead of the capacitive coupling to enable the measurements.

5.4 Motor enamel wire

In the previous section a complex insulation system of a motor stator was investigated and it was shown that the object geometry certainly influenced measurement results. In order to evaluate the performance of motor enamel insulation itself, the twisted pair object is often employed [64]. Results of time-to-breakdown tests have been presented in several publications for traditionally used enamel wires with polyamide–imide insulation. In [45] a need for additionally exploring the performance of new enamel insulation materials has been underlined. Results were also presented showing an increase in the maximum PD charge obtained for shorter rise times. The shortest rise time employed in these investigations was about 140 μs. To further extend the existing knowledge more investigations are needed, particularly under conditions of rapidly changing voltage waveforms as well as considerably shorter rise times. Additionally, investigations should be performed when applying PWM voltage waveforms of different frequencies. Such investigations are presented in this section.

Table 5.3 *Smoothing filter components and their characteristics.*

Level	R_4 (kΩ)	R_5 (kΩ)	C_2 (pF)	Smoothness	T_r (μs)
1	0	-	-	75 μ	0.5
2	2	-	-	298 μ	2
3	12	-	-	0.0017	12
4	100	-	-	0.009	60
5	300	100	-	0.013	88
6	1300	100	-	0.045	300
7	1300	100	100	0.075	500
8	2300	100	100	0.12	800

To allow exposure of twisted pair objects (object capacitance is about 15 pF) to shorter rise times by means of the present setup, the resistors connected to the high voltage switch, R_1 in Figure 5.16, was reduced to 600 Ω. Table 5.3 presents the parameters of the employed smoothing filters.

As the geometry and the resulting electric field distribution in the twisted pair objects are influenced by the way they are manufactured, using the same test object in all the investigations seems to be advantageous. However, the individual measurements must be limited in time for avoiding enamel degradation. A similar hypothesis as the one presented in the previous sections assumes here that the degradation during PD exposure will be severely influenced by the smoothness of the applied voltage. The investigations were performed on an object with a wire diameter of 1.5 mm and the thickness of enamel insulation of 40 μm, as depicted in Figure 5.21. The object is connected in the measuring circuit with one wire to the voltage source and the other one to ground. The test objects were prepared according to the standard requirements [65]. The overvoltage caused by reflections at the open end of the object is not an important factor here since the shortest rise time applied is about 0.5 μs and the influence due to reflections is negligible since the time of wave travelling in the test object is considerably shorter than the rise time of the applied wave form and also the connecting cables are kept as short as possible (below 30 cm). This was verified by measuring the voltage at both ends of the twisted pair object.

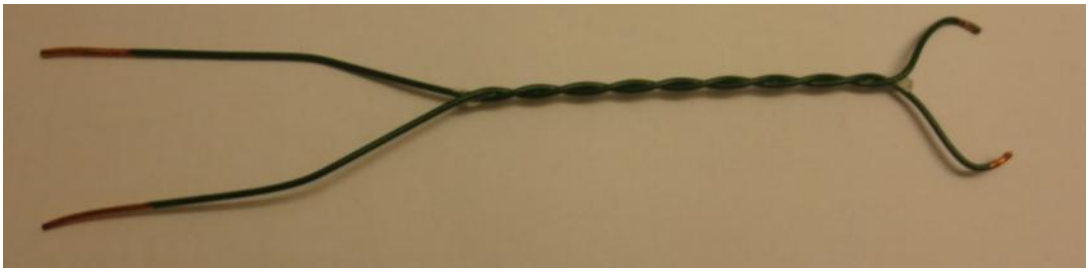

Figure 5.21 *Twisted pair test object. According to standard requirement [65] the number of turns is adapted to wire diameter.*

5.4.1 PWM frequency

The peak voltage level was chosen in these investigations to be 1.25 kV_p, this is more than 10% above the registered inception voltage level. This was kept constant for all the levels of smoothness as well as frequencies employed during a first test series. The applied PWM voltage signals had a modulating frequency of 50 Hz and carrier frequencies of 1, 2, and 3 kHz respectively. Data from 200 cycles were collected at each smoothness level.

Considering the hypothesis from previous sections, a smoothness level between 4 and 5 (see Table 5.3) should be needed for reaching the sinusoidal-like condition of PD activity. At the same time, increasing the carrier frequency implies a shorter remaining step for a given smoothness level. The relation between the maximum and minimum step size as a function of the smoothness level is displayed in Figure 5.22. The extinction voltage is also indicated in the figure. Figure 5.23 shows PRPD patterns for the non-smoothed waveforms with carrier frequencies of 1, 2 and 3 kHz. It can be observed that the maximum PD magnitude remains at about the same level for all the cases, which implies a higher number of large PDs per trace at increasing carrier frequency. Further it becomes apparent that the deviation in duty cycle yields a change in PD pattern density, which becomes more noticeable at the higher carrier frequencies.

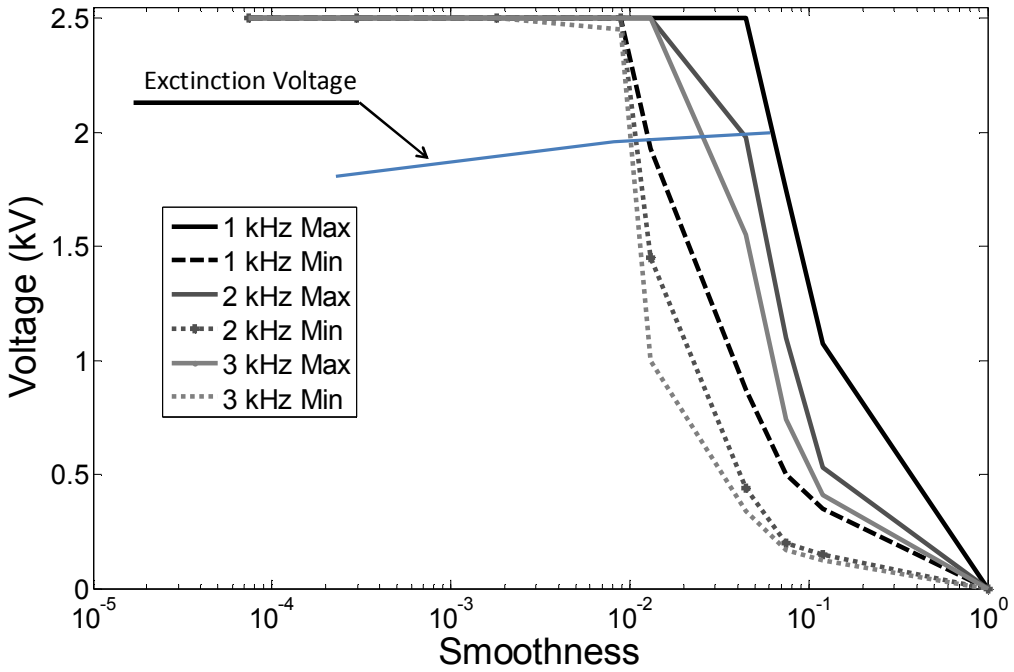

Figure 5.22 *Dependence of PWM voltage step size on smoothness level at different carrier frequencies for constant maximum V_p amplitude of 1.25 kV_p.*

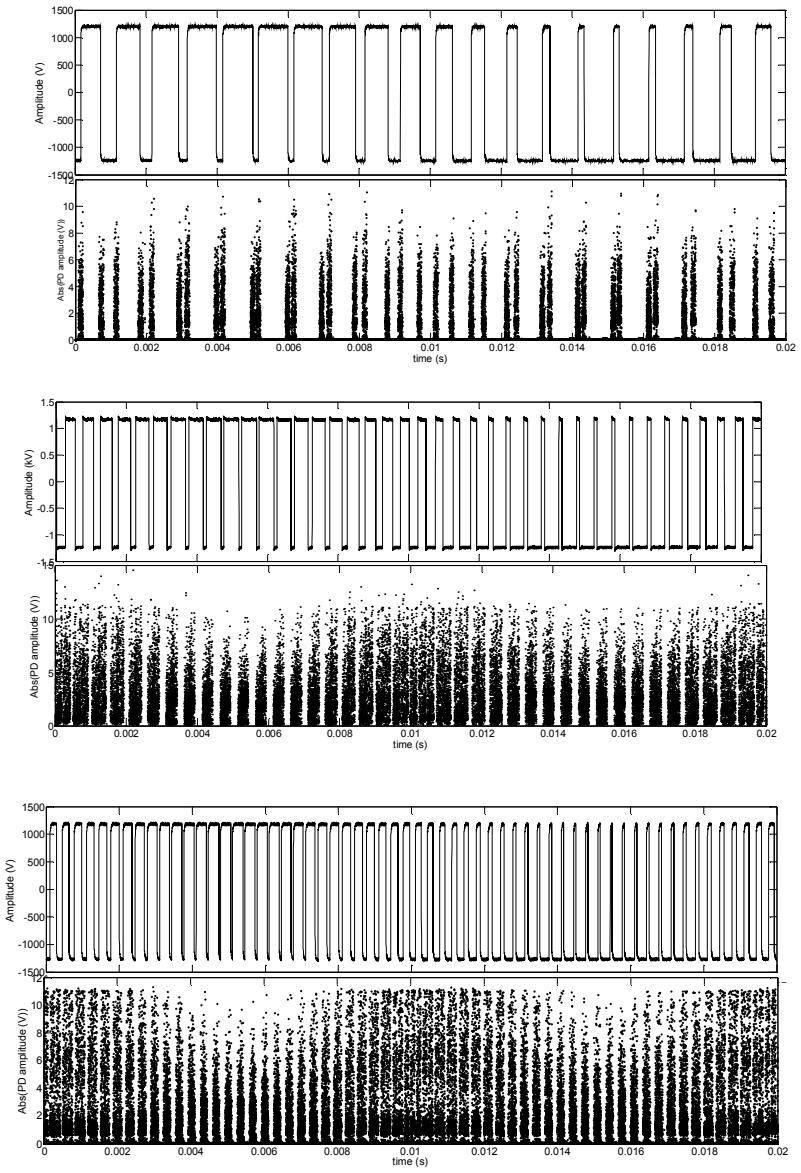

Figure 5.23 *PRPD patterns for non-smoothed PWM waveforms with carrier frequencies of 1, 2 and 3 kHz. Note that the PD pattern density increases due to increased carrier frequency and the influence of duty cycle becomes apparent.*

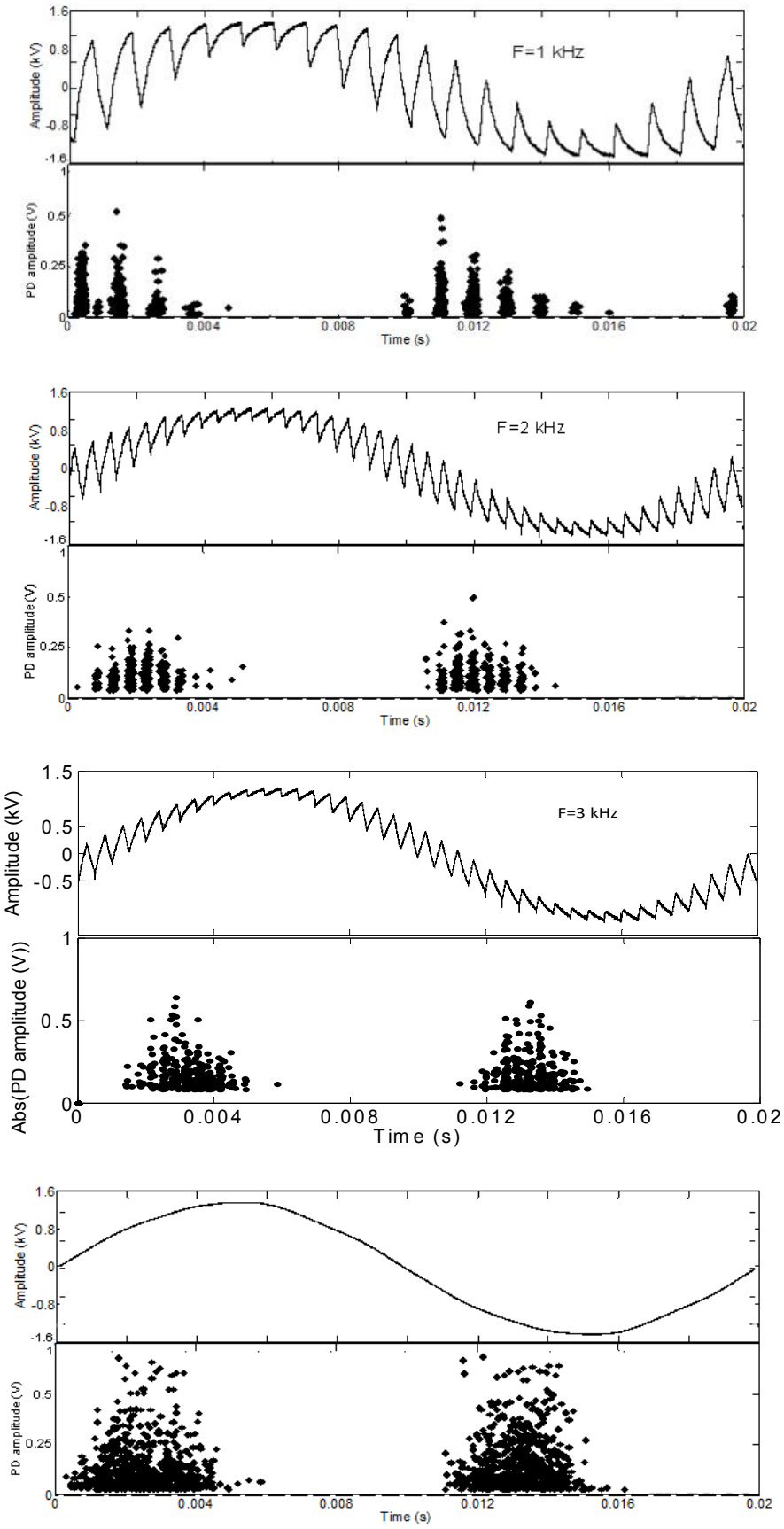

Figure 5.24 *Influence of carrier frequency on PRPD patter for constant peak amplitude V_p for 1, 2 and 3 kHz carrier frequency at smoothness (s = 0.12) as well as for sinusoidal waveform.*

An example when sinusoidal-like conditions are reached for all the carrier frequencies is illustrated in Figure 5.24. For the smoothed PWM waveforms, the PDs also decrease in magnitude and in number. Additionally, the influence of the dips in the synthesized wave form, remnants of voltage steps, is still seen in the PD pattern although faint for the 3 kHz carrier frequency. At 1 kHz, PDs still occur closer to the zero crossing of the synthesized waveform in relation to the sinusoidal PD pattern, while for 2 kHz and upwards little difference can be observed.

The highest carrier frequency will additionally cause the largest number of PDs and the summed PD amplitude until the same smoothness S = 0.009, is reached, as presented in Figures 5.25 - 5.26. As a consequence an increased exposure to PD activity becomes apparent for the lower smoothness levels, similarly as observed in [10], as more than one PD events appear per polarity shift. At the same time, as the remaining voltage steps are higher at 1 kHz carrier frequency, they contribute to slightly increased number of PDs at smoothness levels 6 to 8, meaning that for the higher smoothness the PD exposure will be more severe at lower carrier frequencies.

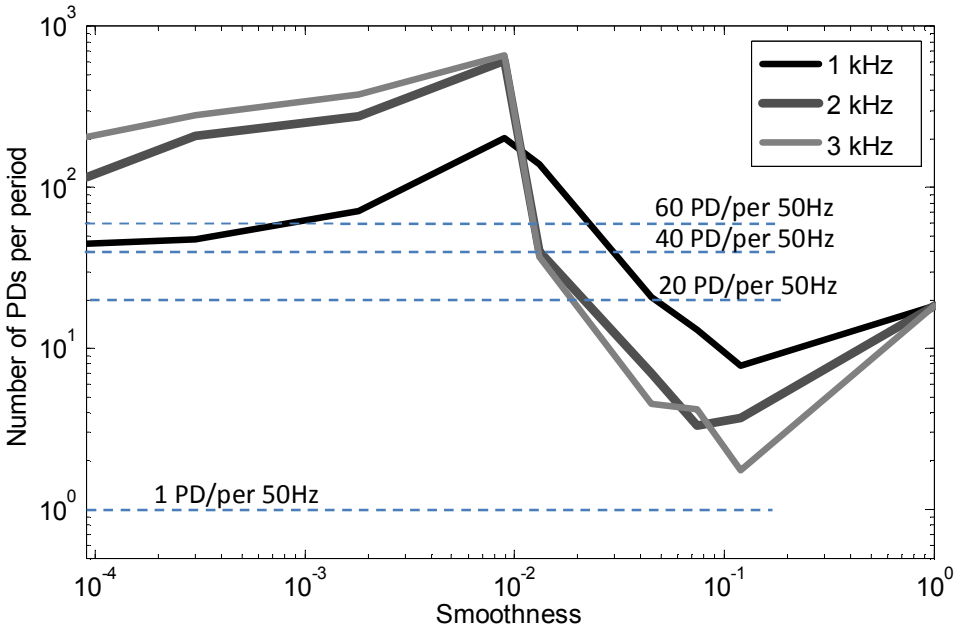

Figure 5.25 *Number of PDs detected for PWM waveforms of different carrier frequencies and smoothness. Note that for low smoothness levels the detected number of PDs follows the number of polarity shifts within a given period but that this relation disappears for higher smoothness.*

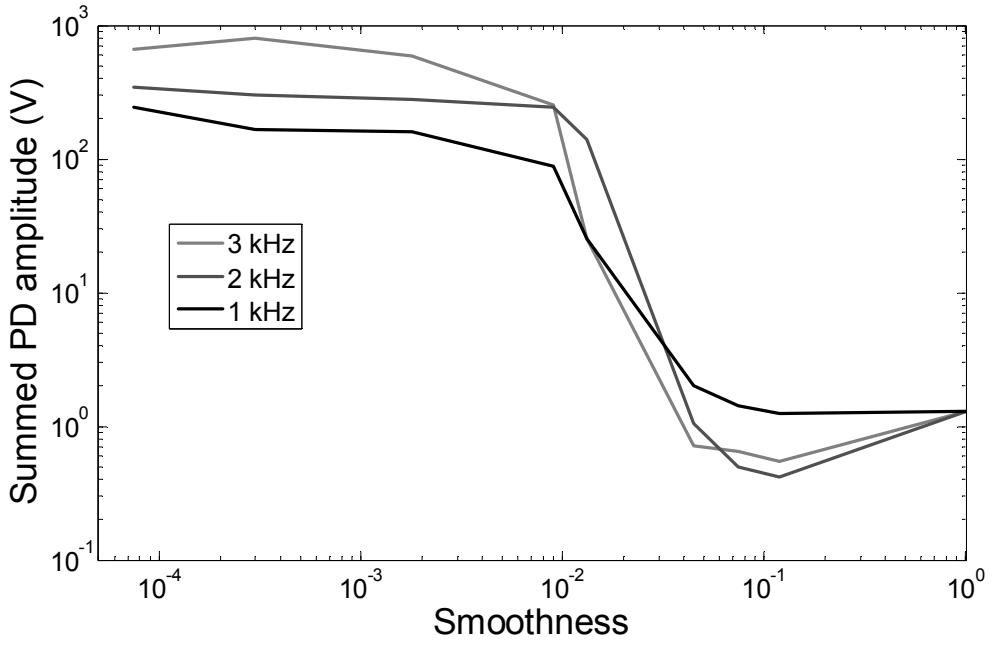

Figure 5.26 *Summed amplitude of PDs detected for PWM waveforms of different carrier frequencies and smoothness.*

Figure 5.27 illustrates how the maximum PD magnitude depends on the smoothness level. At the lowest smoothness, all the investigated cases yield about the same PD magnitude. With increasing smoothness up to S = 0.009, this behaviour is preserved, whereas the magnitude rapidly decreases at the higher levels of smoothness.

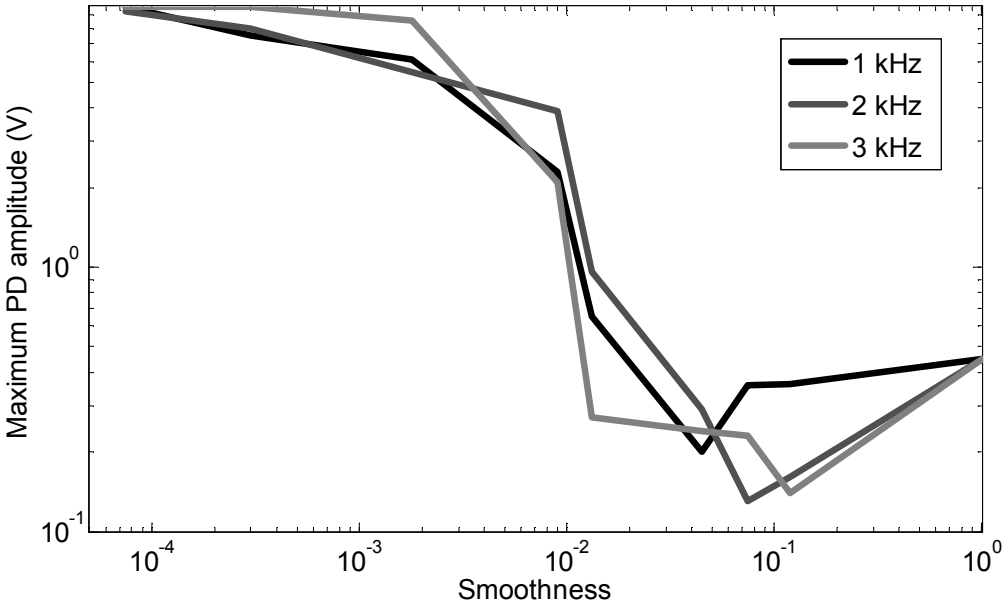

Figure 5.27 *The average maximum PD amplitude captured during each cycle while keeping V_p value constant. Note that sinusoidal conditions are reached at smoothness level 5.*

The observed tendency of increasing PD exposure for higher carrier frequencies (number of PDs) at low smoothness levels highlights the importance of considering application of a stronger insulation or an increased filtering level. On the other hand, it is worth noticing that above certain smoothness level, the PD exposure increases at lower frequencies, which should be considered as well when designing machine insulation systems.

5.4.2 Comparison between constant peak amplitude and constant RMS value

In some articles, a constant RMS value is used on waveforms of different frequency content either including harmonics [45], or by superimposing impulses afterwards [66] to compare PD characteristics. It is the view of this author that maintaining the same peak-to-peak amplitude for such comparisons provides the most suitable approach, because PD behaviour is highly nonlinear. Here, both alternatives are compared. Figure 5.28 presents the maximum and minimum voltage step in relation to the smoothness level for PWM waveform of 3 kHz carrier frequency, while keeping their RMS values constant. The peak amplitude of the maximum voltage steps increases as the minimum decreases at the higher smoothness levels.

It is therefore necessary to understand how the maximum voltage amplitude V_p is affected by the smoothness level while keeping the RMS value constant and how it influences the measured PD characteristics. In addition, also the maximum peak-to-peak value of the voltage step is here important as well as the size of remaining

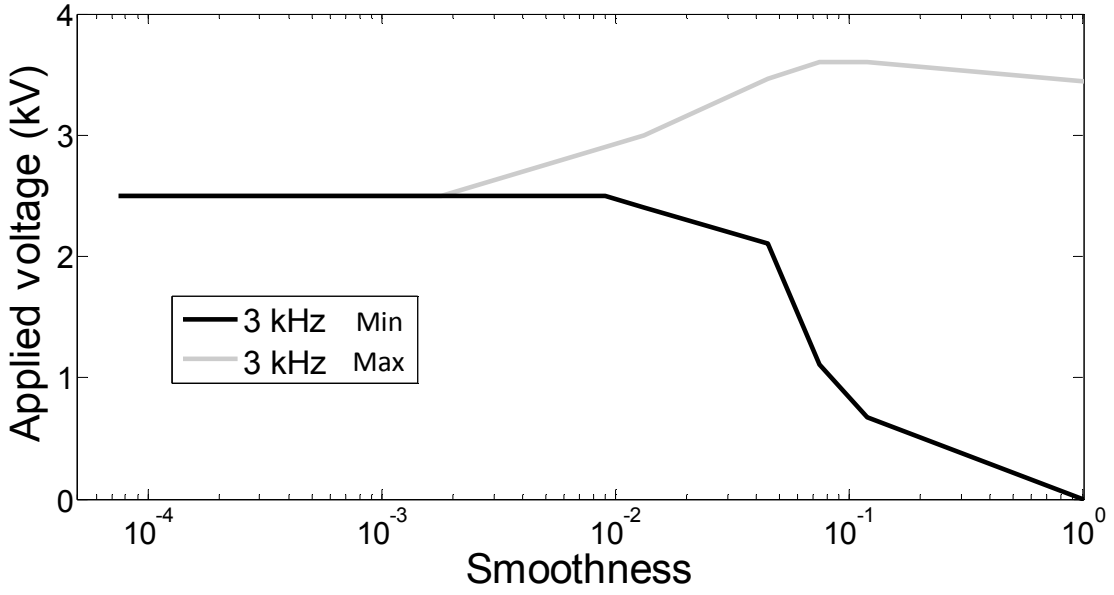

Figure 5.28 *Maximum and minimum level of voltage step for a constant RMS value of PWM waveform of 3 kHz carrier frequency at varying degree of smoothness. Note that an increased smoothness implies increased maximum voltage level.*

voltage steps. For the second test series presented below the RMS value of PWM voltage was kept constant.

Figure 5.29 illustrates how the peak voltage of PWM waveform changes at two different smoothnesses S = 0.09 and 0.26 with the same RMS amplitude. A higher smoothness at a fixed frequency implies smaller voltage steps and higher peak voltage amplitude. This must certainly have an impact on the resulting PD characteristics. When analysing the PRPD pattern for smoothness S = 0.13 presented in Figure 5.30, the maximum PD amplitudes become considerably lower than the ones for the lowest smoothness case (S = 75 μ), presented in Figure 5.23, despite the maximum level of the voltage applied has increased and the applied waveform still contains a considerable amount of harmonics. The change in PRPD pattern follows thus a similar trend as the one presented in the previous section, where the PDs are concentrated close the positions of the maximum voltage steps.

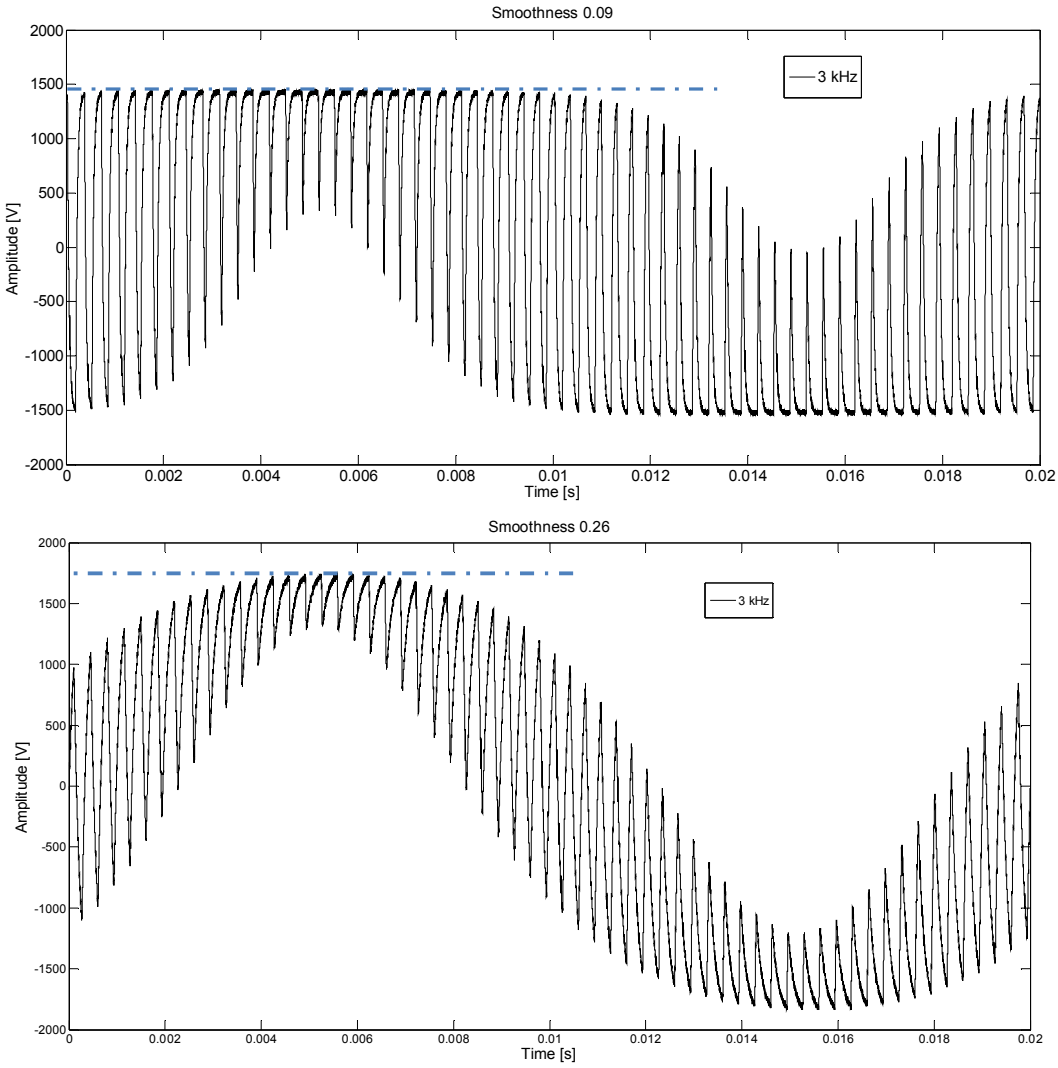

Figure 5.29 *Influence of smoothness level on peak voltage of PWM waveform of 3 kHz carrier frequency while keeping the RMS value constant. Note that peak voltage amplitude differs more than 20 % for the presented smoothness levels.*

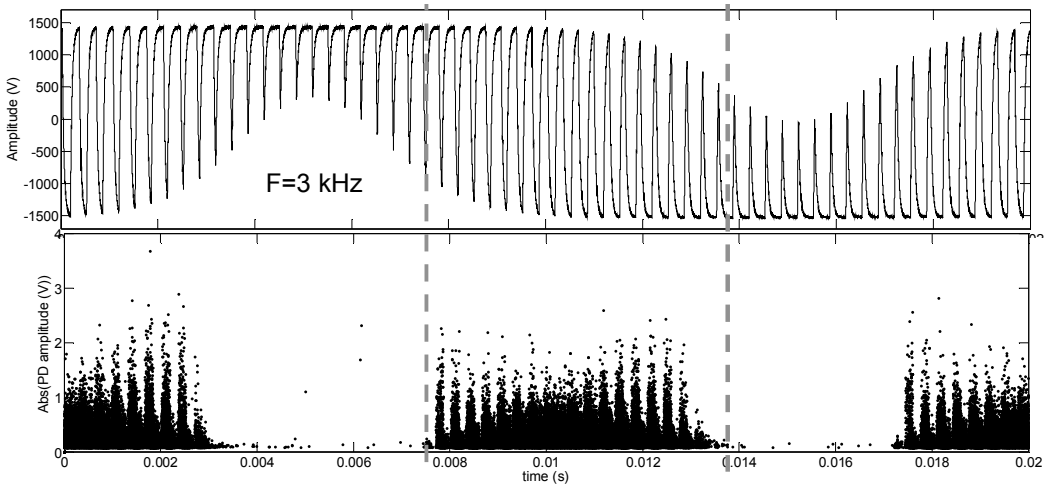

Figure 5.30 *PRPD pattern at smoothness level 5 (0.13) for constant RMS value of PWM voltage at 3 kHz carrier frequency. Note how the PD distribution follows the size of voltage steps.*

It should further be observed that the influence of the remaining contribution from the carrier frequency on the applied waveform is still traceable. To illustrate how the PD characteristics change with the smoothness level, the total and maximum magnitude as well as the number of PDs detected are illustrated in Figures 5.31- 5.33.

The low smoothness still implies considerably higher stress on the insulation material. When comparing the summed PD magnitude (Figure 5.31), for obtaining similar intensity as for the sinusoidal voltage waveform a smoothness level of 4 (S = 0.009) is required independently if RMS or peak values of PWM voltage are maintained constant. The same conclusion is valid for the maximum PD magnitude presented in Figure 5.32. On the other hand, for reaching the number of PDs similar as at sinusoidal condition (Figure 5.33), keeping the RMS value constant implicates a need for maintaining somewhat higher level of smoothness, level 5 (S = 0.013). This is most likely related to the difference in maximum amplitude of the voltage applied when keeping the RMS value constant.

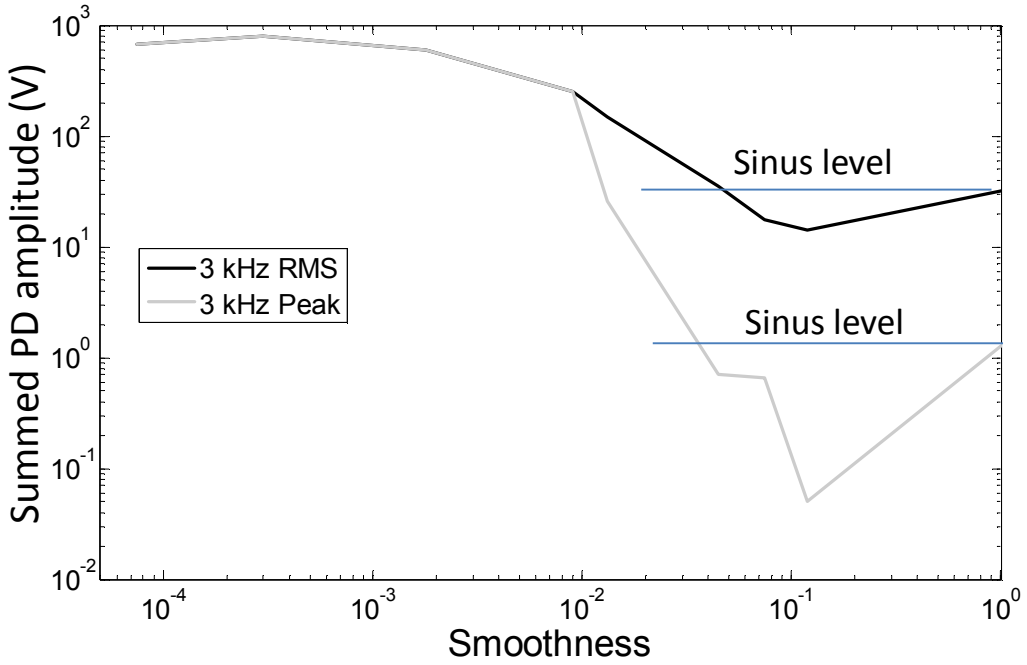

Figure 5.31 *The summed PD magnitude for constant RMS and peak values for different smoothness. At higher smoothness the peak amplitude must increase to maintain RMS constant and thus a difference in summed PD magnitude appears. The applied waveform has about 40% higher magnitude at sinusoidal conditions (smoothness S = 1).*

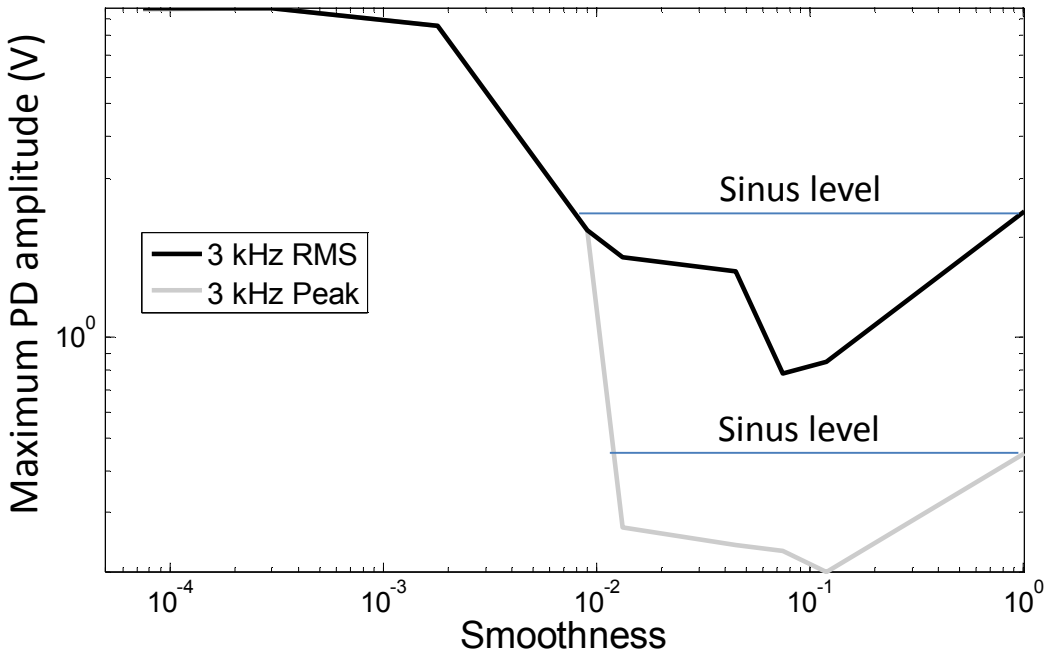

Figure 5.32 *The maximum PD amplitude captured during each cycle while keeping the RMS value of PWM voltage constant. Note that sinusoidal conditions are reached at smoothness S = 0.009.*

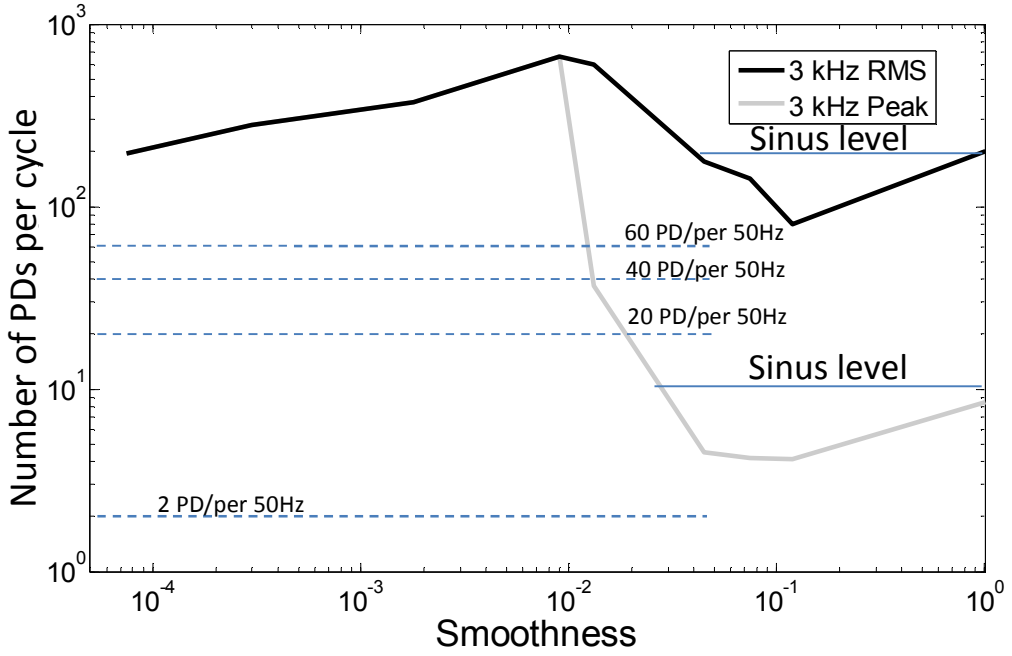

Figure 5.33 *Number of PDs detected for different carrier frequencies and smoothness for constant RMS values.*

To conclude this discussion, the low smoothness implies considerably higher stress on the insulation material for both constant peak and RMS approaches as expected from the tests in previous sections. This although the amplitude level increases for higher smoothness levels while keeping the RMS value constant. For higher smoothness and constant RMS value, the PD exposure increases due to the maximum amplitude. However the level remains well below the low smoothness values.

However one important advantage with keeping a constant peak value to evaluate the PD exposure is that it provides a well-defined maximum voltage level for the different smoothness levels, which makes analysis clearer. This is not the case when applying constant RMS where the peak voltage is dependent on smoothness. The same is valid for the other approaches based on constant RMS values, such for example as when superimposed disturbances are added to the waveform to simulate harmonics on the synthesized waveform [29]. In the latter case the position of the disturbance in relation to the synthesized waveform constitutes an additional factor influencing the PRPD pattern.

5.4.3 Degradation test

As a complement to the electrical measurement, two test samples were exposed to identical number of cycles of PWM voltage waveforms with different smoothness. One sample was exposed to the waveform of the lowest smoothness, (S = 75 μ) and the other one to the waveform of smoothness S = 0.045, i.e. higher than the one

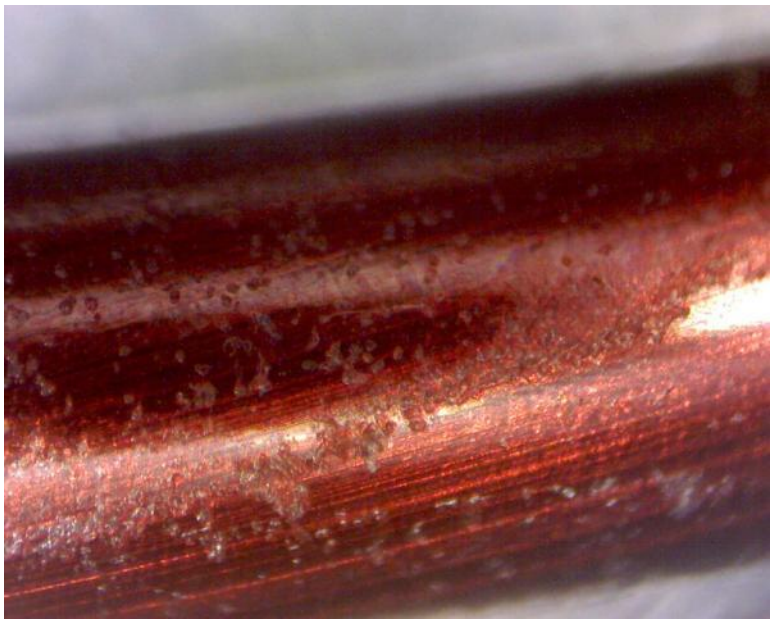

Figure 5.34 *Degradation of enamel wire surface exposed to 8 10^6 cycles of 1.25 kV_p PWM voltage waveform with smoothness S = 75 µ.*

needed for securing the same PD exposure as under sinusoidal conditions. The carrier frequency was kept at 1 kHz for both cases and 8 10^6 cycles were run for each of the cases. The outcome of this investigation for the lower smoothness level (lower rise time), a large number of PDs with high amplitude caused an increased damage of the enamel surface in the area where the two wires were in contact, as illustrated in the microscope picture presented in Figure 5.34. The wear of the enamel surface is likely to result in a decreased life time of windings exposed to PWM voltage waveforms of low smoothness levels.

After treatment with the waveform of the higher smoothness level, the surface remained less degraded, the pits were smaller and the wear less apparent, as illustrated in Figure 5.35. This result confirms the observations that a stronger degradation by PD activity becomes a characteristic feature when using PWM waveforms of low smoothness level. The results discussed here resemble the type of damage in the cavity objects presented in the previous section (Figures 4.33 and 4.34).

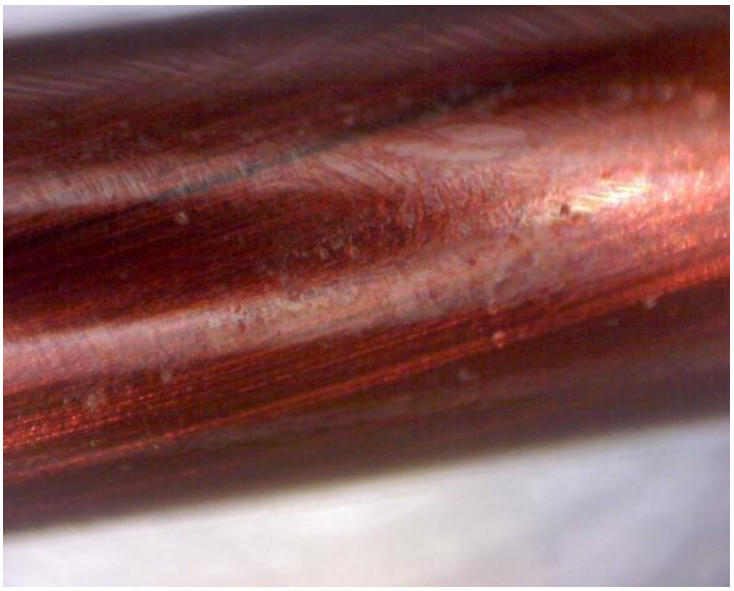

Figure 5.35 *Degradation of enamel wire surface exposed to 8 10^6 cycles of 1.25 kV_p PWM voltage waveform with smoothness S = 0.045.*

If the maximum PD per cycle as well as the total number of PDs per cycle are compared for both smoothness levels (Figures 5.36 -5.37), it can be seen that for the higher level both the number of PDs as well as amplitude remained much lower.

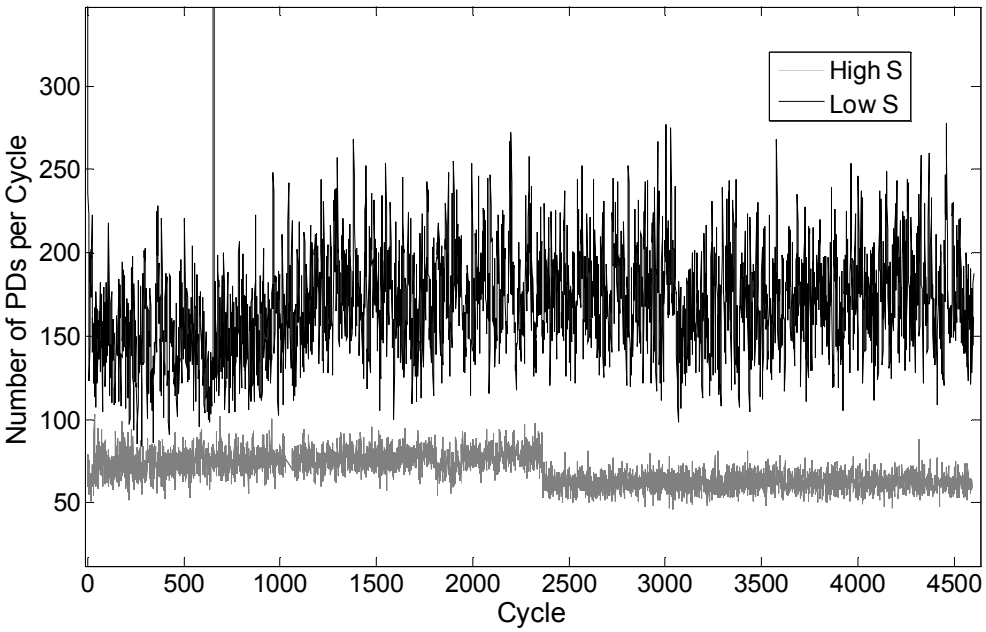

Figure 5.36 *Total number of PDs detected per cycle during treatment of twisted pair by PWM voltage waveforms of different smoothness (S = 75 μ and 0.045 respectively). PD activity during first 4500 cycles is shown.*

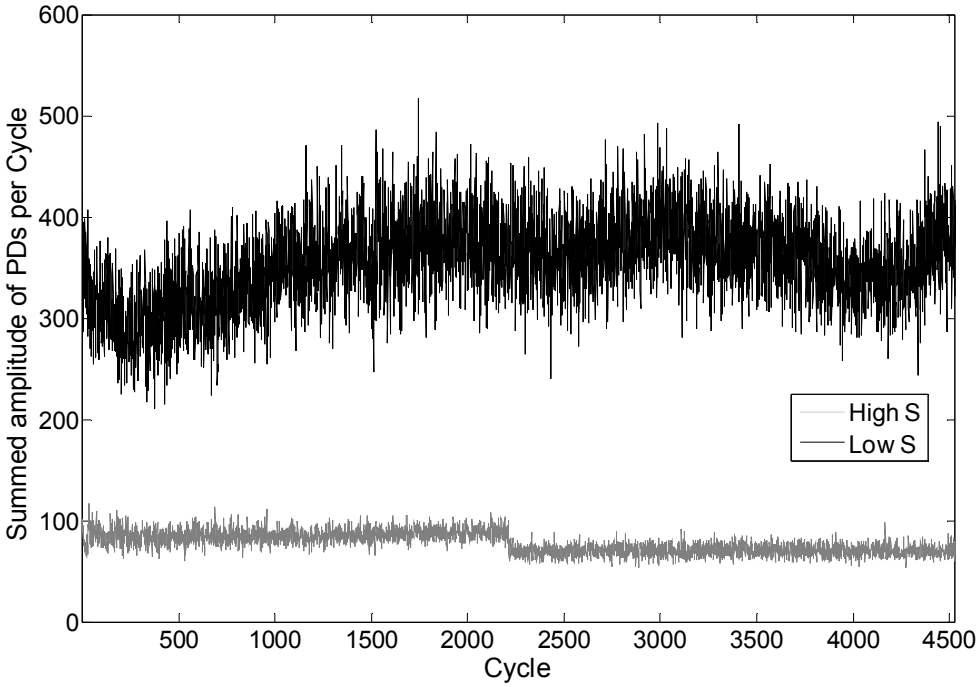

Figure 5.37 *Total summed PD magnitude detected per cycle during twisted pair treatment by PWM voltage waveforms of different smoothness (S=75 μ and 0.045 respectively). PD activity during first 4500 cycles is shown.*

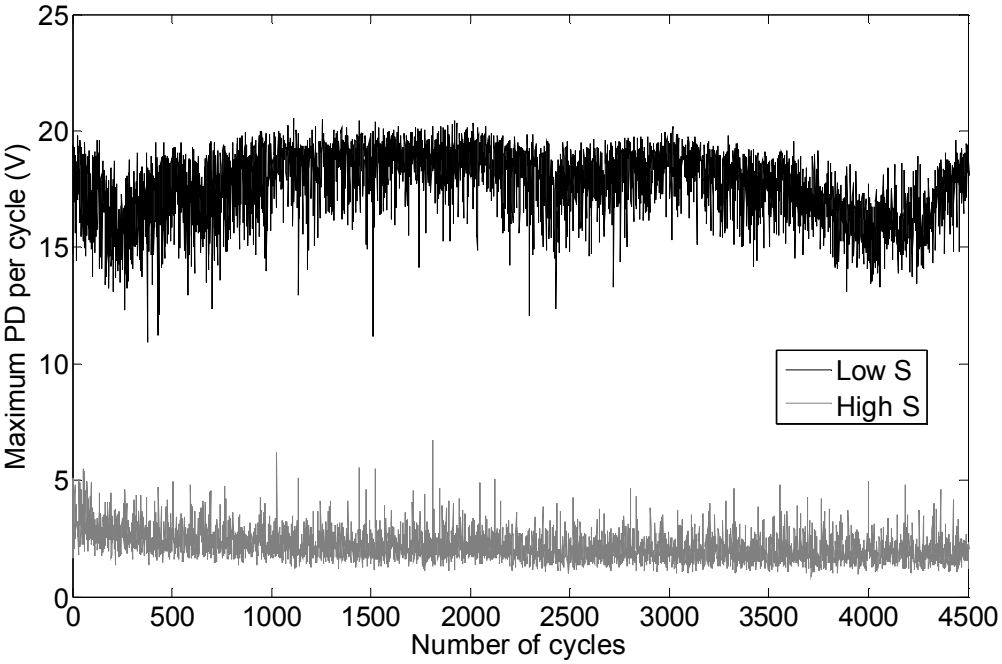

Figure 5.38 *Total maximum PD magnitude detected per cycle during twisted pair treatment by PWM voltage waveforms of different smoothness (S = 75 μ and 0.045 respectively). PD activity during first 4500 cycles is shown.*

The average maximum for the low smoothness is about 17 compared to 2.15 for the higher as illustrated in Figure 5.38. It can be noted that a consistent difference in both maximum individual PD as well as total summed PD remains during the test.

The consistent difference in PD characteristics in the tests with the two smoothness levels indeed confirms the usefulness of the developed approach as a robust tool when evaluating insulation system performance. It also appears that applying only sinusoidal waveforms is insufficient when evaluating the performance of enamel wire insulation for PWM voltage waveform applications.

5.5 Conclusions

In this chapter an approach to measure PDs under PWM voltage waveforms is successfully introduced and applied to several different insulation systems. In all the cases the results display similar tendency of changing PD properties with rise time as the earlier described behaviour of dielectrically insulated cavity exposed to semi-square waveforms. The concept of "smoothness" is introduced and quantified by the level of filtering applied on a PWM voltage waveform. This estimate is designed to provide consistent result regarding the level of filtering needed to reach similar PD exposure as for a sinusoidal waveform.

The study on the dielectrically insulated cavity has shown that the number and amplitude of PDs per modulated period exhibits different characteristics depending on the PWM smoothness level. It also appears that the remaining voltage steps in the smoothened PWM train should remain at lower level than the extinction threshold for reaching the same intensity of PD exposure (in number and amplitude) as under sinusoidal excitation. On the other hand, the short rise time implies on average three to ten times higher PD amplitude per cycle compared to the sinusoidal conditions. Thus the tendencies observed in chapter 4 are confirmed, which emphasises the importance of considering rise time as an important parameter in analyses of PD properties.

Finally, the adapted technique makes measurements of PDs in-service for equipment subjected to PWM voltages possible and the developed algorithm should work equally well for other types of PD decouplers, such as current sensors or antennas.

6 PD Model Analysis

In the previous chapters a number of significant changes in PD properties appearing due to variation of the voltage rise time have been presented. Remarkably, these do not seem to be related to a specific type of test object, grossly the same observations can be made for both cavities and twisted pair objects. However, exceptions exist, as for example discussed in [10, 15] where weak influence of rise time is observed in PD activity from a needle plane geometry in air as well as a pig tail oil paper object.

The main purpose of this chapter is to develop a simple PD model with as few parameters as possible that is able to capture the features presented earlier in this thesis. Preferably, the model parameters should be extracted from measurements or other observations to limit the use of assumptions that are difficult to verify. Additionally, one consistent set of parameters should be valid for all rise times. Due to the geometric complexity of the of the twisted pair test objects, the focus will be on the dielectrically insulated cylindrical cavity.

6.1 Observed PD Properties

Only a few observed experimentally properties of PD behaviour have so far been described through simulations, such as number of PDs per period or visual resemblance of the PRPD patterns [51]. As the studies presented in chapter 4 have resulted in several observations on how the rise time of the applied voltage influences the measured PD characteristics, this information is to be used as the base for the simulation approach presented here. The most apparent observations are as follows:

- One PD per polarity shift is present at shorter rise times whereas a linear relation between number of PDs and voltage level can be observed for longer ones.
- Amplitude of PDs increases for decreasing rise times.

- First PD after a polarity shift appears later for shorter rise times and thus at higher voltage levels.
- A single PD observed at shorter rise times is significantly stronger than the total sum of PDs observed at longer ones.
- Lower extinction voltage level is observed for shorter rise times.

In addition, it has also been noted how the rise time of the PD itself decreases at steeper voltage fronts, however to include this in the model in an adequate way would require an detailed physical description of the discharge process, as undertaken in [54] and falls beyond the scope of this work.

6.2 PD Model

In this section fundamentals of the modelling approach are presented together with details on how different parts of the model are integrated.

6.2.1 Principal approach

The overall main objective with this modelling approach is to reproduce results from the measurements. A starting point is therefore the well-known 'ABC-model' [14, 48], being in particular utilized for sinusoidal voltage shapes of different frequencies [46]. This principle is actually equivalent to a zero dimensional approach of the problem, as

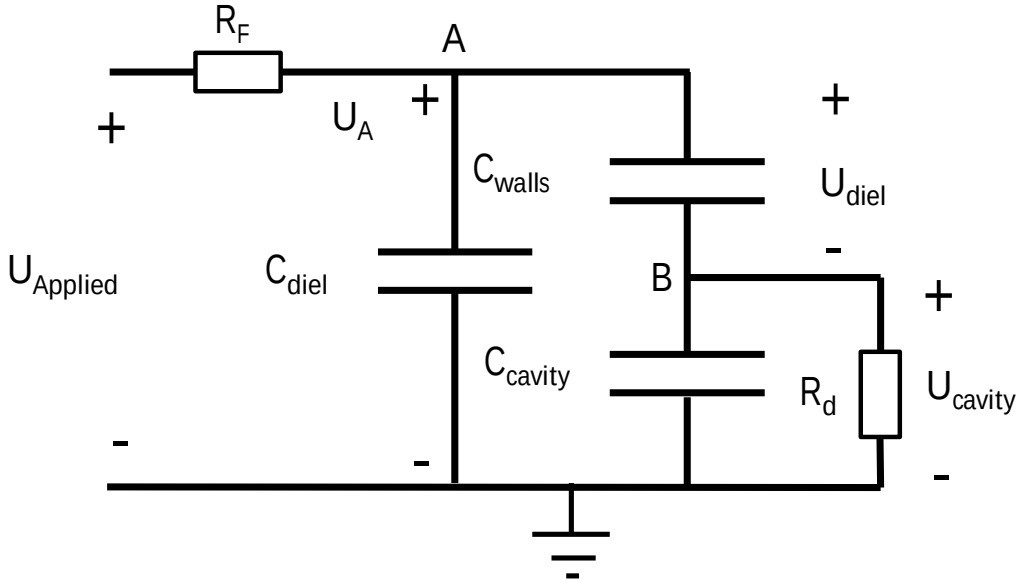

Figure 6.1 'ABC' based model utilized in the simulation. Note that the resistor R_d is controlled to simulate the discharge. Further observe that the parts resembling the cavity walls have been described as one capacitor, C_{walls}, in the model.

introduced by [20]. In Figure 6.1 the insulation material surrounding the defect is introduced as the capacitor C_{diel} and the cavity itself is represented by the capacitor C_{cavity}. The discharge process is modelled with the resistor R_d, the resistance of which is adjusted when a PD occurs. This in principle corresponds to the condition of increasing concentrations of free electrons and ions in physically based models. As the resistivity of polycarbonate material is high, the influences imposed by charge decay and bulk conductivity are neglected. Different properties of the material surface at cavity endplates are represented by C_{walls}.

6.2.2 Simulation algorithm

To facilitate the description of the algorithm, the schematic illustration in Figure 6.2 shows the different steps involved. Each of the steps is described below, while the input includes information about the selected waveform as well as its smoothness, defined similarly as in the measurements:

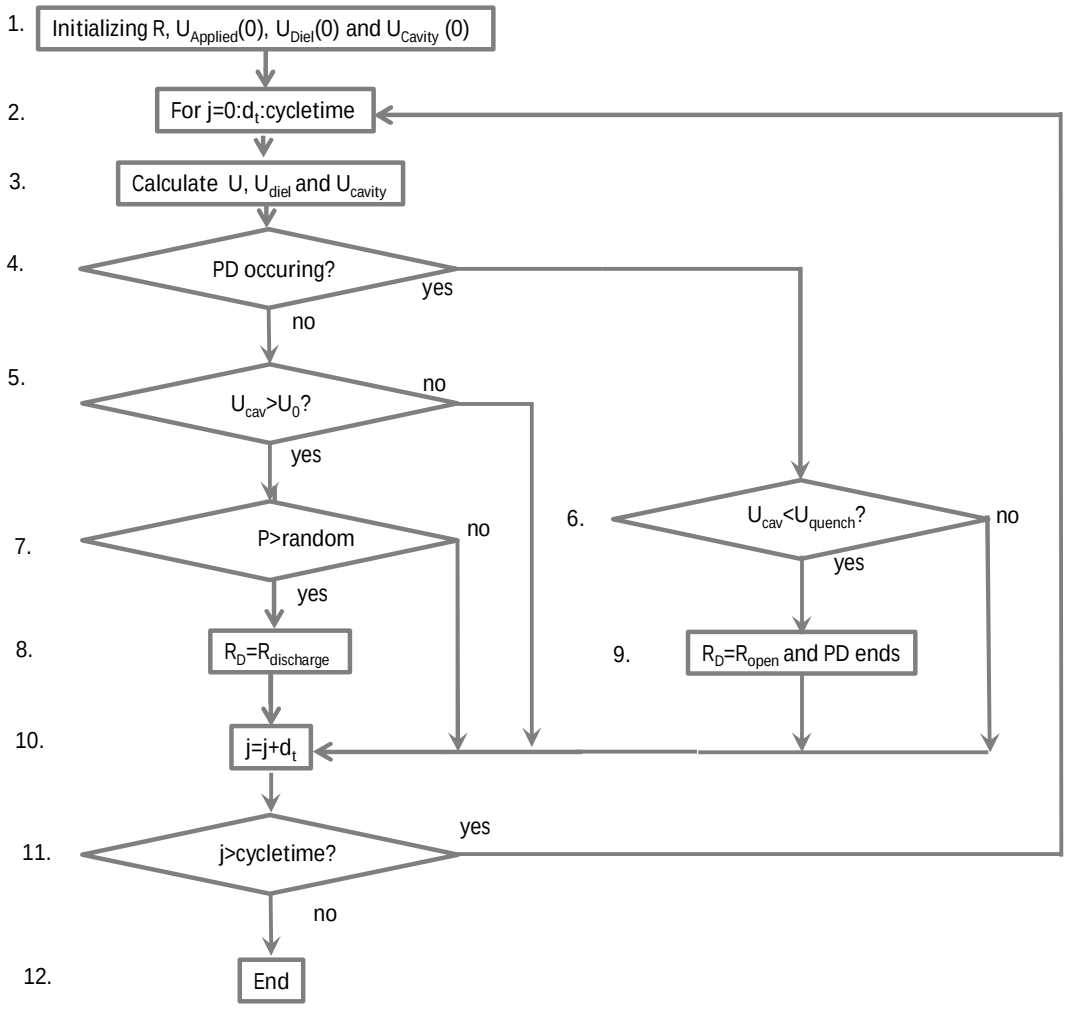

Figure 6.2 The structure of the software algorithm, where steps 2- to 11 are performed for each period studied.

1. The model variables are initiated.
2. Verification whether desired time span has been simulated.
3. In each new time step all the voltages levels within the insulation system are calculated. More details regarding these calculations are introduced below.
4. It is checked whether a PD process is presently occurring or not. If this is the case continue to check the cavity voltage in step 7.
5. The voltage level across the cavity U_{cav} is compared with the minimum value for a PD to occur.
6. Here the electric field level have been found sufficient for a PD, thus a probability expression P is calculated and compared with a random number R. In case that P>R then a PD should occur, otherwise continue for the next time step.
7. A PD occurs, thus the resistor R_d is changed to a low value, $R_{discharge}$, to simulate the discharge.
8. The voltage level across R_D is checked versus the quench voltage, U_{quench}. If the electric field level is low enough the PD ends.
9. The PD ends and the initial, high, $R_d=R_{Open}$ value is used.
10. The time is increased with the time step: $t=t+d_t$.
11. It is checked whether the simulation is completed? If yes the calculation ends.

To derive the voltage across the cavity for each time step, one starts with the Kirchhoff current law in point 'A' in Equation 6.1 below:

$$\frac{U_{Applied}-U_{diel}-U_{cavity}}{R_F}=\frac{U_{Applied}-U_A}{R_F}= \\ =C_{diel}\frac{d(U_A)}{dt}+C_{cavity}\cdot\frac{dU_{cavity}}{dt}+R_d\cdot U_{cavity} \tag{6.1}$$

The second expression is to express the Kirchhoff current law in point 'B':

$$C_{walls}\frac{d(U_A-U_{cavity})}{dt}=C_{cavity}\frac{dU_{cavity}}{dt}+\frac{U_{cavity}}{R_d} \tag{6.2}$$

These equations are expanded to discretized derivatives and solved for the cavity voltage $U_{cavity}(t+dt)$ and $U_A(t+dt)$ as a function of the present voltages and the new applied voltage $U_{Applied}(t+dt)$. Thus $U_{cavity}(t+dt)$ is updated at each time step as:

$$U_{cavity}(t+\ dt) = \frac{C_{wall}(dt-C_{diel}R_F)+C_{Cavity}\left((C_{diel}+C_{wall})R_F-dt\right)}{\left((C_{diel}+C_{wall})C_{cavity}-C_{wall}C_{diel}\right)R_F}U_A(t) +$$
$$+\ dt\frac{\left(C_{Cavity}-C_{wall}\right)}{\left((C_{diel}+C_{wall})C_{cavity}-C_{wall}C_{diel}\right)R_F}U_{Applied}(t+\ dt) +$$
$$+\ dt\frac{C_{wall}}{\left((C_{diel}+C_{wall})C_{cavity}-C_{wall}C_{diel}\right)R_d}U_{cavity}(t) \qquad (6.3)$$

A similar updating Equation holds for U_A.

These are the basic parts of the simulation model. The details will be discussed in the following sections, the model is implemented in Matlab R2011b while the expressions have been derived in Mathematica.

6.2.3 PD occurrence

As measured and discussed in a multitude of papers [12, 14], the PD is a rapid process with short rise time which may introduce issues with convergence of model solutions. Thus to facilitate the calculations the choice of the resistor R_d will be time step dependent to ensure that more than one time step is required for the discharge process to reach the quench voltage. The important issue is that the voltage levels at PD and after are determined in a numerically stable way.

The requirement for a PD to occur is dependent on the electric field level in the defect. In this model is the plane parallel capacitor geometry used to resemble the cavity as well as the surrounding dielectric. This further assumes that both the dielectric insulation and the defect are considered as having equipotential distribution in the radial direction, so the electric field level is constant all across the insulation and the cavity geometry. Thus is the electric field distribution calculated as one value per time step for each part of the test object (dielectric and cavity) in a similar way as in [20, 50]. However, different shapes of the defect can be introduced, such for example as spherical, as long as their geometry allows for a lumped circuit representation and suitable expressions can be applied for describing electric field in each its part. Additionally the presence of volume charges will reduce the accuracy of these assumptions.

As the electric field level in the cavity is dependent on the charge deposited by previous PDs as well as on the externally applied field, it becomes necessary to consider the total resulting electric field in the cavity when estimating if a PD can occur. This model utilizes a minimum total field required, which is determined based on the measured extinction voltage level at the short rise time. Some simulation approaches uses the Paschen curve [52] to determine the minimum required field level. The calculation of this field level is described in the next section.

The resistor applied to simulate the discharge process is adapting the resistance value to simulate the discharge process in a few time steps, until the remaining cavity voltage reaches the level where the PDs cease. A suggested expression for calculating this change in resistance between the off and the on level is as follows:

$$R_d = \frac{k \cdot dt}{C_{cavity}} \tag{6.4}$$

where dt is the time step and constant k is used to provide an additional margin of the time steps for securing convergence of the calculations (typically k = 2 is applied in these simulations). The off value of R_d is selected so that a discharge of the capacitor takes many periods. It must be pointed out that it is necessary to employ a limited value of this resistance. A commonly used level of air resistance in a cavity is about $10^{16}\,\Omega$ [67]. Such an estimate, describing the non-PD state in the cavity, is adopted in the simulations.

The observation that PDs behave symmetrically at both polarity reversals simplifies the model. Thus the employed R_d values are assumed to be polarity independent.

6.2.4 Parameter setting

The measurements in section 4.3.4 have indicated PD rise times shorter than about 15 ns. This would increase the simulation time considerably if obeyed. Introducing instead the change in resistance R_d is advantageous since it allows reducing the simulation time. Thus the simulations can employ a time step of 25 ns for all the considered voltage rise times.

Table 6.2 Capacitance values employed in the ABC model

C_{diel} (pF)	C_{cavity} (pF)	C_{cavity_wall} (pF)	Time step d_t (ns)	R_{open} (Ω)	$R_{discharge}$ (Ω)
50	0.15	0.22	25	10^{16} (off)	$2d_t / C_{cavity}$(on)

The capacitance values are calculated based on a plane parallel cylindrical geometry. And the test object and the cavity diameters are respectively assumed to be 140 and 4 mm. Polycarbonate plates as described in chapter 4 is used and its permittivity ε_r is assumed to be 3. The resulting capacitance values are listed in Table 6.2.

For a PD to occur the electric field must be high enough and a free electron needs to be present in the cavity. A measure of the minimum electric field is thus required. Since the measurements reported in chapter 4 indicated the extinction voltage level of about 5 kV_p at short rise times, the minimum electric field level in the cavity becomes:

$$E_{cavity} = \frac{U_{applied} \cdot C_{cav\_wall}}{\left(C_{cavity\_wall} + C_{cavity}\right) h_{cavity}} = 4\ kV/mm \tag{6.5}$$

When applying Paschen expression for this cavity, the electric field level required for starting PD becomes equal to 4.9 kV/mm. This reproduces well the measured values for a virgin cavity; however at stationary conditions a slightly lower value is expected, as a clear difference in inception and extinction voltage were noticed in section 4.2.1. Thus, in the following simulations a higher value of the electric field level than the one provided by Equation 6.5 is adopted, $E_{cavity\ min}$ = 4.8 kV/mm. The minimum voltage over the cavity for a PD to occur becomes equal to:

$$U_0 = E_{cavity\ \min} \cdot d \tag{6.6}$$

The following sections illustrate the properties of the simulated PD characteristics at different rise times and discuss the implications of different model parameters when relating simulation results to measured observations.

6.3 Reproducing PD observations

The simulations presented below aim to resemble the results of measurements on the cavity objects, presented in chapter 4. It has been observed that the diameter of the cavity influenced PD characteristics, smaller dimensions resulted in fewer PDs. Commonly, for cavity diameters of 4 mm and below, one PD per polarity shift is recorded on average for the shorter rise times. When performing the simulations for such cavity dimensions, it is therefore reasonable to assume that each PD affects the whole volume of the defect.

6.3.1 Probability and time delay

Three different probability densities p per normalized time unit are used in the calculations: 5, 50 and 95 [%/d_{t0}]. At each time step, when sufficient electric field level across the defect is being reached, this probability density is multiplied with the time step d_t. Thus the probability estimation becomes insensitive to changes in time resolution. This probability is then compared with a random number R, representing the influence of the time lag in the discharge development and needs to be accounted for when determining the PD occurrence. Based on measured results in chapter 4, 0.5 µs is assumed as an average time delay, which thereafter is used together with the calculated probability to set different quench voltage levels. An applied voltage of 8 kV_p is employed in these initial simulations to ensure that at longer rise times more than 4 PDs per period should appear.

6.3.2 Constant PD quench voltage

This initial trial explores the relation between the numbers of PDs appearing as well as the PD amplitudes at two voltage rise times, 4 and 40 µs. We initially introduce a

relatively high U_{quench} that reduces the voltage drop across the cavity at PD occurrence to about 2 kV. This results in more than one PD per polarity shift for both the rise times. Figures 6.3 and 6.4 exemplify typical simulation results of the obtained PD characteristics.

Additionally, since the PD amplitude is proportional to the voltage drop, its change due to the rise time variation is small, whereas the included delay time do increase the PD magnitude slightly at short rise times. However to resemble the measured results, the difference in PD amplitude should be up to at least 5 times, as indicated in Figure 4.10, while here at most a factor 2 is seen. One can thus conclude that the adopted value of quench voltage fails in resembling the experimental observations.

To investigate an opposite case, a low quench voltage is used that implies an almost fully discharged cavity (300 V) at each PD occurrence. As a consequence, for the same rise times employed, the simulation is unable to reflect the observed changes in the number of appearing PDs, Figure 6.5 presents the simulated result the shorter rise time. One PD appears here per polarity shift, as expected. However, less PDs as compared to the experimental observations are observed in the simulation for the longer rise time, Figure 6.6. In the latter case only two PDs on average are generated per polarity reversal. Additionally, the difference in PD amplitude is still small. Thus the models needs a further development, based on assumptions motivated on the basis of experimental observations.

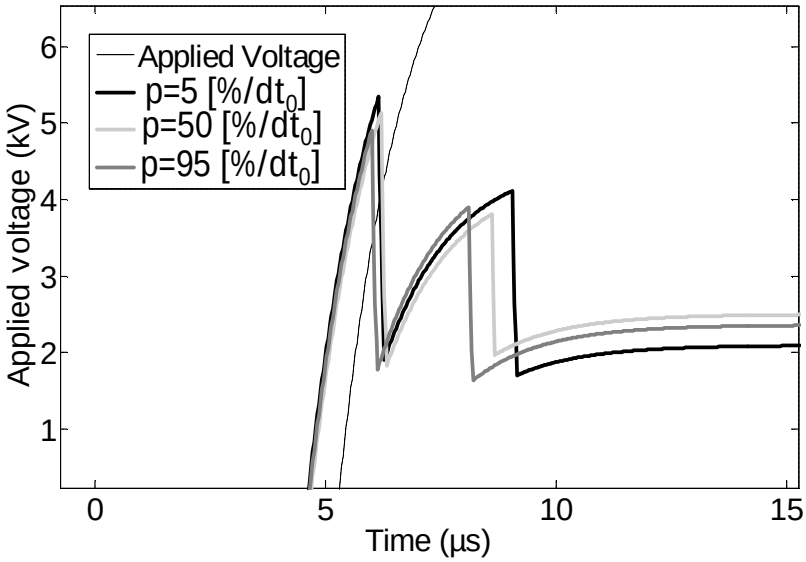

Figure 6.3 Simulation of PDs at rise time of 4 µs for a constant high quench voltage (2 kV) and different discharge probabilities (5, 50 and 95 [%/d_{t0}] probability density).

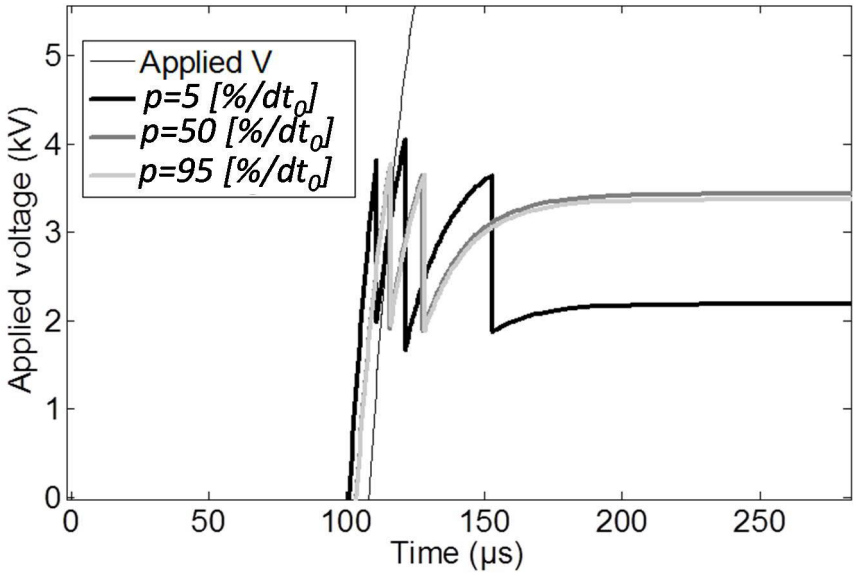

Figure 6.4 Simulation of PDs at rise time of 40 µs for a constant high quench voltage (2 kV) and different discharge probabilities (5, 50 and 95 [%/d_{t0}] probability density). Between 4 and 6 PDs appear per period.

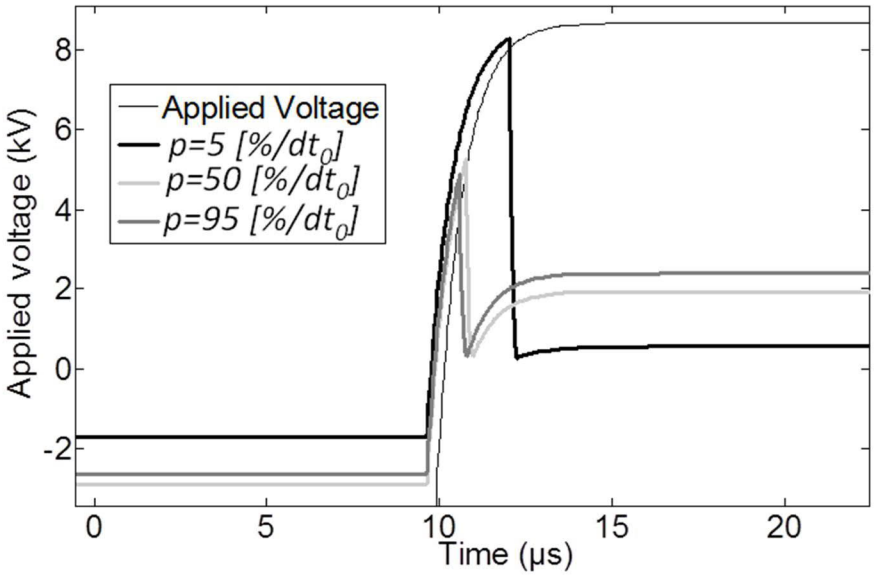

Figure 6.5 Simulation of PDs at rise time of 4 µs for a constant high quench voltage (300 V) and different discharge probabilities (5, 50 and 95 [%/d_{t0}] probability density).One PD is observed per polarity shift.

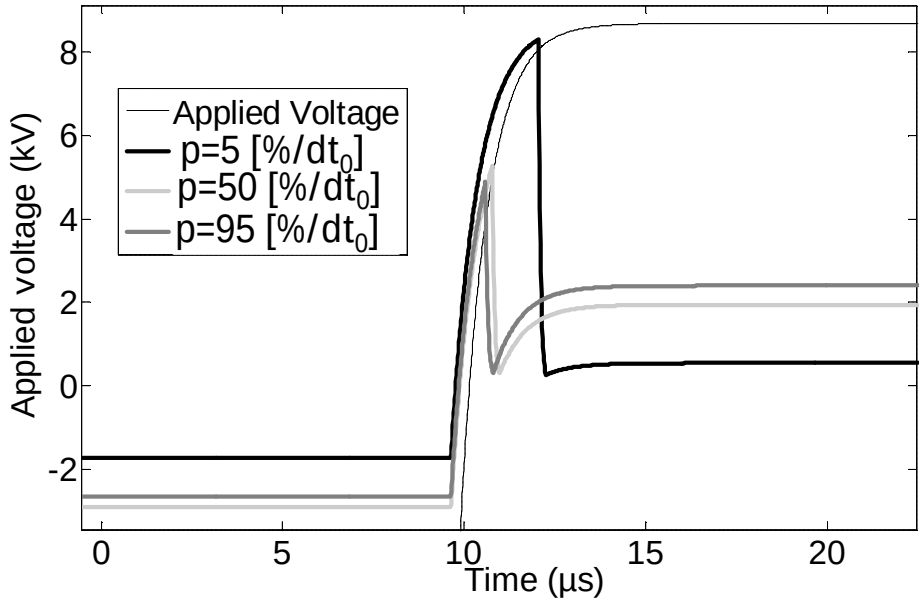

Figure 6.6 Simulation of PDs at rise time of 40 µs for a constant high quench voltage (300 V) and different discharge probabilities (5, 50 and 95 [%/d_{t0}] probability density). The number of PDs per period does not change sufficiently at various probability values.

6.3.3 Experimental indications for quench voltage variation

To properly explore the relation between quench voltage and PD magnitude additional analyses of the previously presented results are required. Since it is impossible to directly measure the quench voltages, the applied voltage as well as the observed PD properties must be considered. An approach suggested in [68], known under the name Pulse Sequence Analysis (PSA), relates the PD appearance to the applied voltage level (or time of occurrence). Here a similar method is employed for cases where more than one PD occurs. For each new polarity shift both the voltage level where the first PD appears as well as the PD magnitude are noted. This is correlated with the difference in voltage until the appearance of next PD within the same voltage half period, as illustrated in Figure 6.7. Here the concept of an overvoltage is introduced that reflects the voltage difference between the minimum voltage at which a PD can occur and the level when it actually takes place. The two PDs indicated in the figure have different voltage drops, here assumed to be two times the overvoltage level at the time of occurrence, the higher the overvoltage the higher the voltage drop. This also implies a higher PD magnitude. The subsequent PDs require thus a longer time until enough voltage builds up (higher differential voltage), as indicated in Figure 6.7 for different overvoltage levels.

The data originating from the measurements on dielectrically insulated cavity exposed to PWM waveforms of different smoothness (section 5.2) are further utilized for estimating the simulation parameters. In Figures 6.8 and 6.9 the position of each PD, measured as reported in chapter 5.2, is indicated as a function of the differential voltage for two different rise times (12 and 2.5 µs). It can be noticed that the differential voltage value increases with the PD amplitude in both cases and that the differential voltage value from the first PD to the next one is indeed dependent on the magnitude of the first PD.

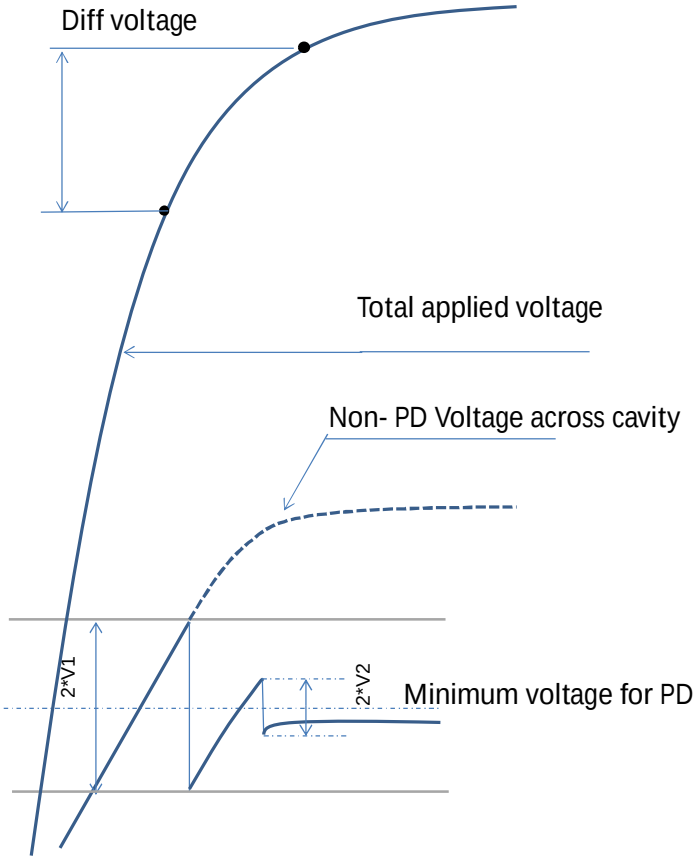

Figure 6.7 Correlation between overvoltage and voltage dip introduced by two PDs. The voltage dip is assumed to be 2 times the overvoltage.

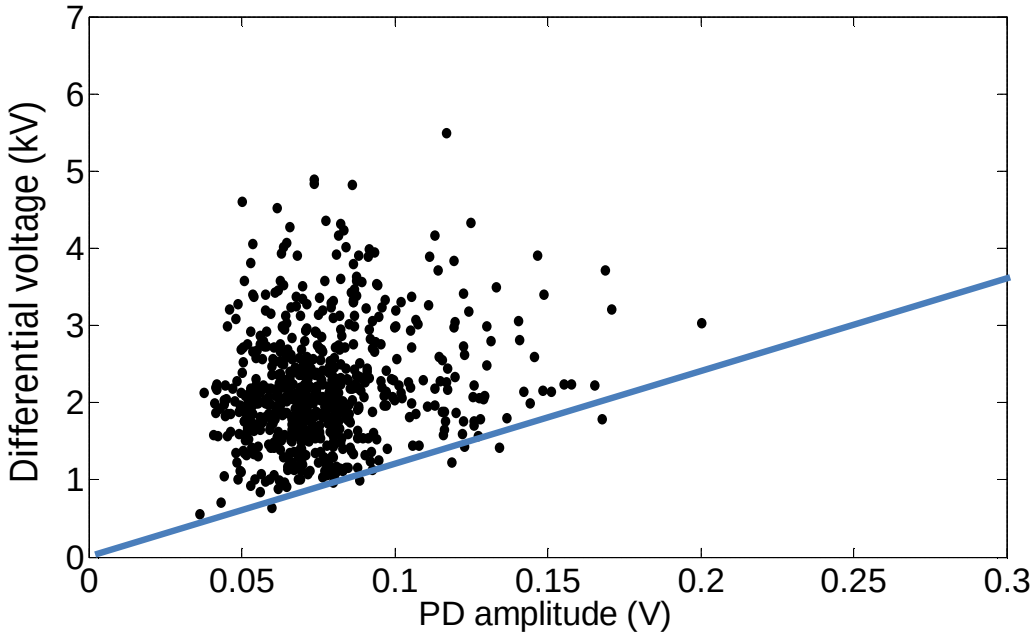

Figure 6.8 Differential voltage level related to amplitude of preceding PD event at 12 µs rise time.

In the relation between the differential voltage level and the PD amplitude illustrated in Figures 6.8 and 6.9 a linear increasing tendency is clearly observable. This relation indicates the required minimum increase in applied voltage level for appearance of a next PD after a PD with specific amplitude takes place. The slope K of the indicated graphs can be calculated as:

$$K = \frac{3750}{0.3} = 12.5\, kV / V_{PD} \tag{6.7}$$

This however only relates the changes in the external voltage level, not across the cavity. By considering a linear relation between the differential voltage and PD magnitude, the ABC-model can be employed to estimate the voltage level slope K' across the cavity by utilizing the capacitance numerical values from Table 6.2:

$$K' = \frac{C_{cavity\_walls}}{C_{cavity} + C_{cavity\_walls}} K = 7.5\, kV / V_{PD} \tag{6.8}$$

It should be emphasized that the differential voltage must always be above 0 V.

As the PD amplitude increases on average with the voltage level, an assumption can be made that the first PDs appearing at a higher voltage level implies reduced quench voltage and lower remaining cavity field strength. The natural assumption when deducing the similar parameters for lower smoothness levels is that the higher PD amplitudes observed should also imply larger differential voltage, which is illustrated in Figure 6.9.

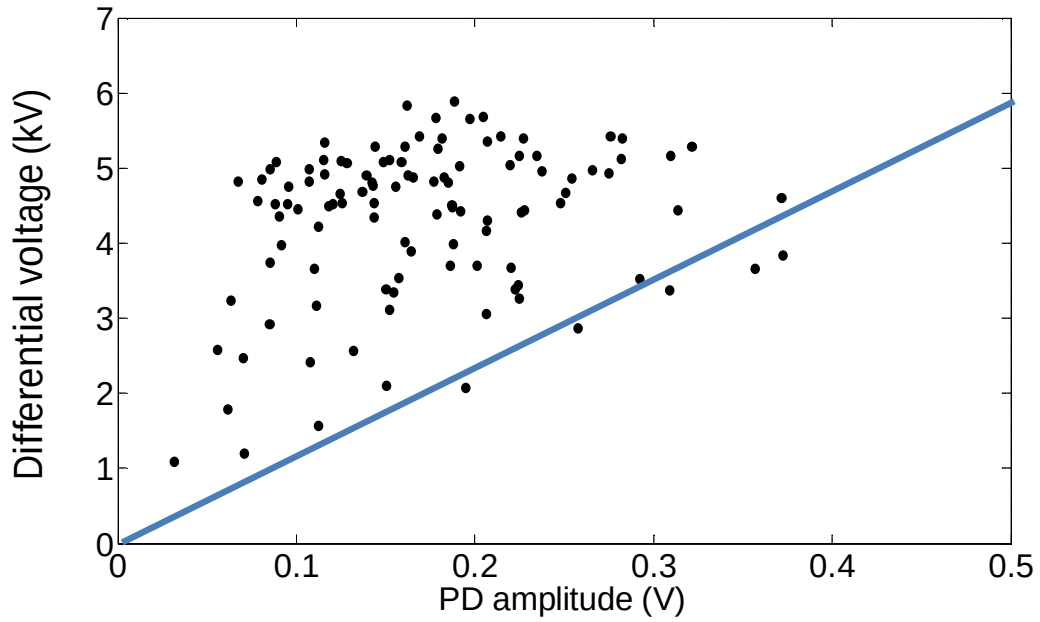

Figure 6.9 Differential voltage level related to amplitude of preceding PD event at 2.5 µs rise time.

Since for the case of data presented in Figure 6.9 the rise time is shorter, fewer secondary PDs are observed and thus less data points presented. The indicated slope is however similar to the one for the longer rise time, but the amplitude of the registered PDs is larger. As a result a robust estimation of the quench voltage level becomes possible for a considerable interval of PD magnitudes.

6.3.4 Quench voltage model

The above presented discussion allows assuming that a suitable expression can be introduced to adjust the quench voltage U_{quench} in relation to the overvoltage, U_{cav}-U_0, at a PD occurrence. It is assumed that $U_{quench,}$, is linearly dependent on the level of the overvoltage U_{cav}

$$U_{Quench} = U_0 - a \cdot \left(abs(U_{cav}) - U_0 \right) \tag{6.9}$$

If a = 2, as indicated earlier, than the voltage dip equals the overvoltage level, as marked in Figure 6.7. This linear relation is however an approximation since the available data is not sufficient to indicate any other type of relation. The quench voltage should not drop below a certain limit, here assumed to be 300 V. This limit agrees reasonably well with the numeric value of 290 V/mm elaborated in [54] for a few mm long air gaps. Thus the procedure to determine the quench voltage is as follows:

$$U_{Quench} = Max\left(U_0 - a \cdot \left(abs(U_{cav}) - U_0 \right), 300\right) \tag{6.10}$$

Different levels of quench voltage were also used in [21] for simulating PD behaviour at voltages of different frequency. At higher frequencies a lover quench voltage value was employed as compared to the lower frequencies. In the latter case, due to a slow rise and decrease in the applied voltage, low overvoltage levels dominated.

6.3.5 PD probability function

One of the most important and difficult parts when performing simulations using the macro modelling approach is to find suitable probability function which, at least quantitatively, describes the influence of the applied voltage waveform on the calculated PD characteristics. The main aim is to include the observations discussed above by means of one set of parameters.

The initiation of a discharge in air cavity requires availability of free electrons under sufficiently high electric field level. The free electrons can originate from different processes, including natural ionization, surface emissions as well as ion and photon impacts at sufficiently high electric field levels. We therefore introduce a probability density function to relate the condition of a PD occurrence in dependence of the applied voltage across the cavity U_{cavity}. Additionally no PD should be introduced until a sufficient voltage level, U_0, is reached across the defect. Thus the expression describing this probability density function is as follows:

$$p(t,U_{cavity}) = \left(\alpha + \beta \cdot \left(\frac{U_{cavity} - U_0}{U_0} \right)^{\gamma} \right) \theta\left(U_{cavity} - U_0\right) \tag{6.11}$$

where the parameters $\alpha[1/d_{t0}]$, $\beta[1/d_{t0}]$ and γ are adopted to fit the measured data. Equation 6.11 provides the calculated probability density value per time unit. By multiplying it by the time step d_t, the probability P(t, U) is obtained to compare with the random variable R. θ is a step function eliminating occurrence of PDs below a minimum overvoltage level.

For analysing the influence of the overvoltage, a similar expression, but without voltage dependence, is introduced, in which the initial probability density is kept constant above minimum voltage level U_0:

$$p(t,U_{cavity}) = \alpha \cdot \theta\left(U_{cavity} - U_0\right) \tag{6.12}$$

It is important to note that expressions 6.11 and 6.12 include time as a parameter. It conditions the appearance of PDs through taking into consideration the statistical and formative time lags in the discharge development. Here a simple time delay is suggested, as defined in Equation 6.13, that includes a random variable (rand) uniformly distributed across the interval (0, 1):

$$t_{\min} = t_{lag} + \Delta t \cdot rand \tag{6.13}$$

Together with the conditions defined in in Equations 6.10 - 6.12, no PDs should happen unless $U_{cavity}>U_0$ longer than the minimum time delay t_{min}. The latter condition is included by adding an additional step function, as in Equation 6.14:

$$P(t,U_{cavity}) = \left(\alpha + \beta \cdot \left(\frac{U_{cavity} - U_0}{U_0} \right)^{\gamma} \right) \cdot \theta\left(U_{cavity} - U_0\right) \cdot \theta\left(t - t_{\min}\right) \cdot d_t \qquad (6.14)$$

where t = 0 is defined by the instant when U_{cavity} first increase above U_0. This expression does not limit the probability for higher overvoltages, despite the presented measured data indicate a limit of the overvoltage level. However, for $\gamma = 1$ the suggested expression resembles a Taylor approximation of an exponential function where the maximum probability is indeed limited:

$$P(t,U_{cavity}) = \left(1 - e^{-\left(\alpha + \beta \cdot \left(\frac{U_{cavity} - U_0}{U_0} \right) \right) dt} \right) \theta\left(U_{cavity} - U_0\right) \theta\left(t - t_{\min}\right) d_t \qquad (6.15)$$

Table 6.2 Parameters employed in the simulations. Note that $\beta = 0$ for the constant probability simulation and that the time step employed is used for both α and β.

Alternative	αd_t	βd_t	γ	t_{lag} (µs)	Δt (µs)	U_0(kV)
1	0.1	0	-	0.5	1	3.6
2	0.1	0.9	1.0	0.5	1	3.6

In chapter 4 the distribution function for the occurrence of the first PD per polarity reversal were determined for both short and longer rise time. To evaluate correctness of the suggested probability expression, a cases with short (4 µs) and long (40 µs) rise times are simulated. As the measured results exhibit a delay in PD appearance for the short rise time, the simulated results should demonstrate a similar property. Expression 6.14 was employed with the parameters defined in Table 6.2. The expected outcome is that the width of the PD distribution should appear narrower for the voltage controlled probability as compared to the constant one since this probability increases with voltage level. At the same instant, the time delay influence should be of a minor importance for the longer rise time. The claimed tendencies are observed for the simulations presented in Figure 6.10, similarly as in the experimental results in Figure 4.6.

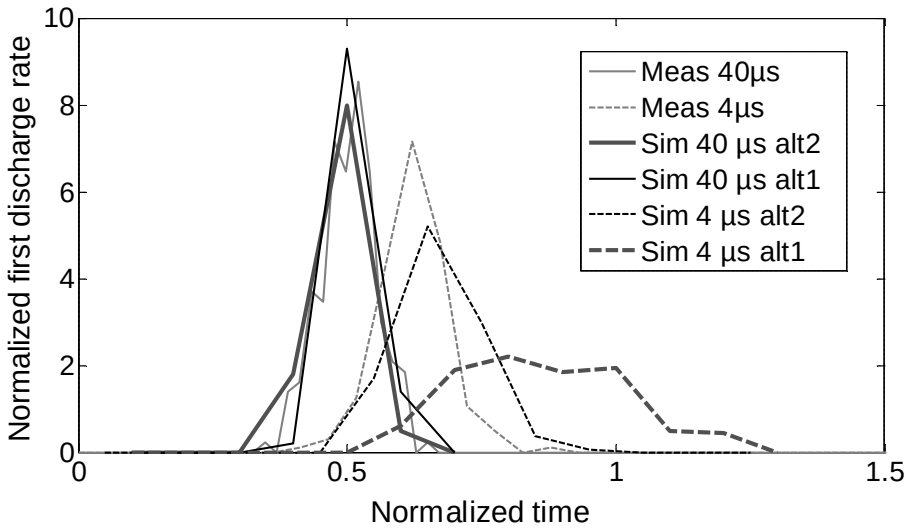

Figure 6.10 Comparison of first discharge rate distributions obtained from simulations using different probability functions at different rise times.

When analysing the widths as well as magnitudes of the distributions presented in Figure 6.10 the two presented cases seem reasonable well represented with the help of Equation 6.14. This suggests that the simultaneous use of voltage and time as variables is sufficient to describe the experimental observations regarding the occurrence of first PDs and their amplitude. The natural continuation is then to elucidate how the number of PDs per period changes when applying the suggested probability function.

The experimental data presented in chapter 4 show a clear relation between the rise time and the number of appearing PDs. This tendency is particularly noticeable from about 7 kV_p and upwards. To illustrate that the proposed probability distribution function yields similar results, a simulation is performed to find the number of PDs per polarity shift at 8 kV_p at some different rise times. The obtained result and its comparison with experimental data is illustrated in Figure 6.11. The model predicts an increase in the number of PDs above 10 µs, while only one PD per polarity shift is found at shorter rise times. The agreement with the experimental observations is here very good.

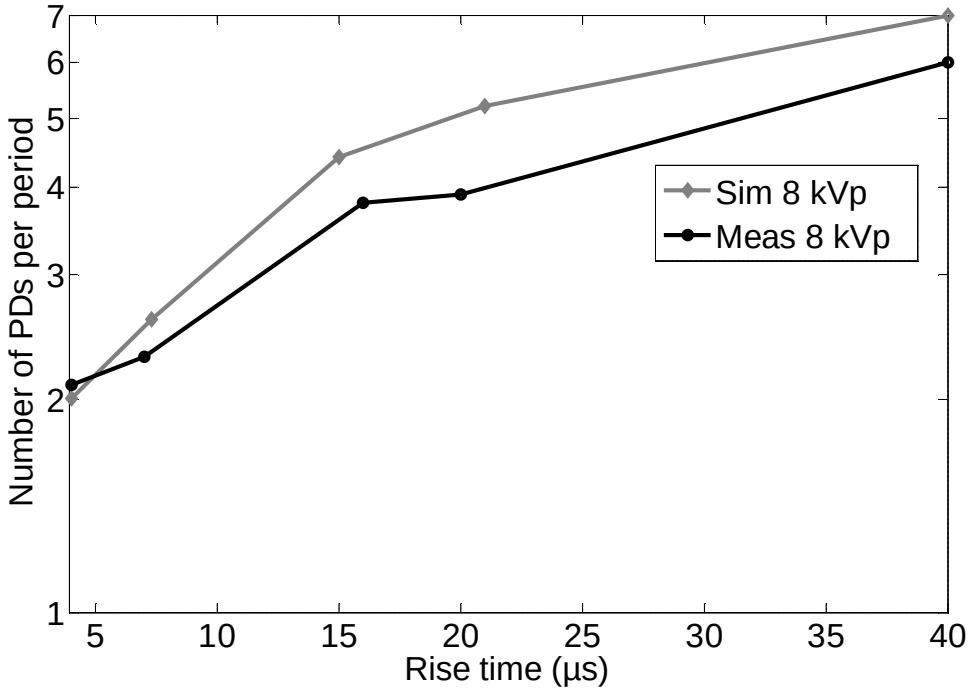

Figure 6.11 Simulated number of PDs per polarity shift for different rise times at 8 kV_p compared with experimental observations from section 4.3.

6.3.6 PD amplitude at various rise times

All the insulation systems tested in this thesis have shown a considerable dependency of PD amplitude on the rise time of the applied voltage. The aim with this section is to evaluate how the experimentally observed behaviour can be reproduced by the adopted the simulation model. The measured data for 8 kV_p were employed to compare in the following differences with the simulations of the summed and maximum PD amplitudes. Since the unit of the simulated PD amplitude is nC and of the measured one V, the results are normalized with the relevant maximum values at the shortest rise time (4 µs) to facilitate the comparison, see Table 6.3.

Table 6.3 Measured and simulated maximum values of PD parameters for the rise time of 4 µs. The data presented in Figure 6.12 are normalized based on these data.

Rise time (4 µs)	Summed PD	Max PD
Measured (V)	2.1	1.8
Simulated (nC)	0.9	0.8

The data presented in Figure 6.12 exemplify how both the maximum and summed PD amplitudes decrease with increasing voltage rise time. It is clear that the observed tendency shows similarity between the simulated and the measured results. The decay

in the normalized maximum magnitude shows however a faster decay for the simulated results.

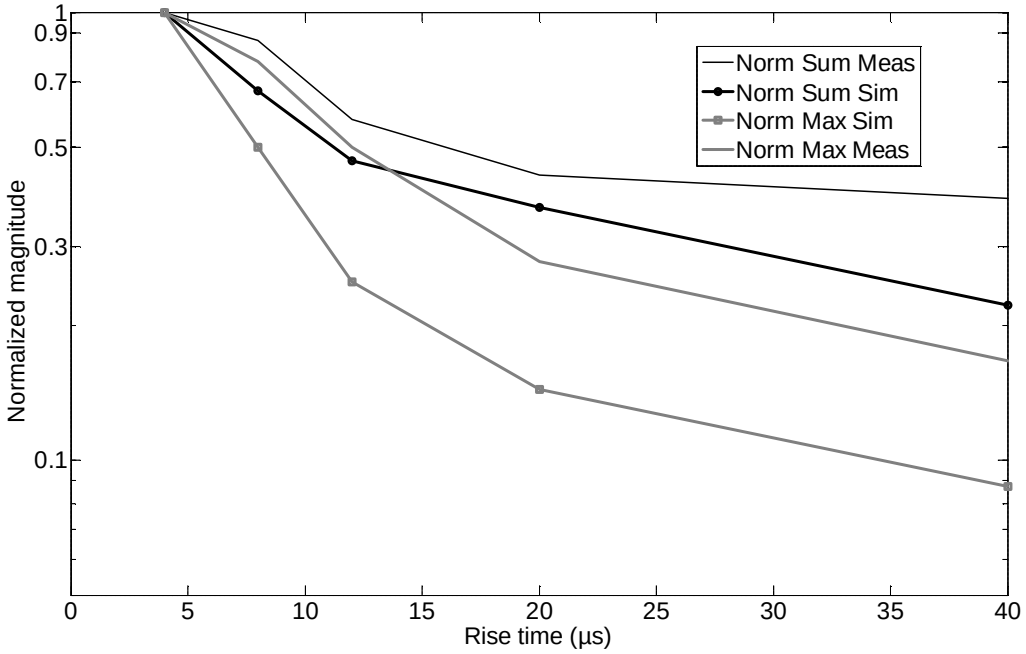

Figure 6.12 Simulated normalised summed and maximum PD amplitudes per voltage polarity shift for different rise times at 8 kV_p and their comparison with experimental data.

6.3.7 Observation of extinction voltage behavior

According to the results presented in chapter 4, the extinction voltage provides a more consistent measure of PD behaviour than the inception level. As this measure is found to be sensitive to the rise time employed, a similar effect should be predicted by the simulation model. To study it, two rise times are selected, 2.5 and 160 µs, for which a difference of about 1 kV_p in the extinction voltage is measured. Each of these cases is simulated by stabilizing the PD process at 8.5 kV_p for at least 200 cycles and thereafter decreasing the applied voltage gradually with one percent per polarity shift until no PDs appear. In Figures 6.13 and 6.14 the gradual voltage change is exemplified for the longer rise time. It can be seen that the quench voltage increases and after reducing the voltage level down to about 6.0 kV_p no PDs occur, the extinction voltage is reached. Since the quench voltage remains higher for the longer rise times, this implies a higher extinction voltage.

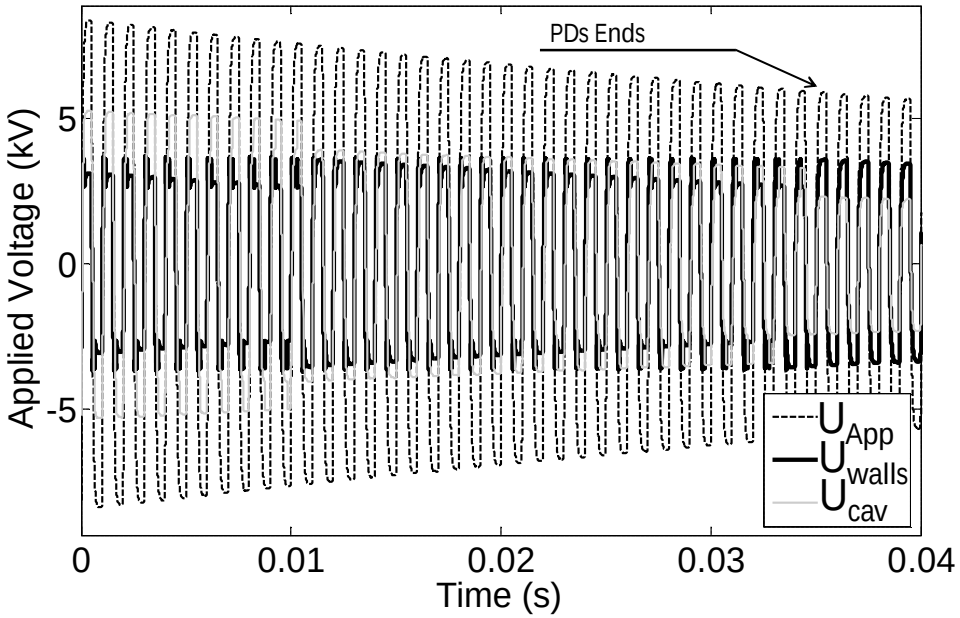

Figure 6.13 Simulation of PD extinction process during gradual decrease of the applied voltage with rise time of 160 µs.

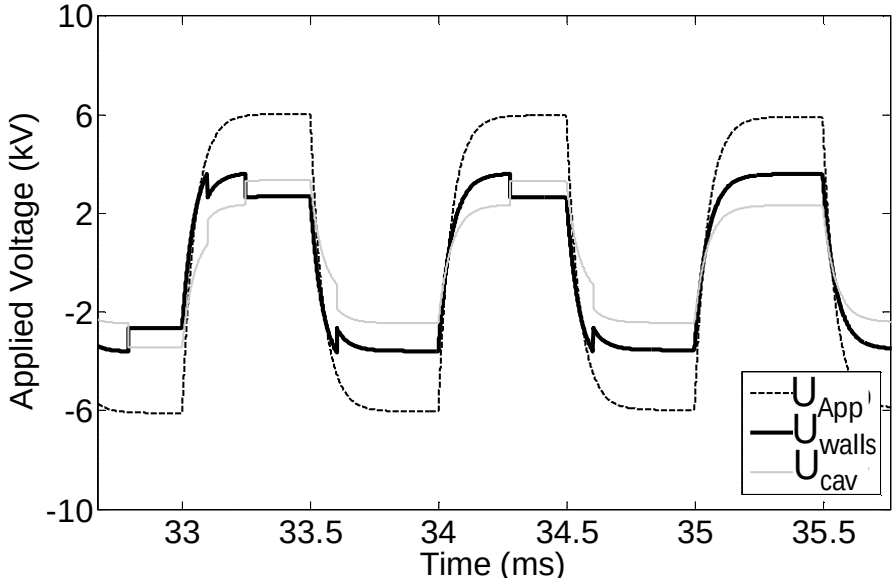

Figure 6.14 Enlargement of Figure 6.13 at the time instant when the extinction voltage is reached. No PDs appear after about 6 kV_p.

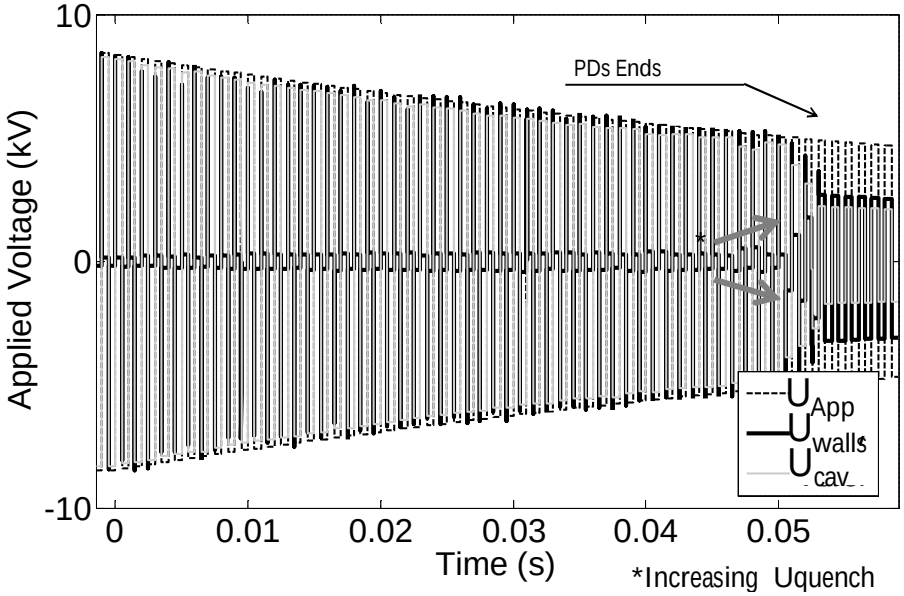

Figure 6.15 Simulation of PD extinction process during gradual decrease of the applied voltage with rise time of 2.5 µs. Note the positions where the quench voltage starts to increase.

When performing simulations for the short rise time, the model predicts occurrence of PDs at higher overvoltage ratios and thus the cavity is discharged to considerably lower quench voltage level, see Figures 6.15 and 6.16. This process contributes to PDs continously appearing at higher voltage levels. As the applied voltage decreases, the quench voltage increases and the amplitude of PDs decreases after each polarity reversal until they cease completely at a lower exctinction level. In this particular case the exctinction voltage was found to be about 4.9 kV_p.

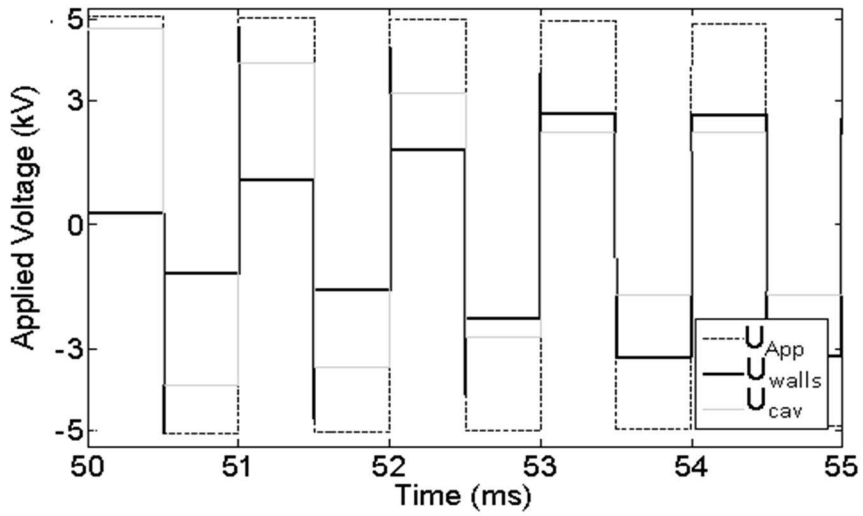

Figure 6.16 Simulated decrease in voltage level until no PDs occur. Note that the decreasing voltage level gradually reduces the over voltage level and subsequently an increase in quench voltage follows. The PDs disappear at about 4.9 kV_p.

6.3.8 Differential voltage

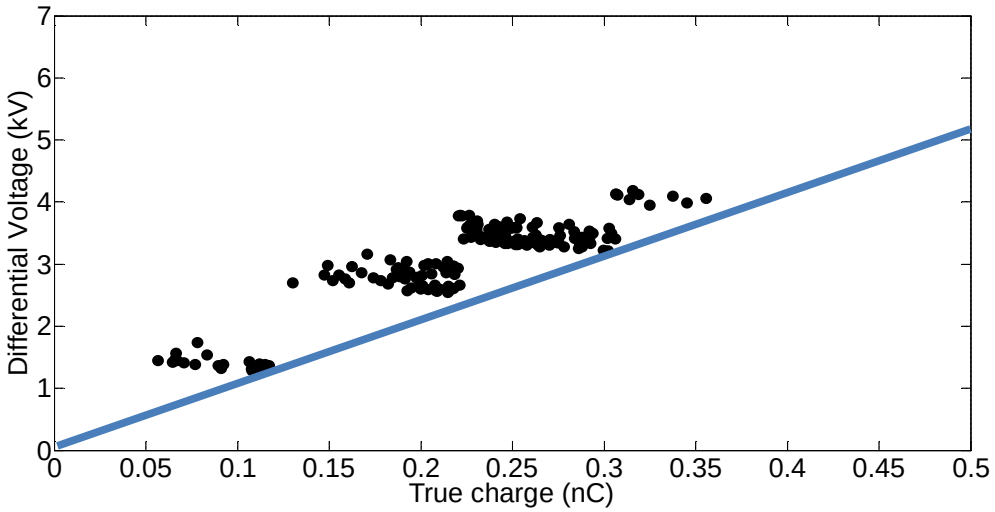

Figure 6.17 Simulated dependence between differential voltage and PD amplitude for 9 µs rise time - on average 4.1 PDs per cycle.

The relation between differential voltage and PD amplitude is elucidated in this section based on the experimental data presented in section 5.1. Two rise times are selected for exemplifying the effect; these are 9 and 18 µs to provide a sufficient amount of second PDs. It is found from the measurements that the differential voltage needed to create a second PD steadily increases with PD amplitude and a similar tendency is clearly observed from the simulation results presented in Figures 6.17 and 6.18. In both the cases a minimum slope of the dependence becomes apparent, similarly as for the measured data presented in Figures 6.8 and 6.9. The deviation of differential voltage for particular PD amplitude appears to be lower, but the general tendency is captured in the simulations well. The shorter rise time also implies larger PD amplitudes and fewer second PDs are observed.

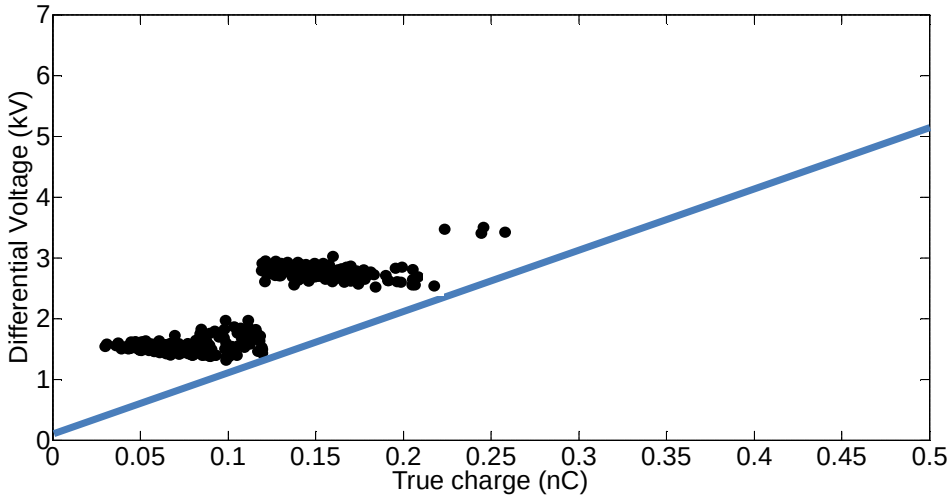

Figure 6.18 Simulated dependence between differential voltage and PD amplitude for 18 µs rise time - on average 5 PDs per cycle.

The small variation in differential voltage from the simulation for various PD amplitudes indicates a need for further exploitation of the probability function as the variation in the experimental data, figures 6.8 and 6.9, is much larger.

To enable comparison to the measured data, the simulated PD magnitudes need to be scaled. In the model the differential voltage is registered between two PDs and the true PD charge is calculated. However to relate this charge to the measured PD amplitude, the relation between the voltage measured by the PD detector and the apparent charge is used, similarly as discussed in chapter 6.3.3. It is estimated that for the dielectrically insulated cavity, 1 mV on the detector corresponds to about 1.5 pC (K''). At the same time the slope of the characteristics in Figures 6.17 and 6.18 is:

$$K = \frac{5100}{0.5} = 10.2 \ \ kV/nC \tag{6.16}$$

The differential voltage is then estimated as:

$$K' = \frac{C_{Cavity\_walls}}{C_{Cavity} + C_{Cavity\_walls}} K \cdot K'' = 9.2 \ \ KV/V_{PD} \tag{6.17}$$

A somewhat larger value of the differential voltage is obtained than the measured one, 7.5 kV/V_{PD}. This, at the present stage, seems to be of a reasonable accuracy as the model applies several simplifying assumptions. Additionally the difference between the true and the apparent charge is neglected.

6.3.9 PWM waveforms at different smoothness

Data presented in Chapter 5 show that the PRPD pattern strongly depends on the smoothness level of PWM voltage waveform. If the magnitude of the voltage steps related to the carrier frequency is lower than the extinction level, the pattern follows the shape of synthesized waveform. This section demonstrates how these observations are reflected by the simulations when applying waveforms of different smoothness. The same amplitude of 8.75 kV_p is used for all the simulated waveforms. Figure 6.19 show the results obtained for a waveform of low smoothness, which indicates that PDs occur mainly at its flanks. The spread in PD amplitude is similar as the one seen in the results of measurements (Figure 5.7). The influence of jitter on PWM waveform is excluded here, which decreases the spread in PD occurrences.

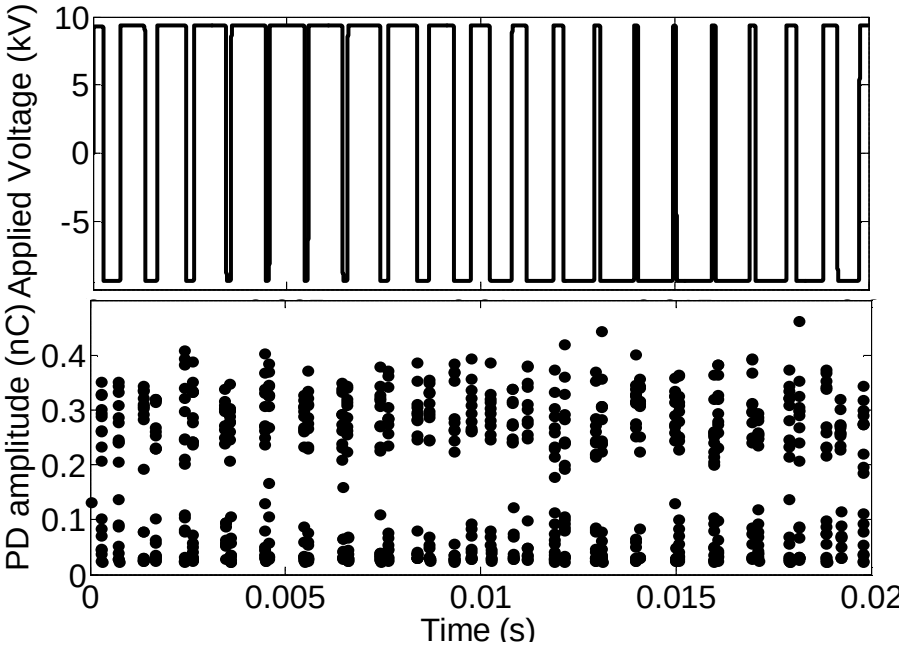

Figure 6.19 Simulated effect of PWM waveform of low smoothness (S = 0.0006) on appearance of PDs.

As the level of smoothness increases, as exemplified in Figure 6.20, the PD magnitude reduces by almost a factor of 10. Additionally, it can be noted that the number of PDs is reduced at phase positions where the voltage steps are decreased. At the same time, at the full voltage steps the PD amount increases as a consequence of the increased rise time.

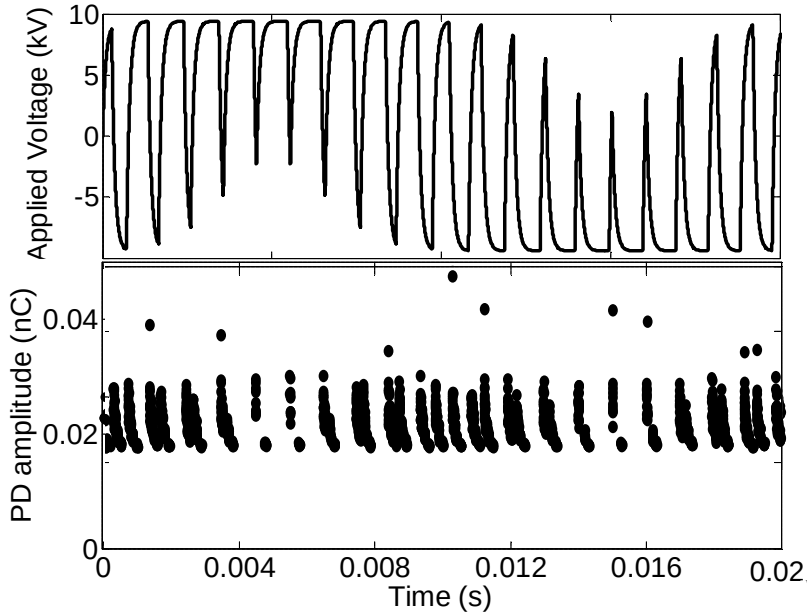

Figure 6.20 Simulated effect of PWM waveform of intermittent smoothness (S = 0.04) on appearance of PDs.

Figure 6.21 illustrates a situation where some of the voltage steps in the applied waveform are lower than the extinction voltage level (S = 0.15). The PRPD pattern becomes here similar to that of the pattern under sinusoidal excitation.

To further elucidate the observed behaviour, Figure 6.22 illustrates how the voltage

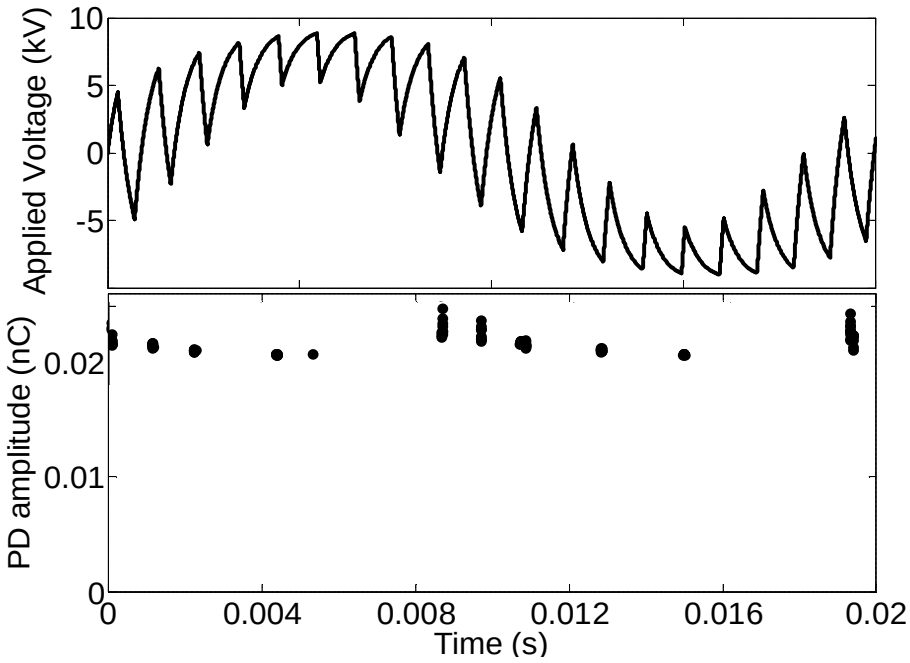

Figure 6.21 Simulated effect of PWM waveform of high smoothness (S = 0.15) on appearance of PDs.

steps of the smoothed waveform influence the simulated voltages across the cavity and the dielectric insulation. When the voltage across the cavity reaches sufficient level for a PD to occur, the corresponding change in voltage distribution is indicated in Figure 6.22.

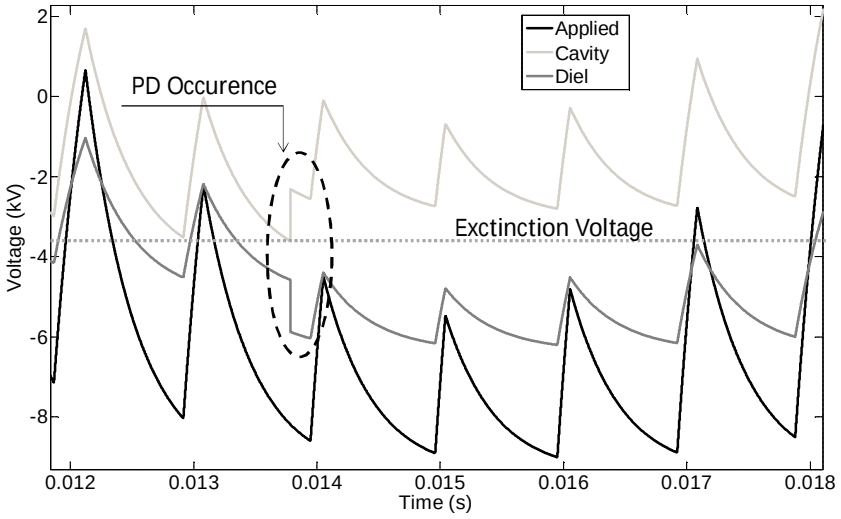

Figure 6.22 Voltage drops on cavity and insulation under exposure to PWM waveform of high smoothness (S = 0.15).

Similarly as above, to improve the similarity to observations, the deviations in PD magnitude should be increased for higher smoothness levels. One way to do this would be to adjust the probability expression more carefully than was deemed necessary above. Additionally the time dependence can be further exploited; however the main aim with this approach is to present a model which quantitatively captures relevant properties of the PD process with a limited number of process elements and parameters. It is observed from the simulations that the PD magnitude decreases and the number of PDs initially increases until the smoothness reaches the required level, as expected. Thus the presented model has successfully accomplished this aim.

6.4 Comments and conclusions

Several approaches to simulate PDs have been presented in the literature based on a multitude of parameters to reproduce various experimental results, see chapter 2. However, as mentioned in the beginning of this chapter, it is often difficult to accurately determine these parameters and thus to obtain a better understanding of the PD phenomena. The model presented in this section is capable of qualitatively reproducing several of the observations discussed in chapters 4 and 5 for a dielectrically insulated cavity. It is based on a modified 'ABC' model and the relevant parameters needed to reproduce most observations are obtained from measurements and gradually introduced.

The presented investigation highlights the introduction of over voltage dependent quench level as well as the minimum time delay before PD as the most prominent contributions. It has been illustrated that the number of PDs, relative number as well as exctinction level dependence of rise time have been included in the descriptive

properties of the model. The probability function has been selected simple enough to reach a similar PD distribution as the measured results.

Certain drawback exists however, such as the limited of ability to consider volume charges, see chapter 2. However since the employed parameters are mostly based on measured quantities, such as the minimum required electric field level for PDs, a reasonably similar behaviour have been reached. Extension of the ABC model is also possible [47, 48]. The simulation result have been tested and verified for different rise times. Further investigations to improve the accuracy can suitably be focused on increasing the spread in PD amplitude for the different smoothness as discussed in chapter 6.3. The influence of surface conductivity is neglected in this model, however from previous investigations it is also known that the charge decay on polycarbonate material is very slow, in the range of hours as observed from the measurements of the extinction voltage in Figure 4.2.

One particularly relevant observation is the relation between the change in PD amplitude and extinction voltage level for the different rise times investigated. Common to all insulation system studied within this thesis is the decreased extinction voltage level for shorter rise times. This was initially noticed for the dielectrically insulated cavity but the same tendency was later observed for the motor winding and the twisted pair test object as well. Applying the same simulation approach on a twisted pair test object would however have presented a challenge due to the amount of possible PD sources.

Tests applying sinusoidal waveforms where the endplates were covered with conducting metal showed little spread in PD amplitude [21] suggesting a complete discharge of the cavity for each PD. A smaller part of the cavity discharged would then result in lower PD magnitude. Thus a relation between rise time and volume of each PD would show similar properties as the suggested approach. In [69] several aspects of such an approach are discussed. However measurements relating voltage difference and PD amplitude in Figure 6.9 support the implemented method in this work.

7. Conclusions

One limitation with measurements at steep voltage shapes is that the decoupler frequency output from PDs should preferably be higher than from the applied voltage. However with the time domain filtering technique, where the stochastic nature of the PDs is used, the test voltage attenuation is less important which reduces this problem significantly.

The resonant PD coupler presented in this thesis gives a considerably increased sensitivity compared to previously used circuits. This is obtained through a more effective use of a coaxial cable as a resonant unit. As a result, a sensitive PD detection is obtained that allows for studies of intrinsic PD properties, such as discharge rise time. The investigations performed also emphasised that to implement a robust PD decoupler with a high bandwidth, it is necessary to consider parasitic impedances when selecting circuit parameters.

Though the circuit applied in this work is not fully optimized, variations in the range of one order of magnitude in the transfer function still enable a sensitive PD detection. Thus the parameters of the circuit need only to be grossly adjusted to specific test situations. An example of optimization of the circuit is however presented, giving a result which almost eliminates the voltage remnant completely, suitable for steeper voltages and/or higher voltage levels than what is applied in this work.

Additionally a calibration procedure is illustrated based on recreation of the voltage dip across the decoupling capacitor. The result has shown equal or better accuracy than direct measurement with 400 MHz bandwidth high voltage probes and eliminates the shortcomings of some PD calibration units on the market.

The studies presented in this thesis for dielectrically insulated cavity exposed to semi-square voltage waveforms, have shown that the number of PDs per period under exposure to short voltage rise times possesses very different voltage dependence as compared to longer ones. When evaluating the extinction and inception voltage tests, it was found that the former provided considerably more repeatable information. The

extinction voltage also provides the lowest voltage level at which PDs occur and for these reasons it is in focus in the work of this thesis.

Further, the first PDs after polarity reversal occur at a higher voltage level at a shorter rise time. Thus the relative time delay to the polarity reversal increases. This effect appears to be repetitive and taking place in cavities of different dimensions while exposed to voltages of several rise times. For one studied cavity in polycarbonate (diameter 3.5 mm), the critical rise time at which the behavior changes lies between 10 and 20 μs. It has additionally been observed that PDs appearing in all the studied cases have larger amplitudes at shorter rise times, which, on average, also increases with voltage level and cavity diameter. In addition, the rise time of the PD event is significantly shorter at short voltage rise times than at longer ones. For the longer rise times the PD amplitude remains approximately constant and at a lower level, though more PDs are generated per period. Additionally these observations were found valid for various cavity sizes and for bipolar and unipolar waveforms.

The studies were continued applying PWM wave forms which forced an adaption of the software algorithm to consider jitter in phase and non-integer relation between carrier and synthesized waveform frequencies. The vital points were to classify the voltage flanks with respect to polarity and to use two time scales to relate PDs both versus flank and within the modulated frequency. The latter enables a direct comparison of PRPD patterns for PWM and sinusoidal wave forms.

The concept “smoothness” was introduced and quantified by the level of filtering applied on a PWM voltage waveform. In principle higher smoothness imply longer rise time. This estimate is designed to give consistent result regarding the level of filtering required to reach the same PD exposure as for sinusoidal wave form. This measure has been applied on all insulation system tested with PWM wave forms.

The studies on the dielectrically insulated cavity confirm that the number and amplitude of PDs per modulated period exhibits different characteristics depending on the PWM smoothness level. For the studied cavity, the most significant change in number of detected PDs lies between smoothness levels of 0.028 and 0.11, whereas the PD amplitude decreases to the same level as for sinusoidal excitation already at lower smoothness. This agrees well with the results in chapter 4 for semi-square shaped voltages. For larger smoothness the PD amplitude remains approximately constant, but at a lower level. Thus the influence of rise time on insulation system behaviour appears similar for both PWM and semi-square voltage shapes. This has been confirmed while maintaining constant voltages as measured by peak value or RMS as well as for different carrier frequencies.

Since the PD amplitude increases considerably for low smoothness for the other insulation systems tested (the motor stator and the twisted pair sample), this

observation can be linked to recent results regarding the evaluation of new motor insulation. Tests in this work shows a considerable increase in PD amplitude and surface wear similar as identified for the dielectrically insulated cavity. As the PD magnitude remain high at low smoothness, differences in PD amplitude appears most important for the life on the insulation. It also appears that the remaining voltage steps in the smoothened PWM train should remain at lower level than the extinction threshold to reach the same intensity of PD exposure (in number and amplitude) as under sinusoidal excitation.

The simulation approach presented shows that a short time delay until a PD occur results in higher over voltage for low smoothness. This is however not sufficient to reach the difference in distribution observed in the measurements. To obtain this the PD quench voltage level was made dependent on the over voltage level. This means that low smoothness lowers the quench voltage and results in larger but less PD per period.

Additionally these simulations showed lower extinction voltage for low smoothness, mainly dependent on the lower quench voltages.

Taken together, these conclusions suggest a possible change of the PD discharge mechanism as the voltage rise time decreases. At the present stage, one may only speculate on the nature and cause of this change and a transition from a Townsend to a streamer-like discharge seems to be a possible scenario. It has been considered in [12] that the evolving PD degradation in gas filled cavities do cause changes in the discharge mechanism, so that streamer, Townsend and pitting phenomena occur as the degradation proceeds. This affects the number of PDs occurring in each period. However, the differences described in this paper reflect behavior attributed to the rise time influence and not to degradation as in [12].

To estimate the effect of the smoothness levels on the insulation system life, additional investigations is needed. Considering the shorter duration and larger amplitude of the streamer-like discharges, it seems probable that the deteriorating effects may be stronger as is supported with the visual degradation tests performed which suggests an increased wear. This effect can potentially have an impact on the service lifetime of insulation systems exposed to rapidly changing voltages and therefore deserve further studies.

Finally it has been shown that the square waveform provides several advantages when studying PD properties. The rise time can be adjusted independent of frequency, which is an advantage compared to sinusoidal waveforms of different frequencies. It is thus possible to measure important PD properties, such as the delay time, with short enough rise times. Further the time at constant voltage gives a possibility to measure charge decay times if they are comparable to the used test voltage period.

8. Future Work

Several directions of the further studies are foreseen. One of them should be devoted to increase understanding of the physics of the observed transition in discharge mechanism and thereby to be able to predict under which circumstances it occurs. Here experiments performed under varying stress conditions should provide important insights, as it appears from the present study that not only the fast PD process but also the magnitude and decay time of the deposited charges become important ingredients in the process description. Also simulations of the discharge process may be very useful as well as studies of other types of sources. PDs under oil, for example, show a long delay time, several ms, as observed in [11]. For such PD sources, fast voltage rise times have presumably no influence on PD magnitude.

Another direction is to define the extent by which the transition from one discharge type to another may reduce insulation service life. Here time-to-breakdown investigations can provide the ultimate answer but such studies require long time and large resources to obtain statistically significant results. A faster alternative may be to study the gradual degradation of the cavity surface, similarly to the studies presented in [12]. Such an investigation should also include studies on other materials than the investigated polycarbonate plates, including characterizations of changes appearing in the chemical structure of material surfaces after exposure of PDs of varying intensities.

The observations described in this thesis suggest that studies of the transition between PWM and sinusoidal waveforms will be essential for elucidating how the stress in the insulation system changes. It is likely that a shortcut to find the level of smoothness required to reach the same PD exposure as for sinusoidal wave forms includes comparisons between the extinction voltage levels. In case no difference can be noted, one may prove that for waveforms with remaining step size lower than the extinction level a similar PD exposure ought to be reached.

An important part of the future work may also concentrate on modifications of the measurement system to enable studies under exposure to voltages from multi-level

inverters. Use of another PD decoupler, such as Rogowski coil or antenna, may be required in case a voltage stiff converter is the source of the voltage. Since the presented software algorithm is not specifically designed for any particular PD detector, such investigations are possible without software changes.

A method to recreate the initial voltage shape across the PD source has been demonstrated. However, the remaining challenge is to recreate the actual rise time of the PD and additional work needs to be performed to accomplish this task. Particular emphasis should be to obtain a reliable transfer function at the highest frequencies. When such method is found, its inclusion into the software of the measurement system will allow for a more flexible use.

9. References

[1] A. Mbaye, F. Grigorescu, T. Lebey and B. Ai, “Existence of Partial Discharges in Low-voltage Induction Machines supplied by PWM Drives”, IEEE Transactions on Dielectric and Electrical Insulation, Vol. 3, pp. 554-560, 1996.

[2] F. Sahlén, L. Ming, K. Johansson, E. Mårtensson and O.Koponen. ”Investigation of Mica Based Insulation for High Voltage Machines Subjected to Repetitive Pulsed Voltage”, IEEE int’l. Sympos. Electr. Insulation (ISEI), pp. 409-413, 2010.

[3] M. K. W. Stranges, G. C. Stone and D. L. Bogh, “Voltage endurance testing, stator insulation systems or inverter-fed machines”, IEEE Industry Applications Mag., Issue: 6, pp. 12-18, 2009.

[4] IEC Publications 60270, "Partial discharge measurements", 3rd ed. 1998.

[5] IEC/TS 61934 Electrical insulating materials and systems – Electrical measurement of partial discharges (PD) under short rise time and repetitive voltage impulses, 1st ed. 2006.

[6] F. Guastavino, G. Coletti, B. Cerutti and E. Torello, “An Experimental Study About the Weight of the (dv/dt) Factor Characterizing Inverter-like Voltages During Pre-selection Tests on Copper Enameled Wires for Adjustable Speed Drives Motors”, IEEE Power Engineering Society Summer Meeting, Seattle, WA, USA, Vol. 4, pp. 2446-2488, 2000.

[7] M.D Judd, S.D.J McArthur, A.J Reid, V.M Catterson, L Yang, B Jacobsson, K.O Svensson, “Investigation of radiometric partial discharge detection for use in switched HVDC testing”, IEEE Power Engineering Society General Meeting, pp. 1-7, 2006.

[8] M. T. Do, J. L. Auge and O. Lesaint, “Optical Measurement of Partial Discharges in Silicone Gel under Repetitive Pulse Voltage”, Int’l. Sympos.

Electr. Insulation Materials (ISEIM), Vol. 2, Kitakyushu, Japan, pp. 360-363, 2005.

[9] E. Lindell, T. Bengtsson, J. Blennow and S.M Gubanski," Measurement of Partial Discharges at Rapidly Changing Voltages", IEEE Transactions on Dielectric and Electrical Insulation, Vol. 15, pp. 823-831, 2008

[10] E. Lindell, T. Bengtsson, J. Blennow and S.M Gubanski, "Influence of Rise Time on PD Extinction Voltage at Semi-Square Voltage Waveforms", IEEE Transactions on Dielectric and Electrical Insulation,Vol. 17, pp. 141-148, 2010.

[11] E. Lindell, T. Bengtsson, J. Blennow and S.M Gubanski, "Cavity Partial Discharges at Semi-Square Voltages at different rise times", 21st Nordic Insulation Sympos., Gothenburg, Sweden pp. 93-96, 2009.

[12] P.H.F Morshuis, Partial Discharge Mechanism, Ph.D. thesis Delft University of Technology, Delft University Press, 1993.

[13] F.H. Kreuger, Industrial high Voltage, 4-6, Delft University Press, ISBN 90-6275-562-3, 1992.

[14] F.H. Kreuger, Partial Discharge Detection in High Voltage Equipment, Delft University Press, ISBN 90-6275-562-3, 1992.

[15] E. Lindell, "Partial Discharges at Repetitive Rapidly Changing Voltages", Ph.D. thesis, ISBN 9789173853125, Chalmers University of technology, Gothenburg Sweden, 2009.

[16] D. Fabiani, G. C. Montanari and A. Contin, "Aging Acelleration of Insulating Materials for Electrical Machine Windings Supplied by PWM in the Presence and in the Absence of Partial Discharges", IEEE 7th International conf on Solid Dielectrics, Eindhoven, the Netherlands, pp. 283-286, 2001.

[17] D. Fabiani and G.C. Montanari, "On the degradation of winding insulation of AC-motors supplied by adjustable speed drivers- An overview," ELECTROMOTION, vol. 8, no. 2, pp. 89-95, Jun. 2001.

[18] F. Guastavino, G. Coletti, B. Cerutti and E. Torello, "Life tests on twisted pairs subjected to PWM-like voltages", Proceedings of the 2004 IEEE , pp. 421-424, 2004.

[19] Suwarno, "Comparison between Discharge patterns in Solid and Liquid Insulation Materials", Proceedings of the 9th International Conference on Properties and Applications of Dielectric Materials, July 19-23, 2009, pp. 561-564, Harbin, China.

[20] L. Niemeyer, “A generalized approach to partial discharge modelling”, IEEE Transactions on Dielectric and Electrical Insulation, 2(4), pp. 510-528, 1995.

[21] C. Forssen, “Modelling of Cavity Partial Discharges at Variable Applied Frequencies”, Doctoral Thesis in Electrical Systems, KTH Electrical Engineering, ISSN 1653-5146, ISBN 978-91-7178-927-3, Stockholm, Sweden, 2008.

[22] F.H. Kreuger, Industrial high Voltage, 1-3, Delft University Press, ISBN 90-6275-561-5, 1991.

[23] H. A. Illias, G. Chen and P.L. Lewin, “The Influence of Spherical Cavity Surface Charge Distribution on the Sequence of Partial Discharge Events”, J. Phys. D: Appl. Phys. 44, pp.1-15, (2011).

[24] C. Forssen, “Modeling Partial Discharges in a Cavity at Different Applied Frequencies”, IEEE Annual Report Conference on Electrical insulation and Dielectric Phenomena, pp. 132- 135, 2007.

[25] G.C. Montanari, A. Cavallini, L. Testa, S. Serra and L. A. Dissado, ”Model of Ageing Inception and Growth from Microvoids in Polyethylen-based Materials under AC voltage”, IEEE Annual Report Conference on Electrical insulation and Dielectric Phenomena, pp. 29- 32, 2008.

[26] F. Gutfleisch and L. Niemeyer, “Measurement and Simulation of PD in Epoxy Voids”, IEEE Transactions on Dielectric and Electrical Insulation, Vol. 2, No.5, pp. 510-528, October 1995.

[27] G.C. Montanari, Cavallini, A.and Ciani, F. “Partial discharges in internal voids: Dependence on defect position with respect to electrodes”, Annual report Conference on Electrical Insulation and Dielectric Phenomena, CEIDP, Vancover, Canada, pp.175-178, 2007.

[28] T. Koltunowicz, A. Cavallini, D. Djairam, G.C. Montanari and J. Smit, ”The Influence of Square Voltage Waveforms on Transformer Insulation Break Down Voltage”, IEEE Annual Report Conference on Electrical insulation and Dielectric Phenomena, pp. 48- 51, 2011.

[29] S. Grzybowski, L. Cao and A. Zanwar, “Accelerated Aging Phenomena of 15 kV EPR Cable Energized by Elevated AC with Switching Impulses Superimposed”, Proceedings of the 17th International Symposium on High Voltage Engineering, CD-rom, ISBN/ISSN: 978-3-8007-3364-4.

[30] S. Grzybowski, P. Shrestha and L. Cao, “Electrical Aging Phenomena of XLPE and EPR Cable Insulation Energized by Switching Impulses”,

International Conference on High Voltage Engineering and Application, Chongqing, China, Nov. 9-13, pp. 422-425, 2008.

[31] F. Guastavino, G. Cotella, A. Dardano, G. F. Massa, A. Ratto, S. Squarcia and E. Torello. "Influence of the Rise Time and of the Temperature on the PD Inception Voltage of Enamelled Wires", IEEE Annual Report Conference on Electrical insulation and Dielectric Phenomena, pp. 29- 32, 2010.

[32] M. Florkowski, B. Florkowska, J. Furga, and P. Zydron," Impact of high voltage harmonics on interpretation of partial discharge patterns" IEEE Transactions on Dielectrics and Electrical Insulation, pp. 2009 – 2016, vol. 20 , Issue: 6, 2013.

[33] T. Jiang, A. Cavallini, G.C. Montanari, J. Li "The Role of HVDC Voltage Waveforms on Partial Discharge Activity in Paper/Oil Insulation". IEEE Conference on Electrical Insulation and Dielectric Phenomena", pp. 424-427, Montreal, 14 -17 October, 2012.

[34] G. Paulsson, F. Sahlen, H. Hillborg, A. Björklund, M. Takala, and J. Andersson, "New type of PD-resistant enamelled wire," 12th Int'l. Electrical Insulation Conf., Birmingham, UK, 2013, pp. 169-174.

[35] N. Taylor, "Dielectric Response and Partial Discharge Measurements on Stator Insulation at Varied Low Frequency", Doctoral Thesis, Royal University of Technology, Stockholm, Sweden 2010, ISBN 978-91-7415-713-0.

[36] X. Wang, "Partial Discharge Analysis at Arbitrary Voltage Waveform Stimulus", Lic Thesis, Royal University of Technology, Stockholm, Sweden 2012, ISBN 978-91-7501-587-3.

[37] C. D. Taylor and S. Grzybowski, "Measurement of Partial Discharge in Machine Winding Insulation During Short-Rise Time Pulse Voltage", IEEE Electric Ship Technologies Symposium, Baltimore, USA, pp.529-532, 20-22 April, 2009.

[38] B. Florkowska, M. Florkowski, J. Furgal, J. Roehrich and P. Zydron, "The voltage stresses of insulation systems under PWM inverter supplies", IEEE Annual Report Conference on Electrical Insulation and Dielectric Phenomena, pp. 372-375, 2009.

[39] Hyang-Eun Jo, Dae-Won Park, Gyung-Suk Kil, Young-Min Kim and Sung-Wook Kim, "Calibration of a Partial Discharge Sensor in a Gas insulated

Switchgear" , Proceedings of the 18th International Symposium on High Voltage Engineering, Seoul, pp. 2094-2097, South Korea 2013.

[40] M. D. Judd, L. Yang and I. B. Hunter, "Partial Discharge Monitoring for Power Transformers Using UHF Sensors Part 1: Sensors and Signal Interpretation", IEEE Electrical Insulation Magazine, Vol,21, No.2, pp. 5-14, March/April 2005.

[41] Alistair J Reid, Martin D Judd, Brian G Stewart and Richard A Fouracre, "Partial discharge current pulses in SF6 and the effect of superposition of their radiometric measurement", J. Phys. D: Appl. Phys.39, pp. 4167–4177, 2006.

[42] T. Billard, F. Fresnet, M. Makarov, T. Lebey, P. Castelan, P. Bidan, S. Dinculescu," Partial Discharges monitoring in twisted pair fed with PWM inverter using non-intrusive sensors", 2013 IEEE International Conference on Solid Dielectrics, Bologna, Italy, June 30 – July 4, pp. 314-317, 2013.

[43] Sang-Hwa Y, "Surge PD Test Setup and a Sensor for Monitoring Turn Insulation of AC Motor Stator Windings", Proc. of the 18th International Symposium on High Voltage Engineering, Seoul, pp. 2000-2004, South Korea 2013.

[44] B. Sonerud, "Characterization of Electrical Insulation Exposed to Arbitrary Voltage Waveforms", Ph.D. thesis, ISBN 978-91-7385-373-6, Chalmers University of technology, Gothenburg Sweden, 2010.

[45] B. Florkowska, M. Florkowski, J. Furgal, J. Roehrich and P. Zydron, "Impact of Fast Transient Phenomena on Electrical Insulation Systems", Wydawnictwa AGH, Krakow 2012, ISBN 978-83-7464-480-8.

[46] U. Gäfert, H. Edin and C. Forssen, "Modelling of Partial Discharge Spectra Measured with Variable Applied Frequency", Proceedings of the 7th International Conference on Properties and Applications of Dielectric Materials, pp. 839-842, Nagoya 2003.

[47] R. Patsch and F. Berton, "The Role of Space Charges in PD-Processes", ISEIM'01, Himeji, pp. 21-24, Japan 2001.

[48] Z. Achillides, G. Georghiou and E. Kyriakides, "A Theoretical Analysis of the Capacitive Modelling and the Induced Charge Concept in Partial Discharges", IEEE Transactions on Dielectrics and Electrical Insulation Vol. 15, No. 6, pp. 1507-1516; December 2008.

[49] J. H. M Blennow, “Active High Voltage Insulation”, Ph.D. thesis, ISBN 91-7197-937-9, Chalmers University of technology, Gothenburg Sweden, 2000.

[50] L. Wang, “Physical Model of PD Behaviour and Relevant Damage Growth from Micro-Cavities in Polyethylene-Based Material under AC Voltage”, Doctoral Thesis Bologna University, 2011.

[51] H. A. Illias, G. Chen and P. L. Levin, “Modelling of Partial Discharge Activity in Spherical Cavities within a Dielectric Material”, IEEE Electrical Insulation Magazine, pp.38 -45, 2011.

[52] H. A Illias, A. H. A. Bakar and M. A Tunio, “Simulation of partial discharge within a void under square waveform applied voltage”, IEEE Conference on Electrical Insulation and Dielectric Phenomena", Montreal, 14 -17 October, pp.76-79, 2012.

[53] A. Alireza, A. Ganjovi, G. Nandini and R. Gorur, R. Govinda, “A Kinetic Model of a PD Pulse”. IEEE Transaction on Dielectrics and Electrical Insulation, Vol. 16, No. 6, pp.1743 -1754: December 2009.

[54] Y. Serdyuk, “Computer Modelling of Electrophysical Phenomena in High Voltage Insulation”, Ph.D. thesis, ISBN 91-7291-431-9, Chalmers University of technology, Gothenburg Sweden, 2004.

[55] S. Kumara, “Electrical Charges on Polymeric Insulator Surface and their Impact on Flashover Performance”, PhD. thesis, ISBN 978-91-7385-5764-2, Chalmers University of technology, Gothenburg Sweden, 2012.

[56] T. Bengtsson, E. Lindell, T. J. Å Hammarström “Stochastic Detection of Partial Discharges” Published in: IEEE Transactions on Dielectrics and Electrical Insulation, Vol. 20, Issue 6, pp. 2203-2211, December 2013.

[57] J. G. Proakis,”Digital Signal Processing”, Prentice-Hall Internal, Inc, 1996.

[58] H. Curtins and A. Shah, “Pulse Behaviour of Transmission Lines with Dielectric Losses”, IEEE Transactions on Circuit and Systems, Vol. CAS-32, No.8, pp.819-826, August 1985.

[59] Orcad Reference manual Version 9.0, October, 1998. Copyright 1998, OrCAD, Inc.

[60] X. Ma, C. Zhou and I. Kemp, “Automated Wavelet Selection and Thresholding for PD detection,” IEEE Electrical Insulation Mag., vol. 18, pp. 37-45, Mar.-Apr. 2002.

[61] P. Wang, A. Cavallini, G. C. Montanari, “The Influence of Square Voltage Rise Time on Partial Discharge Spectra”, IEEE Conference on Electrical Insulation and Dielectric Phenomena", pp. 129-132, Montreal, 14 -17 October, 2012.

[62] U. Fromm, “Partial Discharge and Breakdown Testing at High DC Voltage”, Thesis, ISBN 90-407-1155-0, Delft University of technology, Delft University Press Netherlands, 1995.

[63] P. H. F Morshuis, “Degradation of Solid Dielectrics due to Internal Partial Discharge: Some thoughts on progress made and where to go now”, IEEE Transaction on Dielectrics and Electrical Insulation, Vol. 12, No. 5, pp.905 - 913, October 2005.

[64] D. Fabiani, G. C. Montanari, A. Cavallini and G. Mazzanti,”Relation between Space Charge Accumulation and Partial Discharge Activity in Enameled Wires under PWM-like Voltage Waveforms”, IEEE Transactions on Dielectrics and Electrical Insulation, pp. 393-405, Vol. 11, No.3, June 2004.

[65] IEC 60851-5 Winding wires - Test methods - Part 5: Electrical properties, 2008.

[66] T. L. Koltunowicz, “Accelerated Insulation Aging due to Thermal and Electrical Stresses in Future Power Grids”, Thesis, ISBN 978-90-8891-819-3, Delft University of technology, Delft University Press Netherlands, 2014.

[67] E. Kuffel, W. W. Zaengl, and J. Kuffel, High Voltage Engineering: fundamentals, 2nd ed., ISBN 0 7506 3634 3, 2000.

[68] R. Patsch and F. Bertom, “Pulse-Sequence-Analysis-Chances to Characterize Defects”, IEEE Conference on Electrical Insulation and Dielectric Phenomena, Proceedings pp. 243-248, 1999.

[69] K. Wu, Y. Suzuoki and L.A Dissado, “The Contribution of Discharge Area Variation to Partial Discharge Patterns in Disc-Voids”, J. Phys, D. Appl. Phys. 37 pp. 1815-1823, 2005.